Integrated use of polarimetric Synthetic Aperture Radar (SAR) and optical image data for land cover mapping using an object-based approach

by

Leigh Helen de Beyer

Thesis presented in fulfilment of the requirements for the degree Master of Science in Geoinformatics at Stellenbosch University.

Supervisor: Dr Jaco Kemp

Co-supervisor: Dr Pierre Todoroff

Faculty of Science

December 2015

DECLARATION

By submitting this **thesis**/dissertation electronically, I declare that the entirety of the work contained therein is my own, original work, that I am the sole author thereof (save to the extent explicitly otherwise stated), that reproduction and publication thereof by Stellenbosch University will not infringe any third party rights and that I have not previously in its entirety or in part submitted it for obtaining any qualification.

December 2015

ABSTRACT

Image classification has long been used in earth observation and is driven by the need for accurate maps to develop conceptual and predictive models of Earth system processes. Synthetic aperture radar (SAR) imagery is used ever more frequently in land cover classification due to its complementary nature with optical data. There is therefore a growing need for reliable, accurate methods for using SAR and optical data together in land use and land cover classifications. However, combining data sets inevitably increases data dimensionality and these large, complex data sets are difficult to handle. It is therefore important to assess the benefits and limitations of using multi-temporal, dual-sensor data for applications such as land cover classification. This thesis undertakes this assessment through four main experiments based on combined RADARSAT-2 and SPOT-5 imagery of the southern part of Reunion Island.

In Experiment 1, the use of feature selection for dimensionality reduction was considered. The rankings of important features for both single-sensor and dual-sensor data were assessed for four dates spanning a 6-month period, which coincided with both the wet and dry season. The mean textural features produced from the optical bands were consistently ranked highly across all dates. In the two later dates (29 May and 9 August 2014), the SAR features were more prevalent, showing that SAR and optical data have complementary natures. SAR data can be used to separate classes when optical imagery is insufficient.

Experiment 2 compared the accuracy of six supervised and machine learning classification algorithms to determine which performed best with this complex data set. The Random Forest classification algorithm produced the highest accuracies and was therefore used in Experiments 3 and 4.

Experiment 3 assessed the benefits of using combined SAR-optical imagery over single-sensor imagery for land cover classifications on four separate dates. The fused imagery produced consistently higher overall accuracies. The 29 May 2014 fused data produced the best accuracy of 69.8%. The fused classifications had more consistent results over the four dates than the single-sensor imagery, which suffered lower accuracies, especially for imagery acquired later in the season.

In Experiment 4, the use of multi-temporal, dual-sensor data for classification was evaluated. Feature selection was used to reduce the data set from 638 potential training features to 50, which produced the best accuracy of 74.1% in comparison to 71.9% using all of the features. This result validated the use of multi-temporal data over single-date data for land cover classifications. It also validated the use of feature selection to successfully inform data reduction without compromising the accuracy of the final product.

Multi-temporal and dual-sensor data shows potential for mapping land cover in a tropical, mountainous region that would otherwise be challenging to map using single-sensor data. However, accuracies

generally remained lower than would allow for transferability and replication of the current methodology. Classification algorithm optimisation, supervised segmentation and improved training data should be considered to improve these results.

KEYWORDS

Land cover classification, RADARSAT-2, SPOT-5, object-based, feature selection, fusion, random forest, remote sensing.

OPSOMMING

Beeld-klassifikasie word al 'n geruime tyd in aardwaarneming gebruik en word gedryf deur die behoefte aan akkurate kaarte om konseptuele en voorspellende modelle van aard-stelsel prosesse te ontwikkel. Sintetiese apertuur radar (SAR) beelde word ook meer dikwels in landdekking klassifikasie gebruik as gevolg van die aanvullende waarde daarvan met optiese data. Daar is dus 'n groeiende behoefte aan betroubare, akkurate metodes vir die gesamentlike gebruik van SAR en optiese data in landdekking klassifikasies. Die kombinasie van datastelle bring egter 'n onvermydelike verhoging in data dimensionaliteit mee, en hierdie groot, komplekse datastelle is moeilik om te hanteer. Dus is dit belangrik om die voordele en beperkings van die gebruik van multi-temporale, dubbel-sensor data vir toepassings soos landdekking-klassifikasie te evalueer. Die waarde van gekombineerde (versmelte) RADARSAT-2 en SPOT-5 beelde word in hierdie tesis deur middel van vier eksperimente geëvalueer.

In Eksperiment 1 is die gebruik van kenmerk seleksie vir dimensionaliteit-vermindering toegepas. Die ranglys van belangrike kenmerke vir beide enkel-sensor en 'n dubbel-sensor data is beoordeel vir vier datums wat oor 'n tydperk van 6 maande strek. Die gemiddelde tekstuur kenmerke uit die optiese lae is konsekwent hoog oor alle datums geplaas. In die twee later datums (29 Mei en 9 Augustus 2014) was die SAR kenmerke meer algemeen, wat dui op die aanvullende aard van SAR en optiese data. SAR data dus gebruik kan word om klasse te onderskei wanneer optiese beelde onvoldoende daarvoor is.

Eksperiment 2 het die akkuraatheid van ses gerigte en masjien-leer klassifikasie algoritmes vergelyk om te bepaal watter die beste met hierdie komplekse datastel presteer. Die random gorest klassifikasie algoritme het die hoogste akkuraatheid bereik en is dus in Eksperimente 3 en 4 gebruik.

Eksperiment 3 het die voordele van gekombineerde SAR-optiese beelde oor enkel-sensor beelde vir landdekking klassifikasies op vier afsonderlike datums beoordeel. Die versmelte beelde het konsekwent hoër algehele akkuraathede as enkel-sensor beelde gelewer. Die 29 Mei 2014 data het die hoogste akkuraatheid van 69,8% bereik. Die versmelte klassifikasies het ook meer konsekwente resultate oor die vier datums gelewer en die enkel-sensor beelde het tot laer akkuraathede gelei, veral vir die later datums.

In Eksperiment 4 is die gebruik van multi-temporale, dubbel-sensor data vir klassifikasie ge-evalueer. Kenmerkseleksie is gebruik om die data stel van 638 potensiële kenmerke na 50 te verminder, wat die beste akkuraatheid van 74,1% gelewer het. Hierdie resultaat bevestig die belangrikheid van multi-temporale data vir grond dekking klassifikasies. Dit bekragtig ook die gebruik van kenmerkseleksie om data vermindering suksesvol te rig sonder om die akkuraatheid van die finale produk te belemmer.

Multi-temporale en dubbel-sensor data toon potensiaal vir die kartering van landdekking in 'n tropiese, bergagtige streek wat andersins uitdagend sou wees om te karteer met behulp van enkel-sensor data. Oor die algemeen het akkuraathede egter te laag gebly om vir oordraagbaarheid en herhaling van die huidige metode toe te laat. Klassifikasie algoritme optimalisering, gerigte segmentering en verbeterde opleiding data moet oorweeg word om hierdie resultate te verbeter.

TREFWOORDE

Landdekking, RADARSAT-2, SPOT-5, geografiese objekgebaseerde beeldanalise, kenmerkseleksie, random forest, afstandswaarneming.

ACKNOWLEDGEMENTS

TABLE OF CONTENTS

LIST OF TABLES

LIST OF FIGURES

LIST OF ACRONYMS AND ABBREVIATIONS

CART	Classification and regression trees
CD:NGI	Chief Directorate: National Geo-Spatial Information
CIRAD	Centre International en Recherche Agronomique pour le Developpement
CSIR	Council for Scientific and Industrial Research
CTA	Classification tree analysis
DEM	Digital elevation model
DT	Decision tree
ESA	European Space Agency
GEOBIA	Geographic object-based image analysis
GCP	Ground control point
GIS	Geographic information system
GLCM	Grey level co-occurrence matrix
GLDV	Grey level difference measure
GPS	Global positioning system
KNN	K-means nearest neighbour
LC	Land cover
LCCS	Land cover class system
Lidar	Light detection and ranging
LULC	Land use and land cover
ML	Maximum likelihood
MRS	Multiresolution segmentation
NIR	Near infra-red
NDVI	Normalised difference vegetation index
OA	Overall accuracy
PA	Producer's accuracy
PALSAR	Phased array type L-band synthetic aperture radar
PCA	Principal component analysis
PolSAR	Polarimetric synthetic aperture radar
RADAR	Radio detection and ranging
RF	Random forest
RS-2	Radarsat-2
SAR	Synthetic aperture radar

SEAS-OI	Surveillance de l'Environnement Assistée par Satellite dans l'Océan Indien (Satellite receiving station situated on Réunion Island)
SEaTH	Separability and thresholds
SLC	Single look complex
SPOT	Satellite Pour l'Observation de la Terre (Satellite for observation of Earth)
SVM	Support vector machine
SWIR	Short wave infra-red
UA	User's accuracy

CHAPTER 1   INTRODUCTION

This chapter introduces the study and provides initial background information for context. The problem formulation, aim, and objectives are discussed. The methodology and research design are briefly summarised and the structure of the rest of the thesis is given.

1.1   BACKGROUND TO THIS STUDY

Land cover classification involves assigning real-world land cover types to pixels or areas on an image. It is one of the most important applications of satellite remote sensing (Lee, Grunes & de Grandi 1999), as agricultural planning and natural resource allocation can be optimised by the correct classification of the Earth's terrain. Remotely sensed imagery provides spatially consistent data with large coverage, a variety of information from different sensors, and a short revisit time thereby reducing the need for continual field visits (Herold, Goldstein & Clarke 2003; Pal & Mather 2004). Polarimetric synthetic aperture radar (PolSAR) imagery has shown potential as a unique, rich source of information about the Earth's varying land surfaces. Unlike optical sensors, there are very few limitations to collecting synthetic aperture radar (SAR) image data during inclement weather or at night (Moreira et al. 2013). It is important to focus research efforts on land cover mapping and change analysis around this data type as many new SAR satellites will be launched in the next few years, providing high resolution, accessible multi-temporal SAR data (Moreira et al. 2013).

Developing land cover classifications using remotely sensed data is an area of ongoing research (Rodriquez-Galiano et al. 2012). The increased availability of data from different, complementary sensors and sources has allowed research to focus on using this data for various land cover applications. Although pixel-based classifications have effectively created land cover classifications with acceptable accuracy standards, they have received less attention recently and the focus has shifted to object-based approaches (Lu & Weng 2005). This is due to object-based image analyses' many advantages including the ability to exploit more than just spectral values to differentiate classes and incorporate elements such as texture into analysis (Blaschke 2010). Object-based approaches are particularly important for applications in areas displaying typical spatial patterns, such as agricultural areas similar to this study area, as these inherent patterns can be exploited to improve classifications (Waske & Van der Linden 2008).

There has recently been a shift from traditional statistical approaches to more powerful, flexible machine-learning algorithms for land cover classification. Numerous new techniques and applications have been developed in response (Waske & Van der Linden 2008). The increase in computational power, data size,

and data complexity available to an ever-widening user base has also allowed many new applications to be tested (Waske & Van der Linden 2008).

Single-sensor image data can have limitations; for example, they can generate incomplete, inconsistent, or imprecise information (Fatone, Maponi & Zirilli 2001). The integrity of monitoring studies can also be compromised by the inability to collect data at critical points in time. These risks of single-sensor data reliability need to be mitigated (McNairn et al. 2009) and a fusion approach is an effective tool for overcoming these limitations. Data fusion can be defined as combining data from different sources to improve the interpretation performance and potential value of the raw data (Zhang 2010). Merging multiple data sets allows the exploitation of bands from different areas of the electromagnetic spectrum (Haack & Bechdol 2000).

Fusion techniques have many benefits over single-sensor data use. Images can be sharpened by combining different spatial resolutions and improving geometric corrections. Fusion also allows stereo viewing and the enhancement of features that are not otherwise visible in a single image. Applications such as classifications and change detection can be improved by combining data from different sources, thus supplementing missing information and replacing defective data (Amarsaikhan et al. 2010).

Fusing optical and SAR data exploits the benefits of both data types. Each sensor type discerns certain land cover types better than the other (Lu & Weng 2005). Radar imagery alone can struggle to delineate urban areas well whereas optical data can be ineffective in discerning natural vegetation (Haack & Bechdol 2000). Combining these data sets derived from different sources can correct these misclassifications, improving poorly separated classes of single data sets and poor accuracies (Hill et al. 2005).

Single-date imagery is frequently used for land cover classifications, but can pose some limitations. Vegetation classes can be difficult to differentiate, which can be exacerbated by only using a single-date image. There may exist an optimum time of year at which certain vegetation types display the strongest differences due to growth phases, and this seasonality is key for accurate land cover classifications (Lunetta et al. 2006). A multi-temporal approach is beneficial as it can help overcome some of the limitations of single-date imagery and can allow each land cover to be mapped at its optimum time for discrimination (McNairn et al. 2009). This is particularly relevant when using SAR data, as the signal is affected by the presence of exposed soil at the beginning of vegetation growth (McNairn et al. 2009). The differences between types of vegetation, especially in VH backscatter (vertically transmitted and horizontally received polarised radar signal), are more prominent later in the growing season, thus allowing for better class discrimination (McNairn et al. 2009).

SAR data is becoming more available and accessible as there are more sensors available and a larger user community. This has resulted in a transition from purely research-oriented projects to more operational uses of the data (Cable et al. 2014). Operational uses include products that decision makers can use immediately, such as crop yield estimates for harvest planning or land cover classifications to aid in land assignment to different uses, such as agriculture. Although multi-frequency and multi-polarisation SAR data is preferable for most applications, it is not always practical to obtain such data for operational purposes as such projects often have resource restrictions that limit the type of data that can be used. The ability to define the data requirements for a project's particular output is therefore important. Reliance on a single source of data can also limit operational projects as information derived from multiple sensor sources can mitigate the risk of missed acquisitions and ensures data availability all year round.

There is an opportunity to merge and exploit the promising developments in approaches for classifying remotely sensed data. The fusion of multi-sensor and multi-temporal data sets with an object-based approach and inclusion of texture variables holds compelling application promise for land cover classification and change detection. Due to the practical restrictions of operational projects, it is important to quantify the benefits of using multi-temporal and dual-sensor imagery.

1.2   PROBLEM FORMULATION

Traditionally, land cover analysis using remote sensing has been performed on optical sensor imagery. However, optical image data has some limitations, as it cannot be captured during inclement weather or at night. SAR imaging sensors overcome these limitations by using the microwave portion of the electromagnetic spectrum and provide their own energy source. The current reliance on single-sensor data, mostly from optical sensors, introduces a level of risk when research projects are translated into operational outputs. Fusing image data from multiple sources shows promise in mitigating this risk (McNairn et al. 2009).

Although fusion can overcome some of the limitations posed by single-sensor reliance, it also increases the data volume and complexity and it is difficult to process and analyse high dimensional data (Zhang 2004). Feature selection can help to emphasise which parts of the data are most useful and thus inform feature reduction (Amarsaikhan et al. 2010). Feature selection holds potential to also inform which types of data, and from which types of sensor, the most useful information for discriminating different land cover classes can be derived (Laliberte, Browning & Rango 2012).

Several classification algorithms are available for land cover differentiation, each with their own statistical approach, advantages, and disadvantages (Pal & Mather 2003). Thus, it is important to investigate which classification algorithm can handle both the non-normal distribution characteristic of SAR data and the large volume of features that comes with introducing a multi-sensor and multi-temporal data set.

Single-date imagery can have limitations when it comes to mapping vegetation classes, as most classes will exhibit an opportune time of year, or growth stage, for discriminating one from another (Blaes, Vanhalle & Defourney 2005; El Hajj et al. 2009; Jewell 1989; Shang et al. 2009). Multi-temporal image data sets are not always readily available or practical with research project restraints.

Literature does suggest that multi-temporal data sets are better than single-date imagery for land cover classification (Lunetta et al. 2006; Ma et al. 2013; McNairn et al. 2009; Niu & Ban 2013). However, as with multi-sensor data, the benefits of multiple image dates should be quantified. It is also not yet known whether certain features from specific dates are considered more useful for discriminating between classes when applying feature selection on a multi-temporal and multi-sensor data set.

In summary, this thesis addressed four key questions:

1. How can feature selection be used to determine which are the important features for class discrimination, and do these features differ between single-sensor and dual-sensor data sets and between image dates?

2. Which classification algorithm best handles the increased data dimensionality of fused image data sets and produces the highest accuracies?

3. Does the fusion of optical and SAR data improve accuracy in a single-date classification sufficiently to warrant the additional expense of using two data sources?

4. Does the inclusion of a multi-temporal data set improve accuracy sufficiently over a single-date classification to warrant the additional expense of extra data?

1.3   AIM AND OBJECTIVES

The aim of this study was to assess the benefits and limitations of combining multi-temporal fully polarimetric SAR data with optical image data for creating land cover using an object-based approach. The assessment was carried out for land cover in a tropical region.

This aim was divided into 6 major analytical components, addressed in the following objectives:

1. Assess feature selection as a method for informing feature reduction.

2. Assess whether feature importance rankings exhibit temporal trends across both combined and single sensor data.

3. Determine which classification algorithms handle large dual-sensor data sets better.

4. Quantify the potential benefits of combined SAR and optical data against single-sensor data for land cover classification on single-date imagery.

5. Assess temporal trends of combined SAR and optical data against single-sensor data for land cover classification on single-date imagery.

6. Evaluate multi-temporal, dual-sensor SAR-optical data for land cover classification in a tropical region.

1.4   METHODOLOGY AND RESEARCH DESIGN

An overview of the research design is provided in Figure 1.1. An empirical research approach, using primary quantitative data, based on the six main objectives was followed. Prior to analysis, data acquisition and image pre-processing were conducted. In situ information was acquired through fieldwork and image interpretation. The objectives were addressed in four key experiments. Experiment 1 investigated feature selection as a possible method of optimal data selection, and thus data reduction, using the Classification and Regression Trees (CART) and random forest (RF) algorithms. In Experiment 2 six classification algorithms were tested on the combined image data collected to determine the classification algorithm most suited for the study area. This classification algorithm was then used in Experiments 3 and 4. In Experiment 3 single-date object-based classifications were conducted on four separate image dates and the effect of dual-sensor imagery versus single-sensor imagery performance was assessed. Finally, in Experiment 4 multi-temporal classifications were conducted and compared with the single-date classifications of Experiment 3.

A detailed explanation of the methods used is given in Chapters 3 and 4.

CHAPTER 2: LITERATURE REVIEW AND PROBLEM FORMULATION

CHAPTER 3: DATA ACQUISITION

RADARSAT-2

SPOT-5

IN SITU GROUND TRUTH

Objectives 1 and 2: Experiment 1

FEATURE SELECTION

- CART AND RANDOM FOREST FEATURE SELECTION ALGORITHMS

CHAPTER 3: DATA PREPARATION

RADARSAT-2 PRE-PROCESSING

SPOT-5 PRE-PROCESSING

TRAINING AND VALIDATION DATA

Objective 3: Experiment 2

TEST DIFFERENT CLASSIFIERS

- RANDOM FOREST, CART, DECISION TREE, SVM, MAXIMUM LIKELIHOOD AND KNN

Objectives 4 and 5: Experiment 3

SINGLE-DATE CLASSIFICATION

- RANDOM FOREST CLASSIFIER

CHAPTER 4: DATA ANALYSIS

CHAPTER 5: ACCURACY ASSESSMENTS AND RESULTS INTERPRETATION

Objective 6: Experiment 4

MULTI-TEMPORAL CLASSIFICATION

- RANDOM FOREST FEATURE SELECTION AND CLASSIFIER

CHAPTER 6: SYNTHESIS AND EVALUATION

Figure 1.1 Research design diagram.

1.5   STUDY SITE

The primary study site, seen in Figure 1.2, is situated in the south of Réunion Island, around the town of St Pierre. The extent was determined by the availability of RADARSAT-2 imagery and was complemented by SPOT-5 imagery overlapping the same extent.
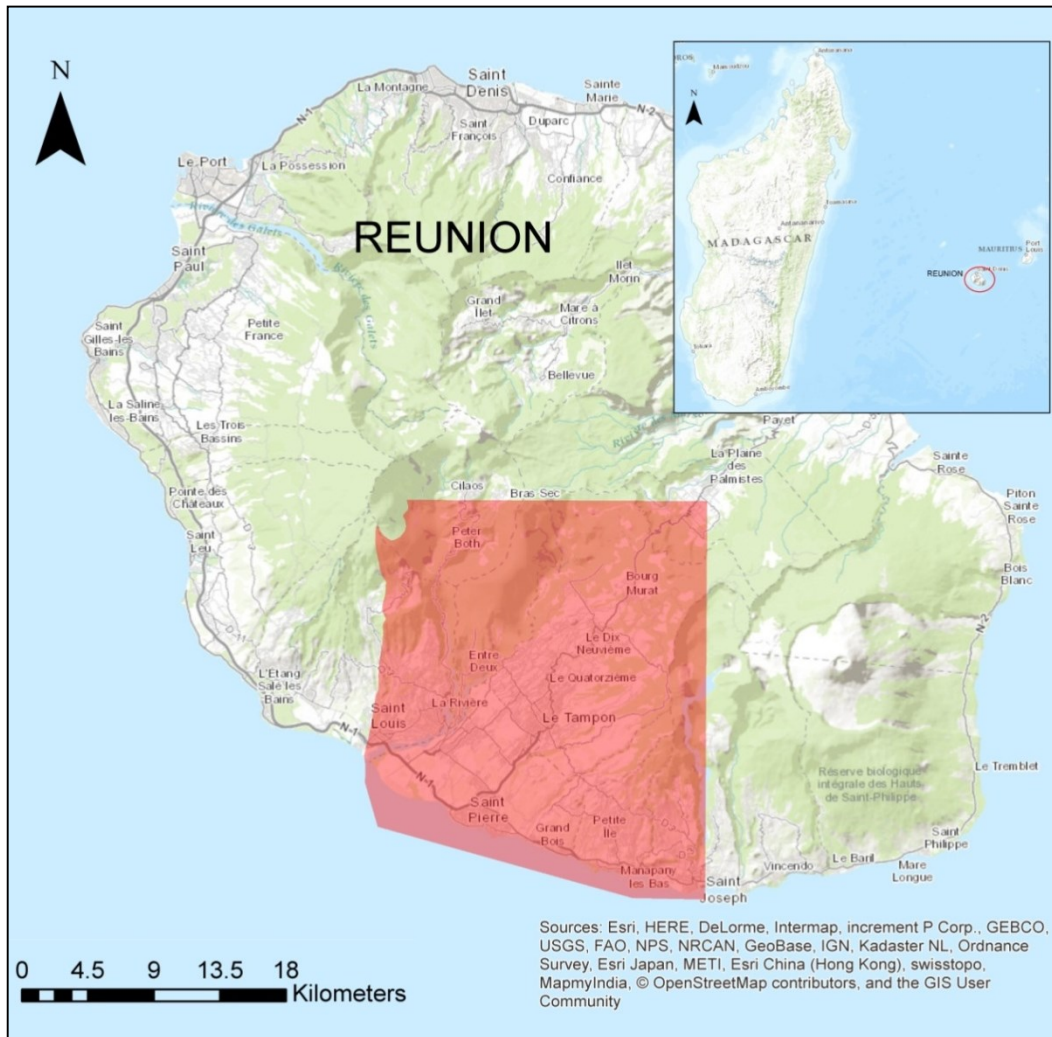
Figure 1.2 The study extent, shaded in red, located on Réunion Island (France) in the South-western Indian Ocean.

Réunion Island is situated in the western Indian Ocean and is approximately 2 500 km² in size (Villeneuve, Bachélery & Kemp 2014). It is located in the tropics and thus has a humid tropical climate. The terrain on Réunion Island comprises mostly rugged mountainous regions in the interior and fertile lowlands running along the coast. The two main seasons are a wet, hot summer from November to March and a cooler, drier winter from April to October.

Rainfall is high (>750 mm) nearly all year round for all areas on the island (Figure 1.3). This tropical climate, coupled with the dense vegetation that is noticeable across nearly the entire island has limited the accurate mapping of the land cover in this area.
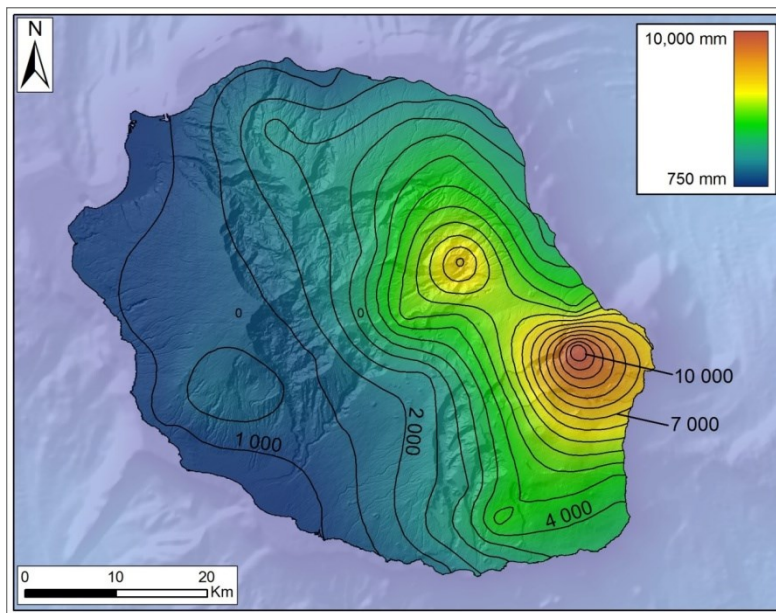
Source: Kemp (2010:27)

Figure 1.3 Mean annual rainfall, with isohyets having a contour interval of 500 mm.

Sixty percent of the cropped area, approximately 26 000 hectares, is planted with sugarcane (Lebourgeas et al. 2010). The sugarcane growth cycle takes about 12-14 months, with harvesting lasting 4-6 months. Harvesting usually begins in the cool season at the beginning of July and spans more than 20 weeks, until the end of November (Lejars & Siegmund 2004). The main difficulties in mapping sugarcane are very high spatio-temporal variability between fields and the long harvesting phase, which is difficult to monitor if gaps in image acquisitions exist (El Hajj et al. 2009).

Another important terrain feature of Réunion are the deep ravines, which are particularly noticeable flanking either side of the study area. The steep gradients of this terrain cause distortion in the radar imagery and makes these areas impossible to map using such data. Rugged terrain resulting in local geometry changes has been noted to affect backscatter values to up to 5 decibels (Loew & Mauser 2007). Thus, Réunion offers a unique and suitable area to assess the benefits of combined SAR-optical data for land cover classification as SAR imagery alone is affected greatly by the terrain and optical imagery is affected greatly by the frequent cloud cover in this tropical region.

1.6   STRUCTURE OF THE THESIS

The rest of the thesis is structured as follows: Chapter 2 presents a review of the literature, provides contextual information for the study, and defines important concepts. Chapter 3 gives detail on the data acquisition and pre-processing methods applied to the imagery. Chapter 4 presents the methods followed to process and evaluate the data, according to the four main experiments. Chapter 5 presents and discusses the study results. Finally, Chapter 6 evaluates the results, draws conclusions, and makes recommendations for future work.

CHAPTER 2 LITERATURE REVIEW

2.1 REMOTE SENSING AND LAND COVER CLASSIFICATION

The field of remote sensing has a long history of image classification (Chen et al. 1996). It is driven by the need for high accuracy maps and, more fundamentally, for the development of conceptual and predictive models for understanding Earth's system processes (Dickinson et al. 2013; Dobson, Pierce & Ulaby 1996).

Knowledge of the spatial distribution of land use and land cover (LULC) is needed to accurately manage land resources (Parihar et al. 2014). This information is used to establish baselines and monitor ongoing change (Evans & Costa 2013). Mapping land cover was originally based on aerial photographs. However, this is expensive, has a small coverage, and is based on interpretation, which leads to problems in repeatability (Evans & Costa 2013). With the recent developments in spatial and spectral characteristics of sensors and improvements in classification algorithms, remotely sensed data are increasingly used to develop LULC maps (Adam et al. 2014).

There are three main factors driving the development in land cover classification using remotely sensed data. First, more data are available from different and complementary sensors and sources today. Second, there has been a shift from traditional statistical approaches to more powerful, flexible machine-learning algorithms for land cover classification. Third, new image segmentation and object-based classification approaches allow data from multiple scales to be processed together, which was not possible with pixel-based classifications. Development has also been bolstered by the increase in computational power, quantity of data, and data complexity available to the widening user base (Waske & Van der Linden 2008).

LULC classification is an important application of remotely sensed data tasks, specifically for PolSAR (Alberga 2007; Lee, Grunes & de Grandi 1999; Pottier & Lee 2000). Urbanisation, population growth, and industrial development drive rapid land use changes. Regional, continental, and global coverage are needed to monitor this change, its sustainability, and the possible adverse environmental effects (Dobson, Pierce & Ulaby 1996). Urbanisation and the impact of human activities and settlements are two of the main causes of global environmental degradation (Ban, Hu & Rangal 2007). By 2008, half of the world's population lived in cities, and this number is growing exponentially. The mapping and monitoring of urban LULC and how they are changing is of great importance (Ban, Hu & Rangal 2007).

Remote sensing provides an ideal platform for gathering empirical data, such as global climate change mapping, to aid decision-makers and support policies that ensure a suitable balance between land

development and environmental protection (Dickinson et al. 2013). Timely LULC information is thus necessary for natural resource and urban planning and management (Parihar et al. 2014).

This literature review introduces some of the elements that should be considered when using remotely sensed data to generate land cover classifications. It also overviews studies that have explored these different elements. The two main kinds of data, optical and SAR imagery, are discussed. Image acquisition considerations, such as data scale and scene selection, are reviewed. The merits of pixel-based and object-based classifications are discussed based on past studies, and the steps of object-based classification are introduced, from pre-processing through image segmentation, to feature selection and the choice of classifier.

2.2   OPTICAL IMAGERY FOR LAND COVER CLASSIFICATION

Optically based remote sensors are passive sensors that generally use the sun's energy to record reflectance from the Earth's surface (Campbell 2006). Images therefore cannot be collected at night or during inclement weather. The data from these sensors have long been used in land cover-based applications. As tried and tested methods coupled with cost effective, high quality optical data are now available, optical data can be effectively used in applications ranging from resource monitoring to urban planning (El Hajj et al. 2009). Optical data from sensors such as Landsat and SPOT can represent the properties of vegetation and crop fields, including retrieving surface characteristics that can be used for crop classification (Guershman et al. 2003; Lebourgeas et al. 2010; Reese et al. 2002; Turker & Arikan 2005). The amount of visible and infrared energy reflected by vegetation is directly related to plant pigmentation, the internal leaf structure, and the leaf and canopy moisture (McNairn et al. 2009). Techniques such as principal component analysis (PCA) can be applied to optical data to select the most useful bands. Hill et al. (2005) used PCA for feature selection to find that the blue band contributed very little towards the mapping of pasture types, and could be discarded in further processing. The use of multi-temporal optical data may significantly improve remotely sensed data applications, especially land cover classifications (El Hajj et al. 2009; Van Niel & McVicar 2004).

A new generation of time series optical sensors, including the SPOT-6 and Landsat 8 satellites, holds potential for detecting and monitoring changes in land cover (El Hajj et al. 2009). The finer spatial resolution provided by these new sensors is particularly useful in urban mapping, where the characteristics of the land cover are often small and very mixed (Lu & Weng 2005). However, missing acquisitions resulting from local weather conditions and uncertain radiometric values due to atmospheric conditions and sensor calibration are problematic for the use of both single-date and multi-temporal optical data (El Hajj et al. 2009). Classification accuracy can be severely affected if even one optical image from an important time in a crop calendar is missing (Blaes, Vanhalle & Defourney 2005; Jewell 1989). Mid-to-

late-season images are essential for accurate crop classification and thus missing acquisitions during key periods can cause major accuracy deficiencies (Shang et al. 2009). El Hajj et al. (2009) documented this issue on Réunion Island, supplementing a SPOT-5 time series with crop growth modelling and expert knowledge as the optical data time series alone was inadequate. Even if images are acquired at every point in the growing season, cloud cover may still render some images unusable, especially in tropical regions. For example, the Global Environmental Facility needed a selection of Landsat imagery collected over five years to create a single cloud-free mosaic of the Brazilian Panatal Wetlands (GEF 2004).

It is important to quantify the potential accuracy gains of using data from the new generation of high spatial and spectral resolution sensors against the additional cost of using this high level imagery. Novack et al. (2011) found that 10 out of 16 classifications achieved higher Kappa values with the inclusion of features derived from the additional bands, Coastal Blue, Yellow, Red Edge, and Near Infrared-2, available from Worldview-2 imagery. All of the classifications also achieved higher overall accuracies when using features from the additional bands, and showed improved distinction of bare soils and ceramic roof tiles (Novack et al. 2011). The newly introduced Red Edge band (705 - 745 nm) also improved classifications and can affect both classification and modelling accuracy (Adam et al. 2014). Adam et al. (2014) used imagery from the RapidEye sensor to map a heterogeneous coastal landscape and found that the overall accuracy dropped by 4.5% when the Red Edge band was omitted.

Some land covers, especially vegetation, can share similar spectral responses for multiple sensor types. Crop separation based solely on spectral signatures can be difficult due to variations in soil properties, fertilisation practices, pest conditions, intercropping, tillage practices, irrigation, and planting dates (Yang, Everitt & Murden 2011). These factors can result in similar reflectance from different crops or even field-to-field variability in the plant reflectance of the same crop and spatial and spectral variability within fields (Yang, Everitt & Murden 2011). Using the short wave infra-red (SWIR) band and taking images during the optimum crop discrimination time can improve reflectance variability issues during classification (Yang, Everitt & Murden 2011). However, crop signatures alter as they grow, due to changes in water content and structure. There is usually an optimum time to map each kind of land cover for optimum discrimination (McNairn et al. 2009). This is the underlying reasoning for using multi-temporal data sets if change analysis is not the focus of a study.

As only the top few millimetres of the vegetation canopy are considered by optical data in vegetation mapping, limited information about the underlying vegetation and soil characteristics can be inferred (Picoli et al. 2013). The effects of solar illumination and the solar azimuth angle must also be considered when interpreting optical imagery (Picoli et al. 2013). Optical data can have significant deficiencies when captured in an area of exposed bright soil, spectrally indeterminate vegetation (a high variability in the spectral signatures within a single vegetation species or class), or in an area with a dead vegetation component that can interfere with the vegetation interpretation (Huang et al. 2010).

Optical imagery can be ineffective for mapping certain urban classes, as some built-up classes generally have similar spectral signatures. As urban areas also display both complex spatial and spectral heterogeneous land cover characteristics, optical imagery alone can be insufficient for classification (Corbane et al. 2008). Accurate repeated mapping of urban areas is an important remote sensing task: these areas are vulnerable due to the complex interactions between infrastructure, humans and the environment and the ever-expanding nature of urban areas (Corbane et al. 2008). Additional information, such as spatial information, should be exploited to accurately differentiate these types of classes (Ban, Hu & Rangal 2007).

2.3   AN OVERVIEW OF SYNTHETIC APERTURE RADAR

SAR has qualities that are advantageous over optical data in remote sensing applications, particularly in target detection mapping and Earth resource management. The key differences between optical and SAR sensors can be found in Table 2.1. SAR sensors provide a wide global perspective with high temporal and spatial coverage (Dickinson et al. 2013). They are sensitive to small changes in surface roughness, slope, and moisture (Deroin, Al-Ganad & Al-Thari 2007), and are illumination-independent, operating both day and night (McCandless & Jackson 2004). SAR is able to capture the large spatial and temporal variability associated with vegetation type, conditions, and soil moisture (McNairn et al. 2000). Most importantly, unlike conventional optical sensors, SAR sensors are unaffected by cloud cover, as they use the microwave region of the electromagnetic spectrum (Dekker 2003).

Table 2.1 Key differences between optical and SAR sensors.

	Optical Multi-spectral	SAR
Platform	Airborne/space borne	Airborne/space borne
Radiation	Reflected or emitted sunlight	Own radiation
Spectrum	Visible/infra-red/thermal	Microwave
Acquisition Time	Day	Day/night
Weather	Blocked by clouds	See through clouds

A SAR image comprises the recorded backscatter response from targets on the Earth's surface. This backscatter is the signal response (Figure 2.1), or return based on the physical and dielectric properties of the ground target. The transmitted signal (Figure 2.1) and received echo can be oriented in specific directions and this is known as polarisation. The signals can be oriented either horizontally (H) or vertically (V). Thus, the HH "band" refers to horizontally transmitted and horizontally received backscatter. SAR has been successfully used in a range of applications, from forest mapping (Karjalainen et al. 2012) to the detection and characterisation of hedgerows (Betbeder et al. 2014). SAR imagery at the

pixel level contains three sets of important information that can be exploited: the radar backscatter intensity, the phase of the backscattered signal, and the range movement based on the time of flight information of the radar pulse (Karjalainen et al. 2012).
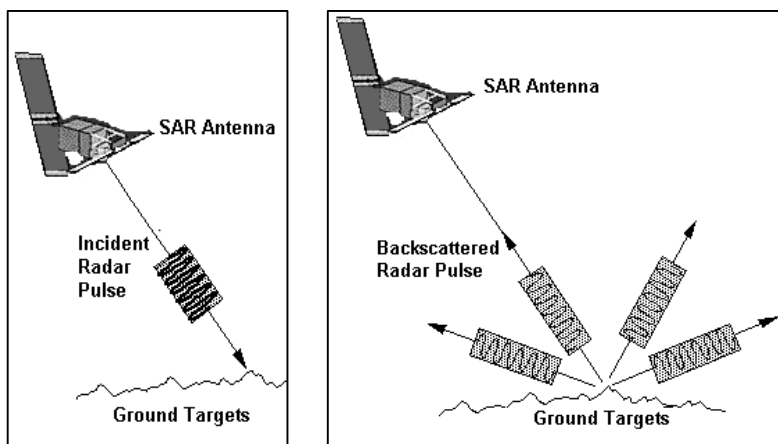
Source: CRISP (2001)

Figure 2.1 (a) Incident ray also known as the transmitted signal, and the resultant (b) backscatter or echo from ground targets.

2.3.1   Factors affecting backscatter in synthetic aperture radar

The backscattered SAR signal is dependent on sensor parameters such as polarisation, incidence angle (Figure 2.2), frequency, and wavelength, and on surface parameters such as topography, surface roughness, and the dielectric properties of the target (Baghdadi et al. 2008).
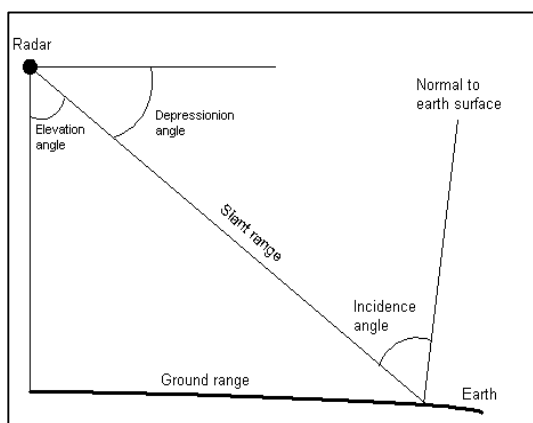
Source: ESA (2014)

Figure 2.2 Geometry of a radar pulse, showing the incidence angle.

The different wavelengths interact with surface roughness in different ways because of their size. Wavelengths will interact with objects of similar or larger size as their wavelength. Ulaby, Moore and Fung (1986) performed a series of experiments to illustrate this phenomenon and a portion of his results

can be seen in Figure 2.3. Figure 2.3 maps the changing backscatter return that the L- (a), C- (b), and X- (c) bands experience depending on the relative surface roughness, soil moisture present and incidence angle. It is important to note that the majority of space radar sensors use an incidence angle of between 20° and 50° thus the right hand portion of each graph is of more importance. The larger the incidence angle (shallow), the lower the backscatter return generally is across all wavelengths. The longest wavelength, the L- band, is most affected by the changing incidence angle and is most sensitive to the change in roughness. The larger the roughness (e.g. 4.1 cm), the higher the backscatter return for all wavelengths. The change in backscatter depending on the roughness is more exaggerated by the longer wavelength (L-band) than the shorter wavelengths (C- and X-bands). Soil moisture also has an important effect on the resulting radar signal strength. As soil moisture increases under wet conditions, the radar signal response generally increases (Baghdadi et al. 2008).
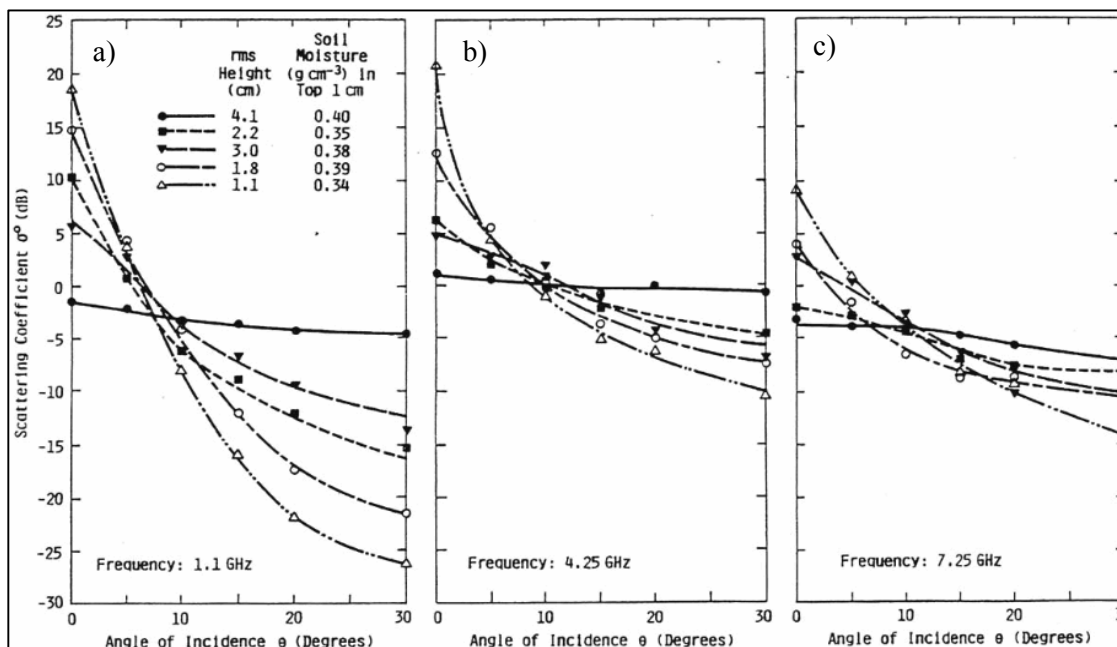
Source: Ulaby, Moore & Fung (1986:1825)

Figure 2.3 The effect of incidence angle and surface roughness have on the backscatter intensity for L-band (a), C- band (b) and X-band (c) SAR.

Due to the complex relationships that exist between the backscatter intensity, frequency, incidence angle, and soil moisture, it can be difficult to determine the optimum scene selections for mapping general land covers. Ulaby & Batlivala (1976) found that like polarisations (HH or VV) at the C-band frequency with small incidence angles (7°-15°) provided the optimum radar parameters for mapping soil moisture, as the sensitivity to surface roughness and soil texture effects were minimised. However, Autret, Bernard and Vidal-Madjar (1989) found that for very small incidence angles, two polarisations, for example the combined HH and VV bands, were necessary to reduce the surface roughness effects.

The intensity of the incident energy scattered by vegetation is primarily a function of the canopy architecture, dielectric properties, and cropping characteristics (McNairn et al. 2009). The canopy architecture has properties such as shape, size, and orientation, which all affect the return signal. Strong signal returns are recorded for buildings due to double bounce off the walls that are perpendicular to the ground. Bare surfaces will have varying returns based on the roughness and, as explained above, the wavelength being used. Water returns very weak signals back to the signal origin, as the incident ray is reflected in all directions.

Both horizontal and vertical surface roughness are dependent on the wavelength and incidence angle of the incoming incident energy. An increase in incidence angle results in an increase in sensitivity to roughness changes and the strength of the radar signal (Baghdadi et al. 2008). Larger (shallower) incidence angles discriminate between rough and smooth areas better than smaller (steep) incidence angles (Baghdadi et al. 2008). Betbeder et al. (2014) used a moderate incidence angle of 37° to map hedgerows as smaller (steeper) angles are more sensitive to ground surfaces, whereas medium to higher angles are more sensitive to vegetation roughness, which is beneficial when mapping vegetation such as hedgerows. When fields appear rough relative to the incident wavelength, multiple scattering is experienced and the response from the HH and VV polarisations are similar (McNairn et al. 2002).

Single-frequency SAR data collected on a single image date can provide limited information for accurate class separability (McNairn & Brisco 2004). Multi-frequency, fully polarimetric data is most useful but is not always accessible or obtainable. The frequency and polarisations of the images used must consequently be carefully selected when designing SAR missions and determining research data requirements (Lee, Grunes & Pottier 2001).

2.3.2   Advantage of phase information

The presence of the phase information inherent in SAR data allows for an array of tools for investigating the geometric properties of the data (Cable et al. 2014). Without the contribution of phase information, the advanced applications of SAR data, including polarimetry and interferometry, cannot be realised. Co-polarised (HH or VV bands) phase information helps to improve discrimination between different targets with the same backscatter intensity, which could otherwise be misclassified (Cable et al. 2014). Phase information can also be used to make polarimetric response plots, which are three-dimensional representations of the transmitted and received polarisations. The peaks and valleys in these plots indicate the minimum and maximum responses respectively (Cable et al. 2014). Co-polarised phase differences make a statistically significant contribution to classification accuracies, especially when mapping crops (Lee, Grunes & Pottier 2001).

2.3.3   Synthetic aperture radar data acquisition considerations

2.3.3.1   Scene selection

There are three major considerations when selecting scenes for a study: seasonality, moisture conditions, and scene overlay (Kellndorfer & Pierce 1998). Seasonality can have a significant impact on the ability to discriminate between land cover types, especially vegetation types. Imagery dated at the peak of the phenological year should be selected when using single-date imagery (Kellndorfer & Pierce 1998). As radar is sensitive to moisture changes in the soil and in vegetation canopies, it is better to choose an image acquired during a relatively dry period. Finally, scene overlap, the section of the scene that is overlapped by multiple images, is particularly important for multi-sensor studies, which should have both time and space overlap (Kellndorfer & Pierce 1998).

2.3.3.2   Wavelength

SAR sensors are available in an array of wavelengths within the microwave region of the electromagnetic spectrum, the most common being the X-, C-, L-, and P-band frequencies (Table 2.2). The use of the microwave region has many advantages for land cover classification applications, such as monitoring vegetation with fast growing cycles, especially with the fine spatial resolution and short revisit times available now with the newer sensors. As a sensor's microwaves reach all parts of a plant, unique information about the size, shape, and orientation of the plant can be derived (Lopez-Sanchez et al. 2014).

Table 2.2 Common frequency bands for SAR sensors, and their frequencies and wavelengths.

Frequency band	Ka	Ku	X	C	S	L	P
Frequency (GHz)	40 - 25	17.6 - 12	12 - 7.5	7.5 - 3.75	3.75 - 2	2 - 1	0.5 - 0.25
Wavelength (cm)	0.75 - 1.2	1.7 - 2.5	2.5 - 4	4 - 8	8 - 15	15 - 30	60 - 120
Example of a sensor	Military Domain	Military Domain	TerraSAR-X-1 COSMO-SkyMed	ERS-1/2 RADARSAT-1/2 ENVISAT ASAR	Almaz-1	JERS-1 SAR ALOS PALSAR	AIRSAR

The X-band uses very short wavelengths and is not suitable for estimating vegetation parameters, as the radar signal does not penetrate deep into the vegetation and is quickly saturated (Baghdadi et al. 2009). However, Baghdadi et al. (2009) found that the X-band differentiated between ploughed fields and

vegetated fields better than the L- and C-bands. The X-band also cannot be used to map surface roughness at useful limits (Baghdadi et al. 2008).

Polarimetric C-band SAR was originally only acquired using airborne sensors, which limited the use and scope of these data (Cable et al. 2014). With the introduction of space-borne sensors such as RADARSAT-2, fully polarimetric C-band data are now more readily available to a larger user community (Cable et al. 2014).

The C-band is generally helpful in discriminating between crop types (Baghdadi et al. 2009) and outperforms the L-band in discriminating between lower biomass crops (Shang et al. 2009). Lower biomass crops with their stable vegetation structures allow for greater penetration through the top canopy. Using a shorter wavelength to visualise these areas, such as the C-band, minimises the soil contribution to the signal response (Shang et al. 2009). However, Lee, Grunes and Pottier (2001) found that the L-band produced better accuracies for mapping crops than the C- and P-bands, as it produced better contrast between the fields. This could have been due to the crop and field type in that study area (Lee, Grunes & Pottier 2001).

C-band data cannot be used to discriminate between roughness classes greater than 1.5 cm (Baghdadi et al. 2008). Baghdadi (2002) recommended using three classes of roughness when taking field measurements and observations: smooth, up to and equal to 1 cm roughness; moderately rough, from between 1 and 2 cm; and greater than 2 cm roughness.

Comparing C- and L- band, Turkar et al. (2012) found that the C- band produced better accuracies for the water and wetlands class, with accuracies of 100% and 95.54%, in comparison with the L-band accuracies of 87.9% and 73.4%. However, the longer wavelength L-band was marginally better (less than 2%) at describing the urban class, with an accuracy of 100%. In the same study, when a Neural Network classifier was used, the C-band was able to discriminate between two slum classes and various built-up classes, with class accuracies over 80%. Prakoso (2003) found that the L-band was better than the C-band at distinguishing between burnt and non-burnt regions of primary forest, showing that the longer wavelength is useful for the denser, larger vegetation found in forests.

When comparing the class performance for the P- and L-bands, Shimoni et al. (2009) found that longer wavelength, specifically the P-band, produced better producer's accuracies for the residential, bare soil, abandoned area and road class. Only the river class achieved a better producer's accuracy (23.9%) in the L-band, and this was only a 2% difference between the two bands. When combining the P- and L-band, all the above-mentioned classes showed an improved user's accuracy and only the residential class suffered a small decrease to 90.3% in the producer's accuracy. The combined frequencies thus defined these urban and bare soil classes far better than the either of the single wavelengths.

The P-band produces better results than the L- and C-bands for forest age classification due to its longer wavelength and higher penetration ability (Lee, Grunes & Pottier 2001). This was supported by Li et al. (2012) who found that the L- and C-band on their own could not accurately separate the detailed forest class. Karjalainen et al. (2012) found that the L- and P-bands could be used to estimate stem volume in forests. Haack and Bechdol (2000) found that L-band SIR-C data produced a slightly better classification than C-band data (88.1% versus 87.8%). However, the two bands differentiated between the vegetation classes equally well, as the area included thick complex canopies that restricted penetration of either wavelength. The L-band has also shown potential in mapping wetland regions with overall accuracies of over 80%, depending on the level of detail included in the classification scheme (Evans & Costa 2013).

Using data from single-frequency sensors can pose limitations for accurate land cover discrimination as they provide limited information. Sensors that also provide polarisation and frequency diversity offer more detailed information about ground targets, resulting in far higher classification accuracies (Shang et al. 2009). However, although multi-frequency and fully polarimetric multi-temporal data are desirable, they are difficult and expensive to acquire and are beyond the scope of many research and operational projects.

The use of multi-channel SAR imagery for classification has interesting applications. A range of input features can be derived from a multi-channel SAR data set, such as radiometric, polarimetric, interferometric, and spatial information. This creates a rich data set with a variety of possible features that can be used in the classification. Borghys et al. (2006) investigated the use of combined P-, L-, C-, and X-band SAR data for the supervised classification mapping of potential areas of minefields. With this aim, they found that using logistic regression and multinomial regression, to combine features from the multi-channel SAR imagery, produced a user's accuracy of 80% for the key land cover class, namely abandoned land (Borghys et al. 2006). In general, the C-band is sensitive to leaves and small branches, the L-band to intermediate branches, and the P-band to trunks and the largest branches in vegetation (Huang et al. 2010). Thus, using a combination of wavelengths can improve the classification accuracy. Adding multi-polarisation SAR data to the combined bands was shown to give an overall accuracy of 95% for a classification with 13 land cover classes (Chen et al. 1996). Turkar et al. (2012) supported this result, finding that the best classification accuracies were achieved when combining X-, C-, and L-band data, in comparison with just using a single wavelength. The best single wavelength classification (L-band) gave an overall accuracy of 89.6%, whereas combining the three bands generated an overall accuracy of 97.4% and 100% class accuracies for both the water and urban classes.

2.3.3.3   Incidence angle

The incidence angle is the angle formed between the radar beam and a line perpendicular to the surface. A greater incidence angle magnifies radar pulse attenuation, reduces single and double scattering (McNairn et al. 2002), and increases volume scattering. At a large incidence angle of 51°, surface moisture does not have a significant correlation with any radar parameter. At a more moderate angle of 30-40°, surface roughness and residue cover contribute significantly to linear polarised radar backscatter (McNairn et al. 2002). A steeper incidence angle results in a more perpendicular signal to the target, which reduces specular reflectance and increases backscatter intensity (Cable et al. 2014).

A change in the incidence angle results in larger differences in the VV and HH band responses than in the other bands. The marsh and water classes have shown larger changes in response to a change in the incidence angle than any other class in a land cover classification. (Cable et al. 2014). At small incidence angles, the HH and VV responses are very similar for areas with little to no residue vegetation cover, whereas at higher incidence angles the responses for HH and VV will differ more, with the H-polarisation penetrating vegetation canopies to a greater extent and providing more information about soil conditions (McNairn & Brisco 2004; McNairn et al. 2002). Rosenthal and Blanchard (1984) suggested that shallower incidence angles improve crop discrimination, as they minimise the soil contribution. Molch (2009) reported on the effects of incidence angle on mapping urban structures by comparing the responses from an HH band with incidence angles of 22° and 40°. The larger angle (40°) was better for the differentiation of urban structures, and specifically for differentiating between urban and vegetation (Molch 2009). However, larger incidence angles result in longer shadows, which can have a detrimental effect on classification results (Molch 2009).

Coulibaly et al. (2012) quantified the effect of the incidence angle on forest classes by comparing RADARSAT-2 images with incidence angles of 26° and 45°. The 45° image produced the best overall accuracy of 79.1%, in comparison with 72.4% from the 26° image, and also produced better forest classes. The 26° image produced better classes for streams and roads. The incidence angle is therefore an important factor to consider when selecting imagery for a specific application.

2.3.3.4   Polarisation

Radar frequency and polarisation are two of the most crucial parameters to be chosen when designing data acquisition and requirements (Lee, Grunes & Pottier 2001). PolSAR imagery discriminates better between different scattering mechanisms than single-polarisation SAR (Lee et al. 2011; Qi et al. 2012). Targets can also be better distinguished by using both the amplitude and phase information (Van Zyl 1989) contained in PolSAR data, allowing for the advance applications of polarimetry and interferometry to be exploited.

PolSAR can transmit and receive both orthogonal components of the electromagnetic wave (Alberga 2007). The extra information provided by the two polarisation states allows the polarisation response of a target to be analysed and the dominant scattering mechanism to be identified (Van Zyl 1989). Li et al. (2012) showed that single polarisations were not able to effectively separate vegetation types.

The benefits of PolSAR data for land cover classification have been quantified: PolSAR frequently results in higher accuracies than single-polarisation SAR (Chen et al. 1996; Da Costa Freitas et al. 2008; Li et al. 2012; Ouarzeddine, Souissi & Belhadj-Aissa 2007). Even for easily mixed classes, such as the low backscatter targets of water, shadow, cement road and bare soil, separability can be improved by using the polarimetric information that can be derived from PolSAR data (Shi 2012). It is however not always possible to attain PolSAR data due to restrictions in project budgets, resolution or area of coverage requirements (Lee, Grunes & Pottier 2001). Lee, Grunes and Pottier (2001) found that if PolSAR data were unavailable, then the combination of HH and VV polarisations was preferable to other combinations of bands.

Each polarisation is most effective for certain land cover type mapping. Vertically oriented waves interact predominantly with the vertical structure of most vegetation, and provide a good contrast between crop types with different vertical canopy structures (Silva et al. 2009; Soria-Ruiz et al. 2007). Differing vertical structures can also be caused by growth stage or health. However, vertically oriented waves experience a lower penetration into the vegetation canopy than HH waves (McNairn et al. 2000). In contrast, horizontally orientated electromagnetic waves penetrate deeper into vegetation canopies and interact better with dense horizontal-leaved canopies. They provide information about the underlying soil condition (Hill et al. 2005; Soria-Ruiz et al. 2007). The steeper the incidence angle, the better the HH wave penetrates the vegetation canopy (McNairn et al. 2000). However, this ability to differentiate crop height does saturate. The backscatter coefficient from HH polarisation has a strong correlation with the Normalised Difference Vegetation Index (NDVI) for the mature and harvesting stages of sugarcane (Baghdadi et al. 2009), which is useful for mapping this land cover. When surface scattering dominates, the VV response is often greater than the HH response (McNairn et al. 2002). The HH band also shows better differentiation for urban areas, as the VV has a reduced ability to differentiate urban areas from vegetation (Molch 2009).

The cross-polarisation channels (HV and VH) show potential for vegetation mapping, particularly for the mapping of sugarcane harvesting (Baghdadi et al. 2009). These channels are related to multiple reflections within the vegetation volume (Silva et al. 2009). They are thus sensitive to crop structure within the total canopy volume. The cross-polarisation bands are particularly good for separating grain crops from other crops (McNairn et al. 2000).

Da Costa Freitas et al. (2008) investigated the use of different combinations of polarisations from airborne P-band SAR data. The HV band was efficient in differentiating forest from other land covers, whereas the

VV band improved the classification of bare soils. They achieved the best overall accuracy using the VV-HV band combination, with the HH band giving little to no contribution. Li et al. (2012) found that if a single polarisation was to be chosen for land cover classification, for their tropical study area, the HH band provided better class separability than the HV band.

The HH band has been found to discriminate between different ice types whereas the cross-polarised channel HV picks up ice edges better (Deroin, Al-Ganad & Al Thari 2007). Both cross-polarised channels, HV and VH, can successfully identify fire scars while VV has been used to identify oil spills (Deroin, Al-Ganad & Al Thari 2007).

Dual-polarised sensors are able to collect HH-VV, HH-VH or VV-HV bands. They generally have wider swaths and greater area coverage than quad-polarised sensors (HH-HV-VH-VV), which is an advantage (Ainsworth, Kelly & Lee 2009). However, the per-pixel information content of data gathered from dual-polarised sensors is vastly inferior to that of quad-polarisations. Quad-polarised sensors are thus favoured over dual-polarised sensors (Ainsworth, Kelly & Lee 2009).

Silva et al. (2009) investigated the effect of using different polarisation bands by performing crop classifications on single polarisations, dual polarisations, and fully polarimetric L-band data. Of the single polarisations, only the HH band was able to distinguish some pasture fields, yielding a Kappa value of only 0.46. Their best dual-polarisation result was achieved with the VV-HH combination, giving a kappa value of 0.74. Due to the HV and VH band often containing similar information, HV is often only used. Using all three polarisation bands (HH, HV, and VV) yielded the best classification, with an overall accuracy of 91% and a kappa value of 0.89. This result is strong evidence for the use of PolSAR data, rather than dual- or single-polarisation data.

Quad-polarised SAR has also been found to be useful in identifying informal settlements (Kleynhans & Salmon 2012). The ability to extract the polarimetric information, and in particular double bounce, from the polarimetric data (HH, VV, and HV bands) allowed for informal settlements along the boundary of the SabiSands game reserve to be delineated (Kleynhans & Salmon 2012).

PolSAR may be useful for retrieving soil moisture measurements with high spatial and temporal resolution, which would be helpful in predicative modelling. However, this potential use has not yet been fully realised as it is not trivial to separate the contributions of soil moisture and surface roughness from the backscatter signal. Inversion techniques can be used to retrieve the surface parameters of soil moisture and surface roughness from PolSAR data (Hajnsek, Pottier & Cloude 2003).

2.3.3.5   Multi-temporal synthetic aperture radar

The use of multi-temporal data enhances land cover applications as it improves class separation. In single-date imagery, if class histograms overlap, separability is poor and confusion between classes with similar response patterns is common. Introducing a multi-temporal aspect to a study allows for explorative data analysis prior to classification, during which the coefficient of variation that shows the overlap between classes can be improved (Erasmi & Twele 2009). In support, Ma et al. (2013) tested combinations of multi-temporal data and found that accuracy increased with more imagery dates. When testing between one and five imagery dates, they obtained the highest accuracy (91%) with all five dates. However, their most significant enhancement in classification accuracy was achieved when moving from a single-date to two dates, with an increase in accuracy of about 20%. Increasing from four to five dates only generated an accuracy increase of 1%. Their results show that studies will have a threshold beyond which the cost of extra imagery will outweigh the accuracy benefits.

Multi-temporal data is particularly useful for classifying various types of vegetation. Imagery from particular times in the growing season allows for greater discrimination between types, due to plant structure, water content, and growth stage (McNairn et al. 2009). Crop yield estimates can be calculated and subsidies controlled by mapping at specific time and growth stages (Mahmoud et al. 2011). Multi-date RADARSAT-1 imagery has been shown to adequately discriminate between major crop types due to these differences at critical times in the growing season (McNairn et al. 2002). Tso and Mather (2010) achieved overall accuracies of more than 75% using multi-temporal ERS-1 data, even though they only used a single polarisation (VV).

Niu and Ban (2013) achieved a Kappa of 0.91 in a land cover classification focusing on detailed mapping of urban areas using a six-date RADARSAT-2 data set. Urban area classification remains challenging, especially when only using SAR data, as the polarimetric properties of urban scatterers are complex and difficult to interpret (Niu & Ban 2013). The multi-temporal classification improved on the single-date Kappa coefficients, which ranged from 0.51 to 0.67 (Niu & Ban 2013). Even the combination of just three of the dates improved the Kappa coefficient to 0.86. In addition to better accuracies, the multi-date imagery improved the object-based segmentation.

2.3.4   Polarimetric decomposition

The polarimetric parameters related to the physical properties of targets are extracted for land classification (Qi et al. 2012) through methods such as polarimetric decomposition (Cloude, Pottier & Boerner 2002). Decompositions are algorithms developed to identify and extract useful information about the individual scattering components of ground targets from SAR data (Cable et al. 2014).

A comprehensive scene can be developed from fully polarised waves. The observed polarimetric signatures of objects are backscattered, recorded, and interpreted as the scattering properties of the objects (Qi et al. 2012). Processing methods such as decompositions separate the received signal into a combination of scattering responses of simple objects (Qi et al. 2012), simplifying physical interpretation so that the corresponding target type of each object in the image can be determined and extracted.

Signal separation requires each target's scattering matrix, from which the targets' physical properties can be inferred (Cloude & Pottier 1996). This matrix is then decomposed into characterised scattering mechanisms for each target. In general, the matrix is composed of four complex variables, S_{HH}, S_{HV}, S_{VH}, and S_{VV} (Equation 2.1), which relate to the scattering component of each polarisation (Wang et al. 2009). The matrix is thus the full description of the ground parameters, which changes the incident electrical signal (E^i) into the scattered electrical signal (E^s).

Equation 2.1

$$\begin{bmatrix} E_H^s \\ E_V^s \end{bmatrix} = \begin{bmatrix} S_{HH} & S_{HV} \\ S_{VH} & S_{VV} \end{bmatrix} \begin{bmatrix} E_H^i \\ E_V^i \end{bmatrix}$$

For ease of operation, this matrix is often restructured as a 3x3 matrix known as the T3 matrix which forms the starting point for most decompositions (Moreira et al. 2013). Decompositions allow the main scattering mechanism to be determined by expressing an average scattering matrix as the sum of independent matrices, all relating to the different scatter types displayed in the particular region of interest (Agashe 2013). There are two types of decompositions, coherent and incoherent decompositions. Coherent decompositions use first-order matrices and are best used to study coherent, or pure, targets, such as man-made objects (Turkar & Rao 2011). They provide detailed information on scattering mechanisms (Cable et al. 2014). Examples of coherent decompositions are the Freeman-Durden (1998) and Cloude-Pottier (1995) decompositions.

Incoherent decompositions were developed to characterise distributed, natural scatterers (Turkar & Rao 2011) and are based on second-order matrices. Examples are the Van Zyl (1989) and Yamaguchi (2005) decompositions. As coherent and incoherent decompositions characterise different land covers best, using a combination of decompositions from both classes can be beneficial. Thus, in this study, a combination of different decomposition parameters were used to train the classifiers.

Helix scattering is a useful added polarimetric parameter introduced by the coherent Krogager decomposition (1988). It is a general scattering mechanism that is seen in urban areas, but almost never appears in natural scattering. The Krogager and Yamaguchi decompositions take advantage of this scattering to separate man-made and natural targets (Turkar & Rao 2011).

Turkar and Rao (2011) compared classifications based on different decomposition algorithms. They found that the Van Zyl incoherent decomposition resulted in the highest classification accuracy. When features from all of the decompositions were combined, volume scattering from the Van Zyl and Freeman-Durden decompositions contributed the most to the overall accuracy. The odd bounce parameters added additional accuracy pay-offs. Similarly, Shi (2012) showed that using entropy and phase standard deviation extracted from X-band polarimetric interferometric SAR data improved the separability of low backscattering targets, with user's accuracies of between 70% and 92.4%, producer's accuracies between 79.5% and 96.2%, and an overall accuracy of 82.8% when classifying roads, water, and bare soil.

2.3.5   Synthetic aperture radar pre-processing

SAR imagery, as with all remotely sensed imagery, requires initial pre-processing steps prior to classification. Pre-processing involves correcting terrain distortions, masking out inherent distortions such as radar layover and shadow, and co-registering multiple image dates to ensure that they overlay correctly. The following section will provide more detail on studies that have investigated the pre-processing steps crucial to preparing SAR imagery for classification.

2.3.5.1   Terrain correction and geocoding

Scenes with hilly or mountainous terrain require a pre-processing step for terrain correction. Rugged terrain, and therefore changing local geometry, results in changes in the local scattering area and in the scattering mechanism as the incidence angle changes. Terrain therefore affects backscatter responses by up to 5 decibels (Loew & Mauser 2007). Relief-induced backscatter changes should be treated as a systematic error and should be compensated for when retrieving surface characteristics. Terrain correction is particularly important when the analysis is focused on multi-temporal data, as systematic terrain distortion must be removed for multiple images to be accurately co-registered (Loew & Mauser 2007).

The side-looking geometry of SAR sensors introduces significant distortions due to height differences in the across track direction. These distortions are corrected by geocoding. In geocoding, the image is reconstructed by finding each pixel's corresponding correct position on the Earth (Loew & Mauser 2007). A forward or backwards geocoding approach can be followed. Forward geocoding uses the Range-Doppler equation to calculate the position of each image pixel on the Earth's surface. Backwards geocoding calculates the image pixel nearest the Range Doppler co-ordinate for each digital elevation model (DEM) element. The Range Doppler algorithm uses a backwards transformation to convert the position of the backscatter elements into slant range image co-ordinates (Badurska 2011). The difference

between the slant range and ground range is explained in Figure 2.4. A truly robust radiometric calibration should incorporate corrections for local incidence angles and antenna pattern distribution effects (Small et al. 1997).
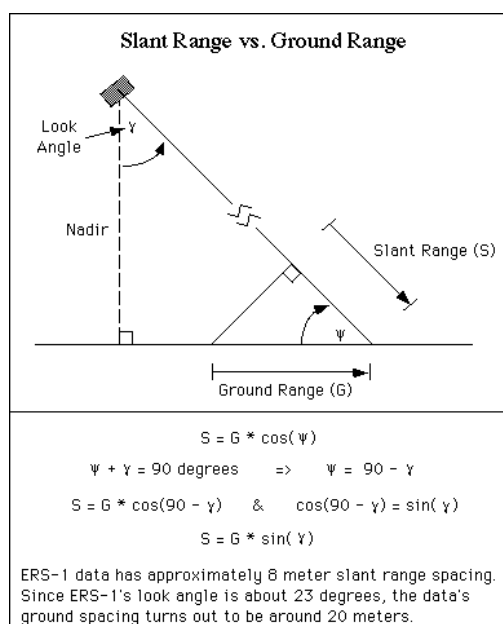
Source: ESA (2014)

Figure 2.4 Difference between the slant range and ground range, with an example based on the sensor ERS-1 to show how the conversion can be done.

Height information is extracted from DEMs and used to geometrically correct each pixel displacement, in a process called orthorectification (Kellndorfer & Pierce 1998). When geocoding SAR data, the range information and georeferencing information from the SAR antenna is combined with the DEM information (Karjalainen et al. 2012) to transform the image into a common reference map geometry (Badurska 2011).

2.3.5.2   Radiometric calibration

Once the accurate description and reconstruction of the SAR imaging geometry is complete (geocoding and terrain correction), the output can be used for more precise radiometric corrections (Loew & Mauser 2007). Geometric correction of SAR imagery transforms the image from ground or slant range geometry to a map reference (Small et al. 1997), whereas radiometric calibration corrects the local incidence angle and the image power replica adjustment (Kellndorfer & Pierce 1998). Radiometric correction removes the terrain-induced distortions that are inherent in radar imagery (Small et al. 1997). Radiometric correction also produces important value-added products that can be used in subsequent processing steps, such as layover and shadow masks.

After radiometric calibration, the average backscattering coefficient over a large number of image pixels should be independent of the local imaging geometry (Loew & Mauser 2007). This backscattering coefficient (called "sigma naught") is a normalised, dimensionless number that expresses the strength of the radar return signal. Although backscattering coefficients tend to decrease as the incidence angle increases, these coefficients tend to be more stable after correction (Loew & Mauser 2007). Calibration has to occur for multiple SAR scenes to be compared.

2.3.5.3   Synthetic aperture radar filtering

SAR imagery is more susceptible to speckle noise than traditional sensors as the images are generated through coherent processing of the scattering signal (Chen et al. 1996). Speckle is a grainy "salt and pepper"-like noise that results from constructive and destructive interference of the pulse by different scatterers (McCandless & Jackson 2004). Speckle filtering has been an area of active research for more than 20 years (Lee et al. 2009).

The high spatial resolution achieved in SAR data has a trade-off with poor radiometric resolution. Speckle causes problems in recognising and distinguishing targets during classification (Wang et al. 2009) and can have a large effect on the accuracy of LULC classifications (Lee et al. 2006). Areas on the ground that should be homogenous are represented with a granular look and a statistical distribution that may be skewed (Durand, Gimonet & Perbos 1987). Speckle degrades both segmentation and classification accuracy (Foucher, Benie & Boucher 2001; Lee, Grunes & de Grandi 1999). It is therefore especially problematic if automatic image segmentation is to be performed on the imagery (Touzi & Lopes 1994). SAR images require a preliminary filtering step to remove speckle (Cloude & Pottier 1996; Ferro-Famil, Pottier & Lee 2001). This filtering is applied prior to information extraction (Lee et al. 2009) and has a positive effect on the accuracy of land cover classifications (Lee et al. 2006). Ban & Wu (2005) compared land cover classifications on five filtered and unfiltered SAR C-band images and found that the overall accuracies improved from just 37.3% to over 70% with the addition of speckle filtering.

The general approaches for filtering are heuristic filtering, statistical adaptive, and wavelet theory (Foucher, Benie & Boucher 2001). Heuristic or "first" filtering techniques were designed for additive noise, so do not correct speckle effectively due to its multiplicative nature (Foucher, Benie & Boucher 2001). Statistical adaptive approaches use optimisation criteria to adapt a filter to the local image information content (Foucher, Benie & Boucher 2001).

As most speckle filtering algorithms are not designed to deal with point target preservation, the resulting targets are severely blurred or suppressed (Lee et al. 2009). In comparison, adaptive filters, such as the min-mean square error filter, are moderately effective in point preservation (Lee et al. 2009). Isolated dark

pixels therefore remain unfiltered due to their very low intensities and resulting very small sigma ranges (Lee et al. 2009).

There are many filters available in open source software packages. The Lee sigma filter (1983) is popular due to its effectiveness and simplicity. It is based on a simple 2-sigma probability that is computationally efficient. However, it produces biased estimates, which result in unfiltered dark spotty pixels. The filter fails to maintain mean values, particularly when there are a number of looks involved (Lee et al. 2009). It can also result in the blurring and depressing of strong reflected targets. The boxcar filter has similar limitations, such as image quality degradation and blurred edges (Lee, Grunes & de Grandi 1999). These deficiencies and the increasing availability of high-resolution, high-dimension SAR data have created a demand for better, more effective speckle filters (Lee et al. 2009).

The refined Lee filter (Lee, Grunes & de Grandi 1999) is an improved version of the original Lee filter (Lee 1981) that offers improved edge preservation. Redundant cells are located within changing neighbourhoods of eight cells, allowing for more accurate filtering of noise (Ju & Molony 1997). It is also available in the free open source software package PolSARPro 4.2 making it a promising option for filtering. This filter effectively preserves polarimetric information and subtle details (Qi et al. 2012).

Lee et al. (1994) suggested five criteria for analysing the performance of a filter and comparing filters:
1. mean value retention in homogenous areas;
2. speckle reduction capability;
3. edge sharpness;
4. thin feature preservation; and
5. point target preservation.

Computational efficiency and the retention of textural information are also important when choosing a filter (Li et al. 2012). When polarimetric information is to be derived, the polarimetric properties must be preserved by filtering each individual term of the covariance matrix by the same amount (Lee, Grunes & de Grandi 1999). Boundary preservation between fields and the mean value retention within fields is particularly important when the study area includes agricultural areas. Although recent literature discusses the need to apply a polarimetric filter, few studies have quantitatively compared the filters that are currently available in open source software such as PolSARPro 4.2. The choice of filter can also be based on the median size of objects, for example the field width. When the size of the moving window is determined using this median object size, boundaries are preserved while object homogeneity is maintained.

2.4   DATA FUSION

2.4.1   Introduction to fusion

As discussed before, single-sensor and single-date data can have limitations, as the information provided may be incomplete, inconsistent, or imprecise (Fatone, Maponi & Zirilli 2001). Reliance on single-sensor image data can introduce a level of risk for operational projects (McNairn et al. 2009). A fusion approach can be used as an effective tool to overcome these limitations. Fusion combines data from different sources to improve the interpretation and potential value of the raw data (Zhang 2010). Research into using different types of sensors for detection and recognition of specific ground targets has been ongoing for many years, driven by factors such as improved coverage and target recognition (Hauter, Chang & Karp 1997). Results from the classifications of fused data are regarded as more reliable, as they are generated by exploiting data with different characteristics (Pohl & Van Genderen 2010). Fusion has been successfully used in a range of applications, including object detection and recognition, classification, change detection, and decision making (Zhang 2010).

Data merging allows the exploitation of bands from different areas of the electromagnetic spectrum (Haack & Bechdol 2000). Using fused data has many benefits over single-sensor data use. Images can be sharpened, as spatial resolutions can be combined, and geometric corrections can be improved (Amarsaikhan et al. 2010). Fusion allows features to be enhanced that are not otherwise visible in a single image (Amarsaikhan et al. 2010). For example, Hu, Tao and Hu (2004) successfully detected and extracted road networks by combining Lidar data with high resolution optical imagery. Missing information can be supplemented and defective data replaced when combining data from different sources, thereby improving applications such as classifications and change detection (Amarsaikhan et al. 2010).

Attempting to fuse multiple data sources is challenging, as the imagery must be accurately co-registered, temporal and spectral variations occur within and between the data sources, and the landscape is often complex (Lu & Weng 2005; Zhang 2010). Finding common ground control points (GCPs) to co-register imagery from different sources can be difficult, as the imagery contains different types of information, for example reflection in optical imagery and backscatter in SAR imagery. Temporal variations due to different image acquisition dates and geometries can cause problems with fusion as discrepancies in the landscape can cause inaccurate co-registering or make interpretation of the fused product difficult.

Fusion can be applied at the pixel, feature, or decision level (Shimoni et al. 2009). Remote sensing applications often use a combination of all three levels. At the pixel level, data from different sources are combined into a single resolution data set. The combined data set is expected to be more informative than the input sources individually, or may reveal changes in multi-temporal data. The spatial resolution of

optical images, for example, can be improved and the structural and textural details are enhanced while preserving the spectral fidelity of the data set (Zhang 2010). Pan-sharpening is a pixel-level fusion approach in which a singular higher resolution optical band is used to improve the rest of the coarser multispectral bands for a single-sensor image. Pixel-level fusion is achieved using component substitution, modulation-based fusion, or multi-resolution analysis-based fusion algorithms.

Feature-level fusion involves extracting features, such as texture, lines, and edges, from different data sources and combining these features into one or more feature maps. Feature maps can be used in further processing steps, such as classification. Feature-level fusion is particularly relevant when considering data sets with too many bands to analyse individually, but it involves precise pixel-to-pixel co-registration. Pixel-level fusion can sometimes result in the deterioration of either the spectral features or backscattering information contained in the original imagery. It is therefore predominantly used when combining optical and SAR, Lidar and optical, optical and GIS, and satellite and aerial data, where deterioration of the original imagery from pixel-based fusion should be avoided to maintain classification accuracies. Combining the classification results produced from different classifiers can be an effective means of fusing these complex data sets. Bayesian formulation is often used to fuse multi-temporal and multi-sensor data for land use classification (Zhang 2010).

Decision-level fusion involves training classifiers with the same data, then combining the outputs (Petrakos & Benediktsson 2001). It allows results from multiple algorithms or processes to be combined for a final fused decision data set. Decision-level fusion can be conducted using soft fusion, which expresses results as confidences, using hard fusion, which expresses results as decisions, or using statistical or fuzzy logic-based methods (Zhang 2010). It has become popular for image classification on remotely sensed imagery as different classifiers may perform better in different regions of a study area (Petrakos & Benediktsson 2001).

Fusion does not only apply to single-date imagery, but can also be applied to multi-temporal, multi-sensor, multi-frequency, multi-polarisation, and multi-resolution data sets (Simone et al. 2002). The literature generally proposes the use of statistical, symbolic, or neural network fusion methods for multi-temporal and multi-sensor data (Simone et al. 2002).

2.4.2   Fusing optical and synthetic aperture radar data

Fusing optical and SAR data exploits the benefits of each and allows data from different parts of the electromagnetic spectrum to be exploited in a complementary manner (Ban, Hu & Rangal 2007). As each sensor type discerns certain land cover types better than the other, a more robust, accurate classification can be obtained. Improvements are thus seen in classification accuracies when dual-sensor imagery is used

(Blaes, Vanhalle & Defourney 2005). SAR data can also fill gaps caused in multi-temporal optical image acquisitions due to cloudy or hazy days (Ban, Hu & Rangal 2007). Radar imagery alone does not delineate urban areas very well, whereas optical data struggles to discern natural vegetation. For example, Haack and Bechdol (2000) found an urban class accuracy of only 38.9% using SAR data and a vegetation class accuracy of 66.9% using optical data. Combining data sets corrects the misclassifications and poorly separated classes of single data sets (Hill et al. 2005).

Ban, Hu and Rangal (2007) successfully used decision-level fusion by vectorising a RADARSAT classification into a thematic map and fusing it with a Quickbird (optical) classification. A new level of segmentation was then performed based on the thematic layer, creating a link between the SAR and optical results. The fusion increased the classification accuracy of the vegetation classes by 17-25% and the low-density building class accuracies by 3.9% and 3.6%, respectively. The overall accuracy of the 16-class classification increased from 87.9 to 89.5% and the kappa value increased from 0.868 to 0.885. In agreement with these results, McNairn et al. (2009) found that target overall accuracies of 85% could not be achieved using individual optical or SAR images, but could be achieved when the two data sets were combined. Similarly, Laurin et al. (2013) found that using optical data produced a maximum overall accuracy of 80.4% and using SAR data, 49.9%. When they used texture variables and fused the data sets, they achieved an overall accuracy of 85.7% with a maximum likelihood classifier and an accuracy of 95.6% with a neural network classifier.

Michelson, Liljeberg & Pilesjo (2000) also found fusion of SAR and optical data to be beneficial for vegetation mapping, specifically for forest and agricultural land cover classes. The percentage of totally separable class pairs was increased from just 17.5% with optical data only and 48.3% with SAR data only to 63.3% with the combined data. Furthermore, the overall accuracies for the classifications were improved in all three instances using different classifiers, showing that the benefits of fusion are not limited to certain cases (Michelson, Liljeberg & Pilesjo 2000)

Urban mapping continues to be a challenging task as it is a highly heterogeneous and complex land cover type (Lu & Weng 2005). However, it remains an important application for monitoring the loss of both natural and agricultural land to urban centres (Pacifici et al. 2008). SAR alone can struggle to delineate these areas due to confusion with rough or wet bare soils, as these areas all have strong radar return signals and thus appear bright in the image (Corbane et al. 2008). Corbane et al. (2008) assessed urban mapping using combined SAR/optical data (RADARSAT-1 and SPOT-4) against single-sensor performance using texture features and a fuzzy classification approach. Information fusion was conducted, allowing for improved precision and accuracy, and the use of flexible fuzzy approaches. The automatic delineation of urban areas was tested and the combined data set resulted in a more precise delineation of the urban area and less false positives. Using just SAR imagery of the same area resulted in an underestimation of urban expanse of nearly 16.1 km², whereas the optical-only imagery led to an overestimate of nearly 13 km².

Work done by Pacifici et al. (2008) supports this result; they achieved a kappa value of 0.9393 for a classification based on combined SAR-optical data using a neural network classifier. They attributed their result to the C-band SAR data providing additional scattering information to the optical data, which improved the separation of the closely situated vegetation and water, which had low returns, from the buildings and roads, which exhibited high returns (Pacifici et al. 2008).

Zhu et al. (2012) provides further evidence of the benefits of combined SAR and optical data for urban land cover mapping. Their classification included 17 land cover classes and compared classifications on multi-temporal Landsat ETM+ and L-band PALSAR data, alone and combined. Their best SAR classification had an overall accuracy of 72.2% and their best optical classification, based on three seasons, had an overall accuracy of 93.8% (Zhu et al. 2012). The magnitude of the optical classification limited the possible increase of the combined classification. However, a statistically significant increase of 1.1% was achieved, predominantly from three urban classes (Zhu et al. 2012).

Combined high resolution SAR and optical data was further proved to be successful in classifying urban areas, particularly in delineating built-up areas and roads, with an overall accuracy for urban classification of 91% (Amarsaikhan et al. 2010). Similarly, Huang, Legarsky and Othman (2007) achieved class accuracies of over 72% for density-building classes, forest, open ground, and water using combined RADARSAT-1 and Landsat-7 ETM+ data.

Combined optical and SAR data have also been successfully used for vegetation mapping. Crop classifications have been reported to have improved by 20-25% when radar and very high resolution optical sensors are combined (Brisco, Brown & Manore 1989; Rosenthal & Blanchard 1984). It also shows potential in wetland monitoring (Li & Chen 2005). Landsat-7 ETM+ data were used with RADARSAT-1 data and a DEM to produce accuracies ranging from 71% to 92% for wetland classification at three sites, in comparison with accuracies of 24% to 89% produced from single-sensor classifications (Li & Chen 2005). Hill et al. (2005) used decision-level fusion, in which classifications from AirSAR and Landsat TM data were combined to improve the mapping of pasture types in Australia. Moghaddam, Dungan and Acker (2002) saw improvements in foliage mass classification, with the root mean square error improving by a factor of two with combined SAR-optical data over just using optical data.

Fusion can also be performed on independent classifications based on different data types. For example, classifications can be performed independently on optical and SAR data, then combined to exploit the "greenness," brightness, and bareness information contained in the optical classification and the height, structure, and water content information in the SAR classification (Hill et al. 2005).

Although the general trend in land cover classifications using optical and radar fusion is to use only the backscatter values extracted from the radar imagery in combination with the optical bands (Laurin et al. 2013), other approaches are also possible. Digital number values can be extracted from multiple optical and radar bands for each land cover type to test the separability through statistical measures, such as the mean and standard deviation of each potential class. Sheroan and Haak (2013) successfully used this method on PALSAR L-band data for crop-type mapping. Polarimetric information can also be extracted and added to the fused data set. This approach is investigated in this study.

2.5   IMAGE CLASSIFICATION

Classification involves the assignment of regions on an image to a real-world "class" (Campbell 2006). Commonly, as in the case of this study, these are land cover classes and refer to real-world ground covers that exist in the study area. Classification is performed on pre-processed, prepared imagery and can be done using an array of approaches, classifiers, and considerations.

2.5.1   Object-based vs. pixel-based classification

In pixel-based classification, each individual pixel is classified as a particular land cover type. Although innovative per-pixel classification approaches for improved accuracy continue to be popular, they suffer from spectral confusion and mixed pixels (Bhaskaran, Paramananda & Ramnarayan 2010). Per-pixel approaches also have limited ability to accurately represent real-world, complex, individual land forms and non-uniform surfaces (Saha, Wells & Munro-Stasiuk 2011). This has particularly become a problem with the new generation of high resolution sensors, such as Worldview and Ikonos. As a result, there has been a paradigm shift from the per-pixel approach to the object-oriented approach.

In object-based classification, pixels are first grouped together into "objects" in a process called segmentation. These objects are then each classified as a particular land cover type. The idea behind representing images through objects is based on mimicking the human brain's ability to recognise and interpret images as distinct regions (Devereux, Amable & Posada 2004). An "object" refers to a group of neighbouring pixels that have been grouped together based on some homogenous characteristics, such as their spectral values. The popularity of object-based approaches has increased due to developments in ecology and the understanding that landscapes inherently embody patchworks of land cover that can be better represented by homogenous objects than by individual pixels (Devereux, Amable & Posada 2004). It is believed that object-based approaches result in a more robust, flexible analysis of landforms and a better representation of the inherent patterns in, and mutual relationships between, the objects (Gamanya, De Maeyer & De Dapper 2007; Saha, Wells & Munro-Stasiuk 2011). There is thus a demand for land

cover object outlines for large areas and object-based classifications remain an important research focus (Devereux, Amable & Posada 2004).

Object-based classification is more appropriate for applications in which the study area has inherent object features, such as the inherent parcel structure of fields in agricultural areas (Mahmoud et al. 2011). For example, a field-based land cover classification using 3 m resolution TerraSAR-X data, texture features, and an object-based approach resulted in a 95.5% overall accuracy (Mahmoud et al. 2011). However, the underlying segmentation should not be based heavily on field boundaries in these applications, as this continues the dependence on digitised layers, produced through manual editing, and not on potentially automated, and therefore more efficient, methodologies.

The two main driving forces behind the growth in object-oriented classifications are the vast quantities of remotely sensed data now available from a multitude of satellite sensors and the increase in the power of geographic information systems (GIS), in particular their computational power and the complexity of the available software and algorithms used to analyse and process image data (Devereux, Amable & Posada 2004). With the popularity and power of object-based classification increasing, it is important for research to focus on producing generalised, standardised image analysis approaches (Gamanya, De Maeyer & De Dapper 2007).

Object-based and pixel-based approaches to classification primarily differ in their classification units and in the features used to separate classes (Liu & Xia 2010). The segmented objects used in the object-based approach reduce the salt-and-pepper effect and spectral variability within classes, but can also result in under- or over-segmentation (Liu & Xia 2010). Pixel-based classifications can be limited as they cannot make use of spatial information (Mas, Gao & Pacheco 2010), whereas object-based classifications characterise objects using a wide variety of features, including spatial, spectral and textural features (Liu & Xi 2010). Relationships between objects can also be exploited (Im, Jensen & Tullis 2014). However, geographic object-based image analysis (GEOBIA) is more likely to be affected by increased data dimensionality, due to the larger number of features and small training sets used to train its statistical classifiers (Myburgh & Van Niekerk 2014).

Object-based approaches are particularly important for applications based in predominantly agricultural areas, such as the study area, as they display typical spatial patterns (Waske & Van der Linden 2008). These inherent patterns can be exploited to improve classifications. The segmentation used to produce objects can also level out the internal variance in spectral reflectance and the backscatter intensity within objects belonging to the same class, caused by differences in soil moisture and plant interactions (Waske & Van der Linden 2008). This helps to reduce the effect of speckle inherent in radar imagery and to decompose the image into piecewise smooth regions (Fatone, Maponi & Zirilli 2001; Qui et al. 2012). In

change analysis applications, pixel-based approaches are over-sensitive to noise and therefore lack the spatial consistency needed for accurate change detection (Im, Jensen & Tullis 2014).

2.5.2   Segmentation

Segmentation is the process of dividing an image into non-overlapping, discrete objects that each represent a homogenous zone on the ground (Devereux, Amable & Posada 2004). It is the first and one of the most important steps in an object-oriented classification as the quality of the classification is directly dependent on the quality of the objects (Gamanya, De Maeyer & De Dapper 2007). The aim of segmentation is to ensure local homogeneity within objects, while still representing the global heterogeneity within the image (Su et al. 2008). Segmentation can be based on either very basic parameters, such as spectral contrast, or can take into account a variety of contributing factors (Devereux, Amable & Posada 2004). A scale factor is used to determine the size of the objects and is set based on the heterogeneity evident in the landscape (Gamanya, De Maeyer & De Dapper 2007). Colour and shape factors can also be weighted, depending on the type of land cover classification being performed, to produce objects that best represent the real world land targets (Su et al. 2008).

Segmentation algorithms are classified as region-growing/merging, boundary detecting, or a combination of both (Stuckens, Coppin & Bauer 2000). Multi-resolution segmentation (MRS) is a region-merging, bottom-up technique (Gamanya, De Maeyer & De Dapper 2007). It begins with single-pixel objects and merges them with neighbouring pixels to form objects, based on the neighbouring pixels' characteristics and heterogeneity within user-defined thresholds (Gamanya, De Maeyer & De Dapper 2007). It is a local optimisation procedure: it considers each step in the growth process against the defined threshold. If the threshold is exceeded, the process stops. It then starts with the next single-pixel starting object (Gamanya, De Maeyer & De Dapper 2007). The scale factor determines the maximum change in total heterogeneity allowed when merging pixels into an object (Dragut & Blaschke 2006). It is important to note that there is no general "ideal" segmentation, especially as the "scale" factor in eCognition is unitless and difficult to directly relate to spatial relationships (Hay et al. 2005). Trial and error is usually needed, thus making this step difficult to optimise (Taubenböck, Esch & Roth 2006). Although MRS generates meaningful objects, it is computational intensive and can be unsuitable for large data sets (Li et al. 2014).

Other segmentation algorithms available include multi-threshold segmentation, chessboard segmentation, and quadtree segmentation. Multi-threshold segmentation splits objects with spectrally high contrast, but does not take the shape of the object into consideration and needs training (Li et al. 2014). Chessboard segmentation is fast and produces regular square objects, but does not take into account the spectral values of the objects and does not produce meaningful objects (Li et al. 2014). Similarly, quadtree segmentation produces square objects of varying sizes.

Li et al. (2014) used a combination of the MRS, chessboard, quad tree, and multi-threshold algorithms in an object-based classification. Although the chessboard and quadtree segmentations are quite rudimentary, they can be useful for creating different hierarchical levels of segmentation. By using all four of these segmentation types together, at varying scales, a good balance was found between computation time and accuracy (Li et al. 2014). An overall accuracy of 91.9% and Kappa of 0.9 was achieved for a 10-class land cover classification (Li et al. 2014). This was nearly a 20% accuracy improvement on a pixel-based classification run on the same imagery. These results show the importance of well-segmented image data for a successful classification.

In agreement with the idea behind using multiple segmentations together, Martha et al. (2011) used the MRS and chessboard segmentations together to delineate landslide object boundaries. The MRS was used first, then the objects were refined and merged using chessboard segmentation. The resulting classification had a 76.4% recognition accuracy for landslides (Martha et al. 2011). The same combination of segmentation algorithms was used by Su et al. (2009) for mapping general land cover using SPOT-5 imagery, obtaining a final overall accuracy of 86.5% and kappa of 0.79.

Hay et al. (2005) designed and implemented a multi-scale segmentation routine to segment meaningful forest-objects at various scales. This approach provided an overview of the dominant structures found in the scene based on the scene components. Although successful, this method was constrained to high resolution imagery and was designed specifically for forest mapping (Hay et al. 2005).

Meinel and Neubert (2004) presented an approach to assess the quality of segmentations and tested it on various segmentation-producing software. Algorithms tested included eCognition 2.1 and 3.0, Data Dissecting Tools, CAESAR 3.1, InfoPACK, Minimum Entropy Approach SPRING 4.0, and the ERDAS Imagine extension for segmentation. Even though outdated versions were used, the eCognition segmentations were deemed the best overall, based on characteristics such as conformity of objects and average difference to the reference areas' perimeters, area, and shape index (Meinel & Neubert 2004).

Over-segmentation occurs when a semantic object is divided into multiple smaller objects, whereas under-segmentation occurs when a single object contains multiple different semantic objects (Liu & Xia 2010). If features are extracted from mis-segmented objects, either due to under- or over-segmentation, they will not represent the properties of the real ground objects. Both under- and over-segmentation can negatively affect the resulting classification. In over-segmentation, however, each object can still belong to a single class. Although too many objects are produced, it is still possible to obtain an accuracy of 100% (Liu & Xia 2010). In contrast, under-segmentation results in objects that contain multiple classes. It therefore introduces classification errors and makes it impossible to achieve 100% classification accuracy (Liu & Xia 2010). Over-segmentation has less of an effect if a subsequent classification will be performed, as the

classifier will merge parcels of the same land cover type to create more generalised products. In contrast, it is impossible for a classifier to split the segments in an under-segmented image (Devereux, Amable & Posada 2004).

The trade-off between accuracy and cost must be considered in light of the requirements of a particular study when choosing the segmentation scale. Using a very fine scale may result in over-segmentation, which can be computationally and resource-expensive, but will result in high accuracy. Processing with less units is more time- and cost-efficient, but is less accurate (Im, Jensen & Tullis 2014).

2.5.3   Feature selection

One of the strengths of object-based classification is that it incorporates the elements that are traditionally used in aerial photograph interpretation, including shape and size. These elements, or features are characteristics that can be derived for an object. They can include the mean spectral value for a specific band for all pixels within that object, a shape characteristic relating to the geometry of the object, or a derived index using band combinations. Features can also be derived from the decompositions of radar imagery, such as the Pauli, Freeman-Durden, Krogager, and H/A/alpha (Cloude-Pottier) decompositions (Chen, Chen & Lee 2003).

This strength is, however, one of the biggest challenges of the object-based approach as the availability of hundreds of spectral, spatial, and contextual features means that data dimensionality can be exceptionally high (Gao et al. 2011; Laliberte, Browning & Rango 2012). This "curse of dimensionality" can result in over-trained classification algorithms, resulting in poor models, poor representations of real-world phenomena, and low classification accuracies. It can therefore be beneficial to only use a subset of features in processing steps such as training classification algorithms. There are numerous ways in which to select these subsets of features. Although user knowledge and past experience can often be some of the main informers of feature selection, they are not always a viable solution (Duro, Franklin & Dube 2012). A commonly used method is PCA which has been discussed extensively in literature and has been successfully applied to many types of remote sensing data (Byrne, Crapper & Mayo 1980; Celik 2009; Li & Yeh 1998; Liu et al. 2003; Townsend, Justice & Kalb 1987; Yonghong 1998).

An alternative to using PCA is to generate rankings of important features for class separation that can inform feature selection and reduction and can be optimised to promote accurate class representations (Laliberte, Browning & Rango 2012). Feature selection is one of the main difficulties in an object-based approach and has received attention in literature (Amarsaikhan et al. 2010; Qi et al. 2012). Feature selection depends on the type of imagery used, the land cover depicted, and the specific output required. It

is therefore difficult to specify a definitive set of features that is applicable to every application. In general, statistical, textural, spatial, and shape-based indicators can be used.

Feature selection algorithms can be assessed based on their efficiency and ease of use, ability to rank and reduce features, and the resultant classification accuracies (Laliberte, Browning & Rango 2012). Many feature selection algorithms have been proposed. A selection of the most common algorithms are presented below.

2.5.3.1   Classification tree analysis

Classification tree analysis (CTA) is non-parametric, fast, and powerful in reducing and ranking features. It can obtain features or specific rules, depending on the user selection. It does not, however, provide class separation distances and can over-fit the decision tree (Laliberte, Browning & Rango 2012). Over-fitting occurs when the parameters fed into an algorithm are too complex or large, and the resultant model describes noise and exaggerates small fluctuations in the data rather than showing general trends. CTA is most useful for applications that have many classes and/or features or that do not need separation distances. It is also useful with data that have non-normal distributions.

Laliberte, Browning and Rango (2012) found that CTA produced better accuracies than feature space optimisation or the Jeffreys-Mutusita distance on sub-decimetre resolution L-band SAR imagery. CTA has been shown to be an effective way to select important features and has been applied successfully within a GEOBIA environment (Chubey, Franklin & Wulder 2006; Laliberte et al. 2007; Yu et al. 2006).

2.5.3.2   Separability and thresholds algorithm

The separability and thresholds algorithm (SEaTH) automatically identifies the relevant features with a purely statistical approach using training samples. It identifies the features that best separate a class pair, then identifies the separation threshold for each feature (Gao et al. 2011). SEaTH uses the Jeffreys-Mutusita distance to measure object separability. It outputs the Jeffreys-Mutusita distances and rules, which makes its output compatible with eCognition software. However, it involves multiple steps, making it less efficient and user friendly. It assumes data normality and performs no initial feature reduction (Laliberte, Browning & Rango 2012).

SEaTH is useful for applications that require separation distances or that have a limited number of classes and features. Gao et al. (2011) found that SEATH outperformed the Nearest Neighbour and Maximum Likelihood classifiers with overall accuracies of 79% versus 66% and 69%, respectively. As with other feature selection methods, it is important to use the first few features that provide the maximum

separability between classes in SEaTH. To maintain method transferability, the minimum number of features possible should be used (Nussbaum, Niemeyer & Cantry 2006). If too many features are used to separate each class pair, there is a risk of introducing features that are only applicable to local conditions.

2.5.3.3   Feature space optimisation

Feature space optimisation is faster than other feature selection methods, especially when used with texture measures. It provides separation distances and can be used for feature reduction with eCognition. It is, however, a black box approach and gives unclear feature ranking without rules. It is most applicable for applications that require feature reduction for neural network classifications (Laliberte, Browning & Rango 2012).

2.5.3.4   Random forest algorithm

The random forest (RF) classifier has the capability to assess and rank features by importance (Rodriguez-Galiano et al. 2012). This is particularly useful for multi-source studies with high data volumes. Importance rankings can be used to select the most useful features for training a classifier. The RF feature selection ranks features by systematically switching a random input variable while keeping the rest consistent. It then considers how the classification accuracy changes with this variable input alteration and uses this to rank the features by importance (Rodriguez-Galiano et al. 2012).

2.5.4   Use of texture in classifications

There exists a variety of features that can be used to train classification algorithms. These include layer values such as the mean or standard deviation for a particular satellite image band as well as derived indices such as NDVI. Furthermore, geometric properties of the actual objects can be assessed. Texture measures have been highlighted in literature as being particularly useful in object-based classifications and especially fusion classifications (Amarsaikhan et al. 2010; Chan, Laporte & Defries 2003; Haack & Bechdol 2000; Herold, Haack & Solomon 2004; Laurin et al. 2013; Nyoungui, Tonye & Akono 2002; Sheroan & Haak 2013).

Texture is a measure of the variation in the reflection intensity of a surface and provides important information about the arrangement of objects and their spatial relationships (Rodriguez-Galiano et al. 2011). It quantifies properties such as smoothness, coarseness, and regularity (Zhang 2010). Texture analysis allows the spatial relationship between neighbouring pixels to be explored within a defined window size, which provides descriptors to separate spectrally similar land cover classes (Chan, Laporte

& Defries 2003). Texture has been shown to improve class separability in land cover classifications, thereby improving mapping accuracy (Berberoglu et al. 2007; Lloyd et al. 2004). It provides useful additional information that can be combined with backscatter information from SAR imagery (Schistad Solberg & Jain 1997). As texture measures vary with the relative depression angle, incidence angle, look direction, and acquisition date, they are a complex addition to a classification (Herold, Haack & Solomon 2004).

The addition of texture measures does, however, considerably increase the data dimensionality of a classification (Rodriguez-Galiano et al. 2011). Often, this increase in data size, and specifically an increased number of features, exceeds the ability of most classifiers (Rodriguez-Galiano et al. 2011). Thus, the classifier must be carefully chosen when using large data sets, such as in this study.

2.5.4.1   Texture measures

Texture analysis can be performed on different orders of statistics. First-order statistics are the simplest and generally result in poor class discrimination (Munoz 2013). They include measurements such as mean, variance, and average energy, and give information about the distribution of grey levels in an image. Second- and third-order derived texture variables are generally considered best for applications such as land cover classification (Nyoungui, Tonye & Akono 2002). Second-order statistics operate on a probability function, also known as a co-occurrence matrix (Munoz 2013). These statistics give the probability that a pair of pixel values will occur some vector apart.

The grey level co-occurrence matrix (GLCM) is one of the most popular textural features (Su et al. 2008). Co-occurrence texture features are based on grey-level spatial dependencies (Haralick, Shanmugam & Dinstein 1973). The computed co-occurrence matrix contains the relative frequencies of all pair-wise combinations of backscatter values, computed at a given distance and direction within a local moving window (Schistad, Solberg & Jain 1997). It can be used to derive a variety of texture measures, such as the second angular moment, contrast, entropy, dissimilarity, mean, and homogeneity. The homogeneity and second angular moment indices describe homogeneity within the objects, whereas the contrast and entropy indices indicate heterogeneity (Su et al. 2008). Correlation measures the grey level linear dependence between specified pixels (Albregsten 2008).

The grey level difference vector (GLDV) counts the occurrence of the absolute difference between a reference pixel and its neighbours (Chan, Laporte & Defries 2003). It is derived from the GLCM and provides additional texture values from those derived solely from the GLCM.

2.5.4.2   Impact of texture measures on classification accuracy

The use of radiometric data alone for a classification is often not sufficient and the addition of textural measures that use inherent spatial information can improve classification accuracy (Li et al. 2012). Texture measures improve class separability by decreasing the coefficient of variation between classes (Erasmi & Twele 2009). Li et al. (2012) found that adding even one texture measure to L- and C-band data provided a better classification and that using all available radiometric and textural images resulted in a 6.6% increase in overall accuracy.

Textural information distinguishes between easily confused classes such as lawn and water (Qi et al. 2012). Herold et al. (2004) included texture variables in a classification on a single wavelength (HH) C-band RADARSAT image, which improved both the overall accuracy and the accuracy of the urban and forest classes. They found that major misclassifications existed between tea plantations and other agricultural areas when only texture was used, but that combining texture and the HH band improved the producer's accuracy of the tea plantation class and general agriculture class by 6% and 1%, respectively (Herold et al. 2004). Combining the textural information with L-band SAR increased the producer's accuracy by 28% and 3% for the water and urban classes, respectively (Herold et al. 2004). These results illustrate the potential that texture variables hold for improved land cover classifications, especially for traditionally confused classes.

Ban and Wu (2005) found that the addition of the mean, standard deviation and correlation texture measures improved overall accuracies from just more than 70%, based only on five C-band SAR images, to 89.7%, with a kappa value of 0.9. All of the land cover classes, ranging from urban classes to water and forest, showed producer's accuracies of 74% and above, as well as user's accuracies of 84% and above (Ban & Wu 2005).

Although recent studies have investigated the use of texture variables to improve classifications, it is still unclear which texture measures are useful for improving the separability of vegetation types, especially in tropical moist regions (Li et al. 2012). Vegetation, particularly tropical vegetation, has complex structures and species compositions. Difficulties also arise from texture variations in the landscape, selecting the size of the moving window, and from the image itself (Li et al. 2012). Choosing the texture images to include in a classification can be difficult. Li et al. (2012) suggested identifying potential combinations using a separability analysis, then choosing the best combinations according to the standard deviation and correlation coefficients.

Texture also has been successfully used in other applications. Kuplich, Curran and Atkinson (2005) found that the correlation between backscatter and biomass increased from 0.7 to 0.8 when the GLCM contrast texture measure was added to SAR data and showed the potential of SAR and texture to produce biomass

evaluations of tropical forests. Chan, Laporte and Defries (2003) saw similar benefits with forest mapping using optical data and texture: the addition of textural measures increased the accuracy of the logged forest class by 36%. However a, trade-off was seen in the accuracies of the other classes and the class accuracy of logged forests remained low at 46.7%.

Addition of texture is especially useful for the characterisation of urban areas as they are described by their structure more than by their reflectance or backscatter alone (Corbane et al. 2008). Su et al. (2009) found that adding GLCM textural measures to spectral imagery improved overall classification results for the city centre of Kuala Lumpur from 81.6% and a kappa of 0.8 to 87.3% and a kappa of 0.8.

The above-mentioned literature shows that texture can have a positive effect, as it leads to accuracy gains and improves classifications over a range of land cover types. It is thus an important addition to the feature set derived from the data set in this study.

2.5.5   Classification algorithms

Once the image objects have been created and features have been selected, a classifier is used to group objects into land cover types based on their feature values. Data requirements, the availability and sensitivity of training data, and computational and operational requirements must all be considered when selecting a classifier (Shang et al. 2009). Automated, efficient methodologies are required to deal with the increasing volume of data available (Chan, Laporte & Defries 2003). Unsupervised classifiers classify pixels into classes based on their reflectance values and require no prior training. They can, however, cause naturally occurring clusters within the image data to drift away from the class centres, resulting in misclassifications (Lee, Grunes & Pottier 2001). More advanced supervised and machine learning algorithms have therefore become popular as they are generally able to handle large volumes of complex data and train quickly and efficiently (Chan, Laporte & Defries 2003; Rodrigeuz-Galiano et al. 2012). These algorithms do not assume normal data distribution and generally produce higher accuracies than unsupervised classifiers (Rodriguez-Galiano et al. 2012).

Supervised learning approaches are generally better than unsupervised approaches as they incorporate prior knowledge into the classification process. However, they require labelled training data to be provided manually by a human expert (Uhlmann, Kiraryz & Gabbouj 2014), which can introduce problems. These problems include having the necessary training data, the introduction of human error and effective training, or parameter setting, of the classifier. Small training data sample sizes often cause the underlying classifier to lack discrimination and generalisation capabilities, a phenomenon known as ill-posed data (Myburgh & Van Niekerk 2013; Uhlmann, Kiraryz & Gabbouj 2014). Semi-supervised learning can be used to overcome small sample sets. This approach first uses a small set of labelled data to

train the classifier, then uses a large amount of unlabelled data to improve the classifier. Choosing reliable training data is crucial in both supervised and semi-supervised approaches (Uhlmann, Kiraryz & Gabbouj 2014).

Past studies using some of the common supervised and machine learning classifiers are discussed next.

2.5.5.1   Maximum likelihood supervised classifier

The maximum likelihood (ML) classifier is a well-known, commonly used classifier of both optical and SAR remotely sensed data (McNairn et al. 2009). It is based on the mean, variance, and covariance statistics of each class's signal responses (Ma et al. 2013). This classifier can be based on different types of distributions, including the Gaussian and Wishart distributions. The Gaussian-based ML classifier has been widely used in optical remote sensing, but is not considered suitable for SAR imagery due to the speckle noise inherent in SAR (Ma et al. 2013). However, the classifier can be applicable if sufficient "looks" are available, which allows the speckle noise to be reduced and makes a Gaussian probability feasible (Ma et al. 2013). It has been successfully used in land cover classifications, attaining an overall accuracy of 84.4% when using combined RADARSAT-1 and Landsat-7 ETM+ imagery (Huang, Legarsky & Othman 2007). The ML classifier is sensitive to small training samples, which can be a limiting factor for using it in certain projects (Clausi 2002). The complex Wishart ML classifier is often used for LULC classifications on PolSAR data, as it is based on the assumption that the data is uncorrelated and is suitable for multi-temporal imagery (Ma et al. 2013).

Although the Wishart classifier is often used, it does not consider phase information (Shimoni et al. 2009). Chen et al. (2007) found that using a supervised Wishart ML classifier on the coherency matrix of L-band PolSAR data achieved better accuracies for each class than numerous other classifiers, but had an overall accuracy of 75.2%. In comparison, the ECHO classifier achieved the highest overall accuracy of 81.3% when applied to all six intensity and three phase images in the data set, but achieved class accuracies as low as 17.8% (Chen et al. 2007). Thus, it is important to choose the correct classifier for the specific application to maximise both overall and individual class accuracies.

Models based on Gaussian and Wishart distributions can be ineffective when texture is present. The integration of the K-means distribution is recommended in applications with texture, such as forest species mapping (Coulibaly et al. 2012).

2.5.5.2   Decision tree classifiers

Decision tree classifiers allow for a multi-stage or sequential approach and do not rely on assumptions about the distribution of the input data (McNairn et al. 2009; Pal & Mather 2003). As non-parametric, sequential classifiers, they are particularly suitable for generally non-normal SAR data (Shang et al. 2009). They are able to handle nonlinear relationships between features and classes, and between defining features (Pal & Mather 2003). They are easier to interpret, quicker to train and execute, and more efficient than artificial neural networks (Friedl & Brodley 1997; McNairn et al. 2009; Qi et al. 2012). Decision tree classifiers are ideal when data gaps are present, for example for cloud masking in optical data or radar layover masking in SAR data (Shang et al. 2009). Decision trees were successfully implemented for feature selection and classification on polarimetric RADARSAT-2 data for LULC classification with an overall accuracy of 86.6%. In comparison, a Wishart supervised classification on the same data achieved only 69.7% (Qi et al. 2012).

2.5.5.3   Support vector machine classifiers

Support vector machine (SVM) classifiers have superior image handling abilities as they can synthesise regression, classify functions based on either discrete or continuous data sets, are insensitive to noise and over-training and can handle unbalanced data sets (Adam et al. 2014). In comparison with other statistical classifiers, SVM is particularly effective when dealing with large data sets and is less prone to suffering from the Hughes effect than the ML classifier, for example (Oommen et al. 2008). SVM is becoming increasingly popular for classification, recognition, and detection as it can deal with high dimension data (Zhang 2010). SVM also handles smaller training sets well (Myburgh & Van Niekerk 2013; Pal & Mather 2005; Lizarazo 2008; Mountrakis, Im & Ogol 2011). This is true not only for pixel-based classifications, but also for object-based classifications (Niu & Ban 2013). Duro, Franklin & Dube (2012) found that SVM produced a statistically significantly better vegetation-focused land cover classification than the decision tree classifier, using an object-based approach. However, SVM can be prone to longer training times and can require parameter tuning to produce the most accurate results (Chan, Laporte & Defries 2003).

2.5.5.4   Artificial neural networks

Conventional statistical classifiers are not optimal for high-dimension data as they do not allow factor weighting and cannot handle large, complex data sets efficiently (Waske & Braun 2009). Although artificial neural networks can be successfully used for larger data sets, they require long training times and have no consistent rules for design or performance (Waske & Braun 2009).

Neural networks outperform statistical classifiers, especially when the feature space is complex and the source data have differing statistical distributions (Nyoungui, Tonye & Akono 2002). They draw their own input-output relations from the data and do not assume a normal distribution (Pacifici 2008). They provide a more rapid performance and allow *a priori* knowledge and realistic physical constraints to be incorporated into the classification process (Nyoungui, Tonye & Akono. 2002). They tend to suffer less from noise and saturation in L-band SAR data (Del Frate & Solimini 2004). Laurin et al. (2013) found that a neural network classifier improved accuracy results by 1.6-1.9% over a ML classifier, although the increase was small, it was statistically insignificant. Chen et al. (1996) achieved overall accuracies up to 95% for land cover classification using multi-frequency PolSAR data, showing this classifier's ability to handle the non-normal distribution of SAR data.

2.5.5.5 Random forest classifier

The RF classifier uses the best split of a random sample of the input features at every node division in a decision tree (Rodriguez-Galiano et al. 2011). It iteratively creates multiple decision trees in this way and reduces generalisation error (Rodriguez-Galiano et al. 2011). The RF classifier is able to compute large time series efficiently even if feature selection is not first conducted on the data set. It also needs limited guidance for parameter setting (Rodriguez-Galiano et al. 2012). The RF classifier is noted specifically for advantages that include (Breiman 2001):

1. It is robust towards outliers and noise;
2. It is efficient with large data bases, such as in this study;
3. It has superior accuracy over other current algorithms;
4. It is computationally lighter than other machine learning algorithms; and
5. It has the capability to determine variable importance (Rodriguez-Galiano et al. 2012).

The RF classifier produced better results than SVM when classifying a heterogeneous coastal landscape, producing an overall accuracy of 93.1% (Adams et al. 2014). Novack et al. (2011) found similar results, with RF producing the best overall accuracies when compared with the SVM, regression tree, and decision tree classifiers, using an object-based approach on WorldView-2 and Quickbird-2 simulated imagery. RF is well-suited for classifications based on multi-temporal data and can perform well even with small training sets (Waske & Braun 2009). Although some classes were poorly separated with this classifier, Waske and Braun (2009) found that adding a single optical image to a SAR time series improved the separation between the urban and forest classes. Performing classification using only SAR data, Du et al. (2015) found that the RF classifier was suited to handling PolSAR data and achieving an overall accuracy of 83.8% and Kappa value of 0.8. Rodriguez-Galiano et al. (2012) saw a positive result from using the RF

classifier for a complex study area and a large number of land cover classes, gaining an overall accuracy of 92%.

A limitation of this classifier is, however, that the splitting rules are unknown and that it is a "black box" type of classifier (Rodriguez-Galiano et al. 2012).

2.5.6   Training data

Training data are necessary when using the above mentioned supervised and machine learning algorithms. It trains the classifier by providing information, or characteristics, about the land cover classes based on samples that are generally collected through field work. Collecting sufficient, accurate, well-distributed ground truth data is often a limiting factor for classifications that rely on remotely sensed data (Lu & Weng 2005). However, a sound ground truth data set is imperative for a successful classification when using supervised classifiers (Myburgh & Van Niekerk 2014).

In an object-based environment, the training data will be information, or features, derived for certain objects known to belong to specific land cover classes. The classifiers will then associate the respective values of the features to characterize each land cover class. Based on these, the classifier can then classify other unknown objects based on their values for the specific defining features.

Inaccurate training data will invariably cause an inaccurate classification. Added to this, if training samples are too few or too many, classification can also be affected. If too few samples exist, the classifier will not be provided enough information to be able to accurately classify the rest of the image. Conversely, if a classifier is over-trained with too many features, misclassifications can also occur. Mislabelling is also a major human error that can cause classification inaccuracies (Rodriguez-Galiano et al. 2012). This can be reduced through inspections as well as using a classifier that is robust against outliers, such as the RF classifier (Rodriguez-Galiano et al. 2012).

CHAPTER 3   DATA ACQUISITION AND PRE-PROCESSING

The data acquisition details and data types used are introduced in this chapter. The classification scheme and land cover classes used in the resultant classifications are also presented, followed by the pre-processing performed on the imagery.

3.1   DATA ACQUISITION

Two sets of remotely sensed data were used for this study: RADARSAT-2 SAR imagery and SPOT-5 optical imagery. Fully polarimetric RADARSAT-2 C-band image data in descending fine beam mode with an incidence angle of 37° was captured every 24 days from January to December of 2014, generating a time series of 13 images. The images were received in the Single Look Complex (SLC) format. The spatial resolution for the raw imagery was 11 m x 9 m. RADARSAT-2 image data is sold under license from MacDonald Dettwiler and Associates. The SEAS-OI station, a partner in this research collaboration, had an existing contract to obtain a quota of RADARSAT-2 image data, under which the data required for this study was captured and obtained.

SPOT-5 optical image data is sold by Airbus Defence & Space and also obtained through SEAS-OI's contract, who routinely capture this imagery over the extent of Réunion Island. SPOT-5 images were selected as close to the acquisition dates of the RADARSAT-2 image data as possible. Thus, a 13-image multi-temporal series was obtained from SEAS-OI to compliment the RADARSAT-2 images. The multispectral bands had a spatial resolution of 10 m and the panchromatic band had a spatial resolution of 2.5 m.

A set of criteria were assessed to identify candidate SPOT-5 and RADARSAT-2 image pairs to be included in the classifications. Firstly, the window period between the image acquisition dates were assessed as a smaller time gap between the two images is favoured in minimize temporal changes within an image pair. Cloud cover in the SPOT-5 image was assessed and images with minimal cloud were favoured. Four images pairs satisfied these criteria and were chosen for classifications. Table 3.1 lists all of the image pairs and their acquisition dates.

Table 3.1 2014 acquisition dates of the 13 pairs of SAR and optical data images. Dates highlighted in grey were used in classifications.

RADARSAT-2	SPOT-5	Days Difference
22 February	22 February	0
18 March	15 March	3
11 April	20 April	9
5 May	1 May	4
29 May	1 June	3
22 June	22 June	0
16 July	18 July	2
9 August	12 August	3
2 September	2 September	0
26 September	23 September	3
20 October	20 October	0
13 November	14 November	1
7 December	11 December	4

3.2 CLASSIFICATION SCHEME DESIGN

One method of organising land cover information is to use a classification scheme (Jensen & Cowen 1999). Determining a suitable classification scheme is one of the major steps in an image classification (Turkar & Rao 2011). A classification scheme defines the land cover classes to be used to classify an image and details their possible hierarchy and any natural breaks between super classes, such as between non-vegetated areas and vegetated areas. A detailed investigation was made of the land covers apparent in the study area through field visits and inspection of high-resolution imagery, and examples of these land covers can be seen in Figure 3.1 A land cover class hierarchy of nine classes (Figure 3.2) was then developed with the aid of the South African full Land Cover Class System (LCCS) classification produced by the Council for Scientific and Industrial Research (CSIR) (2010).
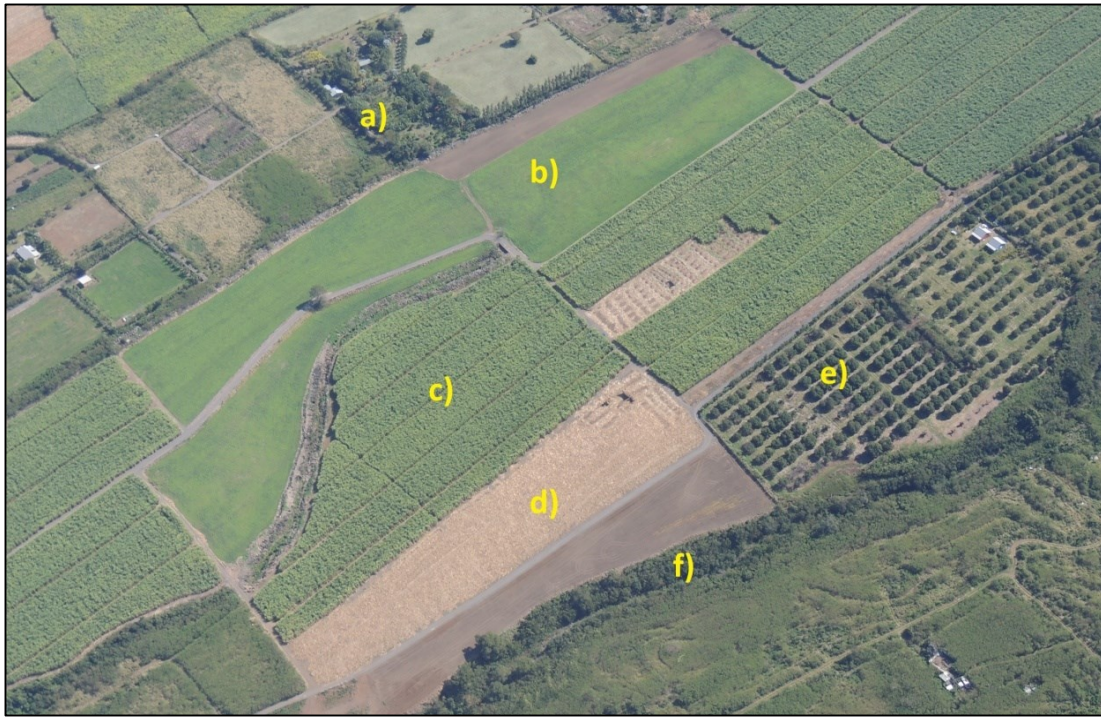
Figure 3.1 Aerial photograph showing some of the typical land covers in the study area: a) natural vegetation, b) grass fields, c) sugarcane, d) harvested sugarcane, e) orchards and f) ravine vegetation.
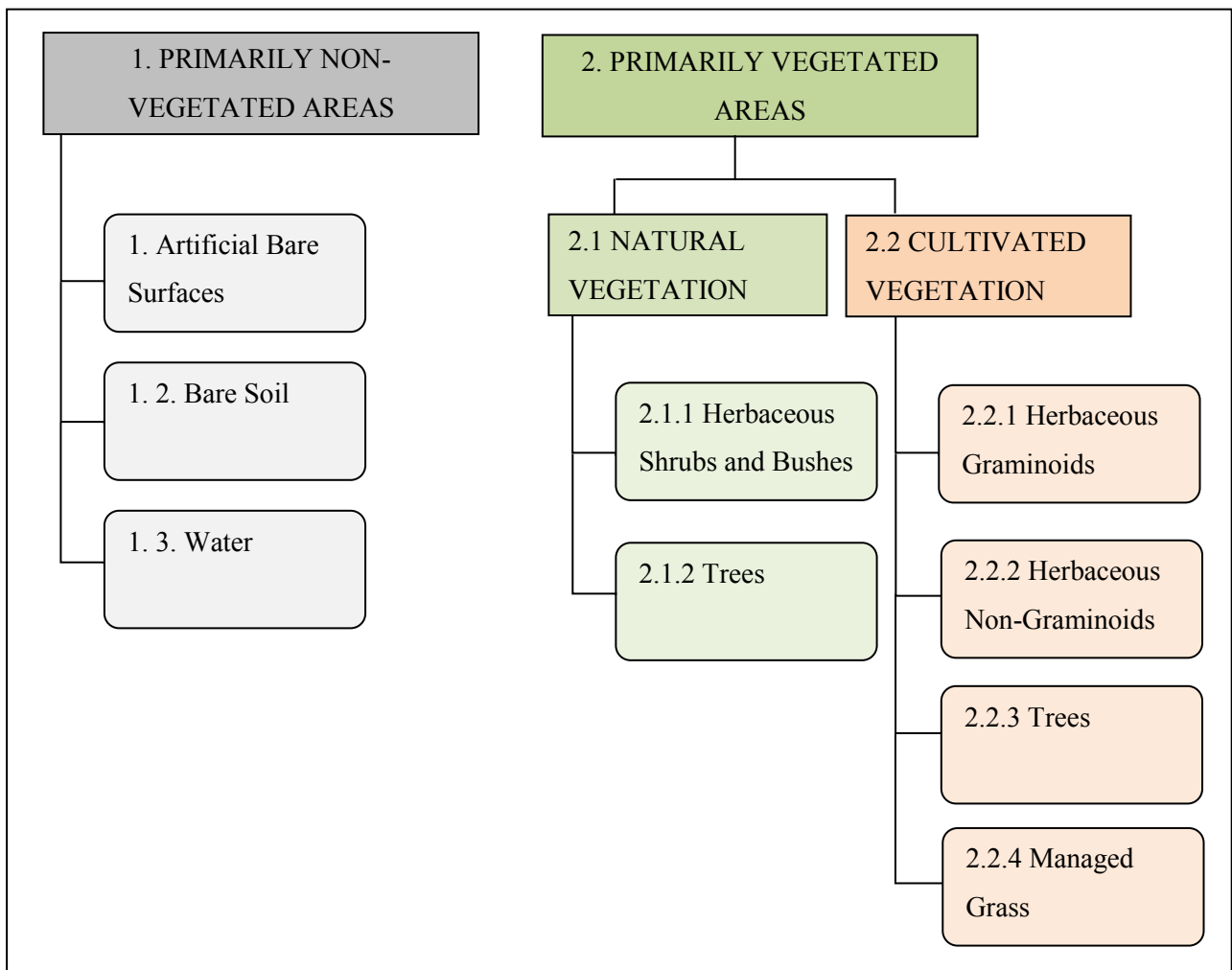
Figure 3.2 Classification scheme used in this study.

The following section will provide a brief description on each of the land cover classes. At the end of Section 3.2.2, Figure 3.3 is presented. This gives photographic examples of each land cover class, as well as the variations within each class. It is referred to within the descriptions of each land cover class but is presented at the end of the section for ease of reference.

3.2.1   Primarily non-vegetated area classes

3.2.1.1   Artificial bare surfaces

Artificial bare surfaces are areas that have artificial coverings due to human activities. They include built-up areas, urban areas, transportation (roads and airport runways), extraction (quarries and open minds), and waste disposal. According to the South African LC Field Guide (CSIR 2010), this class includes built-up, non-linear, and built objects.

Features of interest included the St Pierre runway, located in the south-west corner of the study area, and the built-up coastal towns of St Pierre and St Joseph. Photographic examples of this land cover class can be found in Figure 3.3; a built up residential area along the coast can be seen in Figure 3.3m with a field of solar panels seen in Figure 3.3n.

3.2.1.2   Bare soil

This class can encompass bare soil found in cultivated areas (bare fields), but predominantly refers to naturally occurring exposed soil. These are areas without an artificial covering and have vegetation cover of less than 4%, as defined by the CSIR LCCS. The class includes bare rock, sand, consolidated material on the face of cliffs, landslides, and steep riverbed embankments.

As naturally occurring bare soil was uncommon within the study area and this class was expected to be difficult to classify. The river bed found in the south-western part of the study area is an interesting feature as it is bare at certain times of the year. It was expected that it would be classified into this class at some times of the year and classified as water at other times. This river bed can be seen in Figure 3.3o.

3.2.1.3   Water

The water class refers to areas that are naturally and artificially covered by water. It includes lakes, dams, rivers, and the surrounding ocean. It is important to note when river beds are dry and exposed, these areas

may be classified differently on images from different times of the year. The river bed, with a low water level, can be seen in Figure 3.3o.

The study area did not contain any large lakes. However it contained many small dams that service the agricultural practices in this area and was bordered by the ocean in the south.

3.2.2   Primarily vegetated area classes

3.2.2.1   Natural herbaceous shrubs and bushes

As defined by the LCCS (CSIR 2010), natural vegetation occurs in areas where the vegetation cover is in balance with the abiotic and biotic forces of its biotope. This class includes semi-natural vegetation, which is naturally occurring vegetation that is affected by human activities. It also includes previously cultivated areas that have been abandoned, in which the vegetation is regenerating to a natural state, undisturbed by human activities.

The study area did not contain large expanses of naturally occurring vegetation outside of ravine areas. Small pockets of natural vegetation did occur within the urban areas and around cultivated fields. However the image resolution of 8 m made accurate depictions of these small areas unlikely. Two variations of this land cover can be found in Figure 3.3a and b. Figure 3.3c) depicts a ravine area, showing the dense vegetation characteristic of these regions.

3.2.2.2   Natural trees

Natural trees includes areas with a tree cover density of 15% or higher. An area is considered to contain trees when it holds woody vegetation with a distinct elevation at the top of the canopy no less than 1.5 m above ground level. It can also contain a ground cover of shrubs and bushes no more than twice the area of the tree cover. This class includes indigenous and alien forests.

This study aimed to only classify naturally occurring forests and plantation forests within this class, while excluding trees occurring in cultivated orchards. An example of a natural forest can be seen in Figure 3.3d. The forests and orchards display very different types of vegetation and structural properties and thus were separated.

3.2.2.3   Cultivated herbaceous non-graminoids

This class includes areas where the natural vegetation has been cleared or modified to grow vegetation of anthropogenic origin and uses. This vegetation is "artificial" and requires human activities for maintenance. There may be times of the year when this land has little to no vegetation covering, depending on harvesting and planting regimes. It is possible that these areas may be classified as bare soil on images acquired at certain times of the year, if they remain bare for extended periods.

The crop types in the study area that fell within this class included pineapple fields, commercial gardening containing vegetables and flowers, and herb fields. Two variations of this class can be found in Figure 3.3j and k.

3.2.2.4   Cultivated herbaceous graminoids (Sugarcane)

Within the study area, the main crop type that fell within this land cover class was sugarcane. Fields with any sugarcane growth stages were included in this class. Figure 3.3g, h and i show varying stages in the sugarcane life cycle: Figure 3.3g depicts a harvested field with completely exposed bare ground. At this stage, these areas should be classified as Bare Soil. Figure 3.3h depicts young sugarcane with Figure 3.3i showing the height of full grown sugarcane relative to a vehicle.

3.2.2.5   Cultivated trees

Trees planted and maintained by human activities for commercial purposes fall within this class. It includes cultivated orchards, such as banana trees and mango orchards. Uniform rows and spacing between the trees is characteristic of these areas and is an important consideration when segmenting these images. If segmentation is set at too small a scale, the rows of trees will be separated from the rest of the underlying vegetation, causing classification errors. An example of a mango orchard is shown in Figure 3.3l.

3.2.2.6   Managed grass

Managed grass includes all areas of grass that are managed in some way by human activities, including meadows used for animal grazing and grass fields cultivated for harvest and animal feed, and sports and recreational fields. An example of a Managed Grass is depicted in Figure 3.3e.

Figure 3.3 Photographs of the land cover classes: a), b) and c) Natural Herbaceous Shrubs and Bushes, d) Natural Trees, e) Managed Grass, f) the proximity of different and covers, g) Bare Soil, h) and i) Cultivated Herbaceous Graminoids, j) and k) Cultivated Herbaceous Non-Graminoids, l) Cultivated Trees, m) and n) Artificial Surfaces and o) the river bed showing both Bare Soil and Water.

The study area consists of very limited bare areas. This can be seen in Figure 3.3f. This is an important feature of the study region to note, as the small pockets of varying land cover types lying adjacent to each other, coupled with the high intra-class variability pose limitations in accurately mapping regions such as this.

3.2.3   Naming convention for classes

For ease of reference, a shorthand naming convention for the land cover classes, shown in Table 3.2 is used in the tables and graphs throughout this document:

Table 3.2 Naming convention for the land cover classes used in this document

Name in the classification scheme (Section 3.2.1 and 3.2.2)	Abbreviation used in the rest of this document
Artificial Bare Surfaces	Artificial Surfaces
Bare Soil	Bare Soil
Cultivated Herbaceous Graminoids	Cultivated HG
Cultivated Herbaceous Non-Graminoids	Cultivated HNG
Cultivated Trees	Cultivated Trees
Managed Grass	Managed Grass
Natural Herbaceous Shrubs and Bushes	Natural HSB
Natural Trees	Natural Trees
Water	Water

3.3   SYNTHETIC APERTURE RADAR IMAGE PRE-PROCESSING

Terrain correction and geocoding was done in two parallel stages. The first stage dealt with the backscatter intensity bands. The second stage corrected the polarimetric coherency (T3) matrix, which was extracted from the SLC data using the PolSARPro 4.2 software. The backscatter bands and T3 matrix components were then filtered and polarimetric decompositions were extracted from the T3 matrix. The full pre-processing procedure applied to each SAR image date can be seen in Figure 3.4, which shows the parallel preparation of the backscatter bands and decomposition parameters. The rest of this section will describe how these pre-processing steps were applied to the SAR imagery.

IMAGE PRE-PROCESSING

SAR BANDS (HH, HV, VH, VV)

EXTRACT T3 MATRIX

GEOMETRIC CORRECTION

APPLY POLARIMETRIC FILTER
(Refined Lee 3x3)

POLARIMETRIC
DECOMPOSITIONS

COREGISTERATION BETWEEN
ALL BANDS FROM EACH DATE
(First date used as reference the layer)

DE GRANDI MULTI-TEMPORAL
FILTER

GEOMETRIC AND RADIOMETRIC
CORRECTION

OUTPUTS:

1. Cloude and Pottier Decomposition
   - Entropy, Anisotropy and Alpha
2. Freeman Durden
Decomposition
   - Single, Double and Volume
3. Krogager Decomposition
   - Helix, Diplane and Sphere
4. Van Zyl Decomposition
   - Odd, Even and Double
5. Yamaguchi Decomposition
   - Helix, Double, Single and Volume

OUTPUTS:

1. Filtered backscatter
   - HH, HV, VH, VV
2. Unfiltered backscatter
   - HH, HV, VH, VV

Figure 3.4 Pre-processing chain for the preparation of SAR data.

3.3.1   Pre-processing the backscatter bands

When there are two or more images of different dates, of the same scene, multi-temporal filtering can be performed. This exploits the correlation that exists between the speckle found in each of the images. The De Grandi multi-temporal filter can thus be applied to remove this multiplicative noise. This filter is, however, based on the assumption that resolution is the same and that a ground target in one image is in the exact co-ordinates of all the other images. Therefore, co-registration among all the backscatter bands was applied first, followed by the De Grandi multi-temporal filter in Envi using the SARScape toolbox to remove speckle from the time series. This improved both the visual and radiometric quality of the images, as the grainy salt-and-pepper-like noise was reduced, and this can be seen in Figure 3.5 showing a portion of the scene before and after filtering. This method was preferred as no spatial resolution is lost while speckle is still improved. The bands were then geocoded in SARScape, using a current 5 m Lidar DEM provided by CIRAD. During the geocoding and terrain correction step, the image data were also radiometrically calibrated to sigma-0 (backscattering coefficient) in decibels using the local incidence angle, so that the backscatter intensity could be used in further processing steps.
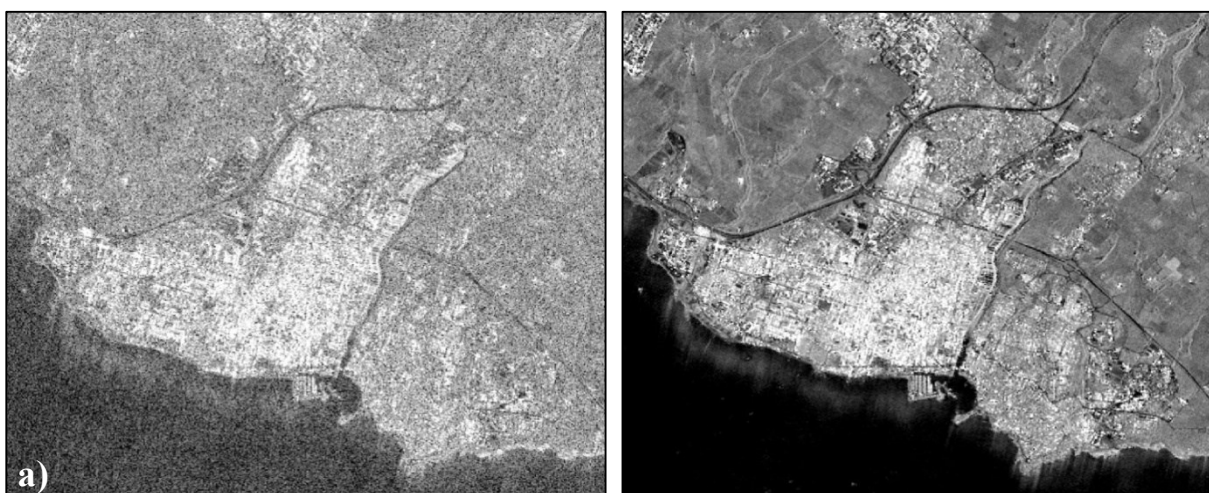
Figure 3.5 The (a) raw backscatter is improved using the De Grandi multi-temporal filter resulting in a more usable (b) product.

A layover and shadow mask was produced during the calibration step. Radar layover and shadow, which were apparent in the image data and inherent in radar, can cause distortion in the backscatter signal and result in misclassification of the affected areas. Two steep ravines flanked the study area, causing large areas of layover on the west and east sides of the images. The layover and shadow mask was prepared for use in eCognition 9.0.3 software for subsequent processing steps.

3.3.2   Pre-processing the T3 matrix

ASF MapReady was used to geocode the T3 matrix elements that had been extracted from the SLC data in PolSARPro 4.2. The 5 m DEM described in Section 3.3.1 was used. The output was generated in PolSARPro-ready formats. Orthorectification of the T3 matrix in MapReady created a longitude coordinate error in the header files, which had to be manually corrected.

3.3.3   Filtering of the T3 matrix

For preserving the full polarimetric phase information of each scene, a multi-temporal filter, like the De Grandi Filter, is not an option for the T3 matrix. Thus, spatial filters need to be used. A review of the current literature available on speckle filtering reveals that there is no definitive opinion on how to choose the optimum method and algorithm for polarimetric filtering. There is thus uncertainty surrounding the choice of filter and the optimum parameters for each filter. Different filters and parameter combinations had to be tested to make a definitive decision on the best choice to use in filtering the T3 matrix for each image data.

Five of the filters available in PolSARPro 4.2 that are commonly used in the literature were selected for this project: the Refined Lee, Sigma Lee, Gaussian Box, Box Car and Lopez filters. Each filter was run on the same RADARSAT-2 image of the study site, dated 22 February 2014. At least three window sizes were tested for each filter (3x3, 5x5, and 7x7). If a filter had additional parameters, as does the Sigma Lee filter, these parameters were varied independently of each other to determine the effect each one had on the resultant output. Table 3.3 shows one example of assessing the effects of a filter's parameters on the output.

Table 3.3 Parameters tested for the Sigma Lee filter and the smoothing effects each one has on the resultant output.

Sigma Lee	Min	Max
Target Window Size	3	5
	More Pixelated	More Smooth
Filter Window Size	7	9
	More Pixelated	More Smooth
Sigma Value	0.5	0.9
	More Pixelated	More Smooth
Number of Looks	1	3
	More Smooth	More Pixelated

The outputs were visually inspected to determine which parameter values for each filter had a generalising (smoothing) or pixelating effect. This was done using the Pauli decomposition as it visualizes a range of scattering mechanisms (ESA 2000). The window size for averaging caused the most smoothing. Figure 3.6 shows the effect of changing window size on the Box Car filter and the Refined Lee filter. From these observations, a "most pixelated" and "most smoothed" output was generated for each filter by compounding the effects of each parameter value choice. The two outputs for each filter were compared using visual interpretation of the five criteria stated in Section 2.3.5.3, along with available literature. The Box Car filter and Refined Lee filter were chosen for further investigation based on the supporting literature and visual inspection of the output.
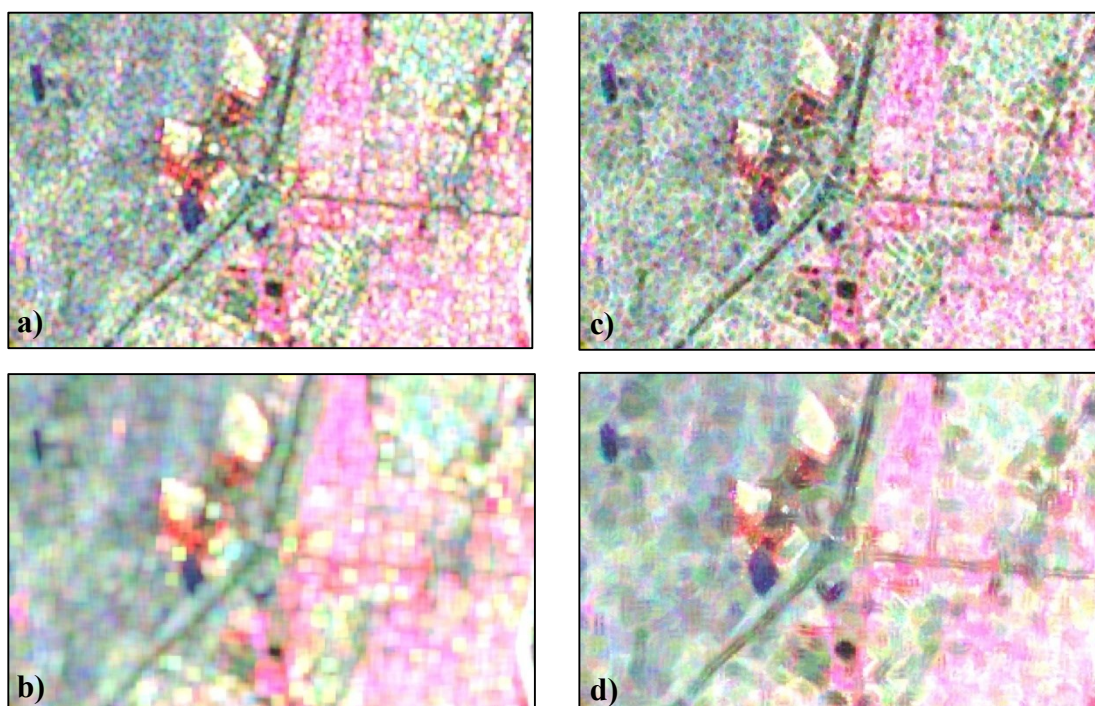
Figure 3.6 Filtering using a) the Box Car filter with a window of 3x3, b) the Box Car filter with window of 7x7, c) the Refined Lee filter with a window of 3x3, and d) the Refined Lee filter with a window of 7x7, displayed in the Pauli decomposition RGB.

A second level of filtering can be introduced at the decomposition stage of the processing chain. This is not an independent filtering step. Instead it determines the window used to estimate the polarimetric parameters, which can have a filtering effect. The outputs from the two chosen filters, the Box Car and Refined Lee filters, were used to extract polarimetric decompositions. The decompositions were extracted without applying an averaging window, ensuring that no further filtering was applied. The outputs were assessed visually and the Refined Lee filter was found to have the most beneficial effect. This filter was thus chosen for use in the study based on its performance as measured by the criteria listed in Section 2.3.5.3. The geocoded and terrain corrected T3 matrix for each image date was subsequently filtered using

the Refined Lee filter with a moving window of 3x3. Polarimetric decompositions were performed on the T3 matrices in PolSARPro 4.2, allowing the following polarimetric parameters to be extracted:

1. Cloude-Pottier Decomposition: Entropy, Anisotropy, and Alpha.
2. Freeman-Durden Decomposition: Volume, Double Bounce, and Single Bounce.
3. Yamaguchi Decomposition: Helix, Single, Double, and Volume.
4. Krogager Decomposition: Helix, Sphere, and Diplane.
5. Van Zyl Decomposition: Odd, Even, and Double Bounce.

These parameters were used as inputs for the feature selection investigations and object-based classifications (Chapter 4).
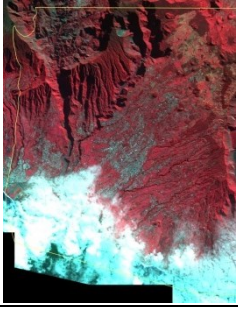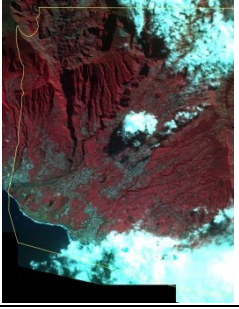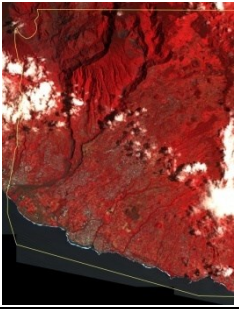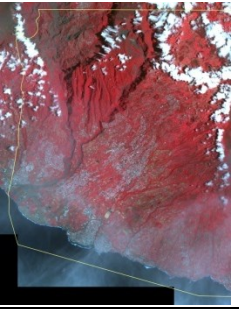
3.4   OPTICAL IMAGE PRE-PROCESSING

The SPOT-5 time series contained 13 images, acquired approximately once every month. The imagery was already orthorectified and atmospherically corrected to ensure radiometric fidelity. Cloud cover can obscure further processing steps and results, and is particularly a problem in multi-temporal data sets over tropical areas. Clouds therefore were manually digitised using ArcMap 10.1, so that areas of cloud cover could be masked out.

The SPOT-5 images were cropped to the same extent as the RADARSAT-2 images to improve processing time and computer resource allocation.

Not all of the 13 RADARSAT-2/SPOT-5 image pairs could be used in the classifications due to large expanses of cloud cover that removed usable portions of the imagery and large time periods between the acquisitions of the two types of images. RADARSAT-2/SPOT-5 image pairs were selected with the fewest number of days between their acquisition dates and with minimal cloud cover in the SPOT-5 image. Four image date pairs were chosen. These dates corresponded to the RADARSAT-2 imagery acquired on 22 February 2014, 5 May 2014, 29 May 2014, and 9 August 2014. A comprehensive evaluation of all 13 image pairs and why each was included or disregarded can be seen in Table 3.4.

Table 3.4 Evaluation of all 13 SPOT-5 images for inclusion in the time series, based on cloud cover and number of days between RADARSAT-2 and SPOT-5 image acquisition dates.

SPOT-5: 2014-02-22 RS-2: 2014-02-22 Included based on identical acquisition dates and areas of interest unaffected by cloud cover	**SPOT-5:2014-03-15 RS-2:2014-03-18** Disregarded based on cloud cover.	**SPOT-5:2014-04-20 RS-2:2014-04-11** Disregarded based on haze and cloud cover, and an unacceptable window between the acquisition dates.	**SPOT-5: 2014-05-01 RS-2:2014-05-05** Included based on limited cloud cover and an acceptable number of days between the acquisition dates.	**SPOT-5: 2014-06-01 RS-2: 2014-05-29** Included based on an acceptable number of days between the acquisition dates and limited cloud cover.
SPOT-5:2014-06-22 RS-2:2014-06-22 Disregarded based on cloud cover and the loss of numerous ground truth points if included.	**SPOT-5:2014-07-18 RS-2:2014-07-16** Disregarded based on cloud cover.	**SPOT-5: 2014-08-12 RS-2:2014-08-09** Included based on the absence of cloud cover and an acceptable number of days between the acquisition dates.	**SPOT-5:2014-09-02 RS-2:2014-09-02** Disregarded based on cloud cover and areas of shadow resulting from the cloud cover.	**SPOT-5:2014-09-23 RS-2:2014-09-26** Disregarded based on cloud cover, resulting in the loss of many ground truth points.
SPOT-5:2014-10-20 RS-2:2014-10-20 Disregarded based on the amount of cloud cover.	**SPOT-5:2014-11-14 RS-2:2014-11-13** Disregarded due to the loss of more than 60 ground truth points.	**SPOT-5:2014-12-11 RS-2:2014-12-07** Disregarded due to haze over most of the image.		

3.5   TRAINING AND GROUND TRUTH DATABASE

Ground truth data are crucial for training supervised and machine learning classification algorithms and for validating the accuracy of classifications. A common method of ground truth data collection is through field visits to collect GCPs. However, this can prove difficult if parts of the study area are inaccessible or the study area is large. High resolution imagery is often used as a substitute.

For this study, GCPs were needed for all nine land cover classes. The aim was to collect at least 40 points for each class, which would be divided between training and validation. Reaching this aim proved difficult for land cover classes that did not extend over large areas or that were not present in large quantities in the study area. The study area had dense vegetation cover, which made accessing some areas at certain times difficult, particularly naturally occurring vegetation. A combination of GCP collection methods was thus used.

Over the course of 2014, field visits were conducted to a selection of predominantly agricultural areas within two days of every RADARSAT-2 image acquisition. These areas were chosen primarily due to access (i.e. permission) to the target areas. GPS co-ordinates, photographs, and general notes of the type of land cover present were collected. The collection of these points was done by the author during June to September 2014 and by a collaborator (Bellon 2014) during February to May 2014. The field visits accounted for most of the ground truth data collected for the classes Cultivated Trees, Cultivated HG and Cultivated HNG.

In addition to field visits, a tour of the study area was conducted by vehicle over several days in August 2014. With the addition of aerial imagery brought along on these trips, GCPs were selected for all of the land cover classes. These points were restricted to areas that could be seen from roads.

To supplement land covers with limited GCPs after the first two steps, high resolution (6 cm) Pleiades imagery was used to perform a purposive desktop collection of points. This was done for easily identifiable classes such as Artificial Surfaces and Water.

Any points in the final, combined ground truth database that fell within areas of layover, shadow, or cloud (for any or all dates) were removed. Training and validation were performed using the same set of points for each image date. The final data set covering all of the classes included 701 points. It was randomly split in half in a class-wise manner using QGIS, forming a training data set (a) of 349 points and an accuracy assessment data set (b) of 351 points, seen in Figure 3.7.
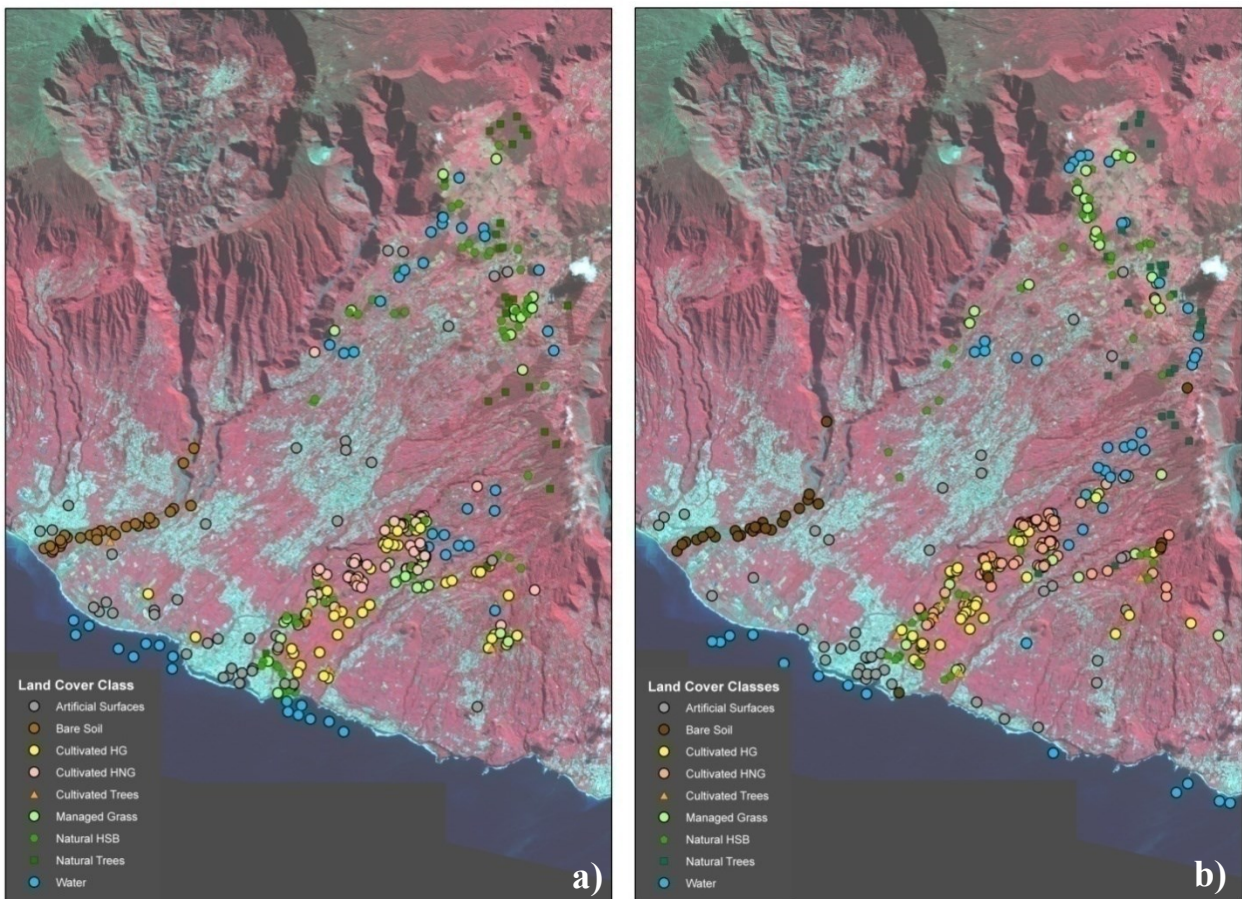
Figure 3.7 Distribution of a) training and b) validation GCPs, colour coded per land cover class.

The training points were used to select the corresponding image objects after segmentation was applied to the satellite imagery in eCognition 9.0.3. The training objects were thus automatically selected for each class. The number of training objects per land cover class is shown in Table 3.5.

Table 3.5 Number of training objects per class used for feature selection and classifier training.

Land Cover Class	Total Training Objects
Artificial Surfaces	41
Bare Soil	30
Cultivated HG	39
Cultivated HNG	63
Cultivated Trees	17
Managed Grass	32
Natural HSB	56
Natural Trees	25
Water	46

CHAPTER 4   DATA ANALYSIS

The following sections give detailed information about the methods and processes used to fulfil the aim of this study and complete the four experiments. The steps followed to conduct the features selection on single-date, multi-date, single-sensor, and dual-sensor data are presented in Experiment 1. Object-based single-date classifications using various classification algorithms are presented in Experiment 2. Experiment 3 compares single-date classification using fused and single-sensor data. Experiment 4 compares multi-temporal and single-date classification. Due to the variety of processes run to fulfil the four experiments, a range of software packages were used in conjunction with each other. Figure 4.1 shows a breakdown of the methods used to accomplish the data processing and the analysis of the prepared data.

DATA ANALYSIS

Experiment 1

FEATURE SELECTION

- Extract indices, textural, mean, standard deviations, geometric and shape features from the training data of both types of imagery
- Run RF and CART feature selection on both the single-sensor and fused-sensor data

Experiment 2

TEST DIFFERENT CLASSIFIERS

- Use combined RADARSAT-2 and SPOT-5 imagery
- Run: RF, CART, decision tree, SVM, maximum likelihood and kNN classifiers
- Use default settings for all

Experiment 3

COMPARE SINGLE-SENOR TO FUSED CLASSIFICATION ON SINGLE-DATES

- Run the RF classifier on three iterations:
  - Fused imagery
  - Only SPOT-5 imagery
  - Only RADARSAT-2 imagery

Experiment 4

COMPARE SINGLE-DATE TO MULTI-TEMPORAL CLASSIFICATION

- Use the combined RADARSAT-2 and SPOT-5 imagery
- Conduct feature selection using the RF algorithm
- Run the RF classifier on increasing numbers of features for training

DATA RESULTS AND INTEPRETATION

- Perform accuracy assessments on Experiments 2, 3 and 4
- Create standard confusion matrices and error metrics based on same validation data set

Figure 4.1 Experimental design.

4.1   PREPARATION FOR THE EXPERIMENTS

The data had to be set up in the correct formats for each software prior to any analysis. This section explains the image stacking to combine all of the image layers together, the segmentation performed on these layers in eCognition 9.0.3, and the extraction of the training objects and their features for the feature selection in Experiment 1, as well as the training of the classifiers in Experiments 2, 3 and 4.

4.1.1   Multi-layer stack

Twenty-eight input layers were prepared from each optical and SAR image pair for input into the object-based classifications. The 28 image layers in each SPOT-5/RADARSAT-2 image pair were converted into a single image stack in ENVI and resampled to 8 m resolution. This stack was imported into eCognition 9.0.3.

The 28 image layers from each SPOT-5/RADARSAT-2 image pair are:
1. Green (SPOT-5 band)
2. Red (SPOT-5 band)
3. NIR (SPOT-5 band)
4. SWIR (SPOT-5 band)
5. HH (RADARSAT-2 backscatter band, filtered)
6. HH (RADARSAT-2 backscatter band, unfiltered)
7. HV (RADARSAT-2 backscatter band, filtered)
8. HV (RADARSAT-2 backscatter band, unfiltered)
9. VH (RADARSAT-2 backscatter band, filtered)
10. VH (RADARSAT-2 backscatter band, unfiltered)
11. VV (RADARSAT-2 backscatter band, filtered)
12. VV (RADARSAT-2 backscatter band, unfiltered)
13. Alpha (derived from the Cloude-Pottier decomposition)
14. Anisotropy (derived from the Cloude-Pottier decomposition)
15. Entropy (derived from the Cloude-Pottier decomposition)
16. Freeman Durden Double Bounce (derived from the Freeman-Durden decomposition)
17. Freeman Durden Volume (derived from the Freeman-Durden decomposition)
18. Freeman Durden Odd (derived from the Freeman-Durden decomposition)
19. Krogager Diplane (derived from the Krogager decomposition)
20. Krogager Sphere (derived from the Krogager decomposition)
21. Krogager Helix (derived from the Krogager decomposition)
22. Van Zyl Double Bounce (derived from the Van Zyl decomposition)

23. Van Zyl Volume (derived from the Van Zyl decomposition)

24. Van Zyl Odd (derived from the Van Zyl decomposition)

25. Yamaguchi Double Bounce (derived from the Yamaguchi decomposition)

26. Yamaguchi Volume (derived from the Yamaguchi decomposition)

27. Yamaguchi Helix (derived from the Yamaguchi decomposition)

28. Yamaguchi Odd (derived from the Yamaguchi decomposition)

4.1.2 Segmentation

The multiresolution segmentation (MRS) algorithm available in eCognition 9.0.3 was used to produce useful image objects. Only the SPOT-5 bands (Red, Green, NIR and SWIR) and SAR multi-temporal, filtered backscatter bands (HH, HV, VH and VV) were used in the segmentation, as this created the most useful objects. The decomposition parameter layers do not contain what would be visually considered "logical" real world objects, so were omitted from segmentation. However, segmentation was applied to the entire multi-layer stack, containing all of the layers.

Segmentation was performed with a scale parameter (10) that ensured a slight over-segmentation, rather than under-segmentation. This scale provided the best represented objects determined by visual inspection. Weightings for all layers were kept equal. The MRS parameters were kept constant so that the classifications could be directly compared with one another.

Segmentations were based on a varying set of layers to analyse feature selection as well as resultant classifications on single-sensor versus dual-sensor data. Firstly, for fused data, segmentation was based on equal weightings for the four filtered backscatter (HH, HV, VH and VV) SAR bands and the four optical bands (Green, Red, NIR, and SWIR). To compare this to single-sensor data, segmentations were also run on just the four backscatter SAR bands and independently on just the four optical bands.

Thematic layers (additional shapefiles) were used to mask out cloud and radar shadow, as well as layover. Training objects for each class were extracted using a thematic layer containing the training points. Objects containing a training point were selected and classified automatically as the correct land cover class based on the attribute information inherent in the point shapefile.

4.1.3 Feature derivation

Features are derived from the input layers, and can include parameters such as "mean green reflectance" or "standard deviation of HH" or "NDVI" per object. Different threshold values for each feature can be used to classify the objects created from an initial segmentation and to train classifiers. Feature selection

depends on the type of imagery used, the land cover depicted and the specific output required. It is therefore difficult to specify a definitive set of features that is applicable to every study.

Features were derived from both sets of image data. This included brightness values from the visible spectrum bands, backscatter and mean digital numbers from the polarisation bands, derived features such as the texture and vegetation indices, geometric features and contextual features. The features were exported for every training object into a single shapefile, which was used in subsequent processing steps, including feature selection. The full list of features derived per image date are presented in Table 4.1.

Table 4.1 Features derived for use in feature selection and classification.

CATEOGRY	TYPE
Customised	Normalised difference vegetation index (NDVI) (NIR - Red) / (NIR + Red)
Layer values	Mean
	Standard deviation
	Brightness
	Max difference
Geometry (extent)	Area
	Border length
	Length
	Length/thickness
	Length/width
	Thickness
	Width
Geometry (shape)	Asymmetry
	Border index
	Compactness
	Density
	Elliptical fit
	Shape index
	Rectangular fit
	Roundness
Texture (GLCM)	Angular second moment
	Contrast
	Correlation
	Dissimilarity
	Entropy
	Homogeneity
	Mean
	Standard deviation

Texture (GLDV)	Angular second moment
	Contrast
	Entropy
	Mean

Each fused SAR/Optical image pair resulted in 208 image features per training object. Only features derived from that sensor's image data were considered when taking into account single-sensor data. For example, NDVI was not considered in feature selection or classifier training for SAR-only data, as it is an optically based vegetation index.

4.2   EXPERIMENT 1: FEATURE SELECTION

The most useful features were selected by performing a CART analysis and RF classification using the default settings of the Salford Systems modelling software (The Salford Predictive Modeller Software Suite 2000-2013). These two algorithms were chosen based on their performance in the above-mentioned literature, efficiency, suitability to multi-source data sets and their availability and ease of use. Furthermore, they both produce rankings with importance scores out of 100 making them directly comparable. They are efficient and quick to run, and the potential agreement between the two sets of rankings allows for more definitive conclusions to be drawn. The CART importance scores are calculated and ranked based on the frequency and significance of a feature as a primary or surrogate splitter of classes in the classification tree (Yu et al. 2006).

The training objects with all of their feature values were imported into the software and the predictors and target variable (land cover class) were selected. Feature selection was performed on the fused and single-sensor image data. For the fused data (dual sensor), 208 features were considered. Only features derived from the four optical bands and the geometric and shape features were used for the SPOT-5 feature selection resulting in 88 features. Similarly, for the RADARSAT-2 feature selection, features derived from the backscatter bands and the polarimetric parameters were used with the geometric and shape features, totalling 149 features. This was done for all image dates and using both CART and RF feature selection algorithms.

The outputs for these algorithms included a ranking of features from the most important to the least important. "Scores" out of 100 are also provided. The CART analysis also generates a decision tree with suggested features and thresholds to split the classes in the most optimal way. The results of Experiment 1 are presented in Section 5.1.

4.3   EXPERIMENT 2: TESTING DIFFERENT CLASSIFICATION ALGORITHMS

A comparison among six of the available classifiers in eCognition 9.0.3 was conducted to determine their relative performance. Two dates were chosen to account for possible variations in classifier performance due to image acquisition date and to allow for more general conclusions. The result informed Experiments 3 and 4 and allowed for the most suitable classification algorithm to be chosen.

The fused image data set was classified using classifiers implemented in eCognition 9.0.3. All of the classifiers were trained using the same set of features (Section 4.1.3) which included texture, layer values and geometric and shape features. The classifiers tested on the 5 May and 8 August 2014 images were:

1. Maximum likelihood (Bayes Classifier);
2. Decision tree;
3. Random forest;
4. K-means nearest neighbour;
5. SVM; and
6. Classification based on the rule set derived from the CART decision tree (Section 4.2).

Performance was measured purely based on the accuracies achieved by the classification algorithms. This was calculated using the same validation data set, using standard confusion matrices and error metrics. The results for Experiment 2 are presented in Section 5.2.

4.4   EXPERIMENT 3: SINGLE-DATE OBJECT-BASED CLASSIFICATIONS

The aim of Experiment 3 was to assess the benefits of fused image data sets over single-sensor imagery for land cover classification, as well as providing a baseline set of single-date classifications to compare with results from Experiment 4 (multi-temporal classifications). Four image dates were therefore used to perform three iterations of classifications. Firstly, a classification based on the combined optical-SAR imagery data, followed by classifications performed using only SAR and only optical data.

The classification algorithm was chosen based on the results obtained from Experiment 2 and thus the RF classifier was used. These single-date classifications were all produced in eCognition 9.0.3 and then assessed based on confusion matrices and error metrics in ArcMap 10.1 using the same validation data set as used in both Experiment 2 and 4. Results for Experiment 3 are presented in Section 5.3.

4.5   EXPERIMENT 4: MULTI-TEMPORAL CLASSIFICATION

A multi-temporal classification was performed to assess whether using multiple image dates improves the classification accuracy obtained from single-date classifications in Section 5.3.

A multi-layer stack of all of the layers from all four image dates was created, resulting in a final stack of 112 input layers. The MRS was applied to the stack using a scale parameter of 10 and equal weightings for all of the filtered backscatter bands and optical bands. These parameters ensured consistency between this segmentation and the segmentation performed on the single-date classifications (Experiment 3).

Features were extracted from all of the layers using the same training data set described in Section 4.1.3. Feature selection was run on a total of 638 features using the RF algorithm in the Salford Systems software. Since the RF classifier emerged as the best performer in the result of Experiment 2, it was used for the multi-temporal classification. The classifier was trained using increasing numbers of top-ranked features, to quantify the benefits of iteratively increasing the number of features. The first 20, 40, 50 and 60 features as well as all of the features was assessed. Results for Experiment 4 are presented in Section 5.4.

4.6   VALIDATION AND ACCURACY ASSESSMENT

A standard accuracy assessment was used to gauge the success and reliability of the classifications. Confusion matrices and standard error metrics (overall accuracy, kappa, errors of omission and commission and user and producer's accuracies) were used to quantify the accuracy measurement. Accuracy was assessed using 351 reference points. The same point data set was applied to each classification output, allowing direct comparisons between class and overall accuracies.

This chapter presented the detailed methods used to fulfil the study objectives. The following chapter will present and discuss the study results.

CHAPTER 5   RESULTS AND DISCUSSION

This thesis aimed to assess the benefits and limitations of using a multi-temporal, dual-sensor image data set for land cover classifications using an object-based approach. Four key questions were explored:

1. How can feature selection be used to determine which are the important features for class discrimination, and do these features differ between single-sensor and dual-sensor data sets and between image dates?

2. Which classification algorithm best handles the increased data dimensionality of fused image data sets and produces the highest accuracies?

3. Does the fusion of optical and SAR data improve accuracy in a single-date classification sufficiently to warrant the additional expense of using two data sources?

4. Does the inclusion of a multi-temporal data set improve accuracy sufficiently over a single-date classification to warrant the additional expense of extra data?

As the results of the investigation of each question were used to optimise the next investigation, the results and discussion of each investigation are presented sequentially.

5.1   EXPERIMENT 1: FEATURE SELECTION

When using multi-temporal and multi-sensor data sets, the large data volume can result in increased computational time and negatively affect the efficiency and ability of classification algorithms to manage these data sets. Feature reduction will counteract these problems. Trends in feature importance can be used to inform feature reduction. Similarities and common important features across dates and between data sets from different sources (fused and single-source) are also useful in determining key features for class separability and the possibility of different sensors changing prevalence in importance across different times of the year.

Feature selection was conducted on all of the features derived from both the optical and SAR image layers (separately and together) using the CART and RF feature selection algorithms available in the Salford Systems software. Selection considered 208 features for the fused data sets, 149 for SAR-only data set, and 88 for the optical-only data set. The features were ranked according to their importance value, which was scored out of 100. The features that scored 0 were disregarded from the analysis.

The Brightness feature was not the same in each iteration of the feature selection. Brightness was calculated using only the layers under consideration for a particular feature selection. In the fused data set classifications, it was calculated using both the SAR and optical image layers, whereas in the optical-only classifications, it was calculated using only the optical bands from the images.

Feature selection was conducted on four image dates from different seasons to determine whether time of year affects the optimal set of features to train the classification algorithm. The February date corresponds to late-summer (the wet season) when vegetation is densest and the sugarcane is generally nearly fully grown. The two May images correspond to the beginning of winter, which is a drier season. Harvesting of sugarcane, which covers 60% of the cropped area, begins in July, thus the August image date is during harvesting season.

The results for Experiment 1 will be presented as follows: the results from feature selection on each date will be discussed for the fusion data sets, including the CART decision trees produced in Section 5.1.1, followed by the single-sensor data sets in Section 5.1.2. Lastly, Section 0 will discuss the feature selection performed on the multi-temporal (all four images combined) fused data set.

5.1.1 Feature selection on the fused data sets

The results of feature selection on the fused optical and SAR data are presented for each date, after which the general findings are summarised. For ease of interpretation, Table 5.1 presented at the end of this section, shows a condensed list of the 15 highest ranked features for both algorithms across all four dates. A glossary defining the features can be found in APPENDIX A.

5.1.1.1 2014-02-22

The RF and CART feature rankings agreed with one another in this late summer image. Seven of the 10 most valued features were selected by both algorithms. Both algorithms ranked the mean texture features derived from the optical bands highly, ranking many of them in the top 20 features. As expected, the NDVI was ranked highly for both algorithms; this vegetation index is usually important for class separability in land cover classifications (DeFries & Townsend 1994; Hansen et al. 2000; Pu et al. 2008).

CART introduced a unique feature to the rankings for this date namely GLCM Contrast based on the Green band. It was not ranked highly for any of the other dates. It was allocated an importance score of 48.4 out of 100, ranking it the 9th most useful feature. The RF selection produced an importance score of only 35.8 for the same feature, dropping it to a rank of 67th. If an identifier is particular to a season or time of year, then it may be important for temporal classification. However, as the two algorithms did not agree on the importance of the feature, its usefulness is inconclusive for temporal classification.

RF ranked one SAR-based feature (8th) in the top 10, namely standard deviation based on the VV image band. In contrast, CART did not rank such features in the top 10. At most, CART gave the mean of the unfiltered HH and the filtered HH almost identical CART importance scores of 19th and 20th.

CART highlighted the importance of features derived from the Green image band for this late summer image date, selecting 8 of its top 20 features from this band. In contrast, RF only selected four features from this band for its top 20.

When considering the classification decision tree produced from the CART process, seen in Figure 5.1, nine (33.3%) out of the 27 features used to split the classes are SAR features. The SAR-derived features are from both the backscatter (three) and polarimetric parameters (six). This shows that the reliance on only backscatter in previous studies is insufficient for optimum class separation. The importance of NDVI and the optical-derived features, seen in the rankings, is mimicked in the decision tree.
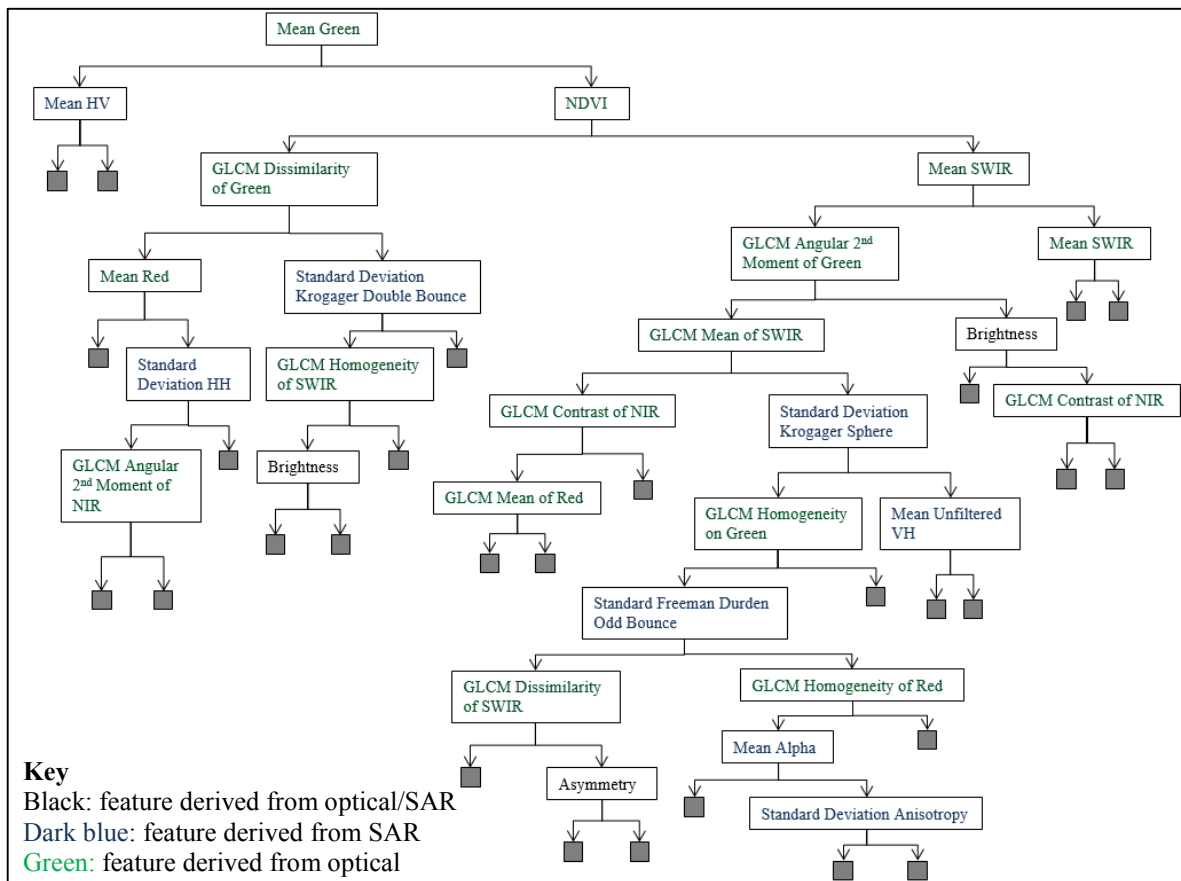
Figure 5.1 CART decision tree (2014-02-22) showing the features used as splitters for class separation.

5.1.1.2   2014-05-05

Feature selection for this May imagery, an autumn date, shows a similar trend to the February image. Once again, CART and RF feature selection have similar results, with six common features across the two top 10 ranked lists. NDVI again featured within the top 10 and the majority of the highly ranked features were derived from the optical image bands.

The 1st ranked SAR-only features were the mean of HH, ranked 8th by RF, and the mean of VV, ranked 19th by CART. This again shows the limited value of SAR-derived features.

The CART decision tree for this date (Figure 5.2) was by far the most complex, with 32 features used as splitters in comparison to 27 for the February date, 23 for the 29 May data set and 11 for the August date. Out of the 32 features, 12 are SAR-derived (37.5%), showing a similar dependence on the optical-derived bands as the other dates. The split between backscatter and polarimetric features is similar to the 29 May and August data sets, with a near even split of five backscatter to seven polarimetric parameters.
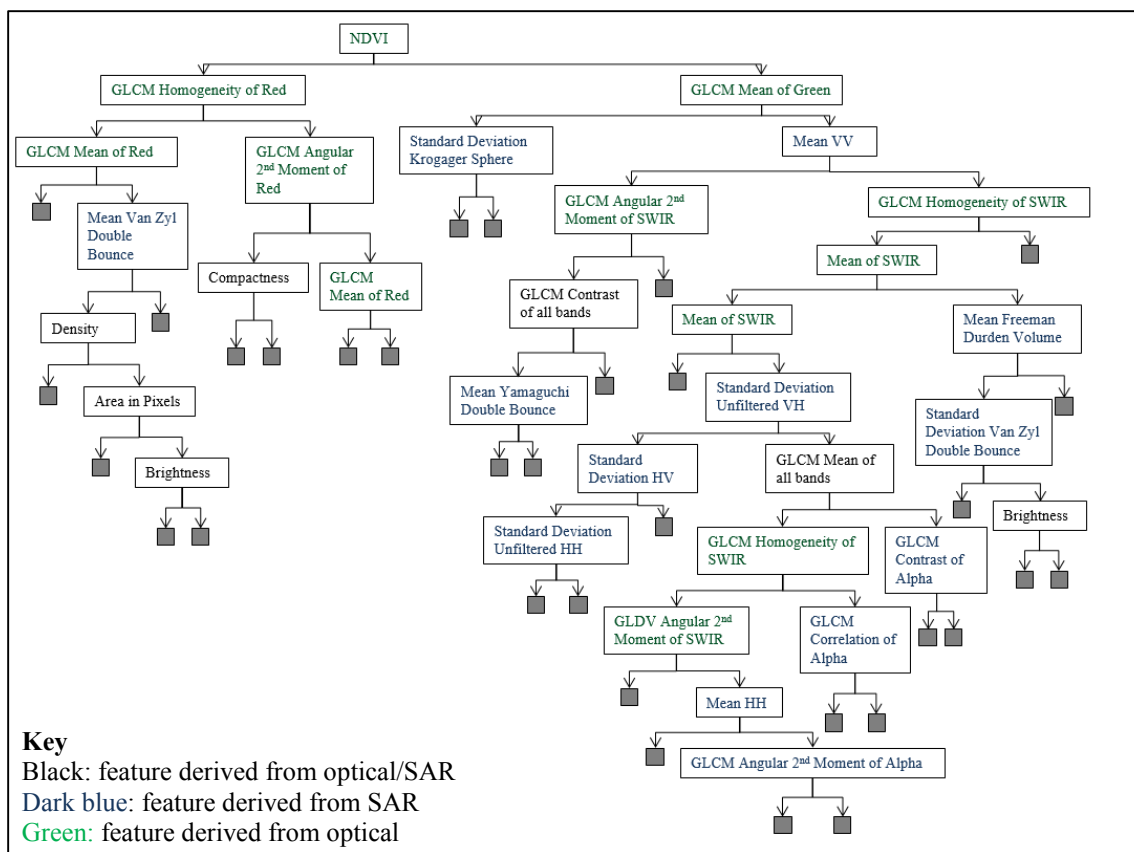
Figure 5.2 CART decision tree (2014-05-05) showing the features used as splitters for class separation.

5.1.1.3   2014-05-29

Feature selection for the second autumn date showed less agreement between the CART and RF feature rankings, with only four features in common between the two top 10 lists.

The RF top-20 included seven SAR-based features, including the Standard Deviations of HH and HV in the top 10 and the mean texture value of alpha ranked 11th. This suggests a difficulty in separating classes based solely on reflectance at this time of year, and the potential of SAR for supplementing optical imagery. The CART rankings introduced the means of VV and HH at 12th and 13th positions, respectively. It included five SAR-based features in the top 20, the second highest number among all four image dates, after the August image date.

The CART decision tree (Figure 5.3), shows similar trends as the other dates, with nine out of the 23 (39.13%) features used as splitters being derived from SAR bands. There is a five-four split between polarimetric and backscatter features, reiterating the need for both types of features for good class separation.
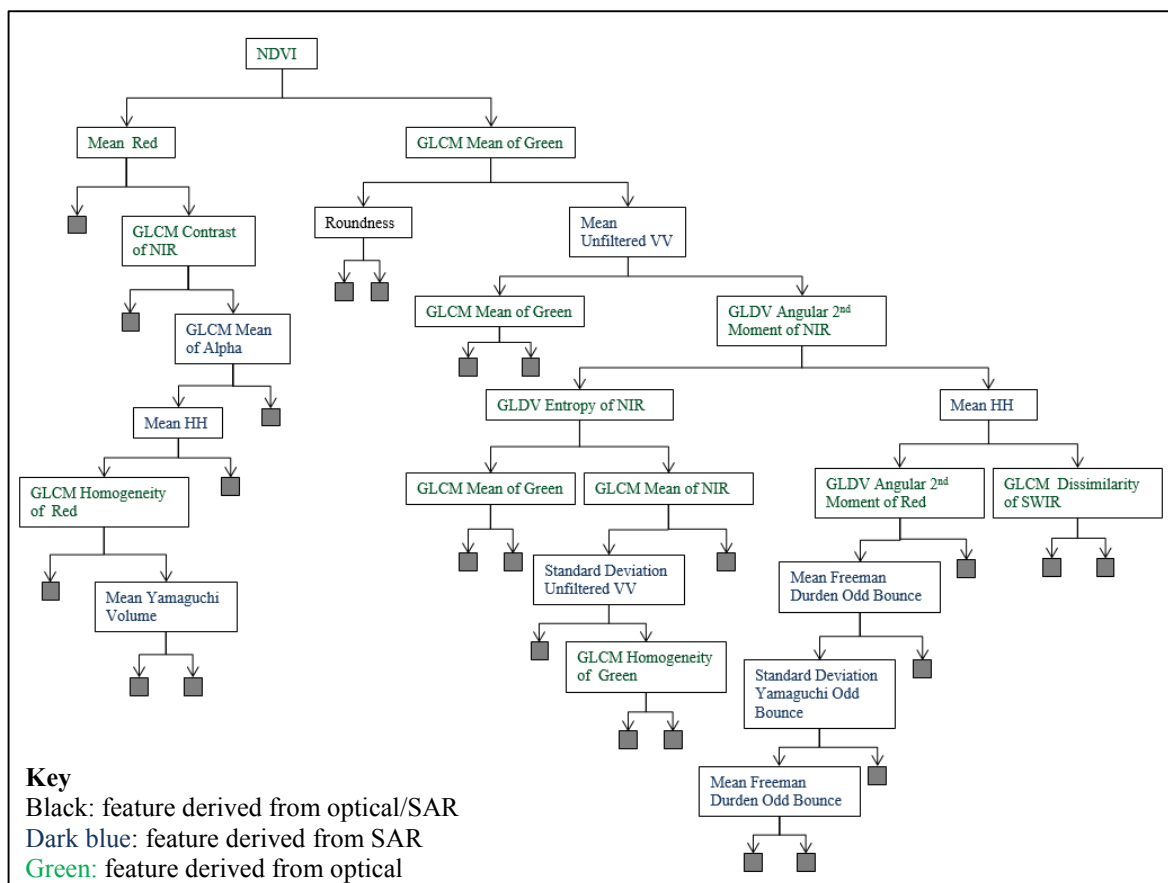
Figure 5.3 CART decision tree (2014-05-29) showing the features used as splitters for class separation.

5.1.1.4   2014-08-09

Compatibility between the two feature selection algorithms was fair for the August image, with five common features in the top 10 ranked features. Both algorithms favoured SAR-based features, ranking eight SAR-based features in their top-20 lists. This result indicates a need for data complimentary to optical data for class separability at this time of year. Much of the sugarcane harvesting occurs from July during the drier season. The changing land cover could result in more information than just the reflectance values being needed. It is also possible that the SAR data at this time is potentially less afflicted by soil moisture issues than in the rainy season. The signal therefore contains more information about vegetation structure and helps in class separability.

CART ranked the mean values for HH and VV and the mean texture value based on the Alpha layer in its top 10, reiterating the importance of both backscatter and polarimetric SAR features for class separability for this date.

The CART decision tree for this winter date (Figure 5.4) is far simpler than the other three dates, with only 11 features being used to separate the nine land cover classes. Similar to the other dates however, four of these 11 (36.6%) are SAR-derived, with an even split between polarimetric and backscatter

features. These four SAR features come from just the HH band and the Alpha parameter. The optical features chosen are also mostly derived from the SWIR band. The prevalence of just three bands in this decision tree, which is a completely different pattern to the other three dates, shows the importance of these three key image bands for classification at this specific time of year.
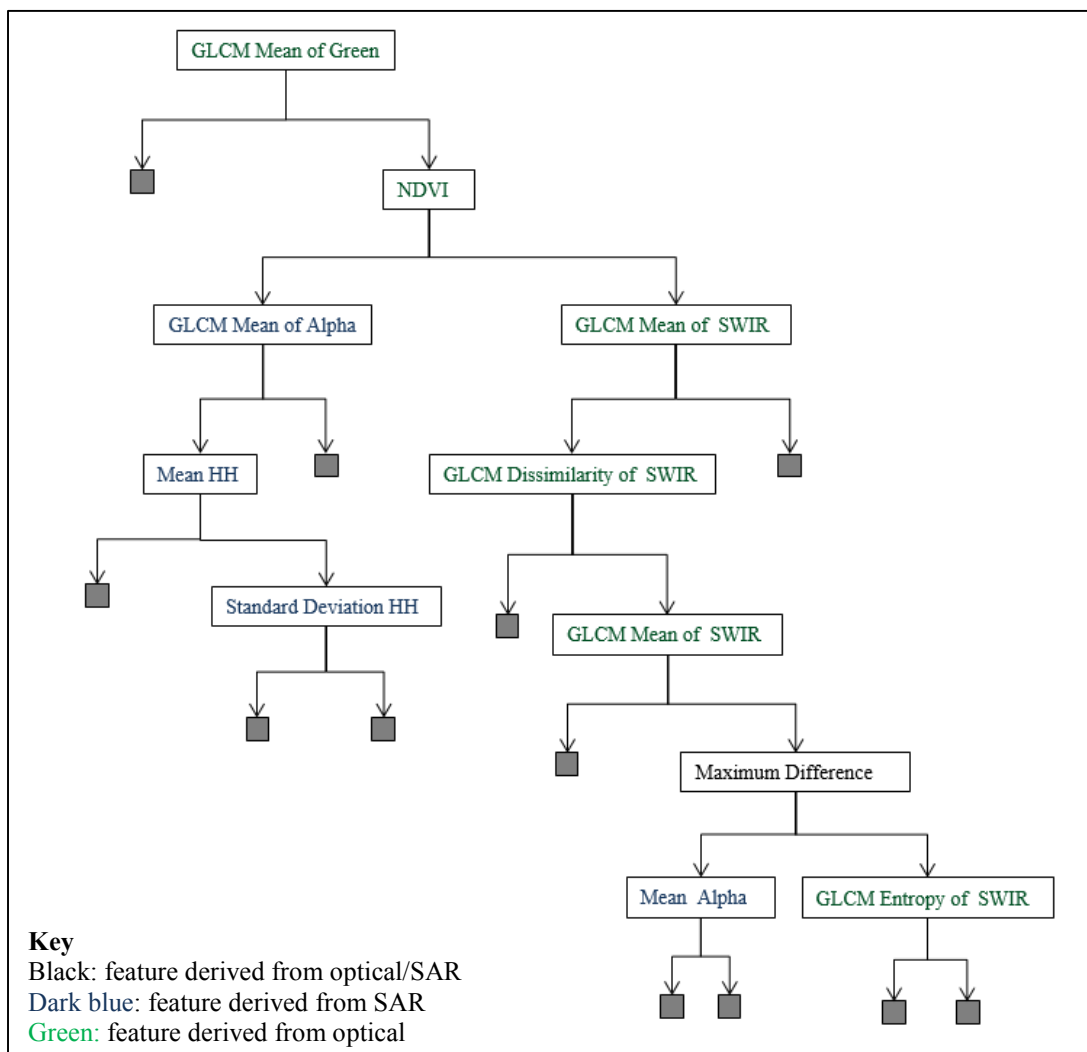
Figure 5.4 CART decision tree (2014-08-09) showing the features used as splitters for class separation.

Table 5.1 Top 15 ranked features for the RF and CART feature selections on the fused data sets for the four image dates.

RANKING	2014-02-22		2014-05-05		2014-05-29		2014-08-09	
	CART	RF	CART	RF	CART	RF	CART	RF
1	GLCM Mean of Red	GLCM Mean of SWIR	GLCM Mean of Red	Mean of Green	GLCM Mean of Red	GLCM Mean of Red	GLCM Mean of Green	Mean of Green
2	Mean of Red	Brightness	Mean of Red	Mean of Red	Mean of Red	NDVI	GLCM Mean of Red	Maximum Difference
3	Brightness	GLCM Mean of Green	Brightness	GLCM Mean of Green	GLCM Mean of Green	GLCM Mean of NIR	Mean of VV	GLCM Mean of Green
4	GLCM Mean of NIR	Mean of Green	GLCM Mean of Green	Mean of SWIR	Mean of Green	Mean of Green	Mean of HH	Brightness
5	Mean of NIR	GLCM Mean of all bands	Mean of Green	GLCM Mean of Red	GLCM Mean of all bands	GLDV Angular 2nd Moment of Red	Maximum Difference	GLCM Mean of SWIR
6	GLCM Mean of Green	GLCM Mean of Red	GLCM Homogeneity of Red	Maximum Difference	Brightness	Mean of Red	Mean of Green	Mean of Red
7	GLCM Mean of all bands	NDVI	GLCM Dissimilarity of Red	GLCM Mean of SWIR	GLCM Contrast of NIR	Standard Deviation of HH	NDVI	GLCM Mean of NIR
8	Mean of Green	Standard Deviation of VV	GLCM Mean of all bands	Mean of HH	GLCM Dissimilarity of NIR	GLDV Entropy of Red	Mean of Alpha	Standard Deviation of HH
9	GLCM Contrast of Green	GLCM Mean of alpha	Maximum Difference	Mean of Alpha	GLDV Mean of NIR	GLCM Mean of Green	GLCM Mean of SWIR	NDVI
10	NDVI	Mean of NIR	NDVI	NDVI	GLDV Entropy of NIR	Standard Deviation of HV	Mean of SWIR	Mean of Freeman-Durden Odd Bounce
11	GLCM Entropy of Green	Mean of SWIR	GLCM Mean of NIR	Brightness	NDVI	GLCM Mean of Alpha	GLCM Mean of Alpha	GLCM Mean of Red
12	GLCM Mean of SWIR	Standard Deviation of HH	Mean of SWIR	Mean of NIR	Mean of VV	GLCM Mean of SWIR	Mean of NIR	Mean of NIR
13	Maximum Difference	Mean of Yamaguchi Double Bounce	Mean of NIR	Standard Deviation of VH	Mean of HH	Maximum Difference	Mean of Red	Standard Deviation of VV
14	GLCM Standard deviation of Green	Maximum Difference	GLCM Homogeneity of SWIR	Standard Deviation of HV	Maximum Difference	Standard Deviation of VV	GLCM Mean of NIR	Mean of HH
15	Mean of SWIR	GLCM Homogeneity of Green	GLCM Dissimilarity of SWIR	Mean of HV	Mean of Unfiltered VV	Mean of HH	Mean of Freedom-Durden Odd Bounce	Mean of Unfiltered HH

5.1.1.5   General findings on combined SAR-optical feature selection

Feature selection on the combined optical and SAR imagery showed definite trends. The importance of textural features was evident. In particular, the Mean GLCM texture measure derived from the Red optical band was either the highest or second highest ranked features for all dates and was ranked highly by both feature selection algorithms. The Mean GLCM derived from the Green optical band was also consistently highly ranked. The added value that texture features provide for separating classes is therefore undeniable, validating the choice of an object-based approach in this study.

The vegetation index, NDVI, was important in class separability for the fused data sets, which mimics its importance in traditional, optical-based classifications. It was consistently ranked highly as an important feature by both CART and RF feature selection. The decision trees created by CART showed that NDVI was used consistently as a primary splitter and was an important splitter specifically for separating vegetation classes (e.g. the cultivated classes) from the non-vegetation classes (e.g. Artificial Surfaces, Bare Soil, and Water). A threshold of around 0.44-0.46 was seen to be useful for separating these two distinct super-classes in the classification hierarchy.

The majority of the top features ranked by both CART and RF were optically based. However, the RF feature selection algorithm tended to rank the SAR-based features higher than CART. Although few SAR features were selected, it is important to note that classifications produced on the combined imagery consistently produced better overall accuracies than those produced on optical imagery alone (see results in Section 5.3). In the CART decision trees across the four dates, there was a relatively stable dependency on SAR features, ranging from 33.3% to 39.13% of features used as splitters being derived from SAR. Figure 5.5 shows the contribution of SAR-only, optical-only, and combination features to the 20 highest-ranked features for each date. The rankings clearly show that the focus on SAR-based features changed during the year, with later dates showing more and higher-ranked SAR-based features. SAR imagery and the features derived from it may therefore be useful for separating classes during vegetation growth stages, and in particular plant senescence, that cause confusion when using optical imagery only. In the drier times of the year and late in the season, the aging plants will have a decrease in NDVI values but SAR can still detect the vegetation structure regardless of the vegetation's chlorophyll productions. Therefore, the SAR data is most complimentary during this senescence stage. This possibility is supported by the single-date classification results in Experiment 3 and is discussed further in Section 5.3.
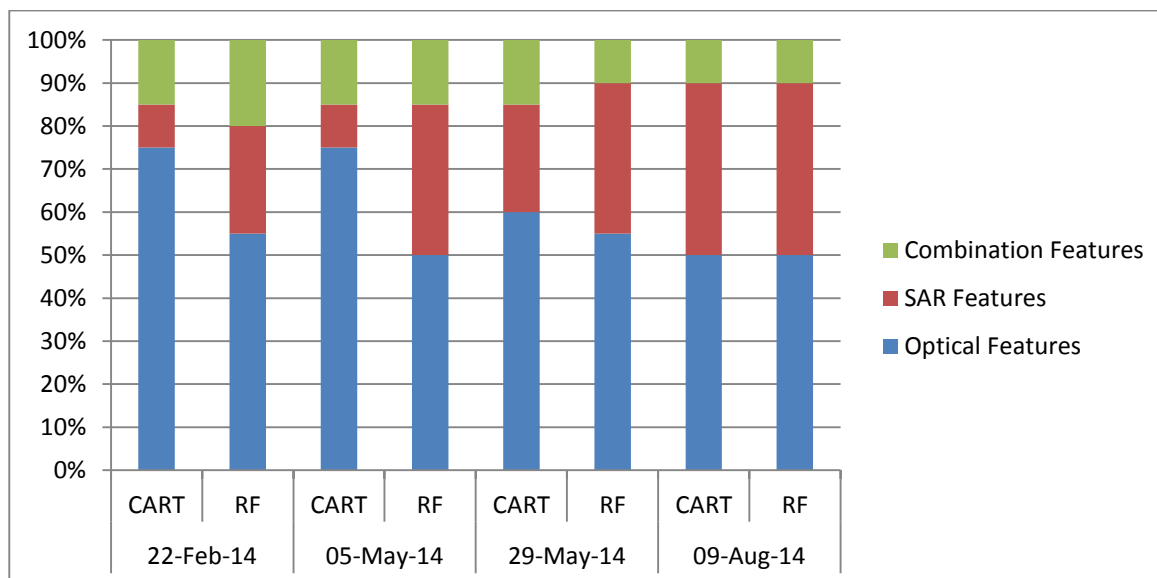
Figure 5.5 Contribution of features derived from the optical data, SAR data and a combination for both, in the top 20 rankings of features for both CART and RF feature selection for all four image dates.

The mean value produced from the Green optical band was ranked consistently highly in all four image dates. The GLDV-derived features and geometric-based features were of limited importance throughout the year. Thus, if time and computational resources are limited, these features could be disregarded from classifier training, as they are not useful for separating classes. Feature selection based on the CART and RF algorithms has therefore informed feature reduction in the large dual-sensor data set in this study. The algorithms may be useful in other studies with large data sets, to provide valuable rankings of important features to inform feature reduction. The effectiveness of the feature reduction and its potential effect on classification accuracy was investigated further in Experiment 4 and is described in Section 5.4.

5.1.2   Feature selection using single-sensor data

Feature rankings for single-sensor data are presented and discussed for each image date. Optical-only data is discussed first, followed by SAR-only data. Table 5.2 and Table 5.3 are presented at the end of the discussion and show the top 10 ranked features for both of these datasets across all four dates. The section concludes with a discussion comparing the general findings on feature selection on single-source data sets with the findings of in Section 5.1.1 on feature selection on fused data sets.

5.1.2.1   Optical-Based Feature Selection

2014-02-22

The two selection algorithms had a high agreement for the February image, with nine features in common across their top-10 lists. Nearly all of these features were either derived from the mean layer values or mean texture values, showing the importance of using combined and averaged pixel values from whole objects to determine class separability. The fused data feature selection also emphasised these two types of features. What is noticeable is the near-complete lack of geometry and shape-based features in the ranked lists. CART assigned an importance score of 0 to all of these features, and RF's highest-ranked geometry feature, area in pixels, was only 59th. Although this low rating of the usefulness of the geometry features could have been due to poorly defined objects from the segmentation, visual inspection of the real-world objects and how they were delineated found this to be unlikely.

2014-05-05

Agreement between the two selection algorithms was slightly lower for the first May date than for the February date, dropping from nine to six features in common between the two top-10 lists. The 2014-05-05 image date was the only date that did not rank the mean value of Green highest in the CART ranking. Instead, the mean texture feature derived from Red was ranked highest. There may be a temporal factor that makes the Red optical band more useful at this time of year. This is supported by the high (2nd) importance of the Red mean value in both algorithms.

Similarly to the results from the February date, the geometry-based features were not ranked highly. They first appeared at position 31 on the CART ranking, with the border index. The geometry features were ranked with low importance and this was supported by similar results with the other three image dates. Completely disregarding these types of features for classifications would thus be detrimental to accuracy. This result further substantiates that poor segmentation was unlikely to have contributed to the absence of these features in feature selection on the February image date. This first May image showed a wider

variety of types of texture measures that were highly ranked. Six of the top 10 CART-ranked features were texture measures, four of which were mean texture values derived from the combination of all four optical image bands. This result shows the prevalence of this type of feature and is in agreement with the fused data feature selection.

2014-05-29

The two feature selection algorithms again agreed well with one another on the second May image date, ranking seven common features in their top-10 lists for optical-only features. Once again, the majority of the highly ranked features were derived from the green and red bands. Eight features in the top 10 were also in common with the top 10 from the 5 May and 22 February images, and seven were in common with the 9 August image date. Time of year may thus have a limited effect on feature selection in optical imagery. The two May dates had similar rankings for the geometry features, as the highest ranked geometry feature for the second date was the border index, ranked 28th.

2014-08-09

Agreement between the two selection algorithms was again high for the August date for optical-only features, with eight features in common between the two top-10 lists. In agreement with the February and 29 May image dates, the mean value of the green band was again the highest-ranked feature by the CART algorithm. Similarly to the other image dates and the fused data sets, both top-10 lists were dominated by mean texture values derived from various bands.

Table 5.2 Top 10 ranked features for the RF and CART feature selections on the optical data sets only for the four image dates.

RANKING	2014-02-22		2014-05-05		2014-05-29		2014-08-09	
	CART	RF	CART	RF	CART	RF	CART	RF
1	Mean of Green	Mean of Green	GLCM Mean of Red	GLCM Mean of Red	Mean of Green	Mean of Green	Mean of Green	GLCM Mean of Green
2	Mean of Red	GLCM Mean of Green	Mean of Red	Mean of Red	GLCM Mean of Red	GLCM Mean of Red	GLCM Mean of Green	GLCM Mean of Red
3	GLCM Mean of Red	GLCM Mean of all bands	GLCM Mean of Green	Mean of Green	Mean of Red	Mean of Red	GLCM Mean of Red	Mean of Green
4	GLCM Mean of Green	NDVI	GLCM Mean of all bands	Mean of SWIR	GLCM Mean of Green	GLCM Mean of Green	Mean of Red	GLCM Mean of all bands
5	GLCM Mean of all bands	GLCM Mean of NIR	Mean of Green	GLCM Mean of SWIR	GLCM Mean of all bands	GLCM Mean of SWIR	Mean of NIR	Brightness
6	Brightness	Mean of Red	Brightness	NDVI	Brightness	NDVI	GLCM Mean of NIR	NDVI
7	Mean of NIR	Brightness	NDVI	GLCM Mean of NIR	GLCM Dissimilarity of all bands	GLCM Mean of all bands	GLCM Mean of SWIR	Mean of NIR
8	Mean of SWIR	Mean of NIR	GLCM Dissimilarity of all bands	Mean of NIR	NDVI	Mean of SWIR	Brightness	GLCM Mean of NIR
9	GLCM Homogeneity of all bands	GLCM Mean of Red	GLCM Homogeneity of all bands	GLCM Mean of all bands	GLCM Standard Deviation of all bands	Brightness	GLCM Dissimilarity of all bands	Mean of Red
10	NDVI	Mean of SWIR	GLDV Mean of all bands	GLCM Mean of Green	GLDV Contrast of all bands	GLCM Mean of NIR	NDVI	Mean of SWIR

5.1.2.2   SAR-Based Feature Selection

2014-02-22

Feature selection performed on SAR-based features for the February image resulted in a far lower agreement between the two algorithms than found with the combined and optical-only feature selections. Only three features were found in both algorithms' top 10 lists for this February image. The mean- and standard deviation-derived features dominated the CART top-10 list, and only one texture measure appeared. Similarly, RF only ranked two texture measures in its top 10. This was quite different to what was found in the feature selections based on optical features, where texture measures were highly ranked and were prominent in both top 10 lists. Features derived from the backscatter bands were not as prevalent as was expected based on the literature where studies have focussed nearly entirely on the use of only backscatter (Pacifici et al. 2008; McNairn et al. 2009; Michelson, Liljeberg & Pilesjo 2000). CART and RF ranked only two and three of these backscatter features in their top 10 lists respectively. The higher-ranked features were predominantly derived from polarimetric features. This was unexpected, as the highest-ranking SAR features found in the fused feature selections were generally based on backscatter. This shift towards the polarimetric parameters when only using SAR-based features is worth noting. When using dual-sensor data, it is generally adequate to derive features from fewer image layers. However, using more derivatives when dealing with single-sensor data is recommended.

2014-05-05

Feature selection performed on only the SAR-derived features for this early May image resulted in good agreement between the two algorithms, with eight features in common between their top 10 lists. Unlike the February image date, the prevalence of backscatter features was high, as expected from the literature, with seven and six backscatter-derived features in the CART and RF top 10 lists, respectively. Similarly to the February image date, texture was not prevalent, with only two texture features on both the CART and RF top 10 list. As in the optical-based feature selection, the geometry- and shape-based features showed little to no importance. In particular, the majority of these features in the CART ranking received an importance score of zero.

2014-05-29

Feature selection based solely on SAR features for this later May image resulted in poor agreement between the two algorithms, with only four common feature in their top 10 lists. As with the other image dates, texture was not prominent in the CART rankings, with only two in the top 10 list. However, four texture features were ranked in the top 10 by RF. There was no obvious reliance on backscatter- derived

features over polarimetric-derived features, with a near-even split of four versus six features in the top 10 CART list, respectively

2014-08-09

The August image showed the greatest agreement between the two selection algorithms, with eight features in common between the two top-10 lists. Similarly to the 29 May feature selection, both algorithms relied equally on the backscatter and polarimetric parameters. Texture was again of less importance, with only two texture-based features appearing in the top-10 for both the CART and RF list.

Table 5.3 Top 10 ranked features for the RF and CART feature selections on the SAR data sets only for the four image dates.

RANKING	2014-02-22		2014-05-05		2014-05-29		2014-08-09	
	CART	RF	CART	RF	CART	RF	CART	RF
1	Mean of Krogager Sphere	GLCM Mean of all bands	Mean of VH	Mean of Alpha	Mean of Entropy	GLCM Mean of all bands	Mean of Alpha	GLCM Mean of all bands
2	GLCM Mean of all bands	Mean of Freeman Durden Odd Bounce	Mean of VV	Mean of VV	GLCM Mean of Alpha	Mean of Alpha	Mean of HH	Mean of HV
3	Mean of Van Zyl Odd Bounce	Mean of Yamaguchi Double Bounce	Mean of HH	GLCM Mean of all bands	Mean of Anisotropy	Mean of Entropy	Mean of VV	GLCM Mean of Alpha
4	Mean of Yamaguchi Odd Bounce	Standard Deviation of HH	Mean of HV	Mean of HV	Mean of Alpha	GLCM Mean of Alpha	Mean of HV	Mean of Freeman-Durden Odd Bounce
5	Mean of Van Zyl Double Bounce	Mean of Alpha	GLCM Mean of all bands	Standard Deviation of VH	Mean of Unfiltered VV	Standard Deviation of VH	Mean of VH	Mean of VV
6	Standard Deviation of Van Zyl Double Bounce	GLCM Dissimilarity of all bands	Mean of Unfiltered VH	Standard Deviation of VV	Mean of VV	Standard Deviation of VV	GLCM Mean of all bands	Standard Deviation of HH
7	Standard Deviation of Freeman Durden Odd Bounce	Standard Deviation of HV	Standard Deviation of HV	Standard Deviation of HV	Mean of HH	GLCM Contrast of all bands	GLCM Mean of Alpha	Mean of Van Zyl Double Bounce
8	Mean of Krogager Diplane	Standard Deviation of VH	GLCM Mean of Alpha	Mean of Entropy	Mean of Unfiltered HH	Standard Deviation of HV	Standard Deviation of HH	Mean of Alpha
9	Standard Deviation of HH	Mean of Krogager Diplane	Standard Deviation of VH	Mean of HH	Standard Deviation of Entropy	GLDV Entropy of all bands	Mean of Freeman-Durden Odd Bounce	Mean of VH
10	Standard Deviation of VV	Mean of Entropy	Mean of Alpha	GLCM Mean of Alpha	GLCM Mean of all bands	Standard Deviation of HH	Mean of Yamaguchi Odd Bounce	Standard Deviation of HV

5.1.2.3   General findings on single sensor feature selection

Feature selection based on single-sensor data produced some interesting trends. Similarly to the feature selection performed on the fused imagery, selection on the SPOT-5 features alone consistently ranked the NDVI, mean GLCM, and mean features as important. The geometric features were of little importance. Brightness was more important in the SPOT-5-only feature selection than the selection on fused imagery.

Beyond the top 10, feature selection on the SPOT-5 data for each image ranked features that were unique for that image and thus time of year. This result suggests that a few key features from specific dates may be useful for optimal class separability, which would be very useful when dealing with a multi-temporal data set. Figure 5.6 shows the SPOT-5-only features and their accumulated occurrence in the top 10 rankings for both algorithms over all four images. Features with a value of 4, such as the NDVI, were ranked in the top 10 for all four dates, whereas features with a value of 1 were ranked in the top 10 for a single-date. Certain features were important for class separation throughout the year, such as the NDVI, the mean values of red and green, and the textural mean of red and green. There thus exists a definitive set of features that must be included in single-sensor classifications and a second set of features that are useful only at certain times of year. This temporal trend was much stronger in the SPOT-5-only feature selection than the SAR-only feature selection.

Key
1: feature occurs in the top 10 rankings for one date
2: feature occurs in the top 10 rankings for two dates
3: feature occurs in the top 10 rankings for three dates
4: feature occurs in the top 10 rankings for all dates
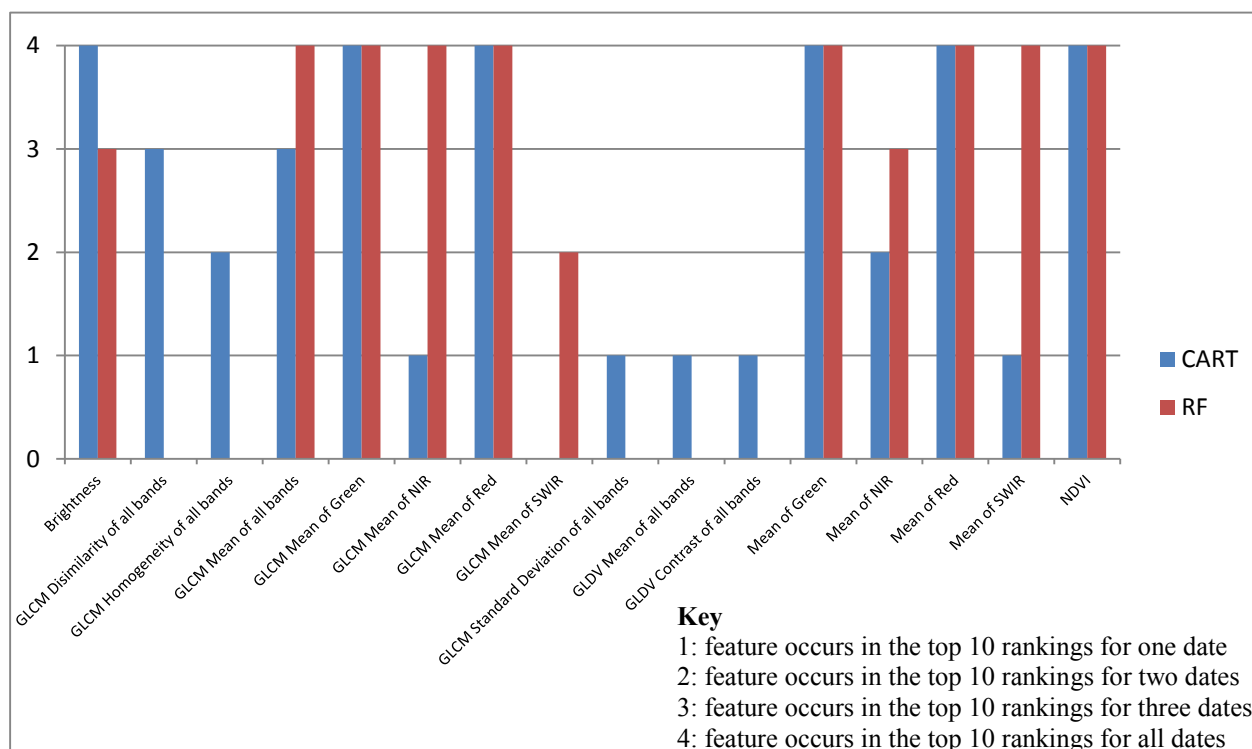
Figure 5.6 Frequency of occurrence of features in all four dates for optical-only data sets.

Feature selection performed on the SAR-only features showed less reliance on the texture measures than the fused data sets. However, the texture measures were still ranked more highly than in the SPOT-5-only feature selection. Feature selection on the SAR-only data resulted in more prominent use of the mean- and standard deviation-based features than selection on the fused data set. The time of year affected the reliance on backscatter-derived and polarimetric-derived features: earlier in the year, there was a greater reliance on the polarimetric features, for the 5 May date this changed completely to a heavy reliance (7 out of top 10) on backscatter-derived features for both algorithms. Later in the year, there was approximately equal reliance on the two sets of features. As in many previous studies, the use of backscatter-derived features alone was not sufficient for optimum class separation.

Figure 5.7 shows the occurrence of features in the top-10 SAR-only rankings for both algorithms across all four dates. The general trend is very different to that seen in the optical-only feature selection (Figure 5.6). As there were far fewer features in common across the rankings and thus far more features in total from all eight sets, only features that occurred in at least two top-10 rankings were included in the Figure 5.7. Far fewer features were included in the top-10 rankings for all four dates than in the optical feature selection. Only the mean textural feature produced from all bands was included in both algorithms' lists for all four dates. The time of year that a SAR image is acquired is therefore of great importance, as a different set of SAR features will better separate a set of classes as the seasons change. As the SAR feature selection did not offer a definitive set of features for use all year round, the optical data set must also be considered, regardless of the time of year.

Key
1: feature occurs in the top 10 rankings for one date
2: feature occurs in the top 10 rankings for two dates
3: feature occurs in the top 10 rankings for three dates
4: feature occurs in the top 10 rankings for all dates
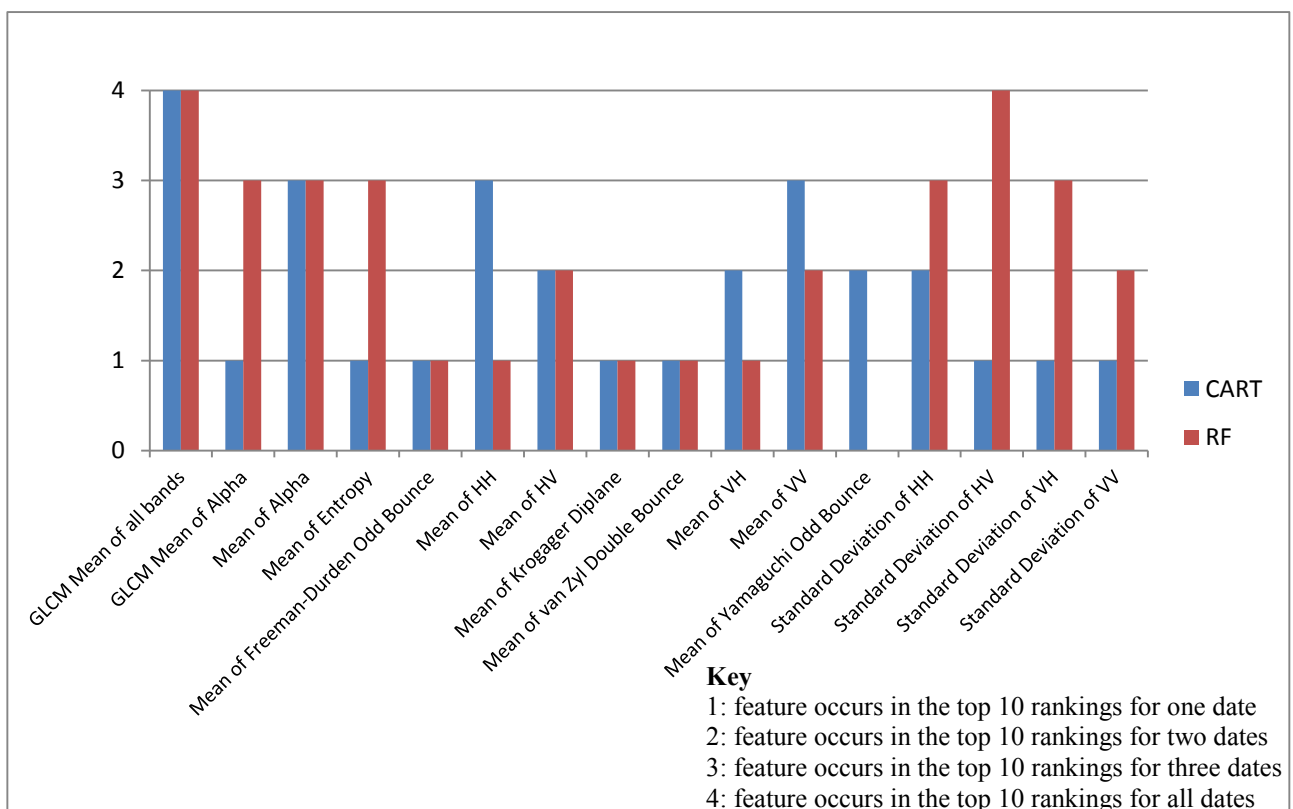
Figure 5.7 Frequency of occurrence of features in all four dates for SAR-only data sets.

5.1.3   Feature selection using multi-temporal data

Feature selection on all 638 of the features derived from all four image dates, and from both sensors, was performed using the RF feature selection algorithm. The geometry- and shape-based features were calculated and added to the feature data set once, as all of the image dates were segmented using the same set of objects. The brightness and maximum difference features were derived for each date and an NDVI layer was calculated for each image. Once again, the features were ranked by their importance score. The full rankings of all features can be found in APPENDIX B, with Table 5.4 showing just the 20 highest ranked features, colour coded by the image date the features were derived from, for ease of interpretation.

Table 5.4 Top 20 ranked features, based on the RF feature selection algorithm, on the multi-temporal, combined SAR-optical data set, colour coded by date.

Ranking	Feature	Importance Score (out of 100)
1.	2014-02-22 GLCM Mean of Green	100.0
2.	2014-08-09 Maximum Difference	75.3
3.	2014-02-22 GLCM Mean of Red	72.0
4.	2014-02-22 NDVI	68.0
5.	2014-05-29 GLCM Mean of Green	66.4
6.	2014-08-09 Mean of Red	64.6
7.	2014-02-22 GLCM Mean of NIR	61.5
8.	2014-08-09 NDVI	59.9
9.	2014-05-29 Standard Deviation of VH	59.7
10.	2014-08-09 GLCM Mean of all bands	57.2
11.	2014-08-09 GLCM Mean of Green	56.7
12.	2014-05-29 GLCM Mean of Red	56.0
13.	2014-08-09 Brightness	55.2
14.	2014-02-22 Mean of Red	52.8
15.	2014-05-05 Brightness	52.2
16.	2014-02-22 Mean of Green	52.1
17.	2014-02-22 Standard Deviation of VV	51.7
18.	2014-08-09 Mean of Green	50.9
19.	2014-05-29 Mean of Red	49.4
20.	2014-05-05 Mean of Green	49.2

The features from the 2014-02-22 and 2014-08-09 images dominated the top 10, 20, 30, 40, 50 and 60 lists: 40 of the top 60 features were generated from just these two image dates, as seen in Figure 5.8. This

result supports the premise that certain dates will be more useful in separating land cover classes than other dates. These two images may have provided the highest contribution because they were acquired six months apart, thereby accounting for most of the temporal variance in the study area.
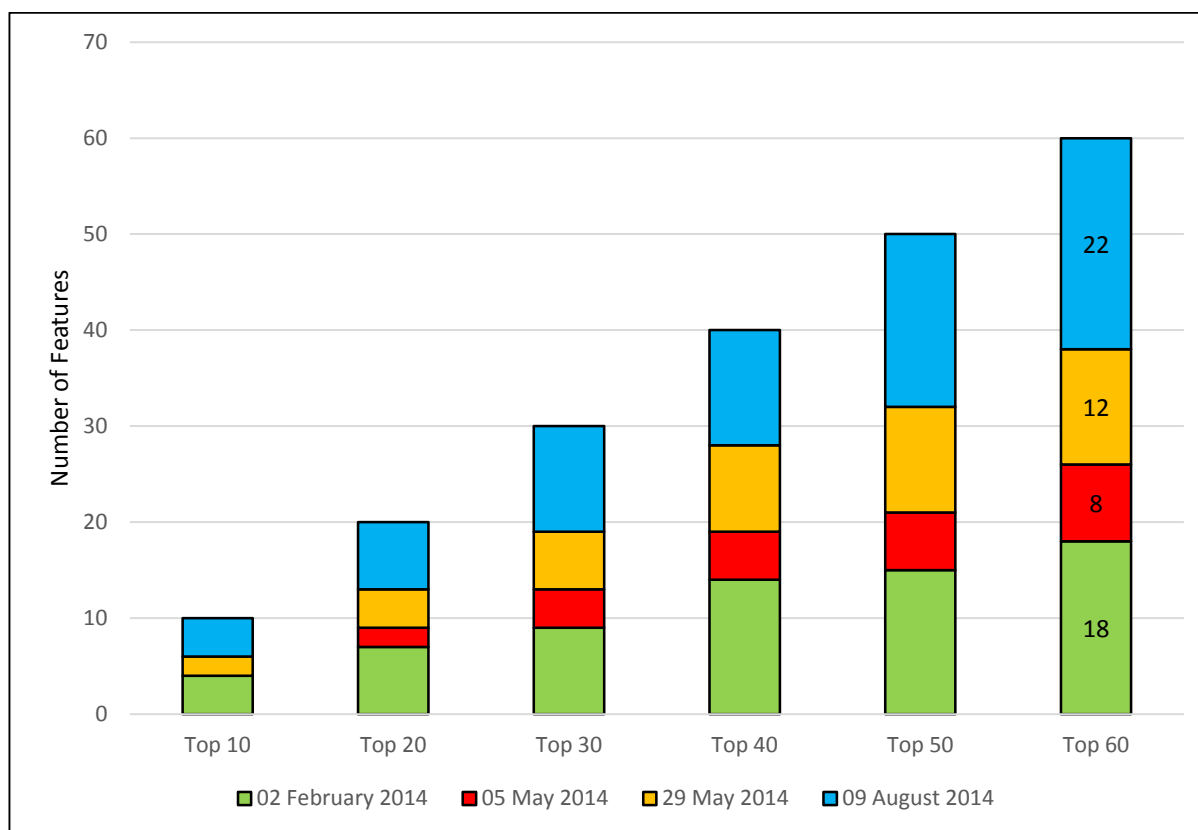
Figure 5.8 Frequency of occurrence of features from each image date found in the top rankings of the RF feature selection performed on the multi-temporal combined SAR-optical data set.

Two NDVI layers were ranked in the 10 most important features, pointing to the need for vegetation indices from different times of the year when attempting to classify land covers containing multiple vegetation classes. These features were also derived from the 22 February and 9 August image dates, further supporting the importance of these two dates in the multi-temporal data set. The top-ranked SAR-derived feature was the standard deviation of the VH layer from 29 May, which was ranked ninth. The SAR-derived features were generally not considered to be the most important, with only one ranked in the top 10, two in the top 20 and three in the top 30. However, four more SAR-derived features were added in the next set of 10, bringing the total to seven in the top 40. As the highest classification accuracies arose when using more than 30 features (Section 5.4), optical-based classification accuracies are likely to benefit from the addition of SAR features, despite their low prevalence. The added SAR-based features were predominantly derived from the mean of the and standard deviation of backscatter bands and the mean of the alpha and various double bounce layers, and provided information about the physical structure of the land cover, not just the chemical structure that is provided by reflectance. These physical features enhance the classification and improve class separability, as will be discussed in detail in Section 5.3.

The importance of the NDVI, textural mean features, and Green and Red bands was reiterated in the feature selections performed on fused data sets from single images. Unlike the SAR-only single-date feature selection, the top-ranked features were primarily backscatter-derived. The polarimetric features only entered the rankings from the mid-20's onwards.

5.2   EXPERIMENT 2: SELECTING A CLASSIFICATION ALGORITHM

A classification algorithm that could handle the high dimensionality of the overall data set and the often non-normal nature of the SAR data was required for the classifications tested in Experiments 3 and 4. To inform this choice and not base it solely on literature, a comparison was done to determine the best-performing classification algorithm based on overall and class-specific accuracies.

Six supervised classifiers were tested using two image dates to determine the classifier that performed best on the Réunion data set. Two dates (5 May and 8 August) were used to ensure a conclusive decision was made that was not biased by the possible variability from using a single image. All of the classifiers were trained with the same set of 208 features derived from the combined SAR and optical image data set and were run using their default settings.

The standard available classification algorithms in eCognition 9.0.3 were used namely SVM, decision tree, RF, K-means nearest neighbour, and Bayes maximum likelihood (ML) classifiers. A CART classification was also tested, based on the decision tree produced in Salford Systems and translated into a rule set in eCognition 9.0.3.

The aim for this experiment was not to produce the best possible classification, but rather to assess the relative performance between classifiers.

This results section presents and discusses the overall performances, judged by accuracy, for each classifier. It then goes into the detail of the class-specific accuracies. A brief discussion focusing on the differences between the classifications produced from the two image dates is also provided. All confusion matrices can be found in APPENDIX C.

5.2.1   Overall performance

All six classifiers produced consistent overall accuracies (Figure 5.9) and Kappa values (Figure 5.10) for the two image dates for most of the classes. The RF classifier outperformed the other classifiers on both image dates and it was the only classifier to achieve an overall accuracy above 65% for both dates and a kappa value of over 0.6. These results show that the RF algorithm can deal with a large number of features. The RF classification for the 5 May date is presented in Figure 5.11.
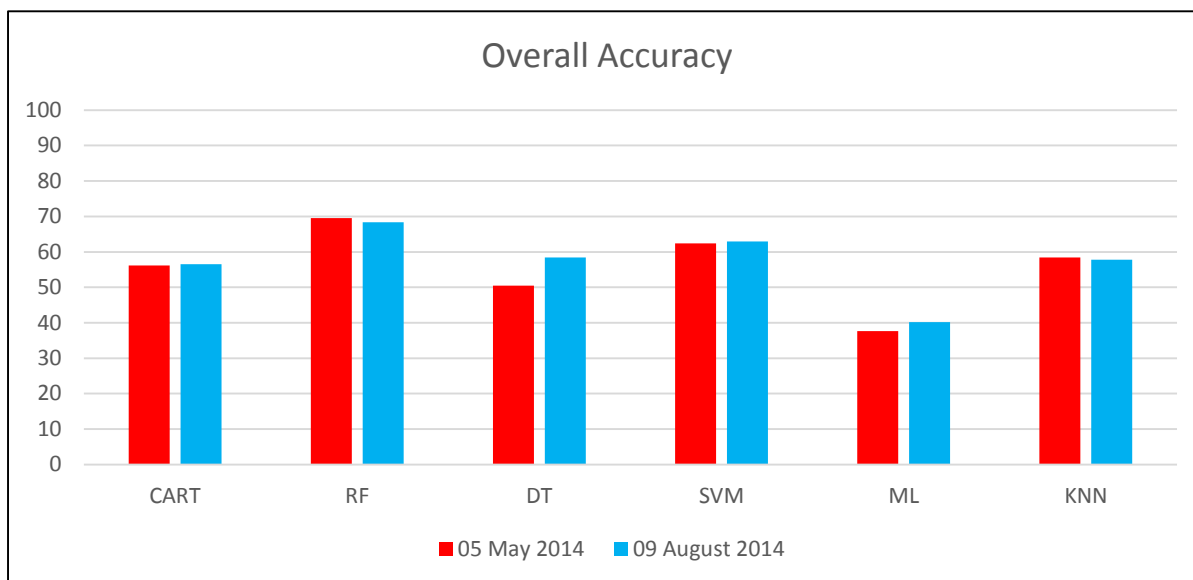
Figure 5.9 Overall accuracy percentages achieved for both image dates by each of the classification algorithms.
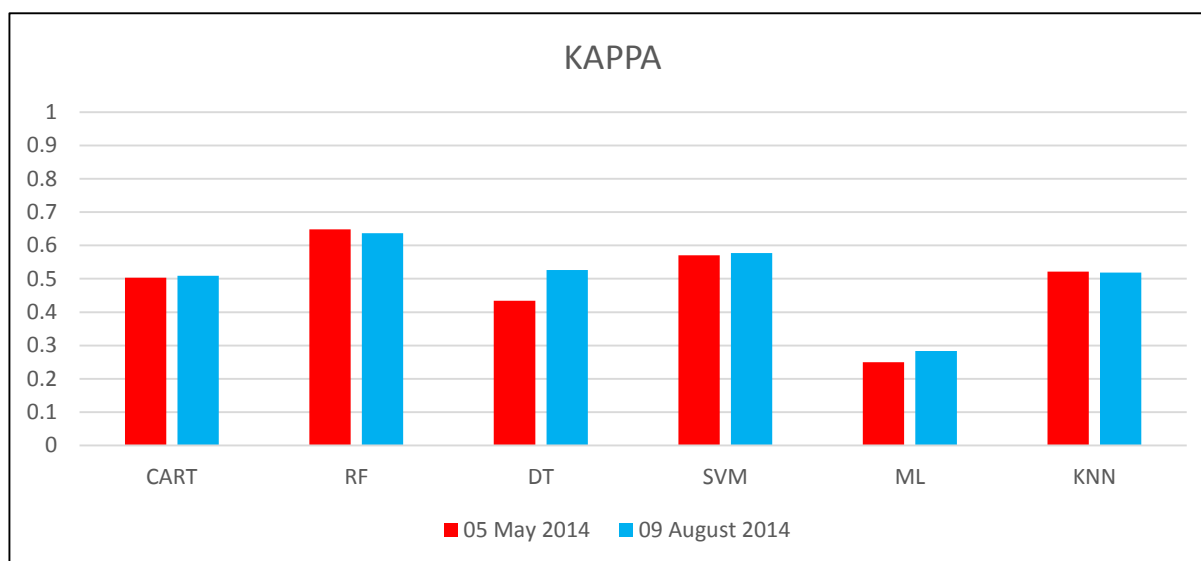
Figure 5.10 Kappa values achieved for both image dates by each of the classification algorithms
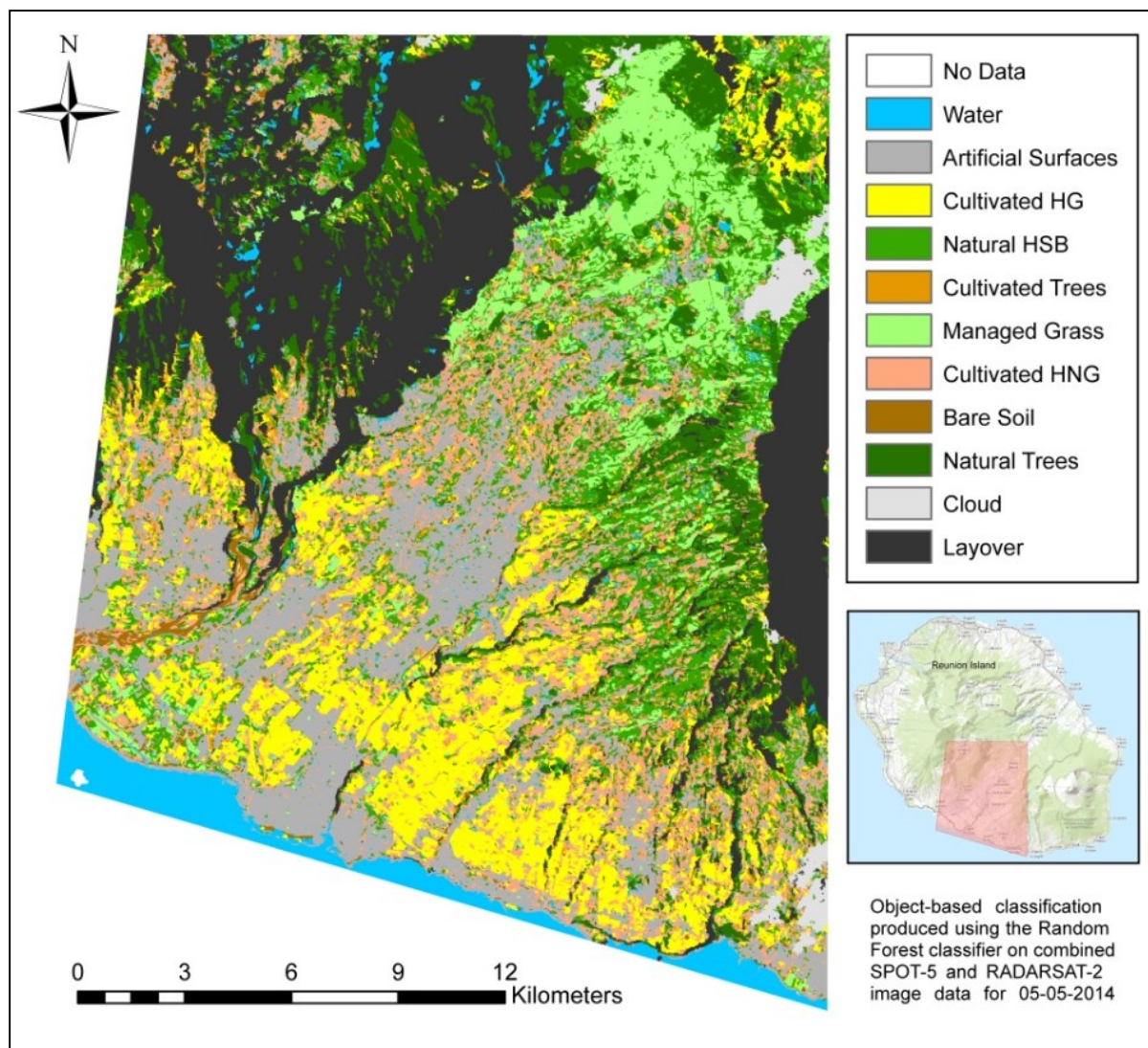
Figure 5.11 Classification produced using the RF classifier for the image date 2014-05-05 on the combined SAR-optical data set.

In contrast, the ML classifier gave consistently poor accuracies and kappa values for both image dates (Figure 5.9 and Figure 5.10). The ML classifier is known to be negatively affected when trained with very large feature data sets that are much larger than the number of training samples, such as that used here. The classifier also assumes that a Gaussian probability exists for the data. As this is generally not the case with SAR data (McNairn et al. 2009) and this assumption may also have caused the poor performance. Figure 5.12 shows the ML classification for the 5 May date using combined SAR and optical features. The majority of the study area was clearly misclassified. Most of the region was classified as Cultivated Herbaceous Non-Graminoids, when in reality this class covers a relatively small area.
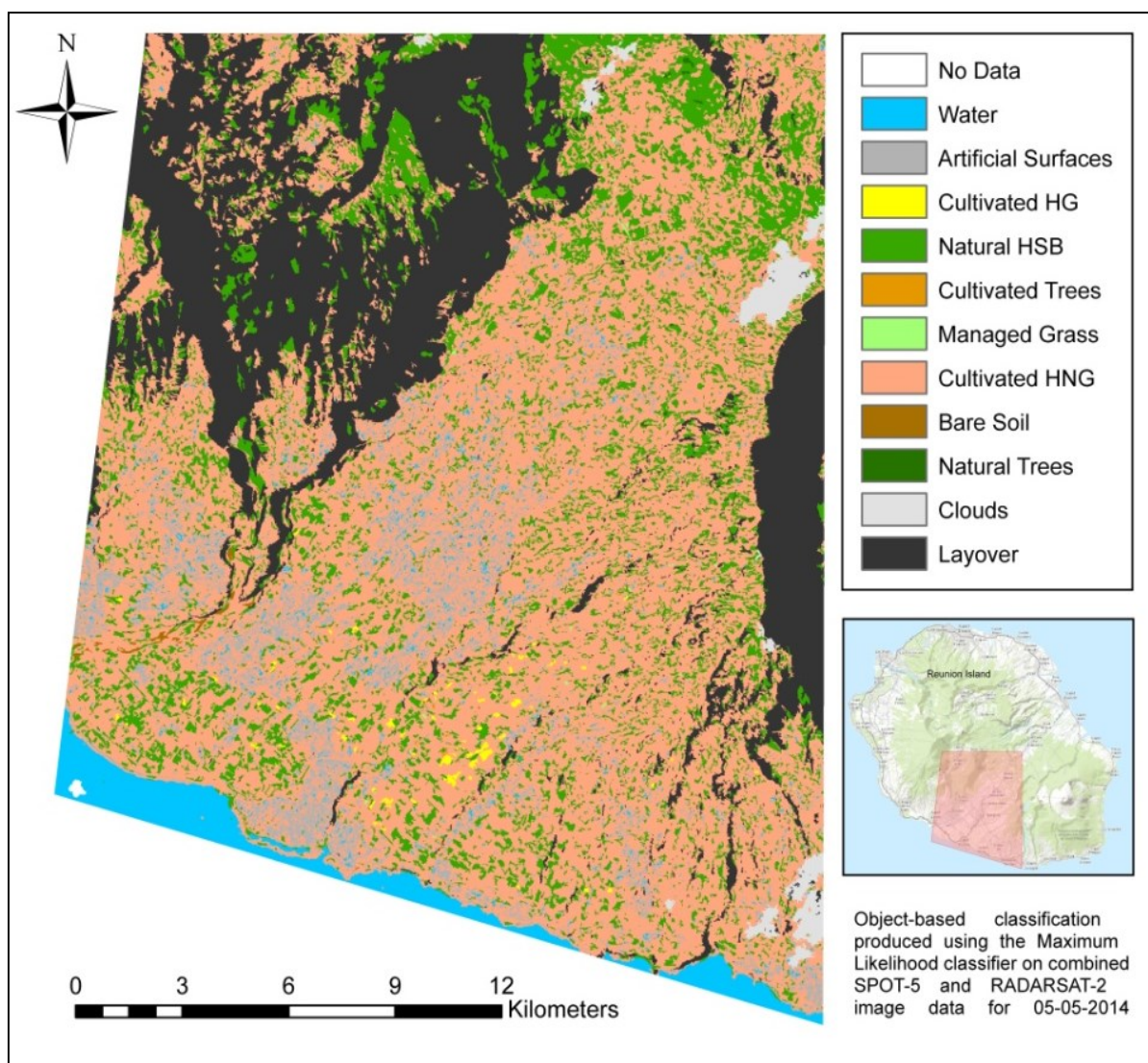
Figure 5.12 Classification produced using the ML classifier for the image date 2014-05-05 on the combined SAR-optical data set.

The SVM classifier performed second best, producing overall accuracies above 60% for both dates (Figure 5.9). This result was not surprising as SVM is known to cope well with large feature sets and has been shown to outperform classifiers such as ML and Nearest Neighbour (Myburgh & Van Niekerk 2014). SVM is a good alternative to the RF classifier.

5.2.2   Class-specific performance

It is important to not only consider overall accuracies, but class-specific accuracies as well. A classification producing an acceptable overall accuracy may not necessarily classify all individual classes adequately.

All six classifiers classified the Cultivated Trees class poorly, yielding exceptionally high (consistently more than 50%) error of omission and commission (Figure 5.13). This class was represented by the fewest

number of training objects (17) and included mango orchards and banana trees, so was likely to exhibit a similar physical appearance to some natural ravine vegetated areas and a similar canopy to natural trees. These similarities with other vegetation classes could have caused the confusion. The textural and geometric characteristics from these objects can also mimic Cultivated Herbaceous Non-Graminoids, creating confusion between all of these classes. Natural and cultivated trees have similar physical and chemical structures, promoting confusion between these two classes. All of the classifiers exhibited a higher producer's accuracy and thus a lower error of omission for Cultivated Trees in the August image date than the May date. The August training data were collected nearer to the August image acquisition date than the May date, which may have driven this discrepancy.
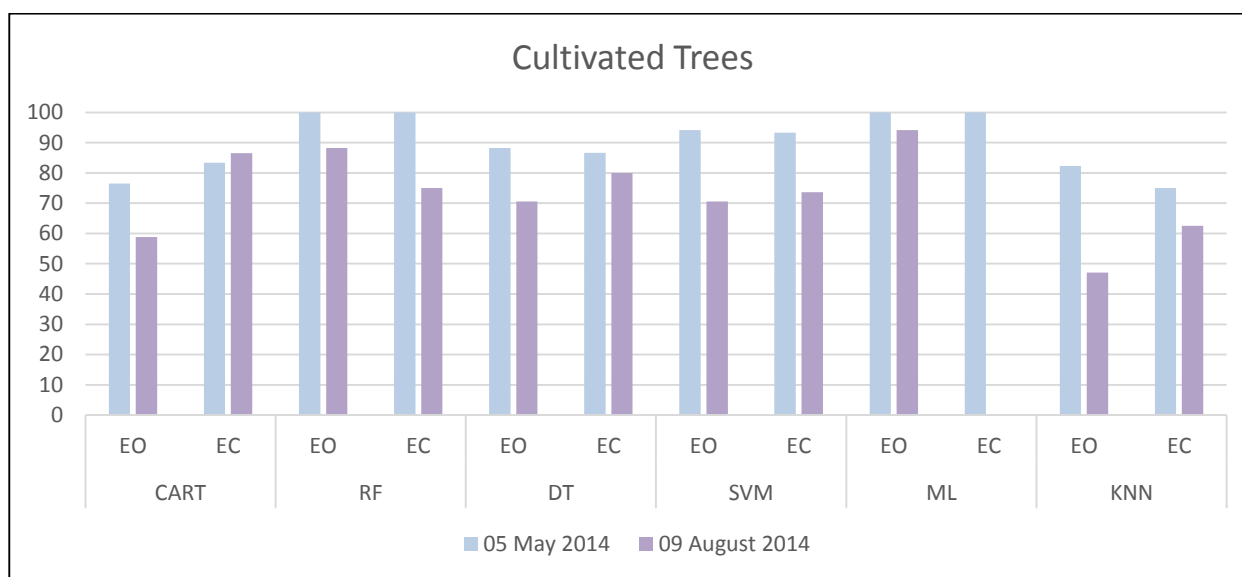
Figure 5.13 Error of omission (EO) and error of commission (EC), in percentage, for each classifier for the land cover class Cultivated Trees

The ML classifier produced an exaggerated user's accuracy and corresponding much lower producer's accuracy for multiple classes, as can be seen in the confusion matrix presented in Table 5.5. With a 0% error of omission for Cultivated Trees and high errors of commission for other classes, the majority of the objects were misclassified into the Cultivated Trees class.

Table 5.5 Confusion matrix for the classification produced on the combined SAR-optical data set for the 2014-08-09 image date using the ML classification algorithm.

		Classification Image										
		Artificial Surfaces	Bare Soil	Cultivated HG	Cultivated HNG	Cultivated Trees	Managed Grass	Natural HSB	Natural Trees	Water	Grand Total	Producer's Accuracy (%)
Reference Image	Artificial Surfaces	21			20						**41**	51
	Bare Soil		7		23						**30**	23
	Cultivated HG			3	29			7			**39**	8
	Cultivated HNG				55			9			**64**	86
	Cultivated Trees				15			2			**17**	0
	Managed Grass			1	21			10			**32**	0
	Natural HSB				34			23			**57**	40
	Natural Trees				11			15			**26**	0
	Water				20			2		23	**45**	51
	Grand Total	**21**	**7**	**4**	**228**	**0**	**0**	**68**	**0**	**23**	351	
	Users Accuracy (%)	100	100	75	24	0	0	34	0	100		
	Overall Accuracy	**38%**										
	Kappa	**0.25**										

The error of omission and commission for each class were averaged across both image dates and all six classifiers and displayed in Figure 5.14. The Artificial Surfaces, Bare Soil, and Water classes were consistently accurately classified, scoring an average error of approximately only 30% or less for both the error of omission and commission. They showed little fluctuation as the classifier changed, except when the Maximum Likelihood classifier was used. These classes therefore appear to be more robust to the time of year and classifier used than the vegetation classes.
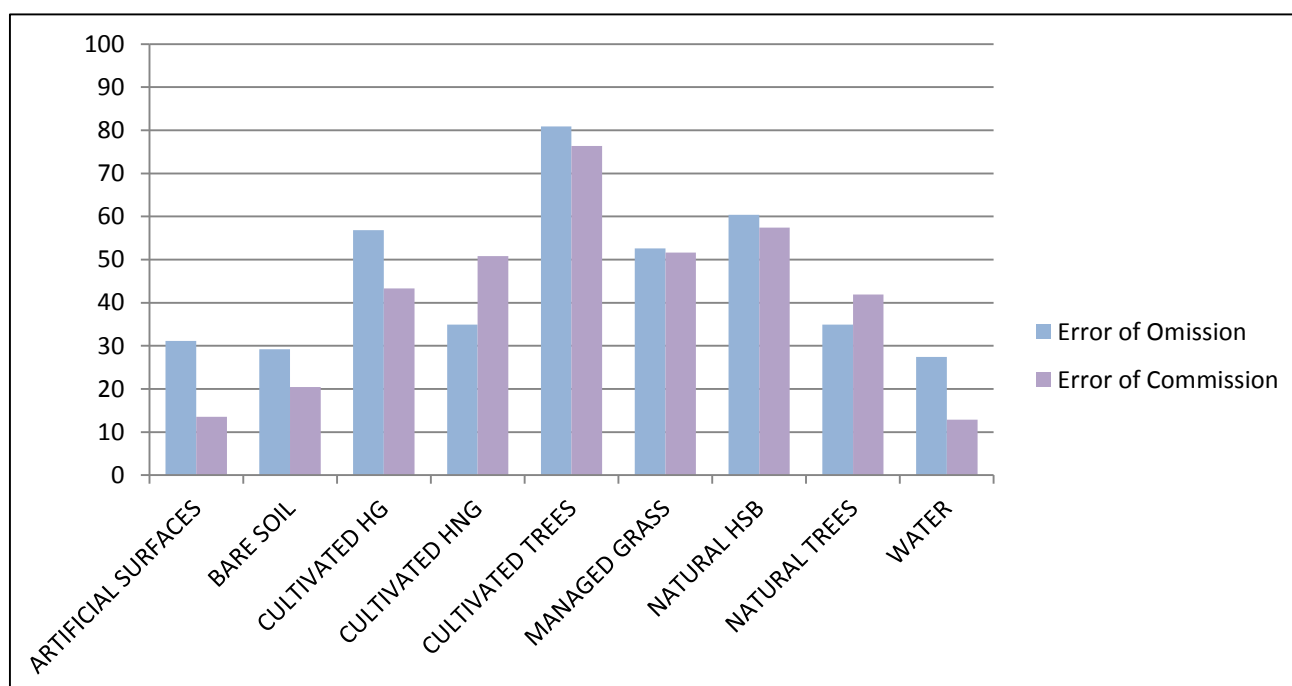
Figure 5.14 Averaged error of omission and commission (%) for each land cover class calculated using both image dates and all six classification algorithms

5.2.3   Choosing a classifier

Taking into account the overall accuracy, consistency between image dates, and class-specific accuracies, the classification algorithms did not perform equally. The RF classification algorithm produced the highest overall accuracy and kappa value for both image dates and showed consistency between the two dates. The class-specific performance of all six classifiers highlighted potentially problematic classes, such as the Cultivated Trees class, which were considered when assessing the classifications produced in Experiments 3 and 4.

As the RF classifier was shown to handle large feature data sets, as is in the case with this multi-temporal, dual-sensor study, and to have acceptable accuracies in this test classification, it was used in the classification comparisons in Experiments 3 and 4, the results of which are presented next in Sections 5.3 and 5.4.

5.3   EXPERIMENT 3: SINGLE-DATE CLASSIFICATIONS

The aim of Experiment 3 was to assess whether dual-sensor imagery yielded improved classification results over single-sensor imagery. The overall classification accuracy and class-specific accuracies were assessed. Four image dates spanning a six-month period were tested to allow more general conclusions and to identify any seasonality trends.

An optical-SAR fused classification, SAR-only classification, and optical-only classification were performed on each image date (2014-02-22, 2014-05-05, 2014-05-29, and 2014-08-09) using the RF classification algorithm chosen in Experiment 2 (Section 5.2). No feature reduction was performed so that the classifications performed on the four different dates could be directly comparable as they were trained using the exact same set, and number, of features. The classifier was trained with all 208 features in the fused classification, 88 features in the optical classification, and 149 features in the SAR classification. The classifications were assessed with cognisance of the feature selection and CART decision trees produced in Experiment 1 (Section 5.1) in order to better understand the potential seasonal variations in the classification accuracies due to key features for class separability for the different dates.

This results section will first compare the fused classifications with the single-sensor classifications, across all four dates in Section 5.3.1. The best classification, 29 May 2014, will then be examined in more depth in Section 5.3.2 in order to note class-specific changes based on the use of dual-sensor imagery. Finally, the temporal trends across the four dates will be presented and discussed in Section 5.3.3. All confusion matrices can be found in APPENDIX C.

5.3.1 General comparison of fused vs. single-sensor classifications

On all four dates, classifications with higher overall accuracies (Figure 5.15) and kappa values (Figure 5.16) were produced when using the fused data set than when using either SAR data or optical data alone. This result corroborates the hypothesis that fusing dual-sensor imagery will produce a higher quality classification.
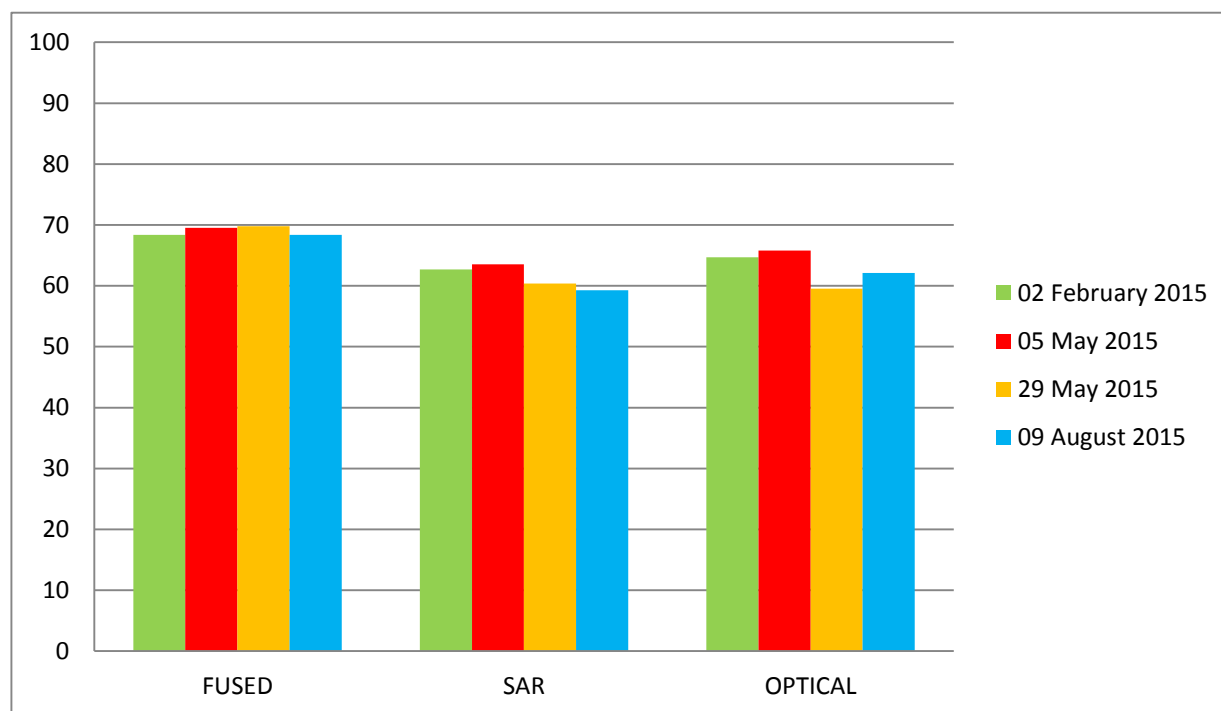
Figure 5.15 Overall accuracies achieved by the RF classifier, for all four separate dates, based on the fused, SAR and optical data sets.
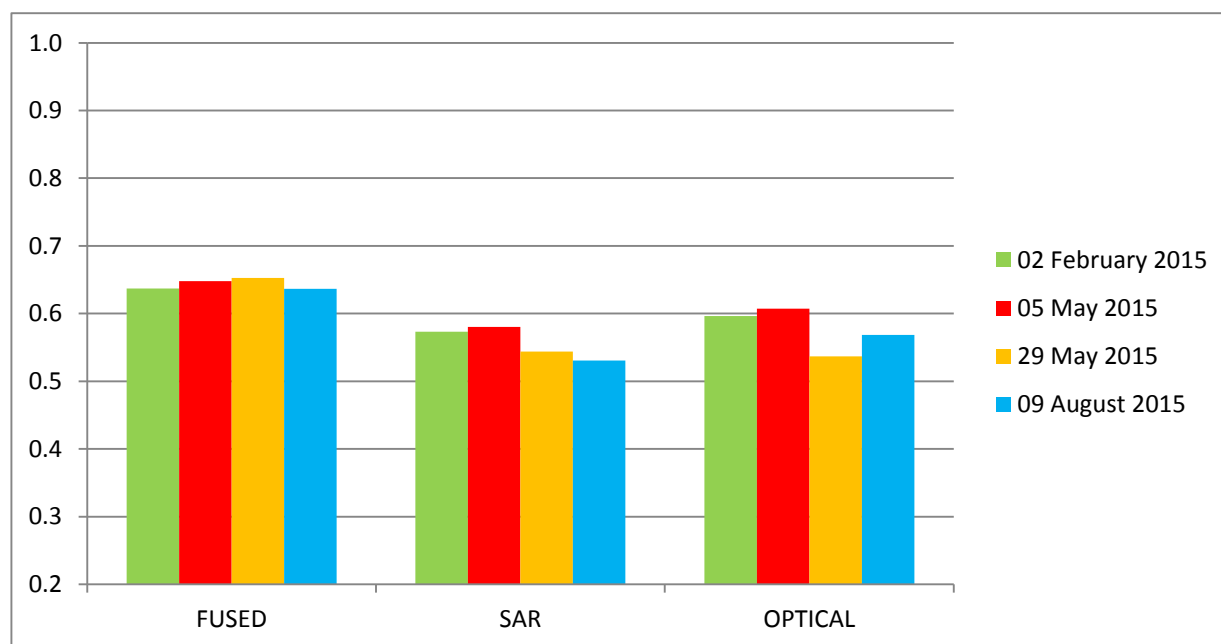
Figure 5.16 Kappa values achieved by the RF classifier, for all four separate dates, based on the fused, SAR and optical data sets.

The accuracies were generally lower than expected. However, the focus was on how the fused imagery performed relative to the single-sensor imagery. Although the low accuracies are not ideal for methodology replication, they do not prevent the clear benefits of using fused imagery over single-sensor imagery from being evident.

The fused data sets produced more consistent results, as measured by both overall accuracy (Figure 5.15) and kappa (Figure 5.16) across the four image dates than either single-sensor data set. The optical-only data set showed a drop in accuracy and kappa for the two later image dates, especially the 29 May image. However, this drop did not affect the fused data set, which recorded the highest accuracy of any classification (69.8%) on the 29 May image. This result echoes what was found in Experiment 1 (Section 5.1), where SAR-based features were ranked more highly in the later images. These two sets of results show that when a single sensor is not sufficient to accurately differentiate between land cover classes during a specific time of year, adding a complementary data source, in this case SAR imagery, can help to maintain classification quality and consistent results.

In the drier winter months, vegetation shows a more generalised reflectance response, which makes it difficult to separate the different vegetation classes with optical imagery alone. Adding SAR data containing information about the physical characteristics of the ground targets can improve class separation and allow a superior classification on fused imagery to be produced. The improvements made in each class by using fused imagery is discussed in the following section. This follows with the recommendations by Kellndorfer and Pierce (1998) who suggest an image acquired in the drier months for single-date land cover classifications.

5.3.2 29 May 2014 classification: Class-specific analysis

Of the four fused classifications, the 29 May 2014 date produced the best classification, with an overall accuracy of 69.8%. This classification was used to investigate class-specific performance in detail. The fused, optical-only, and SAR-only classifications for 29 May 2014 are shown in Figure 5.17 and Figure 5.18, respectively.
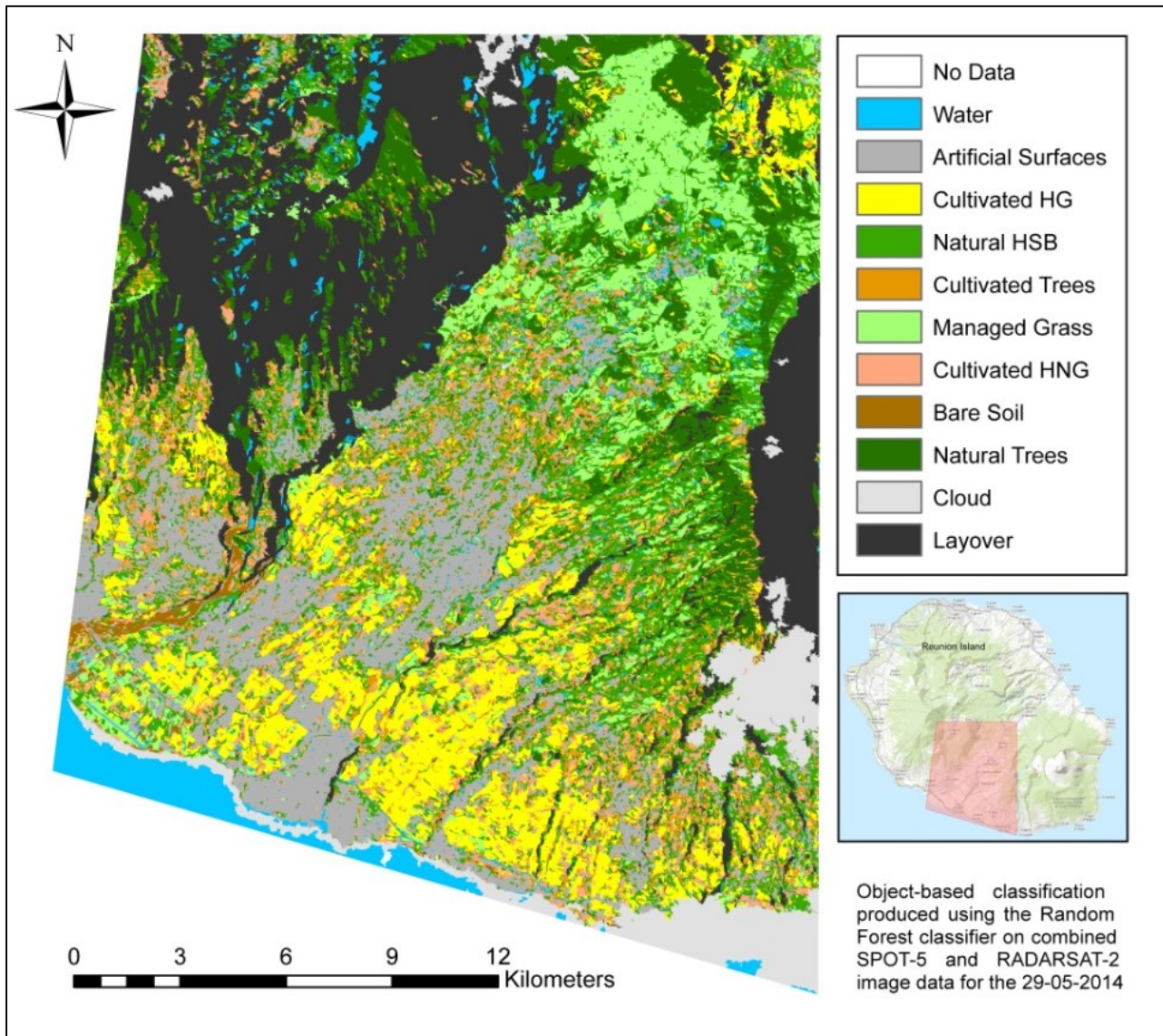
Figure 5.17 Classification produced using the RF classifier on combined SAR-optical 2014-05-29 image data.
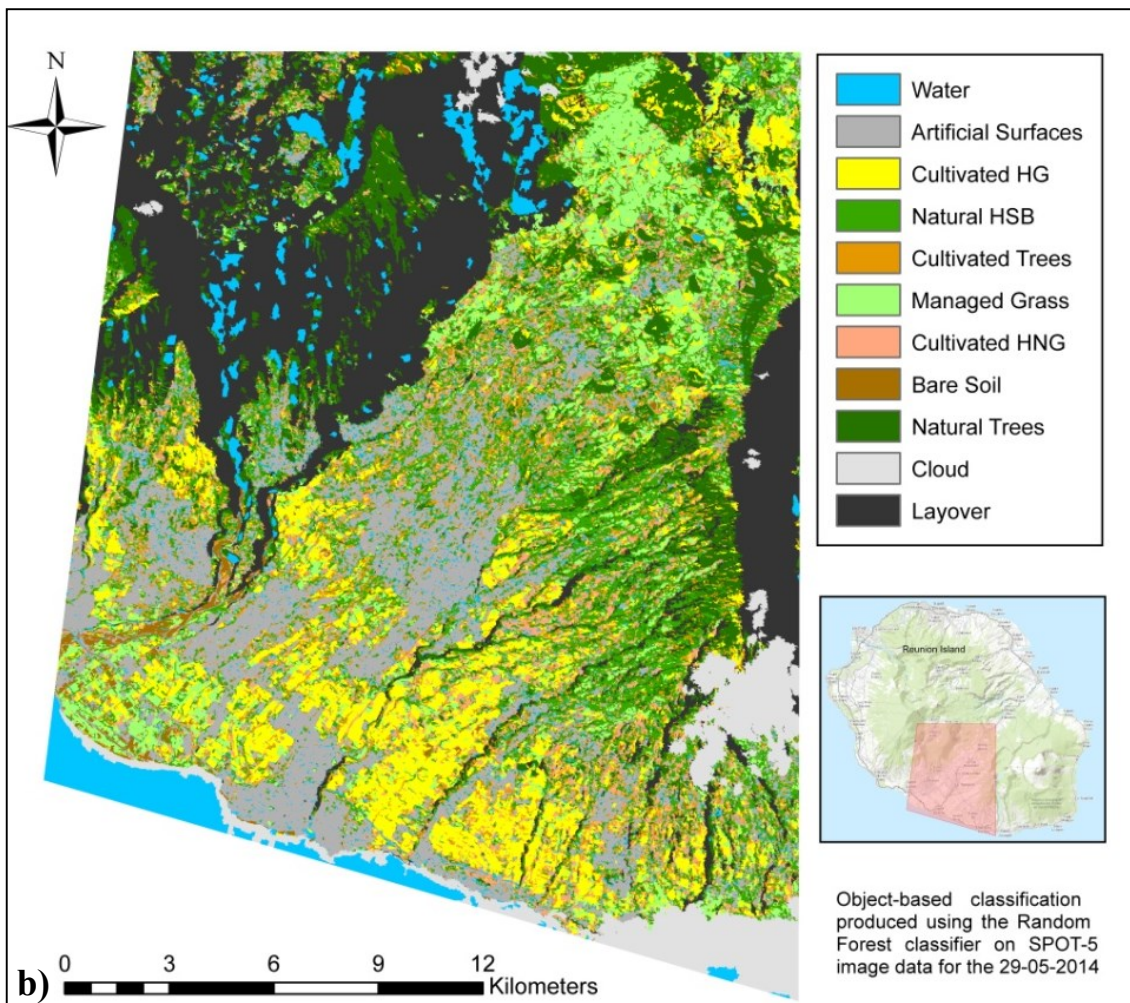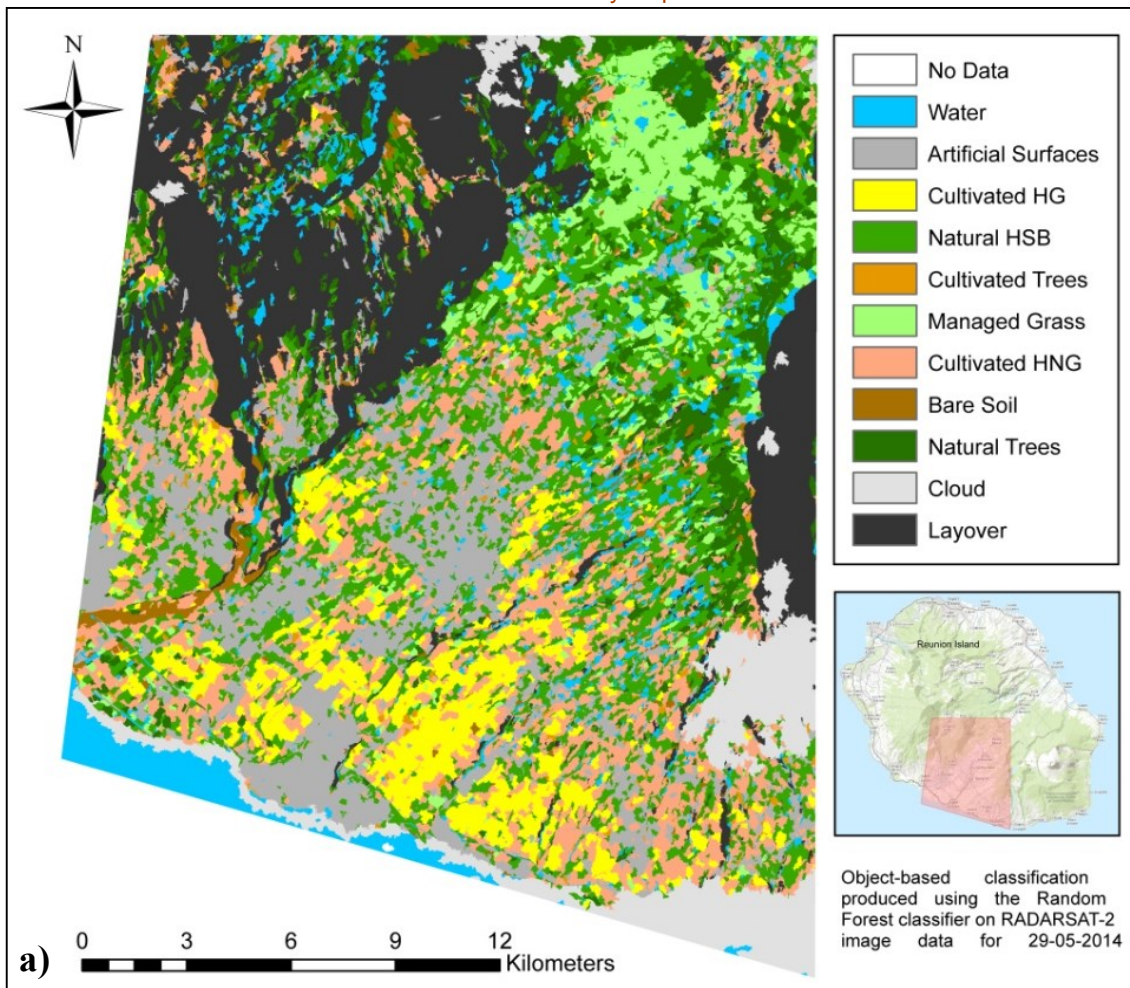
Figure 5.18 Classifications produced using the RF classification algorithm on the a) SAR-only and b) optical-only data for the 2014-05-29 image date.

The confusion between grasslands (Managed Grass) and sugarcane (Cultivated Herbaceous Graminoids) was noted, especially in the optical-only classification. This shows similarities with the findings of Adams et al. (2014) where mature sugarcane was confused with grasslands in a coastal region using the RF classifier. The confusion was however reduced in the fused classification, showing that the introduction of SAR features, and thus information based on physical properties, help to better separate these two particular vegetation classes.

Figure 5.19 and Figure 5.20 show the error of omission and commission for each land cover class in the fused, optical-only, and SAR-only classifications, respectively. The dashed line represents the 40% error mark, which is considered here as a useful threshold for error percentages beyond which outliers can be identified. In the fused classification, two classes exhibited outlying, large errors of omission and commission. The Natural Herbaceous Shrubs and Bushes (mid green) and Cultivated Trees (orange) classes both had large error percentages for both omission and commission, showing that they were misclassified into other classes and that other classes were misclassified into them, respectively. These two classes were thus weakly separated. The Cultivated Trees class was also problematic in Experiment 2. The relatively small (17 objects) training sample and the mixed types of vegetation present in this class could have been the main reasons for these poor accuracies. Natural Herbaceous Shrubs and Bushes also contains a variety of natural vegetation types that are likely to display similar physical and chemical properties to other vegetation classes, which may have driven the omission and commission errors of nearly 60%.
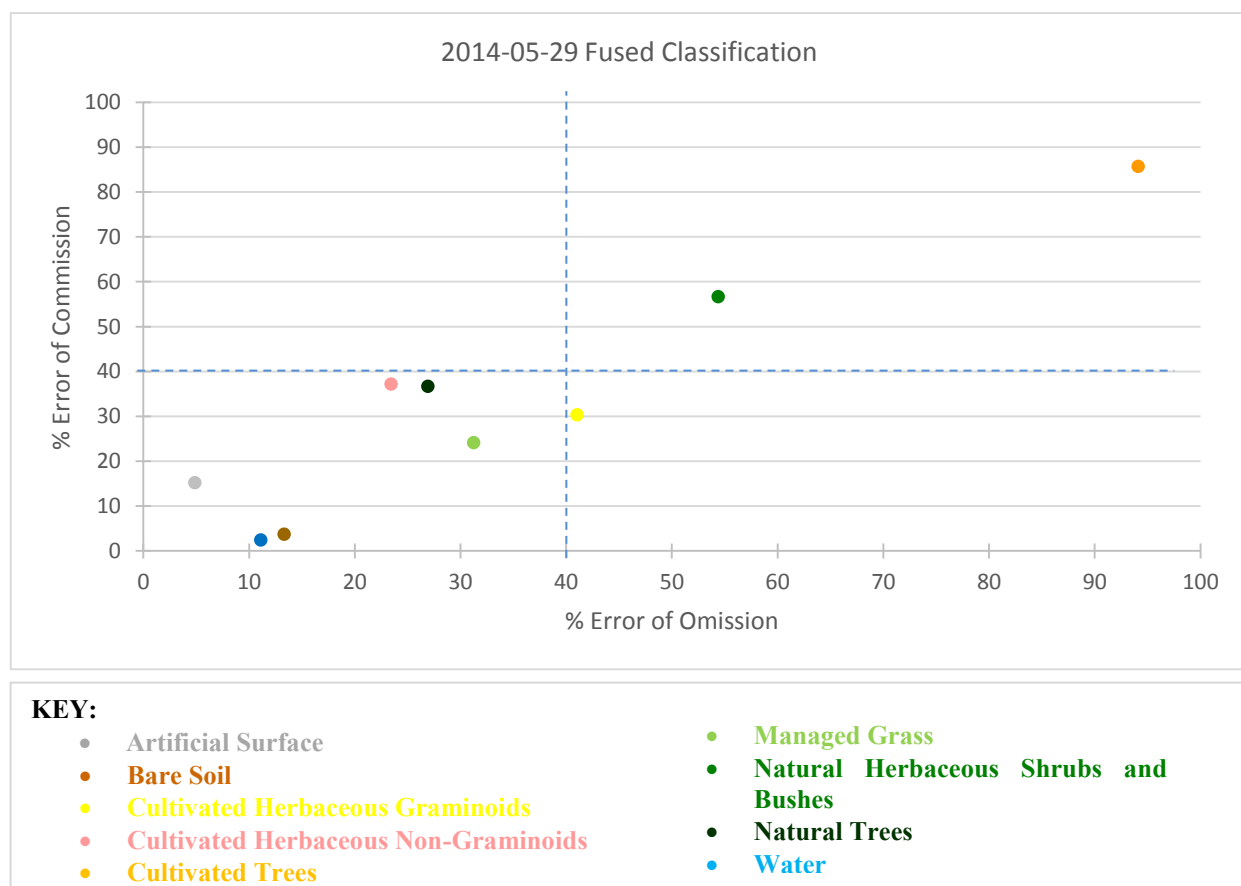
Figure 5.19 Error of omission and commission plotted for each land cover class, based on the combined SAR-optical 2014-05-29 classification.
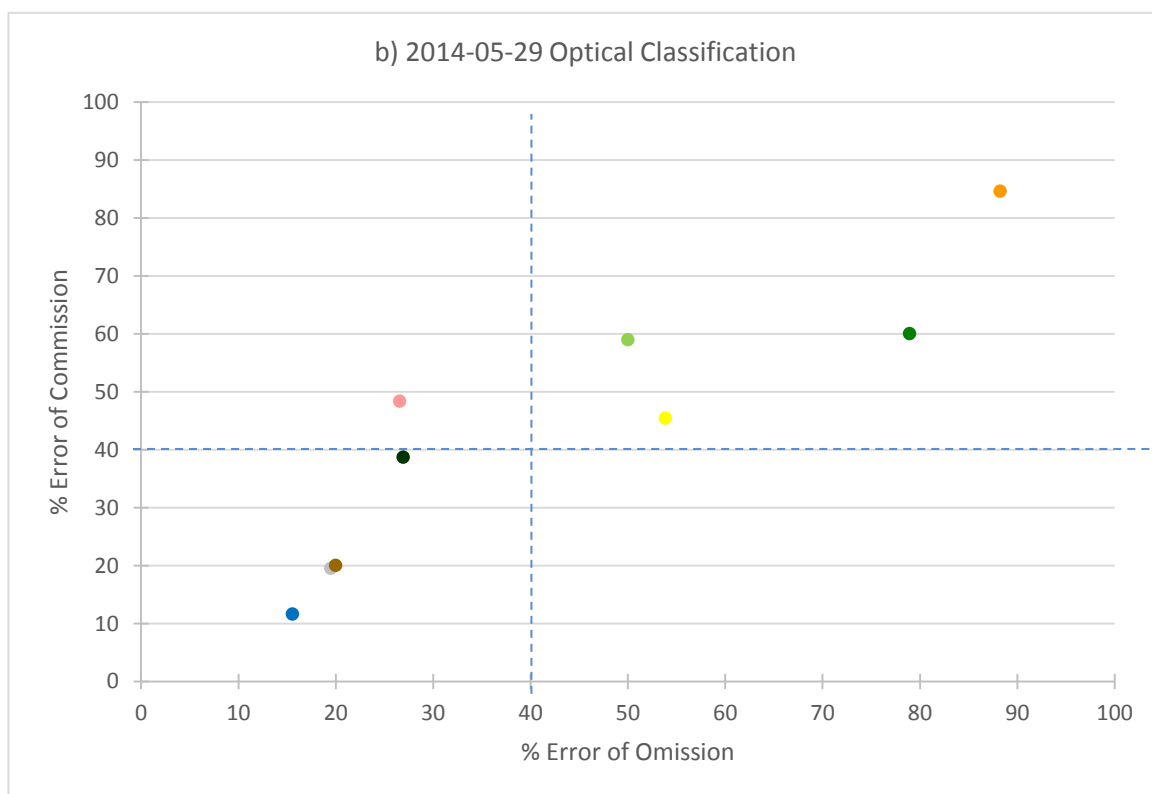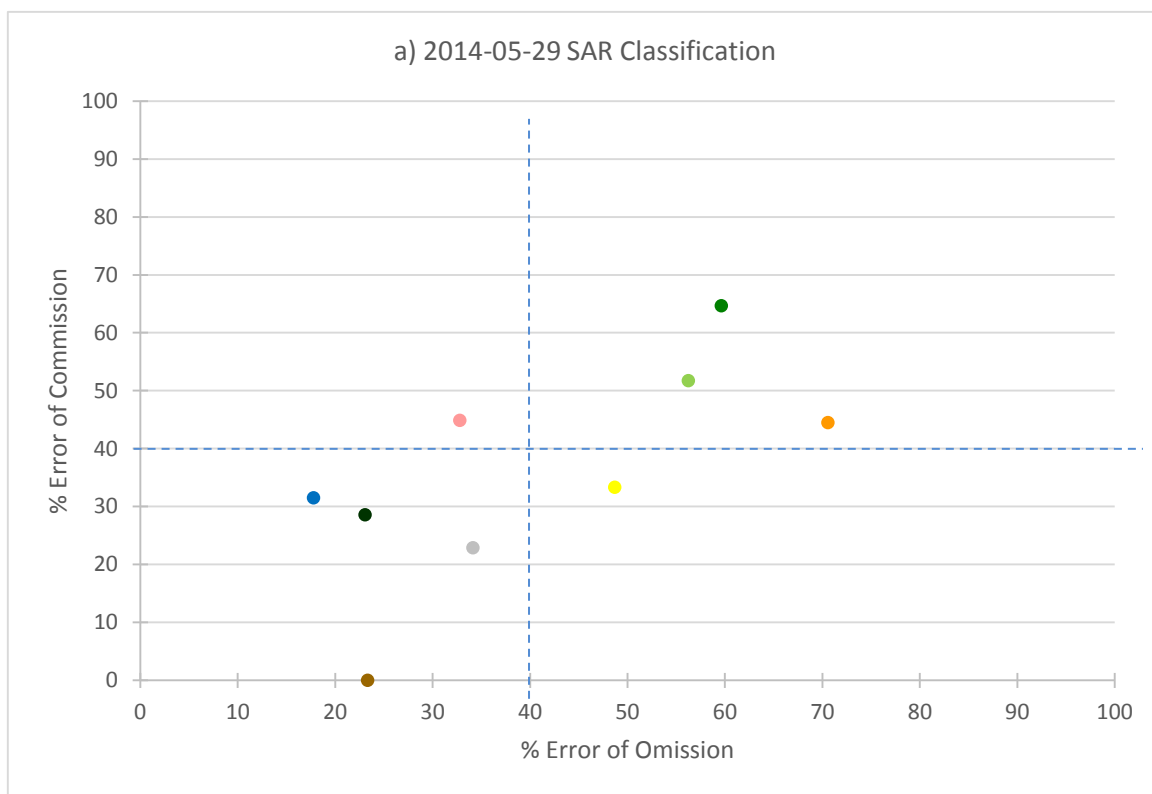
Figure 5.20 Error of omission and commission plotted for each land cover class, based on a) the SAR-only and b) the optical-only 2014-05-29 classifications.

Figure 5.20 clearly shows that both single-sensor classifications performed much worse on a class-wise basis than the fused classification (Figure 5.19). Outlying classes are those found in the right hand top quadrant of the graph, with errors over 40%. Instead of only two outlying classes, the SAR-only classification had three outlying classes and the optical-only, four. Both single-sensor classifications separated the Managed Grass (light green) class poorly. The optical-only classification also failed to clearly delineate the Cultivated Herbaceous Graminoids (sugarcane in yellow) class. Both single-sensor classifications exhibited a higher error of commission for the Cultivated Herbaceous Non-Graminoids (coral) class than found in the fused classification. This class was expected to be difficult to classify as it comprises a mixture of vegetation types such as pineapple fields and strawberries; vegetation with largely varying physical and chemical structures. The Cultivated Herbaceous Non-Graminoids class was over-commissioned when classified using a single data type, lowering the user's accuracy of the final classification. The C-band SAR imagery was expected to discriminate the vegetation classes better than was found as this wavelength has been successfully used in past studies for crop detection (Baghdadi et al. 2009; Shang et al. 2009). Although the SAR-only classification did produce lower errors of omission and commission for the Cultivated Trees and Cultivated Herbaceous Graminoids classes than the optical-only classification, the errors were still above 40% and thus higher than what is acceptable for successful class separation.

The fused classification exhibited the lowest error of omission for seven of the nine land cover classes, and lowest error of commission for five of the nine classes, in comparison with the single-sensor classifications performed on the same date (APPENDIX C). The complementary nature of the SAR and optical imagery thus allowed the fused classification to better separate problematic classes better, especially easily confused vegetation classes, as they offered a combination of physical (SAR backscatter) and chemical-based (reflectance) information.

5.3.3   Temporal changes across the four dates

This section assesses temporal patterns in the fused classifications produced across the four image dates. As the use of fused data for classifying the Réunion study area was validated by the overall and class-wise accuracies in Sections 5.3.1 and 5.3.2, any temporal pattern found can be considered useful.

Figure 5.22 shows the percentage error of omission plotted against the percentage error of commission for each land cover class for the four fused classifications. Overall, the majority of the classes showed stable error percentages across the four image dates, with little variation. This result is supported by Figure 5.23, which shows the standard deviation of the user's and producer's accuracies for each land cover class across the four image dates. However, the Cultivated Trees class had a standard deviation of just over 10% for both the producer's and user's accuracy, showing that this class was the least stable across the four dates. As already mentioned, the Cultivated Trees class was the most problematic class with the highest errors of omission and commission. As it performed poorly for all image dates, the problem was more likely to be the result of incorrect training than seasonality. This class will thus not be discussed further when looking at temporal patterns.

There were micro patterns present in the smaller variations in the errors of omission and commission for each class. The non-vegetation classes (Artificial Surfaces, Water, and Bare Soil) performed best classes, with the lowest errors and among the lowest standard deviations (Figure 5.22). These land covers are usually stable, so were not expected to show much variability in the six months under investigation.

There was a great deal of class confusion between the various vegetation classes, specifically between the cultivated crops and natural vegetation, on all dates. There was a large variance in plant structure, height, and composition within each of these classes. Training for these classes was therefore difficult as all of these variances must be accounted for. The vegetation classes thus displayed generally higher errors of omission and commission. Figure 5.22 shows that the two earlier image dates (22 February and 5 May 2014 in green and red) clearly delineated the Cultivated Herbaceous Non-Graminoids class better than the two later dates, with errors under 30%. The later dates, especially the 29 May 2014 (orange) data, better delineated the Natural Herbaceous Shrubs and Bushes and Managed Grass classes than any of the other three dates.
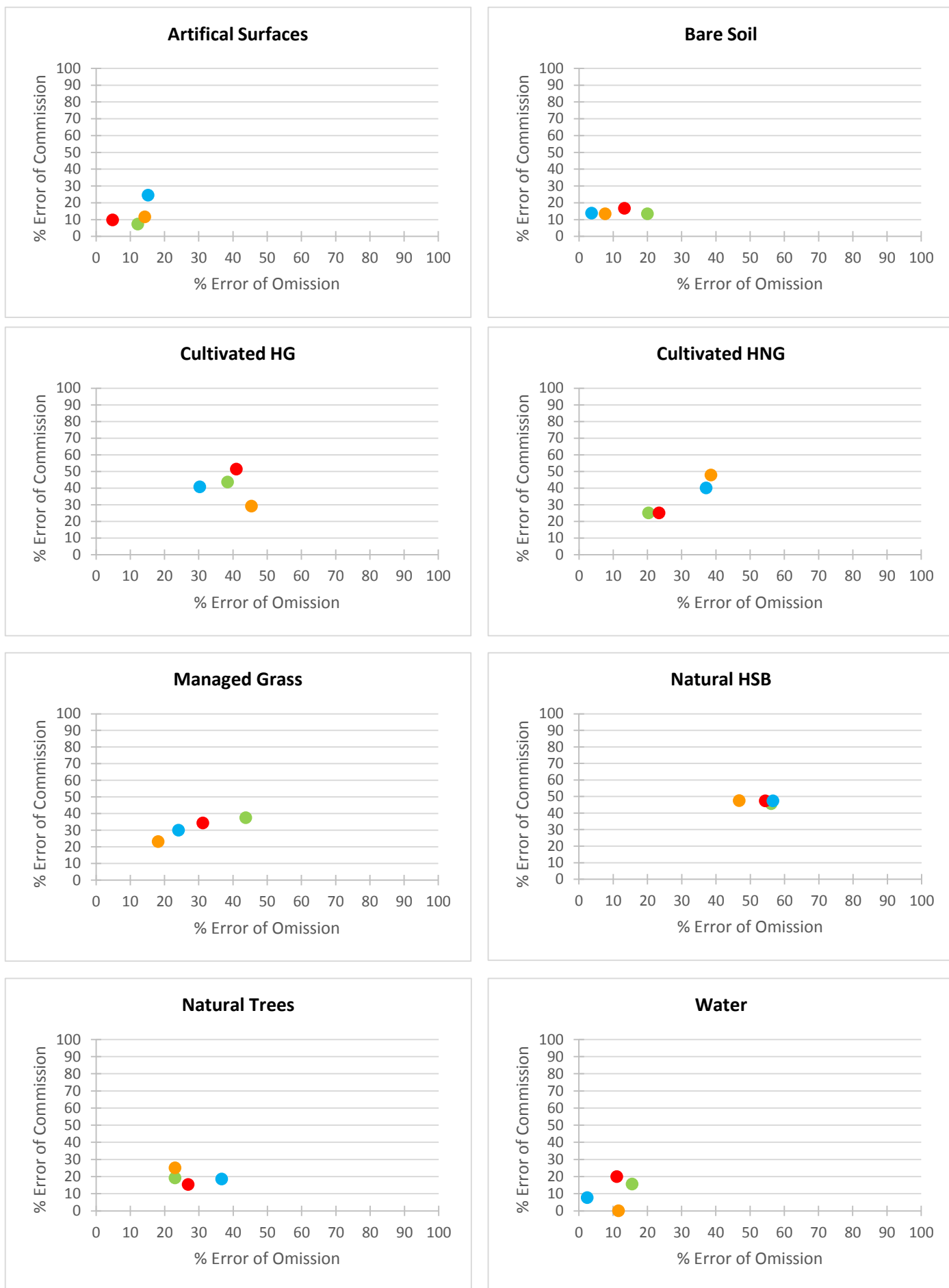
Key
Green: 2014-02-22 | Red: 2014-05-05 | Orange: 2014-05-29 | Blue: 2014-08-09

Figure 5.22 Error of omission and commission plotted for each land cover class, for all four classifications produced using the combined SAR-optical data on each date.
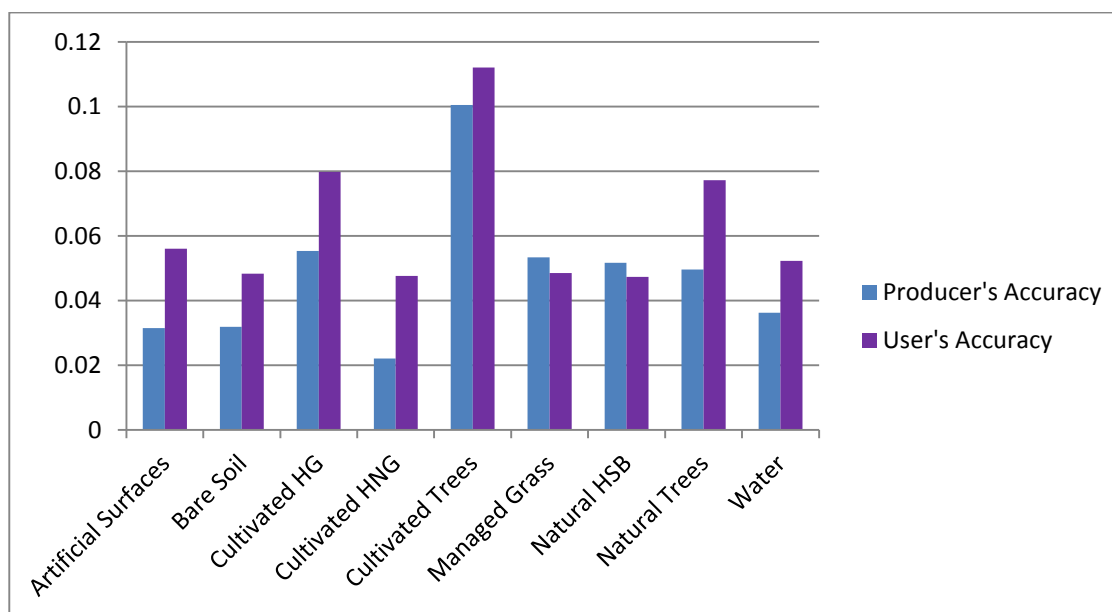
Figure 5.23 The standard deviation for user's and producer's accuracies for each land cover class, calculated using all four classifications produced on the combined SAR-optical data of the separate image dates

Although the best overall accuracies were produced from the fused imagery for the two May image dates, the difference in accuracy between these and the other dates was minimal (less than 1.5%). None of the land cover classes were described significantly better on one date than the other dates. As the training data were collected over the same six months as the images were acquired, the training data may not have clearly accounted for temporal changes in the ground cover. A clear temporal trend may also be lacking because the four image dates only spanned six months. Images spanning a full calendar year should be assessed to better determine the optimum times of the year to map certain classes. This could not be achieved in this study as there was too much cloud cover in the SPOT-5 imagery acquired at the same times as the RADARSAT-2 imagery. As one focus of this study was a comparison of single-sensor and fused classifications, usable single-sensor imagery was a prerequisite. A future study could focus on mapping out optimum times for best delineating the various land cover classes only using fused imagery. Cloud-free optical data would be less of an issue as the combined imagery should overcome the data gaps in cloud regions.

5.4   EXPERIMENT 4: MULTI-TEMPORAL CLASSIFICATION

Experiment 4 aimed to assess the benefits of using fused, multi-temporal data for land cover classification, compared with fused, single-date classifications. The RF classification algorithm was used based on the results from Experiment 2. As the multi-temporal dataset contained 638 features, the RF feature selection algorithm was run first. Based on the feature rankings, different numbers of features (in order of importance) were used to train the classifier.

Section 5.4.1 presents and discusses the results based on the four multi-temporal classifications produced using 20, 40, 50, 60 and all of the features. A class-specific discussion follows in Section 5.4.2 based on the best classification produced (based on 50 features). Finally, Section 5.4.3 compares the best multi-temporal classification with the best single-date classification produced in Experiment 3 (29 May 2014 image). All confusion matrices can be found in APPENDIX C.

5.4.1   Multi-temporal classifications produced using different numbers of training features

The RF classifier was trained with the 20, 40, 50, 60 most important features as well as all of the features to determine the point at which the most accurate classification was produced before over-training negatively affected classification accuracy. The overall accuracies for each classification are shown in Figure 5.24.
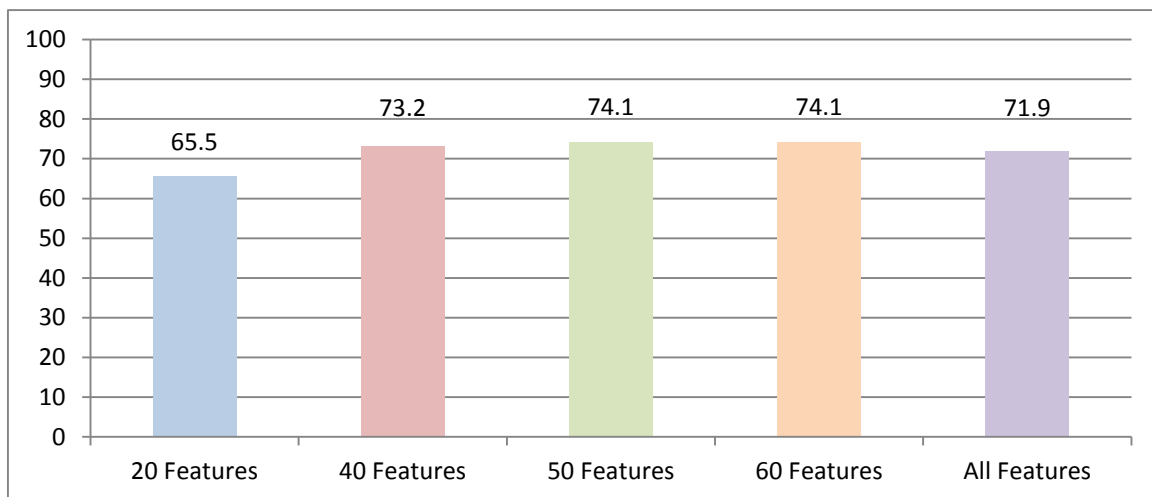
Figure 5.24 Overall accuracies (%) achieved for all iterations of the multi-temporal combined SAR-optical classification, based on different numbers of features.

As expected, the classification that only used 20 features for classifier training resulted in the lowest overall accuracy of 65.5% (Figure 5.24). It also resulted in the highest error of commission for every class (Figure 5.25). The producer's accuracy fluctuated more with the number of features used for training, but

using 20 features still resulted in the highest error of omission for four of the nine classes, with another two classes showing an identical error of omission for all of the numbers of features tested (Figure 5.26).
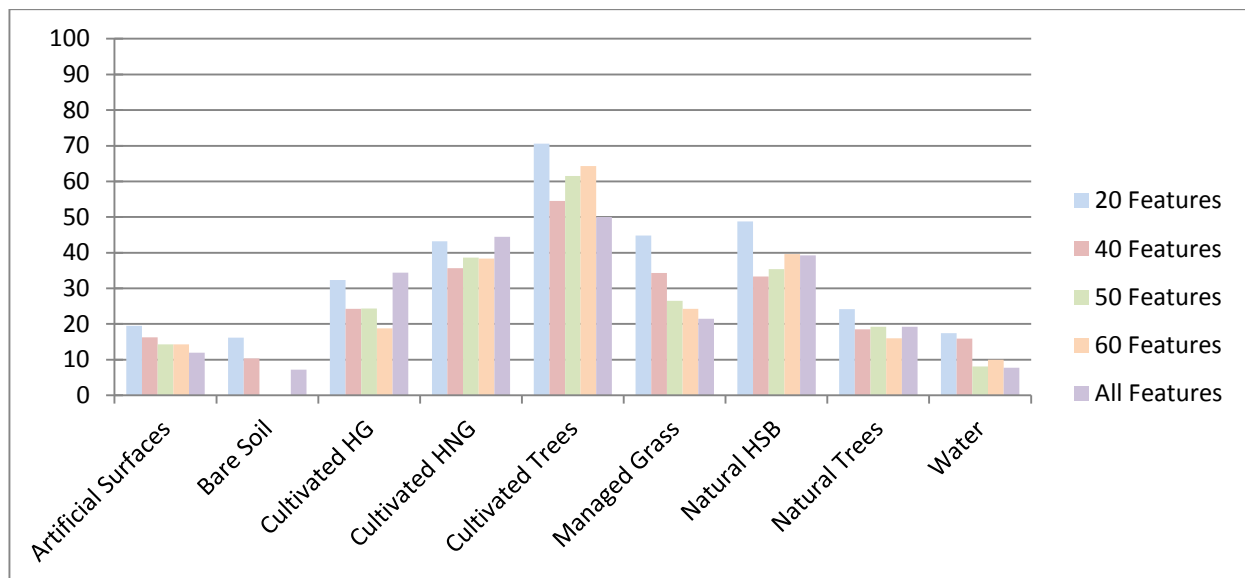
Figure 5.25 The errors of commission (%) of each land cover class for each iteration of the multi-temporal, combined SAR-optical classification, based on different numbers of training features.
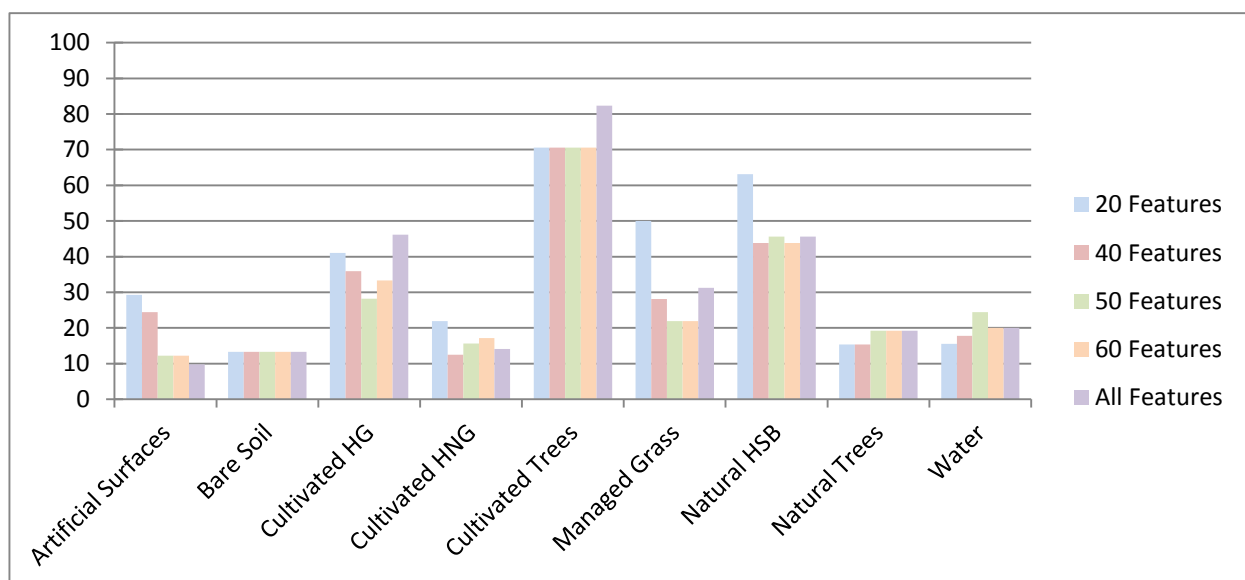
Figure 5.26 The errors of omission (%) of each land cover class for each iteration of the multi-temporal, combined SAR-optical classification, based on different numbers of training features

The greatest difference between overall accuracies was observed between the classifications using 20 and 40 features. Although double the number of features were used, the overall accuracy increases by nearly 8% (Figure 5.24). With the next increase in features from 40 to 50, the accuracy increased by less than 1%. The initial jump to 40 features for training therefore had a significant effect on the classifier's performance. Interestingly, this jump from 20 to 40 features also included a large increase in the number of SAR based-features used. This was discussed in detail in the results from Experiment 1 in Section 0.

The highest overall accuracy, 74.1%, was obtained when training the classifier with 50 or 60 features. The overall accuracy did not change when the number of features was increased from 50 to 60, but the user's and producer's accuracies for individual classes did vary. Increasing from 50 to 60 features for training resulted in a increase in the error of omission for Cultivated Herbaceous Graminoids and Cultivated Herbaceous Non-Graminoids. Simultaneously, the error of omission decreased for Natural Herbaceous Shrubs and Bushes and Water, although these decreases were both less than 5% and thus had a negligible effect on the classifier's performance. Similarly, there was a increase in the error of commission for Cultivated Trees, Natural Herbaceous Shrubs and Bushes, and Water. Thus, although the error of omission improved for Natural Herbaceous Shrubs and Bushes and Water, the error of commission increased simultaneously.

The results from the four iterations show that using no more than 50 features produced the best classification for this particular study area. Using more than 50 features improved some classes, but worsened others, while increasing the computation time. When using all of the features, overall accuracies declined. Within the context of this study, the use of these additional features was not deemed beneficial. This result echoes similar findings from other studies where beyond a certain point, adding additional features resulted in a higher error rate (Schistad Solberg & Jain 1997).

5.4.2   Classification based on 50 features: class-specific performance

The classification produced using the 50 top ranked features is shown in Figure 5.27. Cultivated Trees was problematic for classification throughout this investigation, and this final classification was no exception. The class had a continuous producer's accuracy of below 30% and the highest user's accuracy for the multi-temporal classifications was only 45.45%, as shown in Table 5.6. Assessing all classifications produced in Experiments 3 and 4, the producer's accuracies remain under 30% except for one instance, the single-date classification, produced on the 2014-02-22 RADARSAT-2 data only which produced a producer's accuracy of 41.48%. With other classes reaching a producer's accuracy of 100% (Bare Soil) and a user's accuracy of 87% (Artificial Surfaces) it can be concluded that the Cultivated Trees class was either poorly defined and trained, or is generally a difficult class to separate from other similar classes. As the Cultivated Trees class was also problematic in Experiments 2 and 3, better training data is likely to result in an improvement in classifying this challenging class.
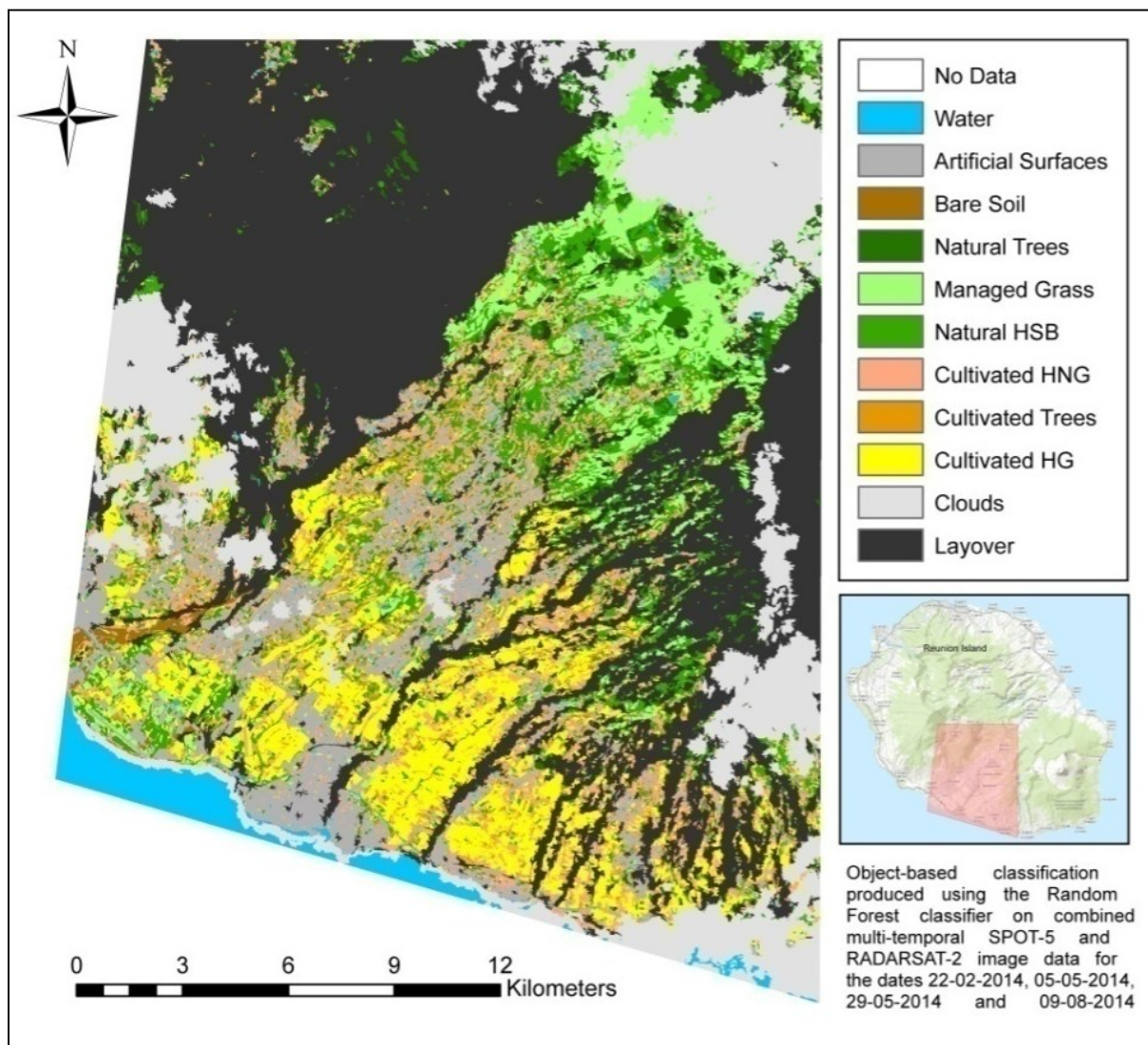
Figure 5.27 Classification produced from the multi-temporal, combined SAR-optical data set, with the RF classifier trained using the 50 highest ranked features.

Table 5.6 User's and producer's accuracies of the Cultivated Trees class for the four multi-temporal classifications performed using different numbers of training features.

	20 Features	40 Features	50 Features	60 Features	All Features
User's Accuracy (%)	29.41	45.45	38.46	35.71	50
Producer's Accuracy (%)	29.41	29.41	29.41	29.41	17.6

Similarly with the single-date classifications, separation between the vegetation classes also remained problematic as the chemical responses of the classes were probably quite similar. Physical structures would have been the most useful way to differentiate between these classes. However, few SAR-based features were included in the training of the classifier, preventing this differentiation factor from being fully exploited.

5.4.3   Multi-temporal classification vs. the best single-date classification

The best multi-temporal fused classification (trained with 50 features) was compared with the best single-date fused classification (2014-05-29). The multi-temporal classification had better overall accuracy and kappa values. It also resulted in less confusion between the classes, as shown by the confusion matrices (Table 5.7 and Table 5.8) for the two classifications. For example, the Artificial Surfaces class was misclassified into five classes (Water, Natural Herbaceous Shrubs and Bushes, Bare Soil, Managed Grass, and Cultivated Herbaceous Graminoids) in the single-date classification, but was only misclassified into three classes (Water, Managed Grass, and Natural Herbaceous Shrubs and Bushes) in the multi-temporal classification. The same trend was seen for Natural Trees, Managed Grass, and Cultivated Herbaceous Graminoids.

Table 5.7 Confusion matrix for the multi-temporal, combined SAR-optical classification produced using 50 training features.

| | | Classification Image | | | | | | | | | | |
		Artificial Surfaces	Bare Soil	Cultivated HG	Cultivated HNG	Cultivated Trees	Managed Grass	Natural HSB	Natural Trees	Water	Grand Total	Producer's Accuracy (%)
Reference Image	Artificial Surfaces	36			3					2	41	87.80
	Bare Soil		26		2			1		1	30	86.67
	Cultivated HG			28	7	2		2			39	71.79
	Cultivated HNG			2	54	2	1	5			64	84.38
	Cultivated Trees			1	4	5	2	5			17	29.41
	Managed Grass	2		4	1		25				32	78.13
	Natural HSB	2		2	8	3	6	31	5		57	54.39
	Natural Trees				2			3	21		26	80.77
	Water	2			7	1		1		34	45	75.56
	Grand Total	42	26	37	88	13	34	48	26	37	351	
	Users Accuracy (%)	85.71	100	75.68	61.36	38.46	73.53	64.58	80.77	91.89		
	Overall Accuracy	74.07										
	Kappa	0.70										

Table 5.8 Confusion matrix for the 2014-05-29 single-date, combined SAR-optical classification.

		Classification Image									Grand Total	Producer's Accuracy (%)
		Artificial Surfaces	Bare Soil	Cultivated HG	Cultivated HNG	Cultivated Trees	Managed Grass	Natural HSB	Natural Trees	Water		
Reference Image	Artificial Surfaces	39						1		1	**41**	95.12
	Bare Soil	1	26		2			1			**30**	86.67
	Cultivated HG			23	6	3	1	6			**39**	58.97
	Cultivated HNG	1	1	2	49	1	1	9			**64**	76.56
	Cultivated Trees			3	5	1	1	6	1		**17**	5.88
	Managed Grass	1		1	2		22	6			**32**	68.75
	Natural HSB	2		3	10	2	4	26	10		**57**	45.61
	Natural Trees			1	3			3	19		**26**	73.08
	Water	2			1			2		40	**45**	88.89
	Grand Total	**46**	**27**	**33**	**78**	**7**	**29**	**60**	**30**	**41**	351	
	Users Accuracy (%)	84.78	96.30	69.70	62.82	14.29	75.86	43.33	63.33	97.56		
	Overall Accuracy (%)	69.80										
	Kappa	0.65										

Figure 5.28 shows the percentage errors of omission and commission for each land cover class for the multi-temporal classification. The analogous plot for the single-date classification was shown in Figure 5.19 in Section 5.3.2. The individual classes were improved in the multi-temporal classification. The Natural Herbaceous Shrubs and Bushes class (mid green) in particular showed a marked improvement in its error of commission with the introduction of multi-temporal data, however it remained outside the 40% mark for error of omission. Only the Cultivated Trees class (orange) remained problematic in terms of both error of omission and commission. The rest of the classes fell well within the bottom left quadrant, which is the acceptable error level.

KEY:
- Artificial Surface
- Bare Soil
- Cultivated Herbaceous Graminoids
- Cultivated Herbaceous Non-Graminoid
- Cultivated Trees
- Managed Grass
- Natural Herbaceous Shrubs and Bushes
- Natural Trees
- Water
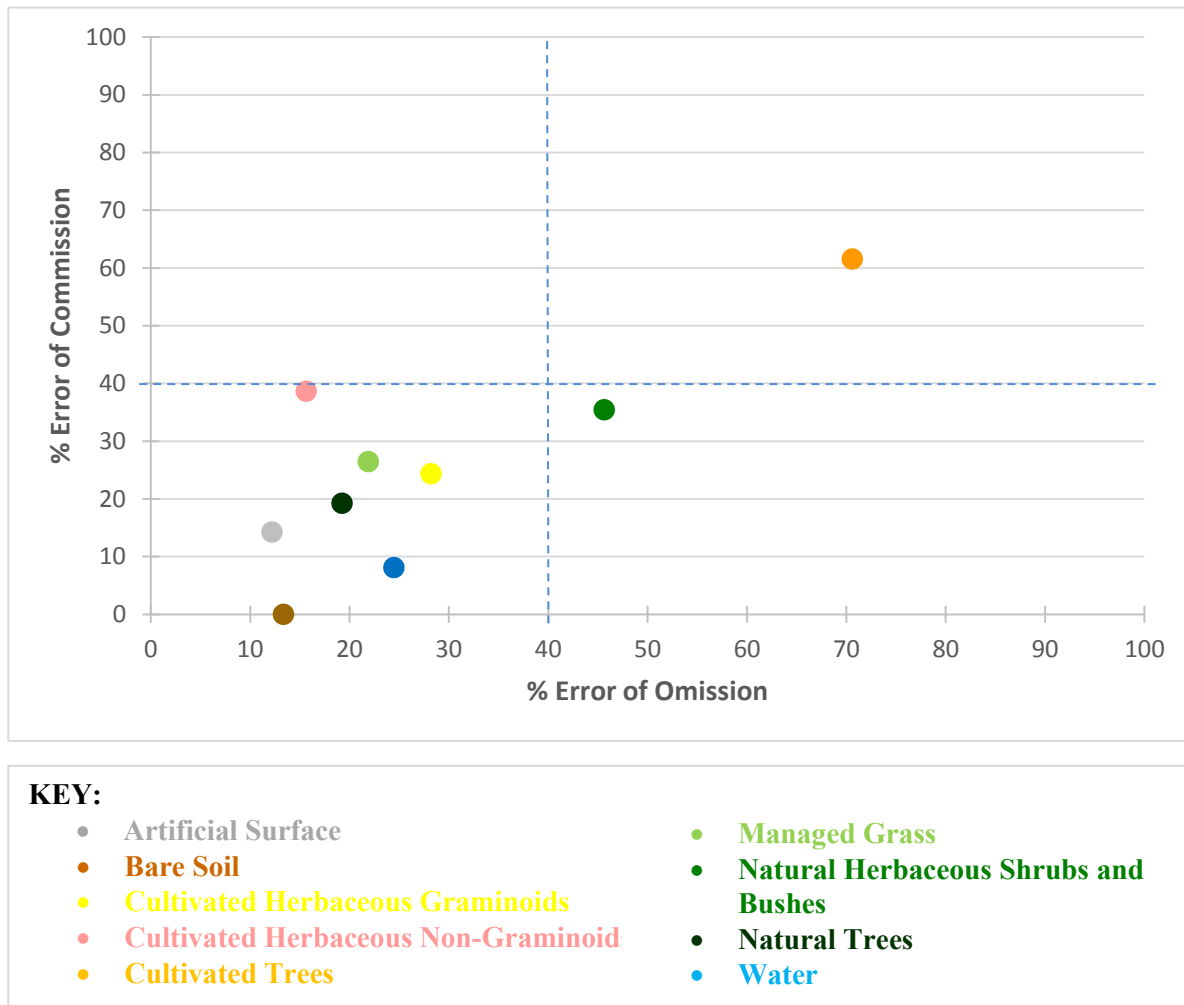
Figure 5.28 Error of omission and commission plotted for each land cover class based on the multi-temporal, combined SAR-optical classification, with the RF classifier being trained using the 50 highest ranked features.

There was an improvement seen in the Managed Grass and Water classes from the single-date to the multi-date classifications. This mimics the results seen by Niu & Ban (2013) using only a RADARSAT-2 time series of six images as well.

All of the results from the four experiments undertaken in this study were presented and discussed in this chapter. In Chapter Six, the results will be summarised and integrated, so that conclusions can be drawn and recommendations can be made.

CHAPTER 6   EVALUATION

Chapter 5 presented the results from the four experiments undertaken to determine the benefits and limitations of using a combined optical-SAR image data set for land cover classification, using an object-based approach. This chapter summarises the key findings from the four experiments and presents an evaluation of the results in context of previous studies. The limitations of this work and opportunities for future studies to extend and improve this work are also discussed. Finally, a concluding section is presented.

6.1   SUMMARY OF FINDINGS

Experiment 1 addressed and achieved Objectives 1 and 2 by assessing feature selection using CART and RF as methods for informing feature reduction as well as assessing possible temporal trends in the importance rankings of both combined and single sensor data. Some features were clearly more useful at particular times of the year, and this was supported by the agreement between the two algorithms as the likelihood of coincidence was low enough to be disregarded. Texture, particularly texture derived from the optical bands, was found to be an important feature addition for class separability for both the fused and optical data sets. Less reliance on texture was seen in the radar-only data sets. The NDVI was important for all of the image dates, both in the fused and optical image data sets. These findings were mirrored in the multi-temporal feature selection rankings.

When assessing the feature rankings across the four dates for the fused data sets, the importance of the SAR-derived features varied. SAR may therefore be a useful addition when optical-only imagery fails to discriminate between classes. When feature selection was performed on SAR-based data alone, the reliance on decomposition-derived and backscatter-derived features varied across the four image dates. Polarimetric information is thus a useful addition to feature selection and relying solely on backscatter is insufficient. The definite trends found in the feature selection tested in Experiment 1 informed the development of Experiment 4, in which the classification algorithm was trained using different numbers of features from the rankings produced in the first experiment.

Objective 3 was achieved through **Experiment 2** which compared the performance of six classification algorithms on two image dates to find the algorithm that performed best in the study site. In agreement with the literature and other studies (Adams et al. 2014; Breiman 2001; Novack et al. 2011; Rodriguez-Galiano et al. 2012), the RF classification algorithm performed best for both image dates. Its ability to handle large volumes of training data and relative insensitivity to outliers meant that it produced superior results. The RF algorithm was thus used further in Experiments 3 and 4. The maximum likelihood classification, as expected, produced the worst accuracies, both overall and class-wise. Its assumption of a

normal distribution in the data (which is not always the case for SAR data) and sensitivity to high dimensionality of data resulted in very poor accuracies.

Experiment 3 compared classifications produced from the fused and single-sensor data sets on four image dates to determine whether introducing data from additional sources increased accuracy. Temporal trends were also assessed but feature selection techniques were not tested, unlike in Experiment 4. The fused data sets consistently produced better accuracies and Kappa values across all four dates than either the SAR-based or optical-based classifications. Classifications with single-date fused imagery also resulted in lower errors of omission and commission in nearly all of the land cover classes than classifications with single-date single-sensor imagery. Clear outliers with high errors of omission and commission were found in optical-only and SAR-only classifications, but were reduced in fused classifications in Experiment 3. These results validated the benefit of dual-sensor data over single-date data, thereby achieving Objective 4.

Consistent overall accuracies and kappa values were obtained for the fused classifications over the four images dates, which spanned February to August. This result showed that the fused data had a lower sensitivity to vegetation growth phases and seasonal changes than the single-sensor data. Single-sensor classifications suffered lower accuracies in the two later dates. Strong temporal trends for the individual land cover classes were not noted. This addressed and achieved Objective 5.

The findings from **Experiment 4** achieved Objective 6 by supporting the use of a multi-temporal data set, as even a classification trained with only 40 key features (out of a total of 638) produced a higher overall accuracy and kappa value than any of the single-date classifications. Training the RF classifier with an increasing number of features showed that the more features the classifier was trained with, the better the accuracy of the resulting classification generally was. However, the accuracy gains for this study area plateaued at 50 training features. The overall accuracy did not significantly increase with increased training information over 50 features but instead decreased when using all of the 638 available features.

The best performing single-date classification had an overall accuracy of 69.8% and kappa value of 0.65. In contrast, the best multi-temporal classification, trained using 50 features, had an overall accuracy of 74.1% and kappa value of 0.70. Confusion between classes was also reduced in the multi-temporal classification, in comparison with the single-date classifications.

6.2   EVALUATION OF RESEARCH

This section evaluates the research in the context of other studies and critically assesses both the impact as well as the limitations of the research.

6.2.1   CONTEXTUALIZATION

In accordance to the results by other authors (Amarsaikhan et al. 2010; Ban, Hu & Rangal 2007; Blaes, Vanhalle and Defourney 2005; Laurin et al. 2013; Lu & Weng 2005; McNairn 2009), there were improvements in the classification accuracy when introducing dual-sensor imagery in comparison to single sensor imagery. Furthermore, misclassifications and poorly separated classes from the single data sets were improved on (Hill et al. 2005). McNairn (2009) found that target overall accuracies of 85% could not be achieved using only SAR or optical imagery but could be achieved through the use of fused imagery. In contrast to this, overall accuracies in this study, even with multi-temporal classifications remained low with the best iteration obtaining 74.1%.

The results from the fused multi-temporal classifications echoed similar findings from other studies where beyond a certain point, adding additional features resulted in a higher error rate (Schistad Solberg & Jain 1997). This was seen with the lower overall accuracy of 71.9% when using all available features to train the classifier, compared to the use of just the 50 highest ranked features from the feature selection, which resulted in an overall accuracy of 74.1%.

Pacifici et al. (2008) attributed the improvements seen in their fused classifications to the addition of C-band SAR providing additional scattering information to optical data thereby improving the separation of vegetation and water from urban classes. This however was not seen in the results if the single-date fused classifications and was only achieved using multitemporal optical/SAR image data.

The vegetation classes, except Cultivated Trees, exhibited increases in accuracies when using the fused imagery over the single-sensor imagery. This is in align with the study by Ban, Hu and Rangal (2007) who found that although a small increase in overall classification accuracy (1.6%) was experienced, larger increases were found with individual vegetation classes. Similarly, Brisco, Brown and Manore (1989) also found improvements in vegetation classes when using combined optical and SAR data. These increases in accuracies were however much larger (20-25%) than what was experienced in this study. This could be attributed to the very high resolution optical imagery that was combined with the radar imagery.

It has been recorded that SAR alone often fails to accurately map urban areas (Corbane et al. 2008). This was seen in this study with the SAR only classification producing errors of omission and commission for the urban class of 34.1% and 22.9% respectively. However, in the fused optical/SAR classification, these errors were improved greatly to 4.9% and 15.2% respectively.

6.2.2 LIMITATIONS

The overall accuracies achieved in this study were lower than what would generally be acceptable for a methodology can be transferred and replicated to other dates or study areas (Congalton & Green 2009). Future work can therefore focus on improving these accuracies to allow this methodology to be transferred to other study sites. The nature of the training data may have contributed to the lower accuracies, as they were collected at different times in 2014. Training data points should ideally be collected at the same time, then recollected on each image acquisition dates. This ideal collection scheme ensures that the training and validation data have higher accuracy and that little error is introduced by changes in land cover due to seasonality or harvesting dates and by changes in seasonally grown crops. Sampling periods should also ideally correspond to key changes in phenology for the major crop types.

The topography of the study area posed some limitations. Large portions had to be masked out due to radar layover and cloud cover present in the optical images. There were thus fewer viable image dates to work with than originally envisaged. Areas containing training points also had to be removed due to layover and cloud cover, compromising the training data set.

Strong temporal trends for the individual land cover classes in the fused classifications were not definitively noted. The results could have been limited by the multi-temporal images chosen for classification only spanning a 6-month period. Imagery spanning an entire calendar year, thereby including all stages of every crop calendar would be better suited to fully achieving this objective. Other studies have shown there to be ideal times of year to map different crop types (McNairn et al. 2009), thus the study was limited by the data used in this aspect.

6.2.3 CONTRIBUTION AND IMPACT

The synthesised results suggest some general conclusions about the potential and benefits of using multi-temporal, fused optical and SAR image data for land cover classification using an object-based approach. Feature selection can be used to assess the importance of features for classifier training, thereby informing feature reduction. This can be used to reduce data volume, complexity, and computational processing time without compromising accuracy standards, as was seen in the multi-temporal classifications in Experiment 4.

The RF classifier handles the large data volumes associated with multi-temporal and dual-sensor data sets well, and is a suitable algorithm on which to base classifications. Fused imagery produces better classifications, based on accuracy, than either SAR or optical imagery alone. Using multi-temporal data

not only improves the overall accuracy of classifications but can also improve class misclassifications, as was shown in this case study.

It was established that it is more beneficial to use fewer key features derived from multiple dates than many features derived from a single image date when performing land cover classifications. For this study area, the best classification resulted from training the RF classifier with 50 top ranked features derived from four image dates. Although the exact specifications and number of features will depend on the study site, the general premise is expected to hold true for many cases. However, the multiple image dates must be strategically chosen to coincide with definitive growth phases of vegetation to improve discrimination between easily confused vegetation classes.

This study investigated multiple facets of the combined use of optical and SAR imagery for land cover classification, investigating both the fused and multi-temporal nature of the data and the potential benefits of both. In this regard, the results provide a novel look into the potential of these large, complex multi-sensor datasets that are now becoming more readily available. The results aid in understanding the processing, potential fusion methods and benefits of such datasets for a land cover classification application and opens up new research questions upon which to base future work.

6.3   RECOMMENDATIONS FOR FUTURE WORK

The fused classifications showed less sensitivity to the senescence of vegetation, with consistent accuracies across the 6-month time period. This was not investigated further as it was beyond the scope of this study, however there remains a possibility of future research into links between vegetation indices and SAR features throughout the vegetation cycle in a tropical environment.

The default settings were used for the classification algorithms for Experiments 2, 3, and 4. Research projects should at least consider, if not work towards, operationally realistic results. Research that remains theoretical runs the risk of quickly becoming obsolete and should be transferred to operational, working projects for its true benefits to be realised. For operational monitoring of land cover for large areas throughout the year, it is not realistic to continually define the optimal structure of each data set and parameters for classification algorithms. This would result in hours of manual editing and reprocessing. Instead, the goal should be an automated, or at least semi-automated, approach to produce useful products to continually aid in decision making. Leaving classifier settings on default and using the same segmentation parameters in every classification promoted the functionality and transferability of the methodology developed here. However, the use of the default settings may have contributed to the lower accuracies experienced in the classifications. The chosen classification algorithm could be improved by optimising the parameters and comparing the results with the final classification reported in this study.

The classifications could be further improved by optimising the segmentation. Recent studies have introduced the idea of supervised segmentation, which can be used to improve segmentation and thus classification accuracies.

The use of high resolution imagery provides another interesting prospect for future work. The 8 m spatial resolution of this SAR data used in this study did not allow smaller fields or pockets of land cover to be delineated during segmentation. A higher spatial resolution could promote a better classification, as objects could be better represented and segmented.

Finally, the results from this research are based on land cover mapping in a tropical region. However, the premise to use fused imagery for general land cover in other climatic regions still holds true. In areas where cloud cover is not as strong a limitation, the fused imagery could hold more potential as ground truth data would not be rendered obsolete due to a single bad acquisition of optical imagery, where cloud cover could remove large portions of data. Further research into using this type of dataset for land cover mapping, including detailed mapping of agricultural regions should be explored.

6.4   CONCLUDING REMARKS

The research presented in this thesis aimed to assess the benefits and limitations of using a combined multi-temporal SAR-optical image data set for land cover classification using an object-based approach. The aim was addressed through six main objectives, all which were achieved through the methods employed. Although data dimensionality is inevitably substantially increased when using a multi-temporal, dual-sensor image data set, data reduction can be successfully achieved by first performing feature selection, using for example the RF or CART algorithms. The produced rankings of importance on features not only help the user to choose the features to train the classification algorithm with, but also provide invaluable information about the usefulness of different sensor-types, and their features, at different times of the year for the study site of interest. The results from this study indicated that SAR and optical data are complementary in nature. Combining the two data types reduces their limitations and exploits their classifying strengths to produce superior land cover classifications, especially during periods when single-sensor imagery is insufficient. The need for multi-temporal data sets for accurate land cover classification was validated by the multi-temporal, dual-sensor data set producing the highest quality land cover classification overall. The feature rankings for this data set revealed dependence on specific dates (2 February and 9 August 2014). Acquisition dates therefore must be strategically chosen in accordance with local vegetation growth phases for optimum class separability. Acquisitions in both the wetter and drier seasons, such as was used in this study, are recommended.

122

Although multi-temporal, dual-sensor data sets can be large and complex to work with, their obvious benefits in accuracy gains and better class separability make them an excellent choice for accurate land cover classifications. This thesis illustrated these benefits in a study region particularly prone to single-sensor classification difficulties, with its tropical climate and mountainous terrain. As software and computational capacity are constantly improving and advanced imagery will soon be available from new sensors, this investigation of combined multi-temporal SAR-optical data should be extended to include new applications in addition to land cover classifications.

CONTINUATION OF THIS RESEARCH

Using the findings from this Master's thesis as a basis, three journal articles are planned for submission by the end of 2015. The broad topic for each paper is as follows:

1. Feature selection as a means to inform data reduction and depict temporal trends in feature importance on single-sensor data in comparison to combined optical and SAR data.

2. Combined optical and SAR data for land cover classification using the Random Forest classifier and an object-based approach.

3. Multi-temporal, object based land cover classification on combined optical and SAR data: A case study of Réunion Island.

REFERENCES

Adam A, Mutanga O, Odindi J & Abdek-Rahman EM 2014. Land-use/cover classification in a heterogeneous coastal landscape using RapidEye imagery: evaluating the performance of random forest and support vector machines classifiers. *IEEE International Journal of Remote Sensing* 35(10): 3440-3458.

Agashe S 2013. Polarimetric decomposition of SAR data for forest structure assessment. Master's thesis. Gothenburg: Chalmers University of Technology, Department of Earth Space Sciences.

Ainsworth TL, Kelly JP & Lee JS 2009. Classification comparisons between dual-pol, compact polarimetric and quad-pol SAR imagery. *ISPRS Journal of Photogrammetry and Remote Sensing* 64(5): 464-471.

Alberga V 2007. A study of land cover classification using polarimetric SAR parameters. *International Journal of Remote Sensing* 28(17): 3851-3870.

Albregsten F 2008. Statistical texture measures computed from gray level co-occurrence matrices. Oslo: University of Oslo, Department of Informatics.

Amarsaikhan D, Blotevogel HH, Van Genderen JL, Ganzorig M, Gantuya R & Nergui B 2010. Fusing high-resolution SAR and optical imagery for improved urban land cover study and classification. *International Journal of Image and Data Fusion* 1(1): 83-97.

Autret M, Bernard R & Vidal-Madjar D 1989. Theoretical study of the sensitivity of the microwave backscattering coefficient to the soil surface parameters. *Remote Sensing* 10(1): 171-179.

Badurska M 2011. Orthorectification and geometric verification of high resolution TerraSAR-X images. *Geomatics and Environmental Engineering* 5(3): 13-25.

Baghdadi N, Boyer N, Todoroff P, El Hajj ME & Begue A 2009. Potential of SAR sensors TerraSAR-X, ASAR/ENVISAT and PALSAR/ALOS for monitoring sugarcane crops on Réunion Island. *Remote Sensing Environment* 113: 1724-1738.

Baghdadi N, King C, Bourguignon A & Remond A 2002. Potential of ERS and RADARSAT data for surface roughness monitoring over bare agricultural fields: application to catchments in Northern France. *International Journal of Remote Sensing* 23(17): 3427-3442.

Baghdadi N, Loumagne C, Ansart P & Anguela TP 2008. Analysis of TerraSAR-X data and their sensitivity to soil surface parameters over bare agricultural fields. *Remote Sensing of Environment* 112: 4370-4379.

Ban Y, Hu H & Rangel IM 2010. Fusion of Quickbird MS and RADARSAT SAR data for urban land cover mapping: object-based and knowledge-based approach. *International Journal of Remote Sensing* 31(6): 1391-1410.

Ban Y & Wu Q 2005. *RADARSAT SAR data for landuse/land-cover classification in the rural-urban fringe of the greater Toronto area*. Proceedings of the 8th AGILE Conference on Geographic Information Science held 26-28 May 2005, Estoril, Portugal: 26-28.

Bellon de la Cruz B 2014. Evaluation du potentiel des images satellitaires a tres haute resolution spatiale et leur analyse orientee objet pour la cartographie du mode d'occupation du sol a la Réunion. Master's thesis. Réunion: University of La Réunion.

Betbeder J, Nabucet J, Pottier E, Baudry J, Corgne S & Hubert-Moy L 2014. Detection and characterization of hedgerows using TerraSAR-X Imagery. *Remote Sensing* 6: 3752-3769.

Berberoglu S, Curran PJ, Lloyd CD & Atkinson PM 2007. Texture classification of Mediterranean land cover. *International Journal of Applied Earth Observation and Geoinformation* 9: 322-334.

Bhaskaran S, Paramananda S & Ramnarayan M 2010. Per pixel and object-oriented classification and methods for mapping urban features using Ikonos satellite data. *Applied Geography* 30: 650-665.

Blaes X, Vanhalle L & Defourney P 2005. Efficiency of crop identification based on optical and SAR image time series. *Remote Sensing of Environment* 96(3): 352-365.

Blaschke T 2010. Object based image analysis for remote sensing. *ISPRS Journal of Photogrammetry and Remote Sensing* 65(1): 2-16.

Borghys D, Yvinec Y, Perneel C, Pizurica A & Philips W 2006. Supervised feature-based classifications of multi-channel SAR images. *Pattern Recognition Letters* 27: 252-258.

Breiman L 2001. Random forests. *Machine Learning* 45: 5-32.

Brisco B, Brown RJ & Manore MJ 1989. Early season crop discrimination with combined SAR and TM data. *Canadian Journal of Remote Sensing* 15(1): 44-54.

Byrne GF, Crapper PF & Mayo KK 1980. Monitoring land-cover change by principal component analysis of multitemporal Landsat data. *Remote Sensing of Environment* 10(3): 175-184.

Cable JF, Kovacs JM, Shang J & Jiao X 2014. Multi-temporal polarimetric RADARSAT-2 for land cover monitoring in Northeastern Ontario, Canada. *Remote Sensing* 6: 2372-2392.

Campbell JB 2006. *Introduction to remote sensing*. 4th ed. New York: Taylor and Francis.

Celik T 2009. Unsupervised change detection in satellite images using principal component analysis and-means clustering. *Geoscience and Remote Sensing Letters* 6(4): 772-776.

Chan JCW, Laporte N & Defries RS 2003. Texture classification of logged forests in tropical Africa using machine-learning algorithms. *International Journal of Remote Sensing* 24(6): 1401-1407.

Chen CT, Chen KS & Lee JS 2003. The use of fully polarimetric information for the fuzzy neural classification of SAR images. *IEEE Transactions on Geoscience and Remote Sensing* 41(9): 2089-2100.

Chen E, Li Z, Pang Y & Tian X 2007. Quantitative evaluation of polarimetric classification for agricultural crop mapping. *Photogrammetric Engineering & Remote Sensing* 73(3): 279-284.

Chen KS, Huang WP, Tsay DH & Amar F 1996. Classification of multifrequency polarimetric SAR imagery using a dynamic learning neural network. *IEEE Transactions on Geoscience and Remote Sensing* 34(3): 814-820.

Chubey Ms, Franklin SE & Wulder MA 2006. Object-based analysis of Ikonos-2 imagery for extraction of forest inventory parameters. *Photogrammetric Engineering and Remote Sensing* 72: 383-394.

Clausi DA 2002. An analysis of co-occurrence texture statistics as a function of grey level quantization. *Canadian Journal of Remote Sensing* 28: 45-62.

Cloude SR & Pottier E 1996. A review of target decomposition theorems in Radar polarimetry. *IEEE Transactions on Geoscience and Remote Sensing* 34(2): 498-518.

Cloude SR, Pottier E & Boerner WM 2002. *Unsupervised image classification using the entropy/alpha/anisotropy method in radar polarimetry*. Proccedings of the NASA-JPL, AIRSAR-02 Workshop held 15-19 July 2002, California, United States of America: 04-06.

Congalton RG & Green K 2009. *Assessing the accuracy of remotely sensed data: principles and practices*. 2nd ed. New York: Taylor and Francis Group CRC press.

Corbane C, Faure JF, Baghdadi N, Villeneuve N & Petit M 2008. Rapid urban mapping using SAR/optical imagery synergy. *Sensors* 8(11): 7125-7143.

Coulibaly L, Tlili A, Hervet E & Adegbidi HG 2012. *Mapping forest stands using RADARSAT-2 quad-polarization SAR images: A combination of polarimetric and spatial information*. Proceedings of the IEEE International Geoscience and Remote Sensing Symposium (IGARSS) held 22-27 July 2012, Munich, Germany: 3359-3362.

CRISP 2001. Microwave remote sensing [online]. Singapore: National University of Singapore. Available from http://www.crisp.nus.edu.sg/~research/tutorial/mw.htm [Accessed 26 September 2015].

CSIR 2010. Land cover field guide. Prepared for: Chief Directorate: National Geospatial Information. Stellenbosch: CSIR Satellite Applications Centre.

da Costa Freitas C, de Souza Soler L, Sant'Anna SJS, Dutra LV, dos Santos JR, Mura JC & Correia AH 2008. Land use and land cover mapping in the Brazilian Amazon using polarimetric airborne P-band SAR data. *IEEE Transactions on Geoscience and Remote* Sensing 46(10): 2956-2970.

DeFries RS & Townshend JRG 1994. NDVI-derived land cover classifications at a global scale. *International Journal of Remote Sensing* 15(17): 3567-3586.

Dekker RJ 2003. Texture Analysis and classification of ERS SAR images for map updating of urban areas in the Netherlands. *IEEE Transactions on Geoscience and Remote Sensing* 41(9): 1950-1958.

Del Frate F & Solimini D 2004. On neural network algorithms for retrieving forest biomass from SAR data. *IEEE Transactions on Geoscience and Remote Sensing* 42(1): 24-34.

Deroin JP, Al-Ganad I & Al-Thari M 2007. *The importance of SAR frequency, polarization and incident angle for mapping arid regions, the Jabali test site, Yemen*. Proceedings of the First Joint PI Symposium of ALOS Data Nodes for ALOS Science Programme held 10 July 2007, Kyoto, Tokyo.

Devereux BJ, Amable GS & Posada CC 2004. An efficient image segmentation algorithm for landscape analysis. *International Journal of Applied Earth Observation and Geoinformation* 6: 47-61.

Dickinson C, Siqueira P, Clewley D & Lucas R 2013. Classification of forest composition using polarimetric decomposition in multiple landscapes. *Remote Sensing of Environment* 131: 206-214.

Dobson C, Pierce LE & Ulaby FT 1996. Knowledge-based land cover classification using ERS- l/JERS-1 SAR composites. *IEEE Transactions on Geoscience and Remote Sensing* 34: 83-99.

Dragut L & Blaschke T 2006. Automated classification of landform elements using object based image analysis. *Geomorphology* 81: 330-344.

Du P, Samat A, Waske B, Liu S & Li Z 2015. Random forest and rotation forest for fully polarized SAR image classification using polarimetric and spatial features. *ISPRS Journal of Photogrammetry and Remote Sensing* 105: 38-53.

Durand JM, Gimonet BJ & Perbos JR 1987. SAR data filtering for classification. *IEEE Transactions on Geoscience and Remote Sensing* 25(5): 629-637.

Duro D, Franklin SE & Dube MG 2012. A comparison of pixel-based and object-based image analysis with selected machine learning algorithms for the classification of agricultural using SPOT-5 HRG imagery. *Remote Sensing of Environment* 118: 259-272.

El Hajj ME, Begue A, Guillaume S & Martine J 2009. Integrating SPOT-5 time series, crop growth modelling and expert knowledge for monitoring agricultural practices - The case of sugarcane harvest on Réunion Island. *Remote Sensing Environment* 113: 2052-2061.

Erasmi S & Twele A 2009. Regional land cover mapping in the humid tropics using combined optical and SAR satellite data- a case study from Central Sulawesi, Indonesia. *International Journal of Remote Sensing* 30(10): 2465-2478.

ESA (European Space Agency) 2000. Polarimetric Decompositions Tutorial [online]. Available from https://earth.esa.int/documents/653194/656796/Polarimetric_Decompositions.pdf [Accessed 24 September 2015].

ESA (European Space Agency) 2014. The Asar user guide: Geometry glossary [online]. Available from https://earth.esa.int/handbooks/asar/CNTR5-5.html [Accessed 24 September 2015].

Evans TL & Costa M 2013. Land cover classification of the Lower Nhecolandia subregion of the Brazilian Pantanal Wetlands using ALOS/PALSAR, RADARSAT-2 and ENVISAT/ASAR imagery. *Remote Sensing of Environment* 128: 118-137.

Fatone L, Maponi P & Zirilli F 2001. *Fusion of SAR/optical images to detect urban areas*. IEEE ISPRS Joint Workshop on Remote Sensing and Data Fusion over Urban Areas held 8-9 November 2001, Rome, Italy. University of Rome: 217-221.

Ferro-Famil L, Pottier E & Lee JS 2001. Unsupervised Classification of Multifrequency and Fully Polarimetric SAR Images Based on the H/A/Alpha–Wishart Classifier. *IEEE Transactions on Geoscience and Remote Sensing* 39(11): 2332-2342.

Foucher S, Benie GB & Boucher JM 2001. Multiscale MAP filtering of SAR images. *IEEE Transactions on Image Processing* 10(10): 49-60.

Friedl MA, Brodley CE 1997. Decision Tree classification of land cover classification - evaluation decision tree approach. *Remote Sensing of Environment* 61(3): 399-409.

Gamanya R, De Maeyer P & De Dapper M 2007. An automated satellite image classification design using object-oriented segmentation algorithms: A move towards standardization. *Expert Systems and Applications* 32: 616-624.

Gao Y, Marpu P, Niemeyer I, Runfola DM, Giner NM, Hamill T & Pontius Jr RG 2011. Object- based classification with features extracted by a semi-automatic feature extraction algorithm–SEaTH. *Geocarto International* 26(3): 211-226.

GEF (Global Environment Facility) 2004. Pantanal/Upper Paraguay Project, Implementation of Integrated River Basin Management Practices in the Pantanal and Upper Paraguay River Basin. Strategic Action Program for the Integrated Management of the Pantanal and Upper Paraguay River Basin. Brasilia.

Guershman JP, Paruelo JM, Di Bella C, Gaillorenzi MC & Pacin F 2003. Land cover classification in the Argentine Pampas using multi-temporal Landsat TM data. *International Journal of Remote Sensing* 24(17): 3381-3402.

Haack B & Bechdol M 2000. Integrating multisensor data and RADAR texture measures for land cover mapping. *Computers & Geosciences* 26: 411-421.

Hajnsek I, Pottier E & Cloude SR 2003. Inversion of surface parameters from polarimetric SAR. IEEE Transactions on Geoscience and Remote Sensing 41(4): 727-744.

Hansen MC, DeFries RS, Townshend JR & Sohlberg R 2000. Global land cover classification at 1 km spatial resolution using a classification tree approach. *International Journal of Remote Sensing* 21(6-7): 1331-1364.

Haralick RM, Shanmugam K & Dinstein I 1973. Textural Features for image classification. *IEEE Transactions on Systems, Man, and Cybernetics* 3: 610-621.

Hauter A, Chang KC & Karp S 1997. Polarimetric fusion for Synthetic Aperture Radar target classification. *Pattern Recognition* 30(5): 769-775.

Hay GJ, Castilla G, Wulder MA & Ruiz JR 2005. An automated object-based approach for the multiscale image segmentation of forest scenes. *International Journal of Applied Earth Observation* 7: 339-359.

Herold M, Goldstein NC & Clarke KC 2003. The spatio-temporal form of urban growth: measurement, analysis and modelling. *Remote Sensing of Environment* 86: 286-302.

Herold ND, Haack BH & Solomon E 2004. An evaluation of radar texture for land use/cover extraction in varied landscapes. *International Journal of Applied Earth Observation and Geoinformatics* 5: 113-128.

Hill MJ, Ticehurst CJ, Lee JS, Grunes MR, Donald GE & Henry D 2005. Integration of optical and radar classifications for mapping pasture type in Western Australia. *IEEE Transactions on Geoscience and Remote Sensing* 43(7): 1665-1681.

Hu X, Tao CV, & Hu Y 2004. Automatic road extraction from dense urban area by integrated processing of high resolution imagery and lidar data. *International Archives of Photogrammetry, Remote Sensing and Spatial Information Sciences*.

Huang H, Legarsky J & Othman M 2007. Land-cover classification using RADARSAT and Landsat imagery for St. Louis, Missouri. *Photogrammetric Engineering & Remote Sensing* 73: 37-43.

Huang S, Potter C, Crabtree RL, Hager S & Gross P 2010. Fusing optical and radar data to estimate sagebrush, herbaceous, and bare ground cover in Yellowstone. *Remote Sensing of Environment* 114: 251-264.

Im J, Jensen JR & Tullis JA 2014 .Object-based change detection using correlation image analysis and image segmentation. *International Journal of Remote Sensing* 29(2): 399-423.

Jensen JR & Cowen DC 1999. Remote sensing of urban/suburban infrastructure and socio-economic attributes. *Photogrammetric Engineering and Remote Sensing* 65(5): 611-622.

Jewell N 1989. An evaluation of multi-date SPOT data for agriculture and land use mapping in the United Kingdom. *International Journal of Remote Sensing* 10(6): 939-951.

Ju C & Molony C 1997. *An edge*-enhanced modified lee filter for the smoothing of SAR image speckle noise. Proceedings of the IEEE Workshop on Nonlinear and Signal Image Processing held 24-26 September 1997, Mackinac Island, Michigan.

Karjalainen M, Kankare V, Vastaranta M, Holopainen M & Hyyppa J 2012. Prediction of plot-level forest variables using TerraSAR-X stereo SAR data. *Remote Sensing of Environment* 117: 338-347.

Kellndorfer JM & Pierce LE 1998. Toward consistent regional-to-global-scale vegetation characterization using orbital SAR systems. *IEEE Transactions on Geoscience and Remote Sensing* 36(5): 1396-1411.

Kemp JN 2010. The application of multi-source remote sensing for sediment transport mapping in an intertropical context (La Réunion Island and South Africa). Doctoral dissertation. Réunion: University of La Réunion.

Kleynhans W & Salmon B 2012. Monitoring informal settlements using SAR polarimetry. *African Association of Remote Sensing of the Environment* 1: 1-6.

Kuplich TM, Curran PJ & Atkinson PM 2005. Relating SAR image texture to the biomass of regenerating tropical forests. *International Journal of Remote Sensing* 26(21): 4829-4854.

Laliberte AS, Browning DM & Rango A 2012. A comparison of three feature selection methods for object based classification of sub-decimeter resolution UltraCam-L imagery. *International Journal of Applied Earth Observation and Geoinformation* 15: 70-78.

Laurin GV, Liesenberg V, Chen Q, Guerriero L, Del Frate F, Bartolini A, Coomes D, Wilebore B, Lindsell J & Valentini R 2013. Optical and SAR sensor synergies for forest and land cover

mapping in a tropical site in West Africa. *International Journal of Applied Earth Observation and Geoinformation* 21: 7-16.

Lee JS 1981. Speckle analysis and smoothing of Synthetic Aperture Radar images. *Computer Graphic and Image Processing* 17: 24-32.

Lee JS, Ainsworth TL, Chen KS & Hajnsek I 2011. *Terrain categorization based on scattering mechanisms for single-pol high resolution TerraSAR-X images*. Geoscience and Remote Sensing Symposium (IGARSS) held 24-29 July 2011, Vancouver, Canada*: 3606-3609.

Lee JS, Grunes MR, Ainsworth TL, Du LJ, Schuler DL & Cloude SR 1999. Unsupervised classification using polarimetric decomposition and the complex Wishart classifier. *IEEE Transactions on Geoscience and Remote Sensing* 37(5): 2249-2258.

Lee JS, Grunes MR & Pottier E 2001. Quantitative comparison of classification capability: fully polarimetric versus dual and single polarization SAR. *IEEE Transactions on Geoscience and Remote Sensing* 39(11): 2343-2351.

Lee JS, Grunes MR, Schuler DL, Pottier E, Ferro-Famil L 2006. Scattering-Model based speckle filtering of polarimetric SAR data. *IEEE Transactions on Geoscience and Remote Sensing* 44(1): 176-186.

Lee JS, Jurkevich L, Dewaele P, Wambacq P & Oosterlinck A. 1994. Speckle filtering of synthetic aperture radar images: A review. *Remote Sensing Reviews* 8(4): 313-340.

Lee JS, Wen JW, Ainsworth TL, Chen KS & Chen AJ 2009. Improved Sigma filter for speckle filtering of SAR imagery. *IEEE Transactions on Geoscience and Remote Sensing* 47: 202-213.

Lebourgeas V, Begue A, Degenne P & Bappel E 2010. Improving harvest and planting monitoring for smallholders with geospatial technology: the Réunion Island experience. *International Sugar Journal* 109: 109-119.

Lejars C & Siegmund B 2004. *Overview of Réunion sugar industry*. Proceedings of the African Sugarcane Technology Association 78: 29-38.

Li G, Lu D, Moran E, Dutra L & Batistella M 2012. A comparative analysis of ALOS PALSAR L-band and RADARSAT-2 C-band data for land cover classification in a tropical moist region. *ISPRS Journal of Photogrammetry and Remote Sensing* 70: 26-38.

Li J & Chen W 2005. A rule-based mapping of Canada's wetlands using optical, radar and DEM data. *International Journal of Remote Sensing* 26(22): 5051-5069.

Li X, Myint SW, Zhang Y, Galletti C, Zhang X & Turner BL 2014. Object-based land-cover classification for metropolitan Phoenix, Arizona, using aerial photography. *International Journal of Applied Earth Observation and Geoinformation* 33: 321-330.

Li X & Yeh AGO 1998. Principal component analysis of stacked multi-temporal images for the monitoring of rapid urban expansion in the Pearl River Delta. *International Journal of Remote Sensing* 19(8): 1501-1518.

Liu D & Xia F 2010. Assessing object-based classifications: advantages and limitations. *Remote Sensing Letters* 1(4): 187-194.

Liu J Y, Zhuang D F, Luo D & Xiao X M 2003. Land-cover classification of China: integrated analysis of AVHRR imagery and geophysical data. *International Journal of Remote Sensing* 24(12): 2485-2500.

Lizarazo I 2008. SVM-based segmentation and classification of remotely sensed data. *International Journal of Remote Sensing* 29(24): 7277-7283.

Lloyd CD, Berberoglu S, Curran PJ & Atkinson PM 2004. A comparison of texture measures for the per-field classification of Mediterranean land cover. *International Journal of Remote Sensing* 25: 3943-3965.

Loew A & Mauser W 2007. Generation of geometrically and radiometrically terrain corrected SAR image products. *Remote Sensing of Environment* 106: 337-349.

Lopez-Sanchez JM, Vicente-Guijalba F, Ballester-Berman JD & Cloude SR 2014. Polarimetric response of rice fields at C-band: Analysis and phenology retrieval. *IEEE Transactions on Geoscience and Remote Sensing* 52(5): 2977-2993.

Lu D & Weng Q 2005. Urban classification using full spectral information of Landsat ETM+ imagery in Marion County, Indiana. *Photogrammetric Engineering and Remote Sensing* 71(11): 1275-1284.

Lunetta RS, Knight JF, Ediriwickrema J, Lyon JG & Worthy LD 2006. Land-cover change detection using multi-temporal MODIS NDVI data. *Remote Sensing of Environment* 105(2): 142-154.

Ma Q, Wang J, Shang J & Want P 2013. *Assessment of multi-temporal RADARSAT-2 polarimetric SAR data for crop classification in an urban/rural fringe area*. Proceedings of the Second International Conference of Agro-Geoinformatics held 12-16 August 2013, Fairfax, USA: 314-319.

Mahmoud A, Elbialy S, Pradhan B & Buchroithner M 2011. Field-based land cover classification using TerraSAR-X texture analysis. *Advances in Space Research* 48: 799-805.

Martha TR, Kerle N, Van Westen CJ, Jetten V & Kumar KV 2011. Segment optimization and data-driven thresholding for knowledge-based landslide detection by object-based image analysis. *IEEE Transactions on Geoscience and Remote Sensing* 49(12): 4928-4943.

Mas JS, Gao Y, Pacheco AN 2010. Sensitivity of landscape pattern metrics to classification approaches. *Forest Ecology and Management* 259: 1215-1224.

McCandless SW & Jackson CR 2004. *Synthetic aperture radar: marine user's manual*. USA: US Department of Commerce, National Oceanic and Atmospheric Administration, National Environmental Satellite, Data, and Information Serve, Office of Research and Applications.

McNairn H & Brisco 2004. The application of C-band polarimetric SAR for agriculture: a review. *Canadian Journal of Remote Sensing* 30(3): 525-542.

McNairn H, Champagne C, Shang J, Holmtrom D & Reicbert G 2009. Integration of optical and Synthetic Aperture Radar (SAR) imagery for delivering operational annual crop inventories. *ISPRS Journal of Photogrammetry and Remote Sensing* 64: 434-449.

McNairn H, Ellis J, Van der Sanden JJ, Hirose T & Brown RJ 2002. Providing crop information using RADARSAT-1 and satellite optical imagery. *International Journal of Remote Sensing* 23(5): 851-870.

McNairn H, Van der Sanden JJ, Brown RJ & Ellis J 2000. *The potential of RADARSAT-2 for crop mapping and assessing crop condition*. Proceedings of the Second International Conference on Geospatial Information in Agriculture and Forestry held 10-12 January 2000, Florida, Unites States of America.

Meinel G & Neubert M 2004. A comparison of segmentation programs for high resolution remote sensing data. *International Archives of Photogrammetry and Remote Sensing* 35(Part B): 1097-1105.

Michelson DB, Liljeberg BM & Pilesjo P 2000. Comparison of algorithms for classifying Swedish land cover using Landsat TM and ERS-1 SAR data. *Remote Sensing of Environment* 71: 1-15.

Moghaddam M, Dungan JL & Acker S 2002. Forest variable estimation from fusion of SAR and multispectral optical data. *IEEE Transactions on Geoscience and Remote Sensing* 50(10): 2176- 2186.

Molch K 2009. Radar earth observation imagery for urban area characterisation [online]. European Commission: JRC Scientific and Technical Reports. Available from http://publications.jrc.ec.europa.eu/repository/bitstream/JRC50451/st_report_sar_urban_final.pdf [Accessed 20 September 2015].

Moreira A, Prats-Iraola P, Younis M, Krieger G, Hajnsek I & Papathanassiou KP 2013. A tutorial on Synthetic Aperture Radar. *IEEE Geoscience and Remote Sensing Magazine* 1(1): 6-43.

Mountrakis G, Im, J & Ogole C 2011. Support vector machines in remote sensing: A review. *ISPRS Journal of Photogrammetry and Remote Sensing* 66(3): 247-259.

Munoz R EA 2013. A dissertation on crops discrimination researches using SAR data. Master's thesis. Cordoba: National University of Cordoba.

Myburgh G & Van Niekerk A 2013. Effect of feature dimensionality on object-based land cover classification: A comparison of three classifiers. *South African Journal of Geomatics* 2(1): 13-27.

Myburgh G & Van Niekerk A 2014. Impact of training set size on object-based land cover classification: a comparison of three classifiers. *International Journal of Applied Geospatial Research* 5(3): 49-67.

Niu X & Ban Y 2013. Multi-temporal RADARSAT-2 polarimetric SAR data for urban land-cover classification using an object-based support vector machine and a rule-based approach. *International Journal of Remote Sensing* 34: 1-26.

Nussbaum, Niemeyer & Cantry 2006. *SEATH–a new tool for automated feature extraction in the context of object-based image analysis*. Proceedings on the 1st International Conference on Object-based Image Analysis (OBIA) held 4-5 July 2006, Salzburg, Austria: University of Salzberg.

Novack T, Esch T, Kux H & Stilla U 2011. Machine learning comparison between WorldView-2 and QuickBird-2-simulated imagery regarding object-based urban land cover classification. *Remote Sensing* 3: 2263-2282.

Nyoungui AN, Tonye E & Akono A 2002. Evaluation of speckle filtering and texture analysis methods for land cover classification from SAR images. *International Journal of Remote Sensing* 23(9): 1895-1925.

Oommen T, Misra D, Twarakavi NK, Prakash A, Sahoo B, & Bandopadhyay S 2008. An objective analysis of support vector machine based classification for remote sensing. *Mathematical Geosciences* 40(4): 409-424.

Ouarzeddine M, Souissi B, & Belhadj-Aissa A 2007. *Unsupervised classification using Wishart classifier*. Proceedings of the Third International Workshop on Science and Applications of SAR Polarimetry and Polarimetric Interferometry (Pol-In-SAR) held 22-26 January 2006, Frascati, Italy.

Pacifici F, Del Frate D, Emery W, Gamba P & Chanussot J 2008. Urban mapping using coarse SAR and optical data: outcome of the 2007 GRSS data fusion contest. *IEEE Geoscience and Remote Sensing Letters* 5(3): 331-335.

Pal M & Mather PM 2003. An assessment of the effectiveness of decision tree methods for land cover classification. *Remote Sensing of the Environment* 86(4): 554-565.

Pal M & Mather PM 2004. Assessment of the effectiveness of support vector machines for hyperspectral data. *Future Generation Computer Systems* 20: 1215-1225.

Pal M & Mather PM 2005. Support vector machines for classification in remote sensing. *International Journal of Remote Sensing* 26(5): 1007-1011.

Parihar N, Das A, Rathore VS, Nathawat MS & Mohan S 2014. Analysis of L-band SAR backscatter and coherence for delineation of land-use/land cover. *International Journal of Remote Sensing* 35(18): 6781-6798.

Petrakos M & Benediktsson JA 2001. The effect of classifier agreement on the accuracy of combined classifier in decision level fusion. *IEEE Transaction on Geoscience and Remote Sensing* 39(11): 2539-2546.

Picoli MCA, Lamparelli RAC, Sano EE, de Mello JRB & Rocha JV 2013. Effect of sugarcane-planting row directions on ALOS/PALSAR satellite images. *GIScience & Remote Sensing* 50(3): 349-357.

Pohl C & Van Genderen JL 2010. Multi-sensor image fusion in remote sensing: concepts, methods and applications. *International Journal of Remote Sensing* 19(5): 823-854.

Pottier E & Lee JS 2000. *Application of the H/A/α polarimetric decomposition theorem for the unsupervised classification of fully polarimetric SAR data based on the Wishart distribution*. Proceedings of the CEOS SAR Workshop held 26-29 October 1999, Toulouse, France: 335-340.

Prakoso KU 2003. *Tropical forest mapping using multiband polarimetric and interferometric SAR data*. Proceedings of the First International Workshop on Science and Applications of SAR

Polarimetry and Polarimetric Interferometry (Pol-In-SAR) held 14-16 January 2003, Frascati, Italy.

Pu R, Gong P, Tian Y, Miao X, Carruthers RI & Anderson GL 2008. Using classification and NDVI differencing methods for monitoring sparse vegetation coverage: a case study of saltcedar in Nevada, USA. *International Journal of Remote Sensing* 29(14): 3987-4011.

Reese HM, Lillesand T, Nagek DE, Stewart JS, Goldman RA, Simppns TE, Chipmand JW & Tessar PA 2002. Statewide land cover derived from multiseasonal Landsat TM data - A retrospective of the WISCLAND project. *Remote Sensing of Environment* 82(2): 224-237.

Rodriguez-Galiano VF, Abarca-Hernandez F, Ghimire B, Chica-Olmo M, Atkinson PM & Jeganathan C 2011. Incorporating spatial variability measures in land cover classification using random forest. *Spatial Statistics* 3: 44-49.

Rodriguez-Galiano VF, Ghimire B, Rogan J, Chica-Olmo M & Rigol-Sanchez JP 2012. An assessment of the effectiveness of a random forest classifier for land cover classification. *ISPRS Journal of Photogrammetry and Remote Sensing* 67: 93-104.

Rosenthal WD & Blanchard BJ 1984. Active microwave responses: An aid in improved crop classification. *Photogrammetric Engineering and Remote Sensing* 50(4): 461-468.

Qi Z, Yeh AG, Li X & Lin Z 2012. A novel algorithm for land use and land cover classification using RADARSAT-2 polarimetric SAR data. *Remote Sensing of Environment* 118: 21-39.

Saha K, Wells NA & Munro-Stasiuk M 2011. An object-oriented approach to automated landform mapping: A case study of drumlins. *Computers and Geosciences* 37: 1324-1336.

Schistad Solberg AH & Jain AK 1997. Texture fusion and feature selection applied to SAR imagery. *IEEE Transactions on Geoscience and Remote Sensing* 35(2): 475-479.

Shang J, McNairn H, Champagne C & Jiao X 2009. Application of multi-frequency synthetic aperture radar (SAR) in crop classification. *Advances in Geoscience and Remote Sensing* Gary Jedlovec (Ed.): 557-568.

Sheroan A & Haak B 2013. Classification of California agriculture using quad polarization radar data and Landsat Thematic Mapper data. *GIScience & Remote Sensing* 50: 50-63.

Shi L 2012. The low backscattering targets classification in urban areas. *ISPRS Annals of the Photogrammetry, Remote Sensing and Spatial Information Sciences* 1-7: 173-176.

Shimoni M, Borghys D, Heremans R, Oerneel C & Acheroy M 2009. Fusion of PolSAR and PolInSAR data for land cover classification. *International Journal of Applied Earth Observation and Geoinformation* 11: 169-180.

Silva WF, Rudorff BET, Formaggio AR, Paradella WR & Mura JC 2009. *ISPRS Journal of Photogrammetry and Remote Sensing* 64: 458-463.

Simone G, Farina A, Morabito FC, Serpico SB & Bruzzone L 2002. Image fusion techniques for remote sensing applications. *Information Fusion* 3: 3-15.

Small D, Holecz F, Meier E, Nuesch D & Barmettler A 1997. *Geometric and Radiometric calibration of RADARSAT images*. Proceedings of the International Symposium on Geomatics in the Era of RADARSAT held 24-30 May, Ottawa, Canada.

Soria-Ruiz J, Fernandez-Ordonez Y, McNairn H & Bugden-Storie J 2007. *Crop monitoring and crop yield using optical and RADARSAT-2 images*. Proceedings of the Geoscience and Remote Sensing Symposium (IGARSS) held 23-27 July, Barcelona, Spain: 3655-3658.

Stuckens J, Coppin PR, & Bauer ME 2000. Integrating contextual information with per-pixel classification for improved land cover classification. *Remote Sensing of Environment* 71(3): 282-296.

Su W, Li J, Chen Y, Liu Z, Zhang J, Low TM, Suppiah I & Hashim SAM 2008. Textural and local spatial statistics for the object-oriented classification of urban areas using high resolution imagery. *International Journal of Remote Sensing* 29(11): 3105-3117.

Su W, Zhang C, Zhu X & Li D 2009. A hierarchical object oriented method for land cover classification of SPOT 5 imagery. *WSEAS Transactions on Information Science and Applications* 6(3): 437-446.

Taubenböck H, Esch T & Roth A 2006. *An urban classification approach based on an object-oriented analysis of high resolution satellite imagery for a spatial structuring within urban areas*. Proceedings of the 1st EARSel Workshop of the SIG Urban Remote Sensing held 2-3 March 2006, Berlin, Germany.

Touzi R & Lopes A 1994. The principle of speckle filtering in polarimetric SAR imagery. *IEEE Transactions on Geoscience and Remote Sensing* 32(5): 1110-1114.

Townsend JR, Justice CO & Kalb V 1987. Characterization and classification of South American land cover types using satellite data. *International Journal of Remote Sensing* 8(8): 1189-1207.

Tso B & Mather PM 2010. Crop discrimination using multi-temporal SAR imagery. *International Journal of Remote Sensing* 20(12): 2443-2460.

Turkar V, Deo R, Rao YS, Mohan S & Das A 2012. Classification accuracy of multi-frequency and multi-polarization SAR images for various land covers. *Selected Topics in IEEE Journal of Applied Earth Observations and Remote Sensing* 5(3): 936-941.

Turkar V & Rao YS 2011. *Applying coherent and incoherent target decomposition techniques to polarimetric SAR data*. Proceedings on the IJCA International Conference on Technology Systems and Management: 23-29.

Turker M & Arikan M 2005. Sequential masking classification of multi-temporal Landsat-7 ETM+ images of field based crop mapping in Karacabey Turkey. *International Journal of Remote Sensing* 26(17): 3813-3830.

Uhlmann S, Kiraryaz S & Gabbouj M 2014. Semi supervised learning for ill-posed polarimetric SAR classification. *Remote Sensing* 6: 4801-4830.

Ulaby FT & Batlivala PP 1976. Optimum radar parameters for mapping soil moisture. *IEEE Transactions on Geoscience Electronics* 14(2): 81-93.

Ulaby FT, Moore RK & Fung AK 1986. *Microwave remote sensing active and passive-volume III: from theory to applications*. Massachusetts: Artech House Incorporated.

Van Niel TG & McVicar TR 2004. Determining temporal windows for crop discrimination with remote sensing: a case study in south-eastern Australia. *Computers and Electronics in Agriculture* 45: 91-108.

Van Zyl 1989. Unsupervised Classification of Scattering Behaviour Using Radar Polarimetry Data. *IEEE Transactions on Geoscience and Remote Sensing* 27(1): 36-45.

Villeneuve N, Bachèlery P & Kemp JN 2014. La Réunion Island: A typical example of a basaltic shield volcano with rapid evolution. In Fort M & Andre MF (eds) *Landscapes and Landforms of France*, 261-270. Netherlands: Springer.

Wang LW, Zhang Y, Lu X & Wang P 2009. Unsupervised classification of polarimetric SAR data using image clustering and H/A/α decomposition. *Proceedings of the ISPRS* 38: 268-271.

Waske B & Braun M 2009. Classifier ensembles for land cover mapping using multitemporal SAR imagery. *ISPRS Journal of Photogrammetry and Remote Sensing* 64: 450-457.

Waske B & Van der Linden 2008. Classifying multilevel imagery from SAR and optical sensors by decision fusion. *IEEE Transactions on Geoscience and Remote Sensing* 46(*5*): 1457-1466.

Yang C, Everitt JH & Murden D 2011. Evaluation high resolution SPOT-5 satellite imagery for crop identification. *Computers and Electronics in Agriculture* 75: 347-354.

Yonghong J 1998. Fusion of landsat TM and SAR image based on principal component analysis. *Remote Sensing Technology and Application* 13(1): 46-49.

Yu Q, Gong P, Clinton N, Biging G, Kelly M & Schirokauer D 2006. Object-based detailed vegetation classification with airborne high spatial resolution remote sensing imagery. *Photogrammetric Engineering and Remote Sensing* 72: 799-811.

Zhang Y 2004. Understanding image fusion. *Photogrammetric Engineering and Remote Sensing* 70(6): 657-661.

Zhang J 2010. Multi-source remote sensing data fusion: status and trends. *International Journal of Image and Data Fusion* 1(1): 5-24.

Zhu Z, Woodcock CE, Rogan J & Kellndorfer J 2012. Assessment of spectral, polarimetric, temporal, and spatial dimensions for urban and per-urban land cover classification using Landsat and SAR data. *Remote Sensing of Environment* 117: 72-82.

APPENDICES

The following can be found in the appendices:

Appendix A: Definitions of features derived from layers

Appendix B: Naming conventions and the full ranking list of the features for the multi-temporal, dual-sensor data set

Appendix C: All confusion matrices, ordered by the analytical components.

9.1   APPENDIX A

GLOSSARY OF FEATURE DESCRIPTIONS

The below table lists the feature types derived for feature selection and classifier training. There are near verbatim definitions from the eCognition Developer v8.7 Reference Book in order to help understanding.

GLCM (page 329-326)	Homogeneity	If an image is locally homogenous, values will be high.
	Contrast	This is the opposite of homogeneity and measures local variance.
	Dissimilarity	Similar to contrast, except in increases linearly and not exponentially. It is high if the local region has high contrast.
	Entropy	Entropy is high when elements of the GLCM are distributed equally.
	2nd Angular Moment	This is another measure of local homogeneity. High values indicate high elements surrounded by smaller ones.
	Mean	This is the average of the GLCM. The pixel value is not weighted by its frequency alone, but by the frequency of its occurrence in combination with a neighbouring pixel value.
	Standard Deviation	Measure of dispersion around the mean and deals specifically with the combination of reference and neighbour pixels.
	Correlation	Measures the linear dependency of gray levels of neighbouring pixels.
GLDV (Sum of the diagonals of the GLCM) (page 327-328)	2nd Angular Moment	This is another measure of local homogeneity. High values indicate high elements surrounded by smaller ones.
	Entropy	This is the opposite to GLDV 2nd Angular Moment. Similar elements will provide high values.
	Mean	Mathematically this is equivalent to GLCM Dissimilarity
	Contrast	Mathematically this is equivalent to GLCM Contrast
Layer (page 235 - 238)	Mean	Mean layer intensity, calculated using the pixel values within the object
	Standard Deviation	The standard deviation of layer intensity, calculated using the pixel values within the object
	Brightness	Calculated using the mean of multiple layers
	Maximum Difference	Calculated using the difference measure between multiple layers

9.2   APPENDIX B

In order to interpret the feature rankings for the multi-temporal, dual sensor data set, the naming convention used is presented first. This was necessary due to the character limits implemented in the shapefile export. The names consist of firstly a letter, corresponding to the image date it was derived from, then a feature name, then a layer value. Use the following tables to understand these codes in the feature rankings.

9.2.1   Naming convention

LETTER CODE AT START OF FEATURE NAME	CORRESPONDING IMAGE DATE
(NO LETTER)	2014-02-22
A	2014-05-05
B	2014-05-29
C	2014-08-09

FULL FEATURE NAME:	ABBREVIATED NAME:
Area	Area
Asymmetry	Asymmetry
Border Index	Border_Ind
Border Length	Border_Len
Brightness	Brightness
Compactness	Compact
Density	Density
Elliptical Fit	Ellip_Fit
GLCM_Angular2_Moment_Layer	GCM_A2_Numbercode
GLCM_Contrast_Layer	GCM_CN_Numbercode
GLCM_Correlation_Layer	GCM_CR_Numbercode
GLCM_Dissimilarity_Layer	GCM_DS_Numbercode
GLCM_Entropy_Layer	GCM_EN_Numbercode
GLCM_Homogeneity	GCM_HM_Numbercode
GLCM_Mean	GCM_MN_Numbercode
GLCM_StandardDeviation	GCM_SD_Numbercode
GLDV_Angular2_Moment_Layer	GDV_A2_Numbercode
GLDV_Contrast_Layer	GDV_CN_Numbercode
GLDV_Entropy_Layer	GDV_EN_Numbercode

GLDV_Mean	GDV_MN_Numbercode
Length	Length
Length/Thickness	Len/Thick
Length/Width	Len/Wid
Maximum difference	Max_diff
Mean of layer	Mean_Numbercode
NDVI	NDVI
Rectangualr Fit	Rect_Fit
Roundness	Roundness
Shape Index	Shape_Ind
Standard Deviation of layer	Std_Dev_Numbercode
Thickness	Thickness
Width	Width

LAYER	NUMBER CODE
Alpha	1
Anisotropy	2
Entropy	3
Freeman Durden Double Bounce	4
Freeman Durden Odd Bounce	5
Freeman Durden Volume	6
Green	7
HH (Filtered)	8
HV (Filtered)	9
Krogager Diplane	10
Krogager Helix	11
Krogager Sphere	12
NIR	13
Red	14
SWIR	15
Unfiltered HH	16
Unfiltered HV	17
Unfiltered VH	18
Unfiltered VV	19
VH (Filtered)	20

VV (Filtered)	21
Van Zyl Double Bounce	22
Van Zyl Odd Bounce	23
Van Zyl Volume Scattering	24
Yamaguchi Double Bounce	25
Yamaguchi Helix	26
Yamaguchi Odd	27
Yamaguchi Volume	28
all directions	29

Example of a feature name decoded:

CGCM_MN_07

     C: 2014-08-09

     GCM_MN: GLCM Mean textural feature

     07: Green band

9.2.2 Full multi-temporal feature ranking

(All features with a score above zero)

	Variable	Score
1.	GCM_MN_07	100.0000
2.	CMAX_DIFF	75.2829
3.	GCM_MN_14	71.9902
4.	NDVI	67.9773
5.	BGCM_MN_07	66.4354
6.	CMEAN_14	64.6253
7.	GCM_MN_13	61.5125
8.	CNDVI	59.8774
9.	STDDEV_20	59.7231
10.	CGCM_MN_29	57.2278
11.	CGCM_MN_07	56.7237
12.	BGCM_MN_14	56.0418
13.	CBRIGHTNES	55.2015
14.	MEAN_14	52.7558
15.	ABRIGHTNES	52.1910
16.	MEAN_07	52.1245
17.	STD_DEV_21	51.6869
18.	CMEAN_07	50.9087
19.	BMEAN_14	49.3611
20.	AMEAN_07	49.1963
21.	BGCM_DS_14	49.1518
22.	CGCM_MN_15	48.5244
23.	BRIGHTNESS	47.3154
24.	GDV_A2_29	46.6736
25.	AGCM_MN_15	46.5902

26.	CMEAN_01	46.2243
27.	CGDV_EN_14	45.6748
28.	CGCM_DS_07	45.2629
29.	AGCM_MN_07	44.4912
30.	BMEAN_13	44.1237
31.	BBRIGHTNES	43.8434
32.	GCM_DS_07	43.7563
33.	GCM_EN_13	43.6043
34.	AMEAN_14	42.8991
35.	CGDV_MN_14	42.7805
36.	MEAN_01	41.9848
37.	MEAN_15	41.3382
38.	MEAN_10	40.9435
39.	BGCM_CN_07	40.9174
40.	BGDV_A2_07	40.5054
41.	CGCM_MN_14	40.3350
42.	CMEAN_22	39.9479
43.	CGCM_MN_13	39.9245
44.	MEAN_13	39.7628
45.	AGCM_MN_29	39.3483
46.	BGCM_HM_14	39.1275
47.	CGCM_HM_29	38.3443
48.	CMEAN_21	38.1756
49.	BGCM_MN_29	38.0477
50.	CGCM_CN_14	37.3495
51.	MEAN_04	36.7698
52.	BNDVI	36.6255
53.	CMEAN_08	36.3027
54.	CMEAN_25	36.2891
55.	CGCM_A2_14	36.2467
56.	GCM_MN_29	36.0065
57.	CGCM_EN_14	35.7572
58.	AMEAN_15	35.6766
59.	MEAN_12	35.3932
60.	AMEAN_16	35.0854
61.	BSTDDEV_21	34.5492
62.	MEAN_05	34.4117
63.	MEAN_28	33.7705
64.	BMEAN_09	33.4871
65.	CGDV_CN_07	32.9513
66.	BMEAN_07	32.8672
67.	AMEAN_21	32.5002
68.	GCM_MN_15	32.4849
69.	CMEAN_05	32.3464
70.	CMEAN_15	32.2994
71.	ANDVI	32.2729
72.	BGCM_MN_15	32.2287
73.	MEAN_20	31.8315
74.	BMEAN_20	31.6936
75.	BGCM_SD_14	31.6105
76.	CGCM_SD_29	31.2274
77.	BMEAN_16	31.1200
78.	MEAN_06	30.7406
79.	CMEAN_20	30.4162
80.	GCM_HM_07	30.2790
81.	GCM_SD_07	30.2214

82. MEAN_25	30.0563
83. GCM_EN_07	30.0331
84. BMAX_DIFF	29.7747
85. CSTDDEV_13	29.6509
86. BGDV_CN_14	29.6404
87. CSTDDEV_21	29.3390
88. GCM_DS_29	29.1312
89. BGCM_EN_13	28.9652
90. MEAN_19	28.9417
91. BMEAN_21	28.7094
92. STD_DEV_20	28.5326
93. MEAN_03	28.5212
94. CGDV_A2_14	28.5212
95. CMEAN_19	28.4979
96. BMEAN_17	28.2540
97. GDV_CN_15	28.2454
98. GCM_DS_13	28.1477
99. STD_DEV_25	27.9880
100. CSTDDEV_04	27.8741
101. BGDV_CN_07	27.8207
102. AGDV_EN_07	27.7729
103. BGCM_SD_07	27.6913
104. GCM_CN_13	27.5779
105. MAX_DIFF	27.4247
106. BSTDDEV_14	27.2021
107. GDV_CN_07	27.0134
108. CMEAN_03	27.0057
109. BMEAN_08	26.6837
110. CGCM_HM_14	26.6521
111. ASTDDEV_09	26.5979
112. CGCM_MN_01	26.5582
113. BGDV_MN_07	26.4803
114. BMEAN_15	26.4511
115. BGCM_DS_13	26.3755
116. GDV_A2_07	26.3407
117. GDV_MN_07	26.1685
118. STD_DEV_22	26.1039
119. BGCM_MN_13	26.0610
120. BGCM_MN_01	26.0238
121. CGDV_CN_14	25.9644
122. AGCM_SD_07	25.8702
123. GDV_A2_14	25.5144
124. AGCM_MN_14	25.3424
125. BGCM_A2_13	25.3280
126. MEAN_23	25.2486
127. ASTDDEV_20	25.1781
128. CGCM_DS_29	25.0347
129. AGCM_SD_14	24.9867
130. GCM_A2_14	24.9668
131. STD_DEV_07	24.7439
132. BSTDDEV_09	24.7401
133. CGCM_DS_14	24.7161
134. MEAN_22	24.2003
135. GCM_HM_14	24.1777
136. CGDV_CN_15	24.1493
137. BGDV_A2_14	24.0975

138. STD_DEV_10	23.8951
139. MEAN_17	23.7779
140. BGCM_SD_29	23.7622
141. AMEAN_09	23.4990
142. CSTDDEV_23	23.4931
143. BMEAN_01	23.3953
144. CMEAN_13	23.2335
145. AGDV_MN_07	23.1688
146. GDV_EN_13	23.0172
147. GCM_MN_01	22.8435
148. BMEAN_04	22.7196
149. MEAN_08	22.6062
150. GDV_EN_29	22.3928
151. STD_DEV_14	22.3815
152. AMEAN_23	22.2551
153. CSTDDEV_08	22.1337
154. BGDV_CN_29	22.1271
155. BGCM_DS_07	21.9866
156. GCM_A2_07	21.8983
157. BGCM_A2_07	21.6077
158. MEAN_11	21.4622
159. GDV_A2_13	21.3110
160. AGCM_SD_29	21.2416
161. CSTDDEV_12	21.0260
162. BGCM_EN_07	20.9708
163. BGCM_A2_14	20.7681
164. GCM_HM_13	20.7413
165. ASTDDEV_14	20.7342
166. BGCM_CN_29	20.7058
167. CGDV_MN_13	20.5463
168. MEAN_18	20.5153
169. CSTDDEV_09	20.5007
170. BMEAN_19	20.3899
171. STD_DEV_27	20.2377
172. STD_DEV_08	20.2057
173. BGCM_CN_15	20.1624
174. MEAN_09	20.1439
175. BGDV_EN_14	20.1412
176. STD_DEV_05	20.1113
177. BGCM_CN_13	20.0010
178. LENGTH_PXL	19.9581
179. MEAN_26	19.9499
180. CMEAN_06	19.9484
181. CSTDDEV_20	19.9151
182. BGDV_MN_14	19.8593
183. CMEAN_12	19.7991
184. CGCM_A2_13	19.7455
185. AGCM_MN_13	19.7078
186. BGCM_EN_14	19.6550
187. CSTDDEV_28	19.5970
188. BMEAN_03	19.5159
189. STD_DEV_04	19.3918
190. GCM_SD_29	19.3077
191. AGCM_MN_01	19.2772
192. GCM_EN_14	19.2738
193. CGCM_HM_13	19.1904

194. BSTDDEV_05	19.1420
195. BSTDDEV_06	19.1019
196. STD_DEV_26	19.0578
197. ASTDDEV_08	19.0168
198. AMEAN_19	18.8659
199. CGCM_EN_15	18.7683
200. GCM_CN_29	18.5422
201. CMEAN_24	18.4790
202. BGDV_EN_13	18.4721
203. CGCM_DS_13	18.4097
204. CGCM_HM_07	18.2917
205. AGCM_DS_07	18.2590
206. BSTDDEV_07	18.1874
207. CGDV_MN_07	18.1534
208. CMEAN_09	18.0288
209. CSTDDEV_10	18.0022
210. GDV_EN_15	17.9180
211. AMEAN_27	17.9129
212. GCM_CN_15	17.7436
213. STD_DEV_23	17.7192
214. MEAN_16	17.5449
215. CGDV_EN_07	17.4894
216. AMEAN_05	17.3907
217. CGCM_A2_07	17.3798
218. GDV_MN_29	17.3572
219. GDV_CN_14	17.3340
220. BGCM_CN_14	17.2280
221. AMEAN_26	17.1479
222. BMEAN_05	17.0084
223. ASTDDEV_25	17.0067
224. VOLUME_PXL	16.8319
225. AMEAN_12	16.7610
226. WIDTH_PXL	16.7281
227. CSTDDEV_11	16.7259
228. AGDV_A2_14	16.6647
229. CGDV_A2_29	16.6112
230. GCM_EN_29	16.5284
231. AMEAN_20	16.5064
232. CGCM_CN_07	16.4081
233. BGDV_MN_15	16.3762
234. ASTDDEV_12	16.3594
235. AMEAN_17	16.2726
236. AMEAN_13	16.1284
237. BSTDDEV_08	16.0424
238. AGDV_EN_14	16.0384
239. GCM_SD_14	15.9197
240. MEAN_24	15.8909
241. CMEAN_10	15.8512
242. BGDV_A2_13	15.8016
243. CGCM_EN_13	15.7827
244. AMAX_DIFF	15.7818
245. AGCM_CR_14	15.6965
246. BMEAN_12	15.6845
247. CGCM_SD_14	15.5871
248. BGCM_CR_14	15.5646
249. MEAN_27	15.4866

250. BMEAN_27	15.4476
251. GCM_CN_07	15.2789
252. CSTDDEV_05	15.2662
253. AREA_PXL	15.1385
254. STD_DEV_24	15.0036
255. CGDV_MN_29	14.9197
256. CGCM_CN_29	14.9054
257. CMEAN_26	14.8784
258. AMEAN_18	14.8714
259. CMEAN_28	14.8404
260. BGCM_SD_13	14.7950
261. CGDV_A2_07	14.7210
262. CGCM_EN_07	14.6855
263. CSTDDEV_14	14.6508
264. GCM_SD_13	14.6343
265. AMEAN_08	14.4099
266. ASTDDEV_21	14.3190
267. GDV_CN_29	14.2245
268. BSTDDEV_27	14.0603
269. GCM_CN_14	14.0163
270. CGCM_DS_15	13.9516
271. GCM_DS_15	13.8335
272. BSTDDEV_15	13.8062
273. CGCM_CN_15	13.7082
274. CMEAN_16	13.7065
275. AMEAN_01	13.7064
276. BGDV_MN_13	13.7008
277. ASTDDEV_28	13.5890
278. CGDV_CN_13	13.4878
279. CMEAN_17	13.4455
280. CMEAN_23	13.4393
281. ASTDDEV_07	13.3589
282. CSTDDEV_26	13.3185
283. BGCM_EN_29	13.3092
284. BSTDDEV_13	13.3074
285. AGCM_EN_14	13.3030
286. AGCM_CN_14	13.2180
287. AGCM_CN_15	13.2081
288. CGCM_HM_15	13.2016
289. STD_DEV_13	13.1802
290. AGCM_HM_14	13.0417
291. CSTDDEV_22	13.0291
292. CGDV_MN_15	13.0114
293. GDV_MN_14	12.9566
294. BSTDDEV_03	12.9301
295. MEAN_02	12.8837
296. GDV_A2_15	12.8799
297. GDV_CN_13	12.7702
298. CSTDDEV_25	12.7368
299. GDV_EN_07	12.6713
300. GCM_DS_14	12.6662
301. BSTDDEV_23	12.6460
302. BMEAN_25	12.6026
303. CSTDDEV_06	12.5985
304. AGCM_EN_07	12.3579
305. ASTDDEV_26	12.2647

306. BMEAN_02	12.1044
307. GDV_MN_15	11.9398
308. BGDV_A2_29	11.9317
309. AGCM_DS_29	11.8938
310. CGDV_CN_29	11.8276
311. CGCM_A2_29	11.7051
312. AGCM_A2_14	11.5908
313. CGCM_SD_13	11.4705
314. CMEAN_27	11.4251
315. STD_DEV_09	11.4151
316. BGDV_CN_13	11.2755
317. CMEAN_04	11.2428
318. GCM_A2_29	11.1411
319. CGCM_CR_15	11.0170
320. GCM_HM_15	11.0155
321. AGCM_CN_07	10.9922
322. CGCM_CR_14	10.9689
323. STD_DEV_28	10.9420
324. AMEAN_03	10.9077
325. ASTDDEV_27	10.8731
326. BGDV_A2_15	10.8402
327. CGCM_CN_13	10.7525
328. CGDV_EN_15	10.7433
329. AGDV_MN_15	10.6131
330. ASTDDEV_10	10.5955
331. AGCM_EN_15	10.5675
332. AMEAN_06	10.4130
333. AGCM_DS_14	10.3219
334. AMEAN_10	10.2898
335. BORDER_LEN	10.2105
336. BMEAN_18	10.1771
337. CSTDDEV_27	10.1639
338. BGDV_MN_29	10.0889
339. AGDV_A2_13	10.0693
340. AMEAN_02	9.9151
341. BGCM_HM_07	9.9103
342. ASTDDEV_23	9.8653
343. BGDV_EN_07	9.7356
344. AMEAN_25	9.7250
345. BSTDDEV_12	9.7142
346. AGDV_CN_07	9.7100
347. BGCM_DS_29	9.6932
348. CGDV_EN_29	9.6751
349. CSTDDEV_03	9.5624
350. GCM_SD_15	9.5086
351. STD_DEV_06	9.3607
352. AMEAN_28	9.3243
353. AGCM_A2_07	9.2983
354. AGDV_MN_13	9.1387
355. GCM_HM_29	9.1117
356. AGDV_CN_14	9.0717
357. CGCM_A2_15	9.0411
358. AGDV_CN_29	9.0268
359. AGCM_HM_13	9.0147
360. ASTDDEV_05	9.0130
361. AGCM_CN_29	8.9831

362. AGDV_EN_15	8.9686
363. BSTDDEV_10	8.9643
364. BSTDDEV_04	8.8847
365. GDV_MN_13	8.6458
366. BGCM_SD_15	8.6253
367. AGDV_A2_07	8.6003
368. MEAN_21	8.5768
369. BMEAN_10	8.5053
370. AMEAN_24	8.4895
371. BGCM_CR_15	8.4546
372. BGDV_CN_01	8.4420
373. STD_DEV_12	8.3763
374. CMEAN_11	8.3708
375. BMEAN_26	8.2140
376. CSTDDEV_24	8.1842
377. CGCM_CR_29	8.1363
378. BGCM_HM_13	8.1239
379. BGCM_EN_15	7.9468
380. GCM_A2_13	7.9391
381. CSTDDEV_07	7.9166
382. CGCM_SD_15	7.9148
383. BGCM_A2_15	7.7778
384. ASTDDEV_15	7.6762
385. BGCM_A2_29	7.6546
386. CSTDDEV_15	7.5056
387. BGCM_A2_01	7.4902
388. BGCM_DS_15	7.4731
389. BGDV_EN_15	7.3936
390. AGCM_DS_13	7.3662
391. CMEAN_18	7.3153
392. GDV_EN_14	7.2666
393. BSTDDEV_25	7.2594
394. AGCM_A2_29	7.2456
395. AGCM_SD_15	7.1502
396. GCM_CR_13	7.1484
397. BSTDDEV_18	7.1075
398. GCM_A2_15	7.1037
399. BGCM_EN_01	7.0827
400. ROUNDNESS	7.0215
401. CGDV_EN_13	6.9575
402. ASTDDEV_06	6.9253
403. BSTDDEV_28	6.8804
404. AGDV_MN_14	6.7691
405. AGDV_CN_13	6.7687
406. AGDV_EN_29	6.7098
407. AGCM_CR_07	6.5900
408. COMPACTNES	6.5562
409. AGDV_A2_15	6.3706
410. STD_DEV_11	6.3641
411. AGCM_SD_13	6.3580
412. CMEAN_02	6.2959
413. AGDV_A2_29	6.2834
414. GCM_CR_14	6.2755
415. AMEAN_04	6.2734
416. RECTANGULA	6.1519
417. CGDV_MN_01	6.0712

418. GCM_EN_15	6.0688
419. ASTDDEV_24	6.0545
420. AMEAN_11	6.0190
421. AMEAN_22	5.9643
422. BMEAN_23	5.9599
423. AGCM_HM_01	5.8711
424. BGCM_CN_01	5.8711
425. CGCM_EN_29	5.8428
426. CGDV_A2_15	5.8291
427. BGCM_HM_29	5.8288
428. AGDV_CN_15	5.7535
429. BSTDDEV_01	5.7432
430. GCM_CR_01	5.7170
431. AGCM_CN_13	5.7009
432. BSTDDEV_02	5.6769
433. BGDV_EN_29	5.6344
434. CGCM_CR_07	5.5634
435. BGDV_EN_01	5.5627
436. ASTDDEV_22	5.5156
437. BMEAN_24	5.4254
438. CGDV_CN_01	5.4143
439. AGCM_CN_01	5.3976
440. BGDV_CN_15	5.3597
441. CGCM_SD_07	5.3537
442. CGCM_CN_01	5.3190
443. STD_DEV_01	5.3112
444. BORDER_IND	5.2320
445. BGCM_CR_29	5.2313
446. BSTDDEV_24	5.1989
447. AGCM_A2_13	5.1294
448. CGCM_EN_01	5.1129
449. AGCM_HM_15	5.1091
450. ASTDDEV_11	5.0836
451. ASYMMETRY	5.0752
452. CSTDDEV_19	5.0641
453. BMEAN_22	4.9594
454. STD_DEV_15	4.9289
455. BMEAN_06	4.9119
456. GCM_CR_29	4.8748
457. CGCM_DS_01	4.8199
458. AGDV_A2_01	4.7481
459. BGCM_HM_15	4.7230
460. BSTDDEV_11	4.7163
461. BGCM_HM_01	4.6938
462. STD_DEV_16	4.6495
463. GCM_CR_07	4.6330
464. ASTDDEV_04	4.6081
465. CGDV_A2_13	4.5992
466. GCM_DS_01	4.5816
467. STD_DEV_03	4.5630
468. ASTDDEV_13	4.5527
469. BMEAN_28	4.5421
470. CGCM_SD_01	4.3801
471. STD_DEV_18	4.3643
472. AGCM_SD_01	4.3537
473. AGDV_MN_29	4.3442

474. BMEAN_11	4.3077
475. BSTDDEV_22	4.2227
476. AGCM_DS_15	4.2148
477. ASTDDEV_17	4.1726
478. SHAPE_INDE	4.1545
479. GDV_A2_01	4.1505
480. GCM_CN_01	4.1175
481. LENGTHWIDT	4.0664
482. CSTDDEV_02	4.0249
483. STD_DEV_02	3.9519
484. AGCM_CR_15	3.9481
485. BGCM_SD_01	3.9298
486. ELLIP_FIT	3.9236
487. BGCM_CR_13	3.8940
488. AGDV_MN_01	3.7919
489. BGDV_MN_01	3.7872
490. AGCM_HM_07	3.7828
491. AGCM_HM_29	3.7713
492. AGCM_EN_29	3.7521
493. AGDV_EN_13	3.6859
494. DENSITY	3.6729
495. BGDV_A2_01	3.6201
496. GCM_CR_15	3.5618
497. BGCM_DS_01	3.5415
498. ASTDDEV_03	3.4371
499. AGCM_CR_29	3.4014
500. AGCM_A2_01	3.3388
501. CGCM_CR_13	3.3303
502. GCM_A2_01	3.3067
503. GCM_HM_01	3.3032
504. AGDV_EN_01	3.2487
505. MAIN_DIREC	3.2433
506. CGCM_CR_01	3.1997
507. AGCM_CR_13	3.1933
508. BGCM_CR_07	3.1769
509. ASTDDEV_02	3.1171
510. AGCM_A2_15	3.1132
511. GCM_EN_01	3.0854
512. BSTDDEV_16	3.0444
513. ASTDDEV_19	2.8731
514. ASTDDEV_16	2.7466
515. BGCM_CR_01	2.7311
516. BSTDDEV_19	2.6957
517. BSTDDEV_26	2.6783
518. CSTDDEV_01	2.6258
519. AGDV_CN_01	2.6030
520. CGCM_HM_01	2.5608
521. CGDV_A2_01	2.5486
522. GDV_EN_01	2.4996
523. CSTDDEV_18	2.4239
524. STD_DEV_19	2.2500
525. ASTDDEV_01	2.2473
526. BSTDDEV_17	2.2196
527. GDV_MN_01	2.1755
528. CSTDDEV_16	2.1481
529. GDV_CN_01	2.1398

530. CGCM_A2_01	2.0983
531. STD_DEV_17	2.0230
532. CGDV_EN_01	2.0009
533. CSTDDEV_17	1.9962
534. AGCM_DS_01	1.9619
535. GCM_SD_01	1.9457
536. AGCM_EN_13	1.9446
537. AGCM_CR_01	1.5023
538. AGCM_EN_01	1.4570
539. ASTDDEV_18	1.2009

9.3   APPENDIX C

9.3.1   Experiment 2: Confusion matrices

2014-05-05 DECISION TREE CLASSIFICATION ON COMBINED SAR-OPTICAL DATA: ACCURACY ASSESSMENT

		Classification Image									
		Artificial Surfaces	Bare Soil	Cultivated HG	Cultivated HNG	Cultivated Trees	Managed Grass	Natural HSB	Natural Trees	Water	Grand Total	Producer's Accuracy
Reference Image	Artificial Surfaces	26	2	1	2		2	1		7	**41**	0.63
	Bare Soil	2	23		1			2		2	**30**	0.77
	Cultivated HG		1	23	8	3	1	2		1	**39**	0.59
	Cultivated HNG	1	8	8	32	2	4	7		2	**64**	0.5
	Cultivated Trees			6	3	2	2	4			**17**	0.12
	Managed Grass	2	2	7	4	1	10	6			**32**	0.31
	Natural HSB	2		7	12	7	8	14	7		**57**	0.25
	Natural Trees				1		1	6	18		**26**	0.69
	Water	3	1		7		3	2		29	**45**	0.64
	Grand Total	**36**	**37**	**52**	**70**	**15**	**31**	**44**	**25**	**41**	**351**	
	Users Accuracy	0.72	0.62	0.44	0.46	0.13	0.32	0.32	0.72	0.71	**351**	
	Overall Accuracy	**0.50**										
	Kappa	**0.43**										

2014-05-05 SVM CLASSIFICATION ON COMBINED SAR-OPTICAL DATA: ACCURACY ASSESSMENT

		Classification Image									
		Artificial Surfaces	Bare Soil	Cultivated HG	Cultivated HNG	Cultivated Trees	Managed Grass	Natural HSB	Natural Trees	Water	Grand Total	Producer's Accuracy
Reference Image	Artificial Surfaces	32			1		3	2		3	**41**	0.78
	Bare Soil	1	22	1	2		3			1	**30**	0.73
	Cultivated HG		1	19	10	7		2			**39**	0.49
	Cultivated HNG		4	6	41	2		10		1	**64**	0.64
	Cultivated Trees			3	5	1	1	5	1	1	**17**	0.06
	Managed Grass	1		1	3	1	20	6			**32**	0.63
	Natural HSB		2	1	5	2	9	23	13	2	**57**	0.40
	Natural Trees					1		5	20		**26**	0.77
	Water	1	1		1	1				41	**45**	0.91
	Grand Total	**35**	**30**	**31**	**68**	**15**	**36**	**53**	**34**	**49**	**351**	
	Users Accuracy	0.91	0.73	0.61	0.60	0.07	0.56	0.43	0.595	0.84	**351**	
	Overall Accuracy	**0.62**										
	Kappa	**0.57**										

2014-05-05 RANDOM FOREST CLASSIFICATION ON COMBINED SAR-OPTICAL DATA: ACCURACY ASSESSMENT

		Classification Image										
		Artificial Surfaces	Bare Soil	Cultivated HG	Cultivated HNG	Cultivated Trees	Managed Grass	Natural HSB	Natural Trees	Water	Grand Total	Producer's Accuracy
Reference Image	Artificial Surfaces	38	1				1	1			**41**	0.93
	Bare Soil		26		1		1	2			**30**	0.87
	Cultivated HG			22	9	1		7			**39**	0.56
	Cultivated HNG	1	3	1	48	2		9			**64**	0.75
	Cultivated Trees			4	12			1			**17**	0
	Managed Grass	1		1	4		20	6			**32**	0.63
	Natural HSB	1		3	11	1	3	31	7		**57**	0.54
	Natural Trees				2		1	2	21		**26**	0.81
	Water	2			5					38	**45**	0.84
	Grand Total	**43**	**30**	**31**	**92**	**4**	**26**	**59**	**28**	**38**	**351**	
	Users Accuracy	0.88	0.87	0.71	0.52	0	0.77	0.53	0.75	1	**351**	
	Overall Accuracy	**0.695**										
	Kappa	**0.65**										

2014-05-05 BAYES (MAXIMUM LIKELIHOOD) CLASSIFICATION ON COMBINED SAR-OPTICAL DATA: ACCURACY ASSESSMENT

		Classification Image										
		Artificial Surfaces	Bare Soil	Cultivated HG	Cultivated HNG	Cultivated Trees	Managed Grass	Natural HSB	Natural Trees	Water	Grand Total	Producer's Accuracy
Reference Image	Artificial Surfaces	21			20						**41**	0.51
	Bare Soil		7		23						**30**	0.23
	Cultivated HG			3	29			7			**39**	0.08
	Cultivated HNG				55			9			**64**	0.86
	Cultivated Trees				15			2			**17**	0
	Managed Grass			1	21			10			**32**	0
	Natural HSB				34			23			**57**	0.40
	Natural Trees				11			15			**26**	0
	Water				20			2		23	**45**	0.51
	Grand Total	**21**	**7**	**4**	**228**	**0**	**0**	**68**	**0**	**23**	351	
	Users Accuracy	1	1	0.75	0.24	0	0	0.34	0	1	351	
	Overall Accuracy	**0.38**										
	Kappa	**0.25**										

2014-05-05 KNN CLASSIFICATION ON COMBINED SAR-OPTICAL DATA: ACCURACY ASSESSMENT

		Classification Image										
		Artificial Surfaces	Bare Soil	Cultivated HG	Cultivated HNG	Cultivated Trees	Managed Grass	Natural HSB	Natural Trees	Water	Grand Total	Producer's Accuracy
Reference Image	Artificial Surfaces	25	1	5	4		2			4	**41**	0.61
	Bare Soil		25	1	1		1	2			**30**	0.83
	Cultivated HG		2	19	7	2	2	6	1		**39**	0.48
	Cultivated HNG	1	2	5	46	2	1	6		1	**64**	0.72
	Cultivated Trees			6	4	3	1	3			**17**	0.18
	Managed Grass	1	1	6	7	2	10	5			**32**	0.31
	Natural HSB	1		7	13	3	5	22	5	1	**57**	0.39
	Natural Trees			1	2				4	19	**26**	0.73
	Water	1		2	3			2	1	36	**45**	0.8
	Grand Total	**29**	**31**	**52**	**87**	**12**	**22**	**50**	**26**	**42**	351	
	Users Accuracy	0.86	0.81	0.37	0.53	0.25	0.45	0.44	0.73	0.86	351	
	Overall Accuracy	**0.58**										
	Kappa	**0.52**										

2014-05-05 CART CLASSIFICATION ON COMBINED SAR-OPTICAL DATA: ACCURACY ASSESSMENT

		Classification Image										
		Artificial Surfaces	Bare Soil	Cultivated HG	Cultivated HNG	Cultivated Trees	Managed Grass	Natural HSB	Natural Trees	Water	Grand Total	Producer's Accuracy
Reference Image	Artificial Surfaces	28	3		5		2			3	**41**	0.68
	Bare Soil	1	24	1	2			1		1	**30**	0.8
	Cultivated HG		2	22	1	9	1	4			**39**	0.56
	Cultivated HNG	1	8	9	25	4	3	13		1	**64**	0.39
	Cultivated Trees			6	2	4	1	4			**17**	0.24
	Managed Grass	1	3	1			22	5			**32**	0.69
	Natural HSB	1		9	5	5	11	20	5	1	**57**	0.35
	Natural Trees			1		1	2	3	19		**26**	0.73
	Water	1	1		2	1	4	3		33	**45**	0.73
	Grand Total	**33**	**41**	**49**	**42**	**24**	**46**	**53**	**24**	**39**	351	
	Users Accuracy	0.85	0.59	0.45	0.59	0.167	0.48	0.38	0.79	0.85	351	
	Overall Accuracy	**0.56**										
	Kappa	**0.50**										

2014-08-09 DECISION TREE CLASSIFICATION ON COMBINED SAR-OPTICAL DATA: ACCURACY ASSESSMENT

		Classification Image										
		Artificial Surfaces	Bare Soil	Cultivated HG	Cultivated HNG	Cultivated Trees	Managed Grass	Natural HSB	Natural Trees	Water	Grand Total	Producer's Accuracy
Reference Image	Artificial Surfaces	31	1	3	1		1			4	41	0.76
	Bare Soil	3	21	5				1			30	0.7
	Cultivated HG		1	17	11	7	1			2	39	0.44
	Cultivated HNG		1	11	31	9	2	4	3	3	64	0.48
	Cultivated Trees			3	6	5		3			17	0.29
	Managed Grass	1		1	3	1	21	5			32	0.66
	Natural HSB			7	13	2	5	21	7	2	57	0.37
	Natural Trees				3			1	22		26	0.85
	Water	2		2	1	1	2	1		36	45	0.8
	Grand Total	**37**	**24**	**49**	**69**	**25**	**32**	**36**	**32**	**47**	351	
	Users Accuracy	0.84	0.88	0.35	0.45	0.2	0.66	0.58	0.69	0.77	351	
	Overall Accuracy	**0.58**										
	Kappa	**0.53**										

2014-08-09 RF CLASSIFICATION ON COMBINED SAR-OPTICAL DATA: ACCURACY ASSESSMENT

		Classification Image										
		Artificial Surfaces	Bare Soil	Cultivated HG	Cultivated HNG	Cultivated Trees	Managed Grass	Natural HSB	Natural Trees	Water	Grand Total	Producer's Accuracy
Reference Image	Artificial Surfaces	37	1		1			1		1	**41**	0.90
	Bare Soil	1	25	1	1			1		1	**30**	0.83
	Cultivated HG		1	19	10	1	4	4			**39**	0.49
	Cultivated HNG	1	2	1	48	2	1	9			**64**	0.75
	Cultivated Trees			4	7	2		4			**17**	0.12
	Managed Grass	3		4			21	4			**32**	0.66
	Natural HSB	2		3	10	2	4	30	5	1	**57**	0.53
	Natural Trees				2			2	22		**26**	0.85
	Water	5			1	1		2		36	**45**	0.8
	Grand Total	**49**	**29**	**32**	**80**	**8**	**30**	**57**	**27**	**39**	351	
	Users Accuracy	0.76	0.86	0.59	0.6	0.25	0.7	0.53	0.81	0.92	351	
	Overall Accuracy	**0.68**										
	Kappa	**0.64**										

2014-08-09 CART CLASSIFICATION ON COMBINED SAR-OPTICAL DATA: ACCURACY ASSESSMENT

		Classification Image										
		Artificial Surfaces	Bare Soil	Cultivated HG	Cultivated HNG	Cultivated Trees	Managed Grass	Natural HSB	Natural Trees	Water	Grand Total	Producer's Accuracy
Reference Image	Artificial Surfaces	29	2		2		1	2		4	**40**	0.73
	Bare Soil		26	2	1		1				**30**	0.87
	Cultivated HG		1	15	5	17		1			**39**	0.38
	Cultivated HNG			5	38	16	1	4			**64**	0.59
	Cultivated Trees			1	3	7	1	5			**17**	0.41
	Managed Grass	1	1	1	1	2	25	1			**32**	0.78
	Natural HSB	1		2	10	9	13	14	8		**57**	0.25
	Natural Trees			1	3	1		2	19		**26**	0.73
	Water	2	4		10		2	2		25	**45**	0.56
	Grand Total	**33**	**34**	**27**	**73**	**52**	**44**	**31**	**27**	**29**	351	
	Users Accuracy	0.88	0.76	0.56	0.52	0.13	0.57	0.45	0.70	0.86		
	Overall Accuracy	**0.57**										
	Kappa	**0.51**										

2014-08-09 KNN CLASSIFICATION ON COMBINED SAR-OPTICAL DATA: ACCURACY ASSESSMENT

		Classification Image										
		Artificial Surfaces	Bare Soil	Cultivated HG	Cultivated HNG	Cultivated Trees	Managed Grass	Natural HSB	Natural Trees	Water	Grand Total	Producer's Accuracy
Reference Image	Artificial Surfaces	28	4	2	4			1		2	**41**	0.68
	Bare Soil	2	22		1		1	3	1		**30**	0.73
	Cultivated HG			14	10	4	4	6		1	**39**	0.36
	Cultivated HNG	1	3	5	42	5		6	1	1	**64**	0.66
	Cultivated Trees			3	3	9		1	1		**17**	0.53
	Managed Grass	1		5	1	1	14	9		1	**32**	0.44
	Natural HSB		1	8	10	2	7	18	11		**57**	0.32
	Natural Trees			1		3		3	18	1	**26**	0.69
	Water			2	4			1		38	**45**	0.84
	Grand Total	**32**	**30**	**40**	**75**	**24**	**26**	**48**	**32**	**44**	351	
	Users Accuracy	0.88	0.73	0.35	0.56	0.38	0.54	0.38	0.56	0.86	351	
	Overall Accuracy	**0.58**										
	Kappa	**0.52**										

2014-08-09 BAYES CLASSIFICATION ON COMBINED SAR-OPTICAL DATA: ACCURACY ASSESSMENT

		Classification Image										
		Artificial Surfaces	Bare Soil	Cultivated HG	Cultivated HNG	Cultivated Trees	Managed Grass	Natural HSB	Natural Trees	Water	Grand Total	Producer's Accuracy
Reference Image	Artificial Surfaces	12			11			15		3	**41**	0.29
	Bare Soil		8		7			15			**30**	0.27
	Cultivated HG			5	24			10			**39**	0.13
	Cultivated HNG				55			9			**64**	0.86
	Cultivated Trees				10	1		6			**17**	0.06
	Managed Grass				14			18			**32**	0
	Natural HSB				18			39			**57**	0.68
	Natural Trees				7			19			**26**	0
	Water				21			3		21	**45**	0.4.7
	Grand Total	**12**	**8**	**5**	**167**	**1**	**0**	**134**	**0**	**24**	351	
	Users Accuracy	1	1	1	0.33	1	0	0.29	0	0.88	351	
	Overall Accuracy	**0.40**										
	Kappa	**0.28**										

2014-08-09 SVM CLASSIFICATION ON COMBINED SAR-OPTICAL DATA: ACCURACY ASSESSMENT

		Classification Image										
		Artificial Surfaces	Bare Soil	Cultivated HG	Cultivated HNG	Cultivated Trees	Managed Grass	Natural HSB	Natural Trees	Water	Grand Total	Producer's Accuracy
Reference Image	Artificial Surfaces	31	1					7		2	**41**	0.76
	Bare Soil	1	26	2				1			**30**	0.87
	Cultivated HG		1	24	10	1	1	2			**39**	0.62
	Cultivated HNG	1	7		39	9	1	6		1	**64**	0.61
	Cultivated Trees			2	6	5		3	1		**17**	0.29
	Managed Grass	1		7	5		19				**32**	0.59
	Natural HSB	1	1	3	15	4	3	16	14		**57**	0.28
	Natural Trees				1				25		**26**	0.96
	Water	4	1		2		1	1		36	**45**	0.8
	Grand Total	**39**	**37**	**38**	**78**	**19**	**25**	**36**	**40**	**39**	351	
	Users Accuracy	0.79	0.70	0.63	0.5	0.26	0.76	0.44	0.63	0.923	351	
	Overall Accuracy	**0.63**										
	Kappa	**0.58**										

9.3.2   Experiment 3: Confusion matrices

9.3.2.1   2014-02-22

2014-02-22 RF Classification on combined SPOT-5 and RADARSAT-2 Imagery: Accuracy Assessment

		Classification Image										
		Artificial Surfaces	Bare Soil	Cultivated HG	Cultivated HNG	Cultivated Trees	Managed Grass	Natural HSB	Natural Trees	Water	Grand Total	Producer's Accuracy
Reference Image	Artificial Surfaces	36			1					4	**41**	0.88
	Bare Soil		24	1	2			2		1	**30**	0.8
	Cultivated HG			24	5	6		4			**39**	0.62
	Cultivated HNG		2	2	51	2		7			**64**	0.8
	Cultivated Trees			4	6	4		3			**17**	0.24
	Managed Grass	2		8		1	18	3			**32**	0.56
	Natural HSB	3		5	11	3	4	25	6		**57**	0.44
	Natural Trees				3			3	20		**26**	0.77
	Water	1			4	2				38	**45**	0.84
	Grand Total	**42**	**26**	**44**	**83**	**18**	**22**	**47**	**26**	**43**	351	
	Users Accuracy	0.86	0.92	0.55	0.61	0.22	0.82	0.53	0.77	0.88	351	
	Overall Accuracy	**0.68**										
	Kappa	0.64										

2014-02-22 RF Classification on just RADARSAT-2 Imagery: Accuracy Assessment

		Classification Image										
		Artificial Surfaces	Bare Soil	Cultivated HG	Cultivated HNG	Cultivated Trees	Managed Grass	Natural HSB	Natural Trees	Water	Grand Total	Producer's Accuracy
Reference Image	Artificial Surfaces	34			2				1	4	**41**	0.83
	Bare Soil		21	4	3	1				1	**30**	0.7
	Cultivated HG		1	20	1	5	2	8		2	**39**	0.51
	Cultivated HNG		1	3	39	1	3	14	2	1	**64**	0.61
	Cultivated Trees			4	4	7		2			**17**	0.41
	Managed Grass	1		4			24	3			**32**	0.75
	Natural HSB	2		2	14	8	5	19	6	1	**57**	0.33
	Natural Trees				5		1	3	17		**26**	0.65
	Water	2			1			3		39	**45**	0.87
	Grand Total	**39**	**23**	**37**	**69**	**22**	**35**	**52**	**26**	**48**	351	
	Users Accuracy	0.87	0.91	0.54	0.57	0.32	0.69	0.37	0.65	0.813	351	
	Overall Accuracy	**0.63**										
	Kappa	0.57										

2014-02-22 RF Classification on just SP0T-5 Imagery: Accuracy Assessment

		Classification Image										
		Artificial Surfaces	Bare Soil	Cultivated HG	Cultivated HNG	Cultivated Trees	Managed Grass	Natural HSB	Natural Trees	Water	Grand Total	Producer's Accuracy
Reference Image	Artificial Surfaces	34	4		3						**41**	0.829268
	Bare Soil		24	2	1	1		1		1	**30**	0.8
	Cultivated HG		3	19	8	8		1			**39**	0.49
	Cultivated HNG	3	3	2	41		1	11	2	1	**64**	0.64
	Cultivated Trees			2	5	5	1	3		1	**17**	0.29
	Managed Grass	1	1	5			20	5			**32**	0.63
	Natural HSB			6	7	5	4	27	7	1	**57**	0.47
	Natural Trees				3	1		2	20		**26**	0.77
	Water	2			3			2	1	37	**45**	0.82
	Grand Total	**40**	**35**	**36**	**71**	**20**	**26**	**52**	**30**	**41**	351	
	Users Accuracy	0.85	0.69	0.53	0.58	0.25	0.77	0.52	0.67	0.90	351	
	Overall Accuracy	**0.65**										
	Kappa	**0.596**										

9.3.2.2   2014-05-05

2014-05-05 RF Classification on combined SPOT-5 and RADARSAT-2 Imagery: Accuracy Assessment

| | Classification Image | | | | | | | | | | |
	Artificial Surfaces	Bare Soil	Cultivated HG	Cultivated HNG	Cultivated Trees	Managed Grass	Natural HSB	Natural Trees	Water	Grand Total	Producer's Accuracy
Artificial Surfaces	38	1				1	1			**41**	0.93
Bare Soil		26		1		1	2			**30**	0.87
Cultivated HG			22	9	1		7			**39**	0.56
Cultivated HNG	1	3	1	48	2		9			**64**	0.75
Cultivated Trees			4	12			1			**17**	0
Managed Grass	1		1	4		20	6			**32**	0.63
Natural HSB	1		3	11	1	3	31	7		**57**	0.54
Natural Trees				2		1	2	21		**26**	0.81
Water	2			5					38	**45**	0.84
Grand Total	**43**	**30**	**31**	**92**	**4**	**26**	**59**	**28**	**38**	351	
Users Accuracy	0.88	0.87	0.71	0.52	0	0.77	0.53	0.75	1	351	
Overall Accuracy	**0.695**										
Kappa	**0.65**										

2014-05-05 RF Classification on RADARSAT-2 Imagery: Accuracy Assessment

| | Classification Image | | | | | | | | | | |
	Artificial Surfaces	Bare Soil	Cultivated HG	Cultivated HNG	Cultivated Trees	Managed Grass	Natural HSB	Natural Trees	Water	Grand Total	Producer's Accuracy
Artificial Surfaces	35						4		2	**41**	0.85
Bare Soil		21	1	6			1		1	**30**	0.7
Cultivated HG		1	24	7	2	2	3			**39**	0.62
Cultivated HNG		1	5	41	7	1	9			**64**	0.64
Cultivated Trees			2	9	4		2			**17**	0.24
Managed Grass	1		4	3	1	17	6			**32**	0.53
Natural HSB	1		4	12	2	5	26	7		**57**	0.46
Natural Trees				5			5	16		**26**	0.62
Water	3			1			2		39	**45**	0.87
Grand Total	**40**	**23**	**40**	**84**	**16**	**25**	**58**	**23**	**42**	351	
User's Accuracy	0.88	0.91	0.6	0.49	0.25	0.68	0.45	0.7	0.93	351	
Overall Accuracy	**0.64**										
Kappa	**0.58**										

2014-05-05 RF Classification on SPOT-5 Imagery: Accuracy Assessment

| | | Classification Image | | | | | | | | | | |
		Artificial Surfaces	Bare Soil	Cultivated HG	Cultivated HNG	Cultivated Trees	Managed Grass	Natural HSB	Natural Trees	Water	Grand Total	Producer's Accuracy
Reference Image	Artificial Surfaces	27	6		4		2	1		1	**41**	0.66
	Bare Soil		27		2			1			**30**	0.9
	Cultivated HG			28	6	1		4			**39**	0.72
	Cultivated HNG	2	1	2	49	2		8			**64**	0.77
	Cultivated Trees			4	6	2	1	4			**17**	0.12
	Managed Grass	2		5	1		16	8			**32**	0.5
	Natural HSB	1		6	8	5	7	26	4		**57**	0.46
	Natural Trees			1	1			5	19		**26**	0.73
	Water	2	2		4					37	**45**	0.82
	Grand Total	**34**	**36**	**46**	**81**	**10**	**26**	**57**	**23**	**38**	351	
	User's Accuracy	0.79	0.75	0.61	0.60	0.2	0.62	0.46	0.83	0.97	351	
	Overall Accuracy	**0.66**										
	Kappa	**0.61**										

9.3.2.3   2014-05-29

2014-05-29 RF Classification on combined SPOT-5 and RADARSAT-2 Imagery: Accuracy Assessment

| | Classification Image | | | | | | | | | | |
		Artificial Surfaces	Bare Soil	Cultivated HG	Cultivated HNG	Cultivated Trees	Managed Grass	Natural HSB	Natural Trees	Water	Grand Total	Producer's Accuracy
Reference Image	Artificial Surfaces	39						1		1	**41**	0.95
	Bare Soil	1	26		2			1			**30**	0.87
	Cultivated HG			23	6	3	1	6			**39**	0.59
	Cultivated HNG	1	1	2	49	1	1	9			**64**	0.77
	Cultivated Trees			3	5	1	1	6	1		**17**	0.06
	Managed Grass	1		1	2		22	6			**32**	0.69
	Natural HSB	2		3	10	2	4	26	10		**57**	0.46
	Natural Trees			1	3			3	19		**26**	0.73
	Water	2			1			2		40	**45**	0.89
	Grand Total	**46**	**27**	**33**	**78**	**7**	**29**	**60**	**30**	**41**	351	
	Users Accuracy	0.85	0.96	0.7	0.63	0.14	0.76	0.43	0.63	0.98	351	
	Overall Accuracy	**0.7**										
	Kappa	**0.65**										

2014-05-29 RF Classification on RADARSAT-2 Imagery: Accuracy Assessment

| | Classification Image | | | | | | | | | | |
		Artificial Surfaces	Bare Soil	Cultivated HG	Cultivated HNG	Cultivated Trees	Managed Grass	Natural HSB	Natural Trees	Water	Grand Total	Producer's Accuracy
Reference Image	Artificial Surfaces	27		1				4		9	**41**	0.66
	Bare Soil		23	3	1	1		1		1	**30**	0.77
	Cultivated HG			20	8		4	7			**39**	0.51
	Cultivated HNG	1		3	43	1		16			**64**	0.67
	Cultivated Trees			2	6	5	2	2			**17**	0.29.
	Managed Grass	3		1	2	1	14	6		5	**32**	0.44
	Natural HSB	4			13	1	7	23	7	2	**57**	0.40
	Natural Trees				1		1	4	20		**26**	0.77
	Water				4		1	2	1	37	**45**	0.82
	Grand Total	**35**	**23**	**30**	**78**	**9**	**29**	**65**	**28**	**54**	351	
	Users Accuracy	0.77	1	0.67	0.55	0.56	0.48	0.35	0.71	0.69	351	
	Overall Accuracy	**0.60**										
	Kappa	**0.54**										

2014-05-29 RF Classification on SPOT-5 Imagery: Accuracy Assessment

		Classification Image										
		Artificial Surfaces	Bare Soil	Cultivated HG	Cultivated HNG	Cultivated Trees	Managed Grass	Natural HSB	Natural Trees	Water	Grand Total	Producer's Accuracy
Reference Image	Artificial Surfaces	33	2		3		1			2	**41**	0.80
	Bare Soil	1	24		2		2	1			**30**	0.8
	Cultivated HG		3	18	9	2	4	3			**39**	0.46
	Cultivated HNG	2		2	47	5	6			2	**64**	0.73
	Cultivated Trees			3	7	2		4	1		**17**	0.12
	Managed Grass	1	1	5	4		16	4		1	**32**	0.5
	Natural HSB	2		5	14	3	10	12	11		**57**	0.21
	Natural Trees				2	1		4	19		**26**	0.73
	Water	2			3			2		38	**45**	0.84
	Grand Total	**41**	**30**	**33**	**91**	**13**	**39**	**30**	**31**	**43**	351	
	Users Accuracy	0.80	0.8	0.55	0.52	0.15	0.41	0.4	0.61	0.88	351	
	Overall Accuracy	**0.6**										
	Kappa	**0.54**										

9.3.2.4   2014-08-09

2014-08-09 RF Classification on combined SPOT-5 and RADARSAT-2 Imagery: Accuracy Assessment

		Classification Image										
		Artificial Surfaces	Bare Soil	Cultivated HG	Cultivated HNG	Cultivated Trees	Managed Grass	Natural HSB	Natural Trees	Water	Grand Total	Producer's Accuracy
Reference Image	Artificial Surfaces	37	1		1			1		1	**41**	0.90
	Bare Soil	1	25	1	1			1		1	**30**	0.83
	Cultivated HG		1	19	10	1	4	4			**39**	0.49
	Cultivated HNG	1	2	1	48	2	1	9			**64**	0.75
	Cultivated Trees			4	7	2		4			**17**	0.12
	Managed Grass	3		4			21	4			**32**	0.66
	Natural HSB	2		3	10	2	4	30	5	1	**57**	0.53
	Natural Trees				2			2	22		**26**	0.85
	Water	5			1	1		2		36	**45**	0.8
	Grand Total	**49**	**29**	**32**	**80**	**8**	**30**	**57**	**27**	**39**	351	
	Users Accuracy	0.76	0.86	0.59	0.6	0.25	0.7	0.53	0.81	0.92	351	
	Overall Accuracy	**0.68**										
	Kappa	**0.64**										

2014-08-09 RF Classification on RADARSAT-2 Imagery: Accuracy Assessment

		Classification Image										
		Artificial Surfaces	Bare Soil	Cultivated HG	Cultivated HNG	Cultivated Trees	Managed Grass	Natural HSB	Natural Trees	Water	Grand Total	Producer's Accuracy
Reference Image	Artificial Surfaces	34		1	1			2		3	**41**	0.83
	Bare Soil		26	2	2						**30**	0.87
	Cultivated HG		1	21	14	1	1	1			**39**	0.54
	Cultivated HNG			10	40	1	1	11	1		**64**	0.63
	Cultivated Trees	1		6	6	3	1				**17**	0.18
	Managed Grass	3		2	2	1	13	6	1	4	**32**	0.41
	Natural HSB	3		4	14	1	6	22	6	1	**57**	0.39
	Natural Trees			2	4		1	3	16		**26**	0.62
	Water		1		8		1	2		33	**45**	0.73
	Grand Total	**41**	**28**	**48**	**91**	**7**	**24**	**47**	**24**	**41**	351	
	Users Accuracy	0.83	0.93	0.44	0.44	0.43	0.54	0.47	0.67	0.80	351	
	Overall Accuracy	**0.59**										
	Kappa	**0.53**										

2014-08-09 RF Classification on SPOT-5 Imagery: Accuracy Assessment

		Classification Image									
		Artificial Surfaces	Bare Soil	Cultivated HG	Cultivated HNG	Cultivated Trees	Managed Grass	Natural HSB	Natural Trees	Water	Grand Total	Producer's Accuracy
Reference Image	Artificial Surfaces	31	5	1	1			2		1	**41**	0.76
	Bare Soil	1	26		2			1			**30**	0.87
	Cultivated HG	2		17	5	3	9	2		1	**39**	0.44
	Cultivated HNG	1	1	3	46	5		8			**64**	0.72
	Cultivated Trees			3	4	5	1	4			**17**	0.29
	Managed Grass	1		8			16	5		2	**32**	0.5
	Natural HSB	1		8	4	11	5	21	6	1	**57**	0.37
	Natural Trees				1	1		2	22		**26**	0.85
	Water	4			4	1		2		34	**45**	0.76
	Grand Total	**41**	**32**	**40**	**67**	**26**	**31**	**47**	**28**	**39**	351	
	Users Accuracy	0.76	0.81	0.43	0.69	0.19	0.52	0.45	0.79	0.87	351	
	Overall Accuracy	**0.62**										
	Kappa	**0.57**										

9.3.3 Experiment 4: Confusion matrices

Multi-Temporal, combined SAR-optical classification based on 20 training features

		Classification Image										
		Artificial Surfaces	Bare Soil	Cultivated HG	Cultivated HNG	Cultivated Trees	Managed Grass	Natural HSB	Natural Trees	Water	Grand Total	Producer's Accuracy
Reference Image	Artificial Surfaces	29	4		2					6	**41**	0.71
	Bare Soil	1	26		2			1			**30**	0.87
	Cultivated HG			23	5	4	4	3			**39**	0.59
	Cultivated HNG		1		50	3	1	9			**64**	0.78
	Cultivated Trees			1	6	5	1	2	1	1	**17**	0.29
	Managed Grass	3		8	2		16	3			**32**	0.5
	Natural HSB	1		2	15	4	7	21	6	1	**57**	0.37
	Natural Trees				2				2	22	**26**	0.85
	Water	2			4	1				38	**45**	0.84
	Grand Total	**36**	**31**	**34**	**88**	**17**	**29**	**41**	**29**	**46**	351	
	Users Accuracy	0.81	0.84	0.68	0.57	0.29	0.55	0.51	0.76	0.83	351	
	Overall Accuracy	**0.66**										
	Kappa	**0.60**										

Multi-temporal, combined SAR-optical classification based on 40 training features

		Classification Image										
		Artificial Surfaces	Bare Soil	Cultivated HG	Cultivated HNG	Cultivated Trees	Managed Grass	Natural HSB	Natural Trees	Water	Grand Total	Producer's Accuracy
Reference Image	Artificial Surfaces	31	3		2					5	**41**	0.76
	Bare Soil		26		2		1			1	**30**	0.87
	Cultivated HG			25	8	1	2	3			**39**	0.64
	Cultivated HNG			1	56	2	1	4			**64**	0.88
	Cultivated Trees			1	6	5	2	2		1	**17**	0.29
	Managed Grass	2		4	1		23	2			**32**	0.72
	Natural HSB	2		2	8	2	6	32	5		**57**	0.56
	Natural Trees							4	22		**26**	0.85
	Water	2			4	1		1		37	**45**	0.82
	Grand Total	**37**	**29**	**33**	**87**	**11**	**35**	**48**	**27**	**44**	351	
	Users Accuracy	0.84	0.9	0.76	0.64	0.45	0.66	0.67	0.81	0.84	351	
	Overall Accuracy	**0.73**										
	Kappa	**0.69**										

Multi-temporal, combined SAR-optical classification based on 50 training features

		Classification Image									
		Artificial Surfaces	Bare Soil	Cultivated HG	Cultivated HNG	Cultivated Trees	Managed Grass	Natural HSB	Natural Trees	Water	Grand Total	Producer's Accuracy
Reference Image	Artificial Surfaces	36			3					2	**41**	0.88
	Bare Soil		26		2			1		1	**30**	0.87
	Cultivated HG			28	7	2		2			**39**	0.72
	Cultivated HNG			2	54	2	1	5			**64**	0.84
	Cultivated Trees			1	4	5	2	5			**17**	0.29
	Managed Grass	2		4	1		25				**32**	0.78
	Natural HSB	2		2	8	3	6	31	5		**57**	0.54
	Natural Trees				2			3	21		**26**	0.81
	Water	2			7	1		1		34	**45**	0.76
	Grand Total	**42**	**26**	**37**	**88**	**13**	**34**	**48**	**26**	**37**	351	
	Users Accuracy	**0.86**	1	0.76	0.61	0.38	0.74	0.65	0.81	0.912	351	
	Overall Accuracy	**0.74**										
	Kappa	0.70										

Multi-temporal, combined SAR-optical classification based on 60 training features

		Classification Image									
		Artificial Surfaces	Bare Soil	Cultivated HG	Cultivated HNG	Cultivated Trees	Managed Grass	Natural HSB	Natural Trees	Water	Grand Total	Producer's Accuracy
Reference Image	Artificial Surfaces	36			2					3	**41**	0.88
	Bare Soil		26		1			2		1	**30**	0.87
	Cultivated HG			26	9	1		3			**39**	0.67
	Cultivated HNG			1	53	1	1	8			**64**	0.83
	Cultivated Trees			2	6	5	1	3			**17**	0.29
	Managed Grass	2		2	1		25	2			**32**	0.78
	Natural HSB	2		1	7	5	6	32	4		**57**	0.56
	Natural Trees				1	1		3	21		**26**	0.81
	Water	2			6	1				36	**45**	0.8
	Grand Total	**42**	**26**	**32**	**86**	**14**	**33**	**53**	**25**	**40**	351	
	Users Accuracy	0.86	1	0.81	0.62	0.36	0.76	0.6	0.84	0.9	351	
	Overall Accuracy	**0.74**										
	Kappa	**0.70**										